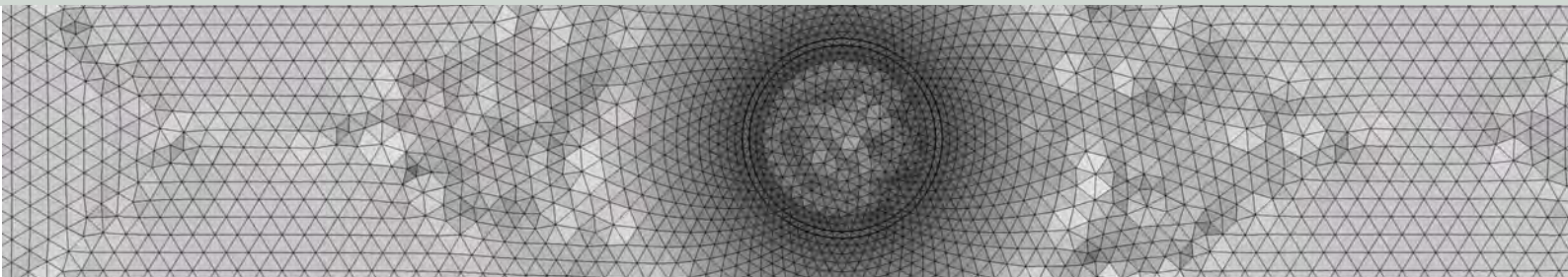




Schweizerische Eidgenossenschaft
Confédération suisse
Confederazione Svizzera
Confederaziun svizra

Swiss Confederation

Eidgenössisches Nuklearsicherheitsinspektorat ENSI
Inspection fédérale de la sécurité nucléaire IFSN
Ispettorato federale della sicurezza nucleare IFSN
Swiss Federal Nuclear Safety Inspectorate ENSI



Review of the kinematic interpretation of the tectonic structures in northern Switzerland

Expertenbericht

im Rahmen der Beurteilung des Vorschlags von mindestens zwei geologischen Standortgebieten pro Lagertyp, Etappe 2, Sachplan geologische Tiefenlager

C. Nussbaum
P. Bossart

swisstopo

Mai 2016

Disclaimer:

Die im Bericht dokumentierten Ansichten und Schlussfolgerungen sind diejenigen der Autoren und stimmen nicht notwendigerweise mit denen des ENSI überein.



**Expertenbericht von swisstopo, Landesgeologie zu Handen
des Eidgenössischen Nuklearsicherheitsinspektorates ENSI**

31. Mai 2016

**Review of the kinematic interpretation of the
tectonic structures in northern Switzerland**

**Based on structural and geological interpretation of new 2D-
seismic and recently reprocessed and depth-migrated 2D
reflection seismic profiles**



Schweizerische Eidgenossenschaft
Confédération suisse
Confederazione Svizzera
Confederaziun svizra

Bundesamt für Landestopografie swisstopo
Office fédéral de topographie swisstopo
Ufficio federale di topografia swisstopo
Uffizi federal da topografia swisstopo

www.swisstopo.ch

SQS-Zertifikat ISO 9001:2000

Eidgenössisches Departement für Verteidigung,
Bevölkerungsschutz und Sport VBS

armasuisse

Bundesamt für Landestopografie swisstopo, Landesgeologie

Authors: Christophe Nussbaum and Paul Bossart

and external experts: Anna Sommaruga, Armelle Kloppenburg, Typhaine Caër, Bertrand Maillot, Pascale Leturmy and Pauline Souloumiac

© 2016 **swisstopo**
Bundesamt für Landestopographie
Office fédéral de topographie
Ufficio federale di topografia
Uffizi federal da topografia
Federal Office of Topography
www.swisstopo.ch

Landesgeologie
Seftigenstrasse 264
CH-3084 Wabern
Tel: +41 58 469 05 87



E-mail: christophe.nussbaum@swisstopo.ch

Content:

1	Introduction	7
1.1	Rationale	7
1.2	Questions to be answered, our approach, and structure of the report	7
1.3	Reports considered for the expertise	10
2	Geological overview and model building	12
2.1	Brief overview of the geology	12
2.2	Why build a 3D model for the expertise?	12
3	Analysis of tectonic structures of northern Switzerland	14
3.1	Fault inventory and comparison between SGT Etappe 1 and 2	14
3.1.1	Siting region Zürich Nordost and Südranden	15
3.1.2	Siting region Nördlich Lägern	15
3.1.3	Siting region Jura Ost	16
3.1.4	Siting region Jura Südfuss	16
3.2	Tectonic map of northern Switzerland	32
3.3	Transfer zone	35
3.4	Role of inherited structures on present-day geometry	37
4	Tectonic history of northern Switzerland	39
4.1	Variscan inheritance and Late Palaeozoic wrench faulting	39
4.2	Jurassic basement-rooted fault reactivation	40
4.3	Paleogene extension (European Cenozoic rift system)	41
4.4	Resulting tectonic setting of the three main inherited fault trends	41
4.5	Late Oligocene/ Early Miocene uplift of the Black Forest Massif and subsidence of the Molasse Basin	42
4.6	Late Miocene (Jura thin-skinned deformation)	43
5	Kinematic tectonic interpretation	46
5.1	Balanced cross sections	46
5.2	Discrepancy between balanced cross section and seismic interpretation	46
5.3	The kinematic evolution of the BIH triangle zone	48
6	Present-day deformation front, future evolution, and recent thick-skinned tectonics	50
6.1	Present-day deformation front	50
6.2	Future evolution of the deformation?	50
6.3	Recent / future thick-skinned tectonics (?)	51
6.4	Limitations of the applied mechanical approach	55
6.5	Neoseismicity	55
7	Key outcomes and recommendations for further investigations	57
7.1	Role of inherited faults and transfer zone	57
7.2	Kinematic evolution	58
7.3	Present-day deformation front	58
7.4	Recent and future thick-skinned tectonics?	59
7.5	Nanoseismic monitoring	59

7.6	Assessment on the siting areas	60
8	References	61

List of appendices

Appendix 1: 2D-seismic interpretation (Dr. A. Sommaruga, Univ. Fribourg)

Appendix 2: 2D kinematic modelling (Dr. A. Kloppenburg, 4DGEO Structural Geology)

Appendix 3: Mechanical analysis of the eastern end of the Jura: Role of basement ramps and inherited faults (T. Caër et al., Univ. Cergy-Pontoise, France)

List of Figures

Figure 2-1: View of the 3D model built in <i>MOVE</i> showing the two superposed tectonic maps (from NTB 14-02 and NAB 14-17) and interpreted basement faults (in red). Image by M. Verdon (swisstopo)	13
Figure 2-2: View of the 3D model built in <i>MOVE</i> (image by M. Verdon, swisstopo) with the seismic profiles, borehole data and balanced cross sections and the top basement tectonic map in underground (from NAB 14-17).....	13
Figure 3-1: Sketch illustrating how the faults (in red) were projected on the map views presented in Figure 3-2 to Figure 3-16. A fault is represented by two polylines forming a surface. When the fault is vertical, the corresponding fault will be illustrated by only one polyline. The width of the surface informs about the steepness of the fault.	15
Figure 3-2: Comparison of tectonic elements Stage 1 vs. Stage 2 Survey Map – Base Tertiary	17
Figure 3-3: Comparison of tectonic elements Stage 1 vs. Stage 2 Survey Map of 5 potential siting areas – Base Malm.....	18
Figure 3-4: Comparison of tectonic elements Stage 1 vs. Stage 2 Survey Map – Base Mesozoic	19
Figure 3-5: Comparison of tectonic elements Stage 1 vs. Stage 2 Zürich Nordost & Südranden – Base Tertiary	20
Figure 3-6: Comparison of tectonic elements Stage 1 vs. Stage 2 Zürich Nordost & Südranden – Base Malm.....	21
Figure 3-7: Comparison of tectonic elements Stage 1 vs. Stage 2 Zürich Nordost & Südranden – Base Mesozoic	22
Figure 3-8: Comparison of tectonic elements Stage 1 vs. Stage 2 Nördlich Lägern – Base Tertiary	23
Figure 3-9: Comparison of tectonic elements Stage 1 vs. Stage 2 Nördlich Lägern – Base Malm	24
Figure 3-10: Comparison of tectonic elements Stage 1 vs. Stage 2 Nördlich Lägern – Base Mesozoic	25
Figure 3-11: Comparison of tectonic elements Stage 1 vs. Stage 2 Jura Ost– Base Tertiary	26
Figure 3-12: Comparison of tectonic elements Stage 1 vs. Stage 2 Jura Ost– Base Malm (image by R. Allenbach, swisstopo).....	27
Figure 3-13: Comparison of tectonic elements Stage 1 vs. Stage 2 Jura Ost– Base Mesozoic	28
Figure 3-14: Comparison of tectonic elements Stage 1 vs. Stage 2 Jura Südfuss– Base Tertiary	29
Figure 3-15: Comparison of tectonic elements Stage 1 vs. Stage 2 Jura Südfuss– Base Malm	30
Figure 3-16: Comparison of tectonic elements Stage 1 vs. Stage 2 Jura Südfuss– Base Mesozoic	31
Figure 3-17 : Tectonic map of northern Switzerland (from Nagra, NAB 14-105, Beilage 1-1).....	33
Figure 3-18: Tectonic map of northern Switzerland with the main fault trends: “Variscan” WNW-striking faults, “Permo-Carboniferous” ENE-striking faults, “Rhenish” NNE-striking faults and “Jura” E-W striking faults (from Nagra, NAB 14-105, modified by C. Nussbaum, swisstopo).....	34
Figure 3-19: The Jura front is affected by a significant transfer zone located between the potential siting areas Jura Ost and Nördlich Lägern (NL). Note that the western edge of NL lies	

- within the transfer zone (from Nagra in NAB-14-105, modified by C. Nussbaum, swisstopo).... 35
- Figure 3-20: The transfer zone is characterized by the apparent interruption of most of the thrusts and faults and changes in orientations of some of them. The E-W lateral continuity of the tectonic structures within the transfer zone is questionable (image by C. Nussbaum, swisstopo, modified from baillage 1-1-in NAB 14-105)..... 36
- Figure 3-21: The transfer zone is composed of two oblique thrust ramps having opposite dip directions. These sidewall ramps are spatially correlated with basement-rooted faults (image by M. Verdon, swisstopo)..... 36
- Figure 3-22: Tectonic map of top basement including the northern Swiss Permo-Carboniferous trough (from Nagra, NAB 14-105)..... 38
- Figure 4-1: Conceptual tectonic map of inherited structures prior to Late Oligocene/Early Miocene uplift of the Black Forest Massif and subsidence of the Swiss Molasse Basin. At least three different inherited fault systems can be identified and traced: 1) WNW-ESE striking faults (“Variscan” trend), 2) ENE-WSW striking faults (“Permo-Carboniferous” trend), and 3) NNE-SSW striking faults (“Rhenish” trend). Note that the eastwards continuation of the Eggberg-Fault may eventually intersect the western part of the Siggenthal-Fault within the siting region Jura Ost (?). The Unterendingen-Fault may intersect the Siglistorf-Fault at the western part of the siting region Nördlich Lägern (?)...... 39
- Figure 4-2: Isopach map of the “Dogger” interval between horizons nTOpa - BMa (map elaborated by R. Allenbach, swisstopo)..... 41
- Figure 4-3: Conceptual tectonic map of tectonic elements after Late Oligocene/Early Miocene uplift of the Black Forest Massif and the subsidence of the Swiss Molasse Basin. Both WNW-ESE-trending faults (“Variscan trend”) and ENE-WSW trending faults (Permo-Carboniferous) were reactivated as normal faulting during the uplift related to the Alpine forebulge 43
- Figure 4-4: Conceptual tectonic map including the superposition of major top basement and surface tectonic elements after Late Miocene thin-skinned thrusting. The pronounced curvature of the Siglistorf-Anticline may be tentatively explained by a NNE trending oblique ramp developed in the sedimentary cover as a result of basement-rooted fault having the same direction..... 44
- Figure 4-5: Tectonic map of northern Switzerland with Unterendingen dextral (to the left) and Siglistorf sinistral (to the right) oblique ramps propagating through the sedimentary sequence consequently to basement-rooted fault reactivation (image from 3D model *MOVE*, swisstopo).45
- Figure 5-1: Interpretation of seismic profile 83-NF-15 (siting region Jura Ost). Comparison between interpreted structures by Meier et al., 2014 and balanced cross section by Jordan et al., 2015. Note the tectonic differences for the Jura Main Thrust and Chestenberg-Anticline.... 47
- Figure 5-2: Proposed kinematic sketch from Malz et al., 2015 illustrating the evolution of the BIH triangle with respect to the Jura Main Thrust: A: initial state with less than 200 m shortening, the inherited normal faults are not affected by the shortening so far; B: Shortening of approximately 200m. The pre-existing normal fault is contractionally overprinted leading to the fully developed BIH triangle structure. C: shortening exceeds the maximum horizontal strain assimilated from the BIH triangle; on-going shortening results in the formation of new thrusts in the hinterland of the BIH; D: shortening strongly exceeds ~200 m; the stationary BIH triangle is overthrust by foreland propagating thrust-faults associated with the Jura belt. Inherited normal faults are completely cut by thrust-faults. 48
- Figure 5-3: Alternative kinematic interpretation proposed by A. Kloppenburg by forward modelling (refer to Appendix 2). In-sequence thrusting and consideration for alternative scenario for section 91-NO-58 (from Beilage 6-6 in NAB 14-105). Thrust faults are numbered according to their temporal sequence of activation. There are no direct constraints from cross-cutting relationships or kinematic considerations for the relative timing of the BIH and Lägern-

Anticline.....49

Figure 6-1: Synthetic map view of the present-day deformation front for various friction angles and assuming a cohesion on the Triassic décollement of 1 MPa (from Caër et al, see Appendix 3).....51

Figure 6-2: Conceptual sketch of the eastern end of the Jura fold-and-thrust belt illustrating the regional kinematic role of the Baden-Irchel-Herdern Lineament (BIH). This major tectonic structure is interpreted by Malz et al. (2015) to separate the study area in two compartments characterized by different tectonic styles. The southern part is dominated by thin-skinned thrusting and the northern side by thick-skinned tectonics (figure from Malz et al., 2015).53

Figure 6-3: Results obtained with Optum G2 for the thick-skin hypothesis tested on profile 12-NS-42 (siting area JS). Three cases for the lower décollement D2 were calculated: $C_{D2} = 0\text{MPa}$ fixed and $\varphi_{D2} = 3^\circ$, $\varphi_{D2} = 7^\circ$, $\varphi_{D2} = 10^\circ$. For the upper décollement D1, cohesion values ranging from 0 to 2 MPa and friction values from 0 to 12 ° are represented by a matrix. The calculated cases are represented by different square colours (from Caër et al., 2015, see details in Appendix 3)54

Figure 6-4: View of the 3D model including the hypocenters of 217 earthquakes published in the SED-database for the period between 1975 and 2008 (image by swisstopo). The tectonic map is from Nagra (Beilage 1-1, NAB 14-105).....56

List of Tables

Table 1.1: List of Nagra reports used for this review 10

Table 1.2: List of peer-reviewed papers provided for the review 11

1 Introduction

1.1 Rationale

In October 2013, swisstopo was commissioned by ENSI to review the kinematic interpretation of the tectonic structures in northern Switzerland proposed by Nagra. We used geological and structural interpretation of new 2D-seismic profiles and recently reprocessed and depth-migrated older 2D reflection seismic profiles were used to unravel the tectonic and kinematic evolution of the study region. These investigations were carried out in the framework of the second stage of the Sectoral Plan for Deep Geological Repositories (SGT) in northern Switzerland (in German: Sachplan Geologisches Tiefenlager, SGT Etappe 2). This second stage consists in selecting at least two potential siting areas for further investigations in SGT Etappe 3. The area of interest encompasses six potential siting regions for the construction of a deep geological repository. There are from southwest to northeast: Jura Südfuss (JS), Jura Ost (JO), Nördlich Lägern (NL), Südranden (SR); and Zürich Nordost (ZNO) and Wellenberg to the south. The present study focuses on the siting regions for which 2D-seismic profiles are available (JS, JO, NL, SR and ZNO). The siting region Wellenberg is not part of this report, since no seismic investigations have been performed in that area.

With the support of external experts, Nagra has proposed a detailed in-depth structural analysis of tectonic elements at the front of the easternmost Jura fold-and-thrust belt in northern Switzerland. The aim of the present review is to check the geological and structural interpretation of new 2D-seismic profiles acquired in 2011/2012 and of reprocessed and depth-migrated 2D reflection seismic profiles acquired in the 1980s and 1990s. Extensive reprocessing of these older 2D-seismic profiles resulted in substantial enhancement of their data quality and interpretability. Nevertheless, complex fault zones and anticlines remain characterised by low quality and/or highly ambiguous seismic imagery.

The seismic data available for this review comprises two sets:

- thirty-three reprocessed 2D-seismic reflection profiles acquired by Nagra between 1982 and 1992
- twenty new 2D-seismic reflections profiles acquired in 2011 and 2012.

1.2 Questions to be answered, our approach, and structure of the report

Our review is based on the structural and geologic interpretation of available reflection seismic data. The expertise contract from ENSI requires swisstopo to provide answers to three specific complex questions, written below first in the original German and then in English:

- 1) Ist das von der Nagra vorgelegte Inventar an tektonischen Elementen der Nordschweiz vollständig?
(Is the inventory of tectonic elements in northern Switzerland, provided by Nagra, complete?)
- 2) Ist die vorgelegte Interpretation der 2D-Seismiklinien nachvollziehbar und schlüssig?
(Is the tendered interpretation of the 2D seismic lines accountable and conclusive?)

3) Welche Folgerungen ergeben sich daraus bzgl. kinematischer Entwicklungsgeschichte der Nordschweiz?

(What are the consequences of the interpretation for the kinematic evolution of northern Switzerland?)

The aim of the first question is that swisstopo compares and verifies the proposed tectonic interpretation from Nagra based on new 2D-seismic and recently reprocessed 2D-seismic reflection profiles with its own geological maps and LIDAR datasets. We have made this comparison and we conclude that Nagra has not omitted any faults in the investigated area. In turn, thanks to the data acquired from 2D seismic profiles, Nagra has significantly improved the tectonic map of northern Switzerland by adding numerous new faults. It should be recalled that the federal geoportal geo.admin.ch provides all existing geological maps of Switzerland edited by swisstopo (GeoCover) as well all digital maps, elevation models, and images (swissALTI3 Hillshade). Furthermore, we decided to focus our effort on the comparison of faults identified from the SGT Etappe 1 with those from SGT Etappe 2 to check and validate the quality of the tectonic interpretation of seismic profiles. This comparison and verification is presented in section 3.1.

In order to assess question 2), swisstopo mandated Dr. Anna Sommaruga (University of Fribourg), first author of the Seismic Atlas of the Swiss Molasse Basin (swisstopo, 2012) to apply her expertise and experience to interpreting the seismic profiles. ENSI and swisstopo agreed that Ms. Sommaruga focus her efforts on a selection of about 20 profiles covering the five potential siting areas. Her analysis encompasses the regional fault area, the tectonic zones to be avoided, and also local tectonic features within the siting areas. In this framework, she was asked to make a statement on a series of specific questions addressed by ENSI. Her assessment is included here as Appendix 1.

Question 3) requires an understanding of past deformation sequences that have resulted in the present-day geometry of the study region to provide a well-evidenced prediction of the most likely future tectonic evolution, at least for the next few million years. We point out that the future kinematic evolution of northern Switzerland was not part of the work carried out by Nagra for SGT Etappe 2. We found few attempts to explore the kinematic evolution in the literature provided to us. Only two examples applying forward modelling are presented for some selected structures, such as the Jura Main Thrust (in report NAB 14-105), and the triangle zone associated with the Baden-Irchel-Herdern Lineament (in Malz et al., 2015). We point out that question 3) was addressed very late in the course of this expertise since both reports of interest (NAB 14-105 and the paper by Malz et al., 2015) were made available to us only at the end of May 2015. Regarding the lack of time to address the kinematic evolution of the study region, we suggest considering our report as a starting point for further investigations to be conducted in the future, especially in Stage 3 (SGT Etappe 3).

Jordan et al. (2015, NAB 14-105) present 18 cross sections distributed over the five siting areas. In this report, we constructed a balanced cross section (deformed section) and a restored section for each of these 18 cross sections. The aims and benefits of balanced cross sections is to have a geometrically viable and tectonically plausible 2D deformed cross section that can be restored to an initial state predating deformation (the "restored" section). However, the Nagra report contains no intermediate deformation steps. The best and only way to verify the viability of a cross section is to run forward modelling that documents each step of

incremental deformation. For this reason, swisstopo commissioned an external expert, Dr. Armelle Kloppenburg (4DGEO Structural Geology), to test the validity of the existing section interpretation for two representative cross sections: Section_83-NF-15 (see Beilage 6-6 in NAB 14-105) and Section_91-NO-58 (see Beilage 6-8 in NAB 14-105). These sections cross the siting areas Jura Ost and Nördlich Lägern, respectively. Kinematic validity of the existing section interpretation was tested using tools and workflows available with the *Move2015.1* program by sequentially restoring and forward modelling deformation due to contraction and fold and thrust development. This forward modelling procedure can test the validity of the geological interpretation and can help better understand the structural history (i.e. order of thrusts: in-sequence vs. out-of sequence), structural style, and structural domains. The report on 2D kinematic modelling by A. Kloppenburg is included here as Appendix 2.

Question 3) may be further explored by attempting to determine where the present-day deformation front is located and how the structure could potentially evolve in the near future (i.e. 1-2 myr). For this reason, we asked the team of Prof. B. Maillot from the University of Cergy-Pontoise to apply his experience on mechanical analysis of thrust-and-fold belts to this question. He and his team utilise a simplified mechanical approach originally developed in Civil Engineering and called limit analysis (Salencon, 2002). The kinematic approach of limit analysis consists in calculating an upper bound to the tectonic force associated with a given distribution of deformation by accounting for mechanical equilibrium and maximum resistance of rocks, as defined by the Coulomb criterion (friction coefficients and cohesions). There are no elastic or viscous parameters. Two programs (*Optum G2* and *SLAMTec*) based on the theory of limit analysis were used to predict the deformation and stress fields resulting from horizontal compression applied to a selection of seven cross sections proposed by Jordan et al. (2015). *Optum G2* has the advantage of putting no constraints on the deformation field (apart from mesh discretisation), and it can include faults as true velocity discontinuities. Also, pre-existing faults and heterogeneity of the mechanical parameters are accounted for, allowing us to analyse our structural interpretations in detail. *SLAMTec* was applied to simulate the possible future evolution of deformation with 1000 m of shortening, corresponding to 10 myr assuming a rate of 0.1 mm/a. The report on the mechanical analysis, written by T. Caër et al. is included here as Appendix 3.

1.3 Reports considered for the expertise

The reports used for this expertise are listed in Table 1.1. In addition, two accepted peer-reviewed papers were provided by their authors (Table 1.2). The literature used by our three external experts are listed in their reports included here as Appendices 1 - 3.

Nagra reference	Title	Authors	Publication date
NAB 10-39	Kompilation und Interpretation der Reflexionsseismik im Tafeljura und Molassebecken der Zentral- und Nordostschweiz	Ph. Roth, H. Naef, M. Schnellmann	July 2010
NAB 13-10	Regionale strukturgeologische Zeitinterpretation der Nagra 2D-Seismik 2011/12. Textband und Beilagenband	H. Madritsch, B. Meier, P. Kuhn, P. Roth, O. Zingg, S. Heuberger, H. Naef, P. Birkhäuser	June 2013
NTB 14-02 - Dossier II - Anhang	SGT Etappe 2: Vorschlag weiter zu untersuchender geologischer Standortgebiete mit zugehörigen Standortarealen für die Oberflächenanlage. Geologische Grundlagen. Dossier II. Sedimentologische und tektonische Verhältnisse.	Nagra	December 2014
NAB 14-17	Tektonische Karte des Nordschweizer Permokarbons: Aktualisierung basierend auf 2D-Seismik und Schwere-Daten.	H. Naef, H. Madritsch	December 2014
NAB 14-34	Tiefenkonvertierung der regionalen Strukturinterpretation der Nagra 2D-Seismik 2011-12	B. Meier, P. Kuhn, S. Muff, P. Roth, H. Madritsch	September 2014
NAB 14-105	Regionale geologische Profilschnitte durch die Nordschweiz und 2D-Bilanzierung der Fernschubdeformation im östlichen Faltenjura: Arbeitsbericht zu SGT-Etappe 2	P. Jordan, A. Malz, S. Heuberger, J. Pietsch, J. Kley, H. Madritsch	March 2015 (only available at end of May)

Table 1.1: List of Nagra reports used for this review

Title	Authors	Journal
An unusual triangle zone in the external northern Alpine foreland (Switzerland): Structural inheritance, kinematics and implications for the development of the adjacent Jura fold-and-thrust belt	A. Malz, H. Madritsch, B. Meier, J. Kley.	Tectonophysics 670, January 2016
Improving 2D-seismic interpretation in challenging settings by integration of restoration techniques: A case study from the Jura fold-and-thrust belt (Switzerland).	A. Malz, H. Madritsch. J, Kley	Interpretation 3(4), November 2015

Table 1.2: List of peer-reviewed papers provided for the review

2 Geological overview and model building

2.1 Brief overview of the geology

The Jura fold-and-thrust belt forms the northwestern rim of the Swiss Molasse Basin and represents the external deformation front of the Central Alps. Laubscher (1961, 1977, 1987) suggested that the Jura belt has been formed by “distant push” (Fernschub) as a consequence of nappe stacking in the Central Alps (Helvetic and Penninic nappes). Shortening in the Central Alps has been transferred into the foreland in a thin-skinned manner along a décollement horizon located in Middle to Upper Triassic evaporites (Jordan et al., 1990). Deformation was restricted to the Mesozoic and Cenozoic sediments while the underlying basement remained largely unaffected during the thin-skinned thrusting (Burkhard, 1990, Laubscher, 1961). The study area is located in the easternmost part of the Jura belt in northern Switzerland. The onset of the thin-skinned deformation is constrained to Late Miocene (11 Ma, Serravallian) in the east of the Jura Mountains. The main phase of thin-skinned deformation is essentially synchronous to the deposition of the Upper Freshwater Molasse (Willett & Schlunegger, 2010). An increasing number of authors consider that the Jura underwent a main change in its deformation style from thin-skin to thick-skin since Late Pliocene times (i.e. Becker, 2000, Madritsch et al., 2008, Ustaszewski & Schmid 2007). These authors assume that thick-skin tectonics lasted at least until recent times. We identify a deformation as being thin-skinned when the sediments are entirely detached from Pre-Triassic basement, the basement is passive beneath the Jura folds, and the corresponding basement shortening is confined to northern front of the Alps (“distant push”). In contrast, thick-skinned deformation is when the basement and cover are shortened by equal amounts, and decoupling between basement and cover is minor or absent."

2.2 Why build a 3D model for the expertise?

Kinematic interpretation of tectonic structures in northern Switzerland requires that we describe the geometry of the tectonic framework in three dimensions. Understanding the geometry and kinematics of fault systems is a 3D challenge. Since the data were collected on 2D-seismic profiles and on horizontal maps, a 3D extrapolation of the tectonic structures is necessary. We expected that we would be provided with a 3D representation of tectonic data. On the contrary, we received a huge amount of very precise descriptions compiled in various reports. For this reason we decided to build a regional 3D model of northern Switzerland using the *MOVE* software. We integrated the available tectonic data as horizontal maps and vertical profiles. For our expertise (Figure 2-2) we used the tectonic map of northern Switzerland (from NTB 14-02 and NAB 14-105), the top-basement tectonic map (from NAB 14-17) (Figure 2-1), and all available interpreted seismic profiles provided by ENSI. We also included 18 balanced cross sections from Jordan et al. (2015), borehole data, and finally the swisstopo digital model of the Earth's surface combined with earthquakes hypocentres from the SED catalogue. Our model helped us to better understand the 3D relationship between the basement-rooted faults and the tectonic elements in the overlying sedimentary cover. Thanks to the 3D model constructed by Marco Verdon, we could identify and image a major transfer zone affecting the northwestern edge of the siting area Nördlich Lägern (see section 3.3).

We emphasise that this 3D model allows us to gain insight into the regional tectonic structures and the tectonic areas to be avoided, but not about the local faults (i.e. faults identified on one

seismic profile only). We used this 3D model largely for our statement described below in sections 3.3, 0 and 4.6.

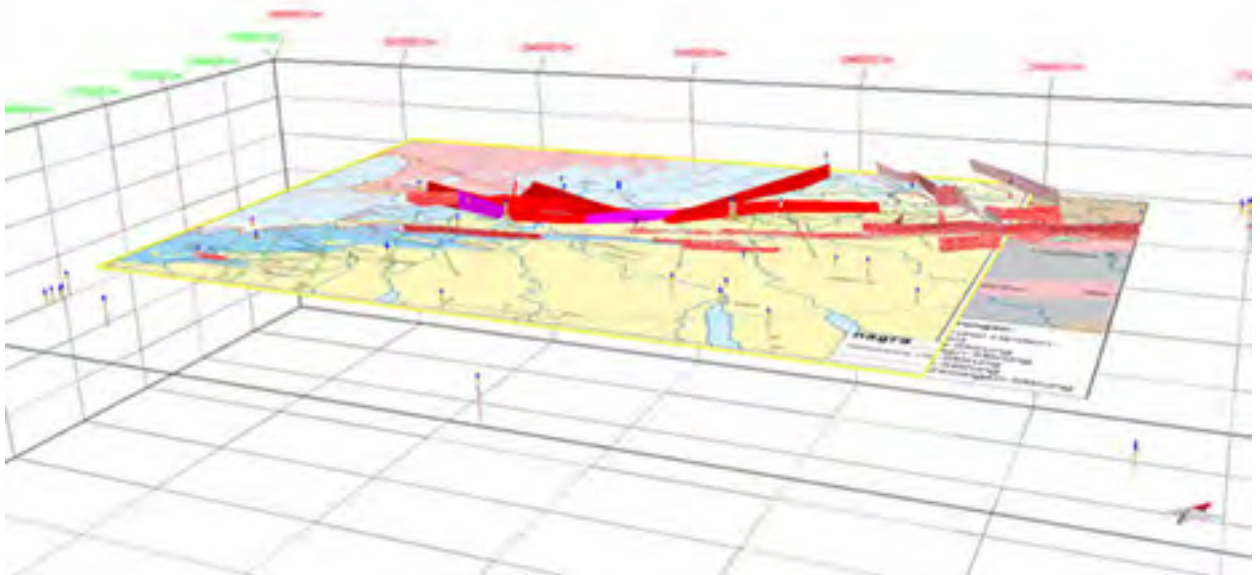


Figure 2-1: View of the 3D model built in *MOVE* showing the two superposed tectonic maps (from NTB 14-02 and NAB 14-17) and interpreted basement faults (in red and orange). Image by Marco Verdon (swisstopo)

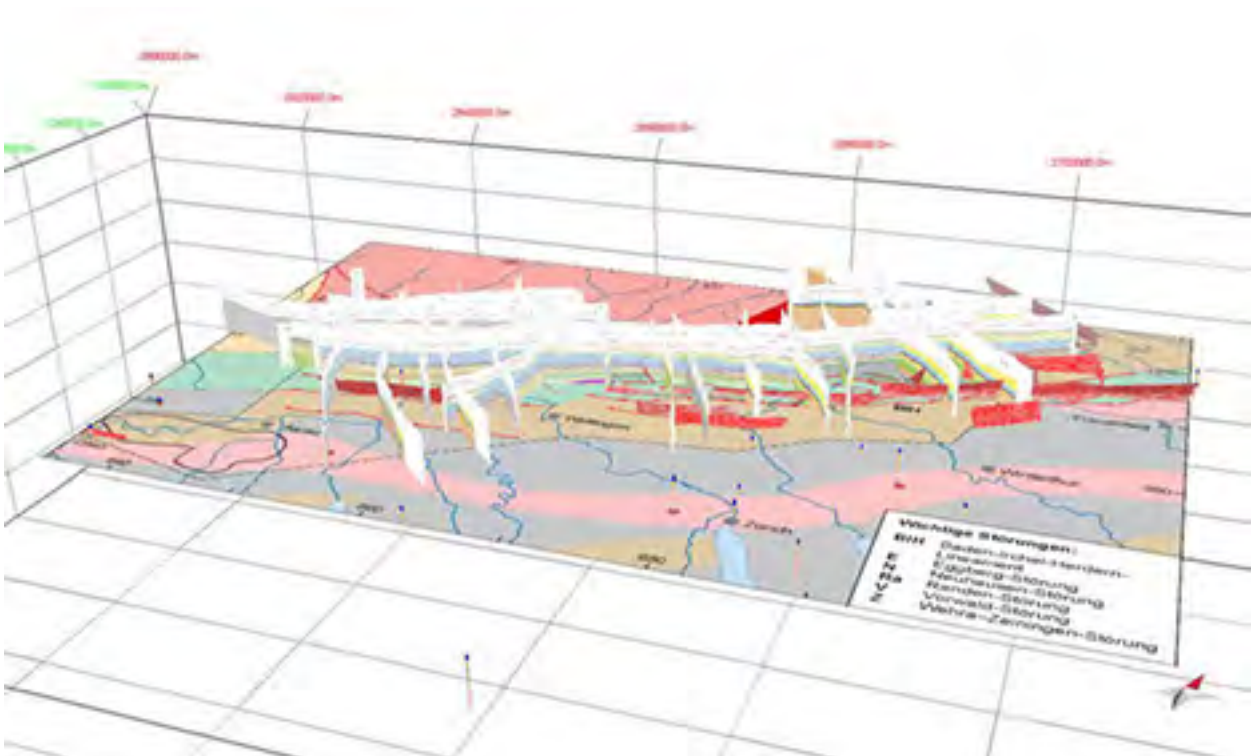


Figure 2-2: View of the 3D model built in *MOVE* with the seismic profiles, borehole data, and balanced cross sections with the top-basement tectonic map as underground (from NAB 14-17). Image by M. Verdon (swisstopo)

3 Analysis of tectonic structures of northern Switzerland

In this chapter we present our analysis of the interpreted tectonic structures extracted from 2D-seismic profiles. We have constructed two different kinds of 3D models:

- For the fault inventory, Robin Allenbach integrated all interpreted faults from the 2D-seismic profiles using the *SeisVision* software, a powerful, fully integrated 2D and 3D seismic interpretation system. From this model he extracted a series of survey maps which are illustrated in section 3.1.
- The analysis of tectonic structures at regional scale and their kinematic relationships is based on the 3D model built with *MOVE* as described in section 2.2. The results are discussed in sections 3.2, 3.3, and 0.

3.1 Fault inventory and comparison between SGT Etappe 1 and 2

To address Question 1) concerning the fault inventory, we compared the tectonic elements as defined in Stage 1 (SGT Etappe E1) with those of Stage 2 (SGT Etappe 2). We have represented the results with survey maps for three main horizons: “Base Tertiary” (Figure 3-2), “Base Upper Jurassic” (Malm) () and “Base Mesozoic” (Figure 3-3). The 2D-seismic profiles were integrated as pre-stack depth migration (PSDM) in the software *SeisVision*. Fault heaves for each horizon are calculated with the “Fault Heave” calculator. Fault polygons are exported to *Petrosys* to be represented in the model. Every fault that cannot be extrapolated onto other seismic profiles is shown by a red circle in map view. When a fault can be identified on more than one profile, it is indicated by a polygon which ends on 2D-seismic profiles. This explains the uncommon abrupt fault trace in map view. As an additional consequence, faults which do not intersect any seismic profiles were not traced by swisstopo (e.g. Wölflinswil graben).

To compare faults interpreted from the first stage (SGT Etappe 1) with those from the second stage (SGT Etappe 2), we plotted both on a series of maps (Figure 3-2 to Figure 3-16) one for each lithology. A fault interpreted from SGT Etappe 2 is represented by two red polylines forming a surface. When the fault is vertical, the corresponding trace in map view is illustrated by only one polyline. When the polyline represents a dipping fault, it is shown in map view by two lines forming a surface. The width of the surface indicates steepness of the fault, the wider the distance between two polylines, the less inclined the fault. Figure 3-1 illustrates how the faults interpreted from SGT Etappe 2 (in red) are drawn in profile and map view. This technique was not used in SGT Etappe 1 by Nagra. Hence, all faults interpreted from SGT Etappe 1 are always represented by single green lines in map view. The background maps used in Figure 3-2 to Figures 3-16 are taken from Beilagen of NAB 10-39, SGT Etappe 1. The reader is referred to Nagra report NAB 10-39 for detailed information.

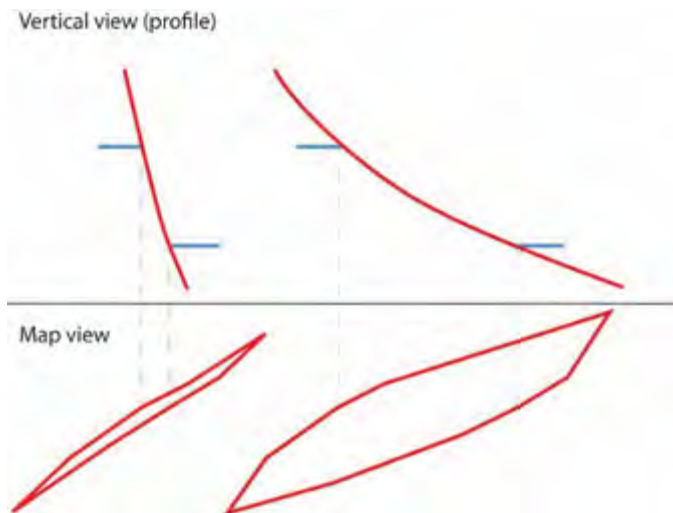


Figure 3-1: Sketch illustrating how the faults (in red) were projected on the map views presented in Figure 3-2 to Figure 3-16. In map view, a fault interpreted from stage 2 (SGT Etappe 2) is represented by two red polylines forming a surface. When the fault is vertical, the corresponding fault will be illustrated by only one polyline. The width of the surface indicates the steepness of the fault.

Due to reprocessing of old seismic lines and new 2D-seismic lines acquired in 2011/2012, we identify two main improvements in Stage 2:

- 1) correction and refining of regional fault traces and tectonic zones that should be avoided in any deep geological repository, and
- 2) detection of additional faults in SGT Etappe 2 not found in SGT Etappe 1. Most of these faults are local since they cannot be correlated with other seismic profiles (these are illustrated by red circles).

Furthermore, superposition of maps “Base Mesozoic,” “Base Malm,” and “Base Tertiary” show the spatial fault propagation. In general, SGT Etappe 2 gives a better definition and clearer refinement of fault features compared to SGT Etappe 1.

3.1.1 Siting region Zürich Nordost and Südranden

Detailed maps of “Base Tertiary,” “Base Malm,” and “Base Mesozoic” are illustrated in Figures 3-5, 3-6, and 3-7, respectively. Additional local faults were observed in the siting area Südranden, especially on the map “Base Mesozoic”. Traces of both faults observed in the southern part of the siting region Zürich Nordost were slightly improved compared to the same features identified in SGT Etappe 1.

3.1.2 Siting region Nördlich Lägern

Detailed maps of “Base Tertiary,” “Base Malm,” and “Base Mesozoic” for the siting region Nördlich Lägern are illustrated in Figures 3-8, 3-9, and 3-10 respectively.

A major improvement in SGT Etappe 2 is the identification of the Siglistorf thrust, bordering the northern part of the siting area (Figure 3-9). This fault was not, or only partially and poorly, defined in SGT Etappe 1. The significance of the Siglistorf thrust as tectonic area to be avoided is important as pointed out in section 4.6. The trace of the Stadel-Irchel-Anticline bordering the southern edge of Nördlich Lägern was slightly refined.

3.1.3 Siting region Jura Ost

Detailed maps of “Base Tertiary,” “Base Malm,” and “Base Mesozoic” are illustrated in Figures 3-11, 3-12, and 3-13, respectively. Additional local faults could be identified in SGT Etappe 2 on the survey map of “Base Mesozoic” (Figure 3-13).

3.1.4 Siting region Jura Südfuss

Detailed maps of “Base Tertiary,” “Base Malm” and “Base Mesozoic” are illustrated in Figure 3-14, Figure 3-15 and 3-16, respectively. In comparison with the SGT Etappe 1, a fault found on at least two seismic profiles has been identified in the north-eastern part of the siting area.

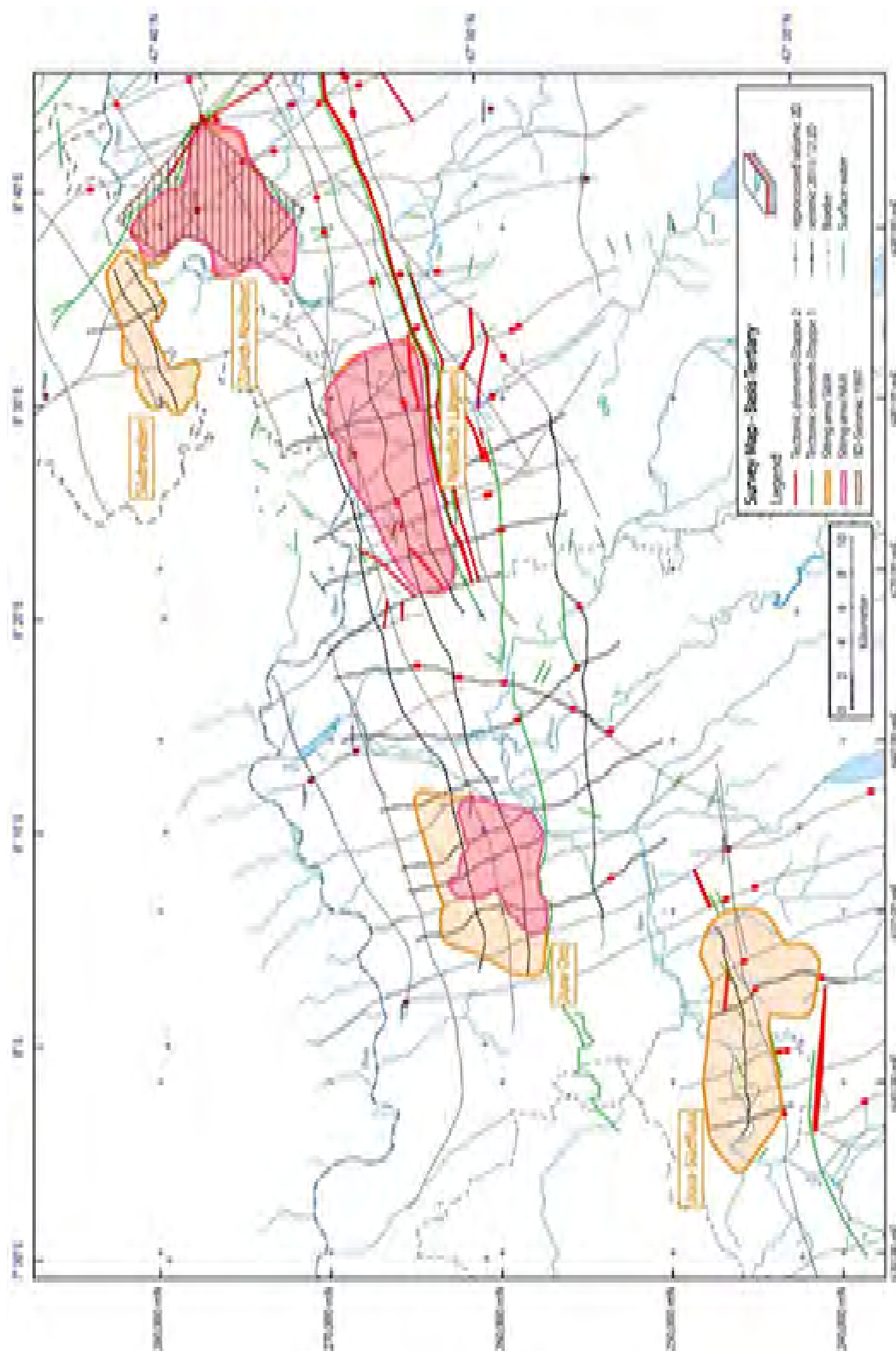


Figure 3-2: Comparison of tectonic elements Stage 1 vs. Stage 2 Survey Map – Base Tertiary. Each fault which cannot be extrapolated onto another seismic profile is shown by a filled red circle in map view. Small red circles with black rings near locality names correspond to boreholes

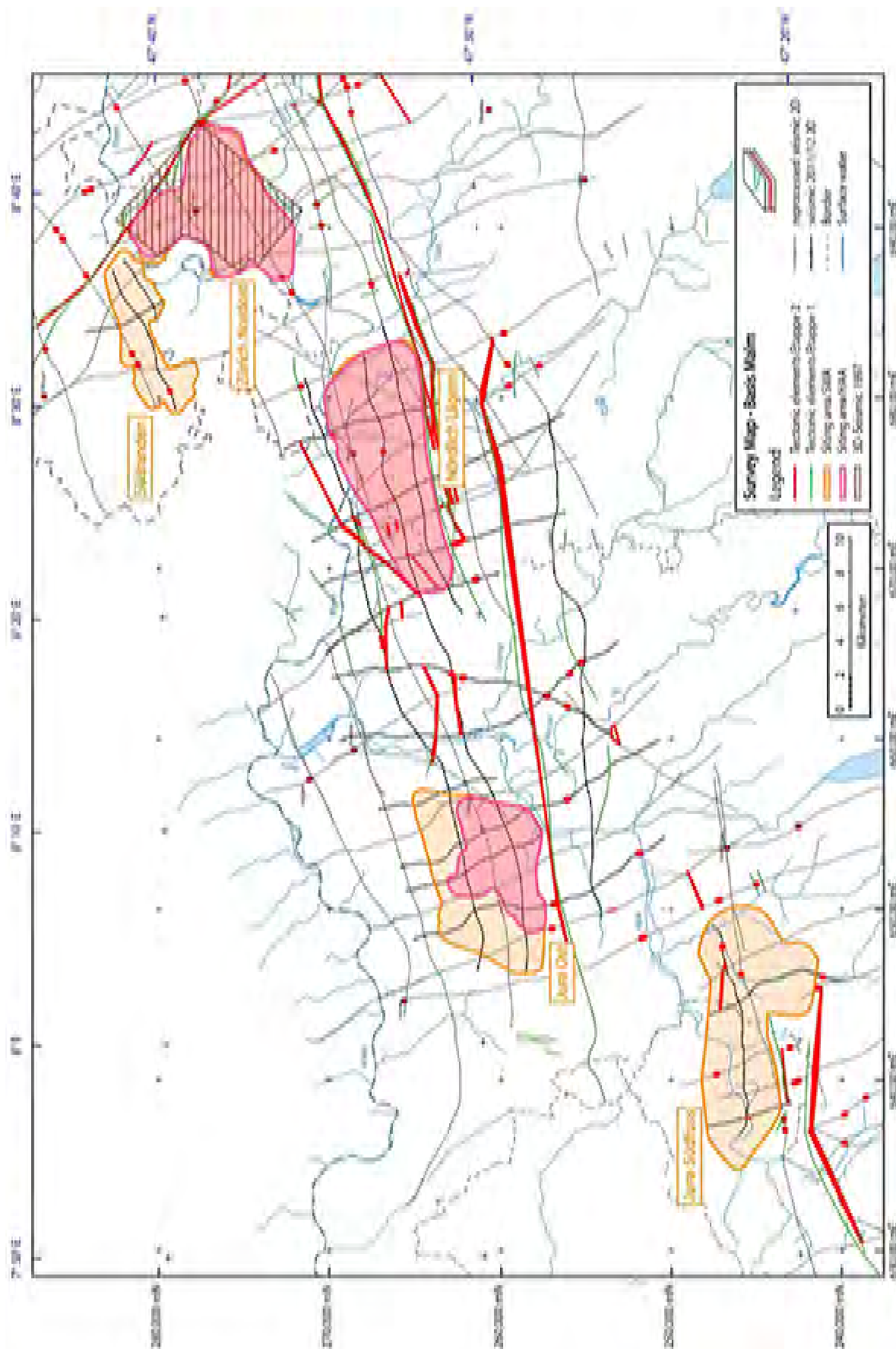


Figure 3-3: Comparison of tectonic elements Stage 1 vs. Stage 2 Survey Map of 5 potential siting areas – Base Malm

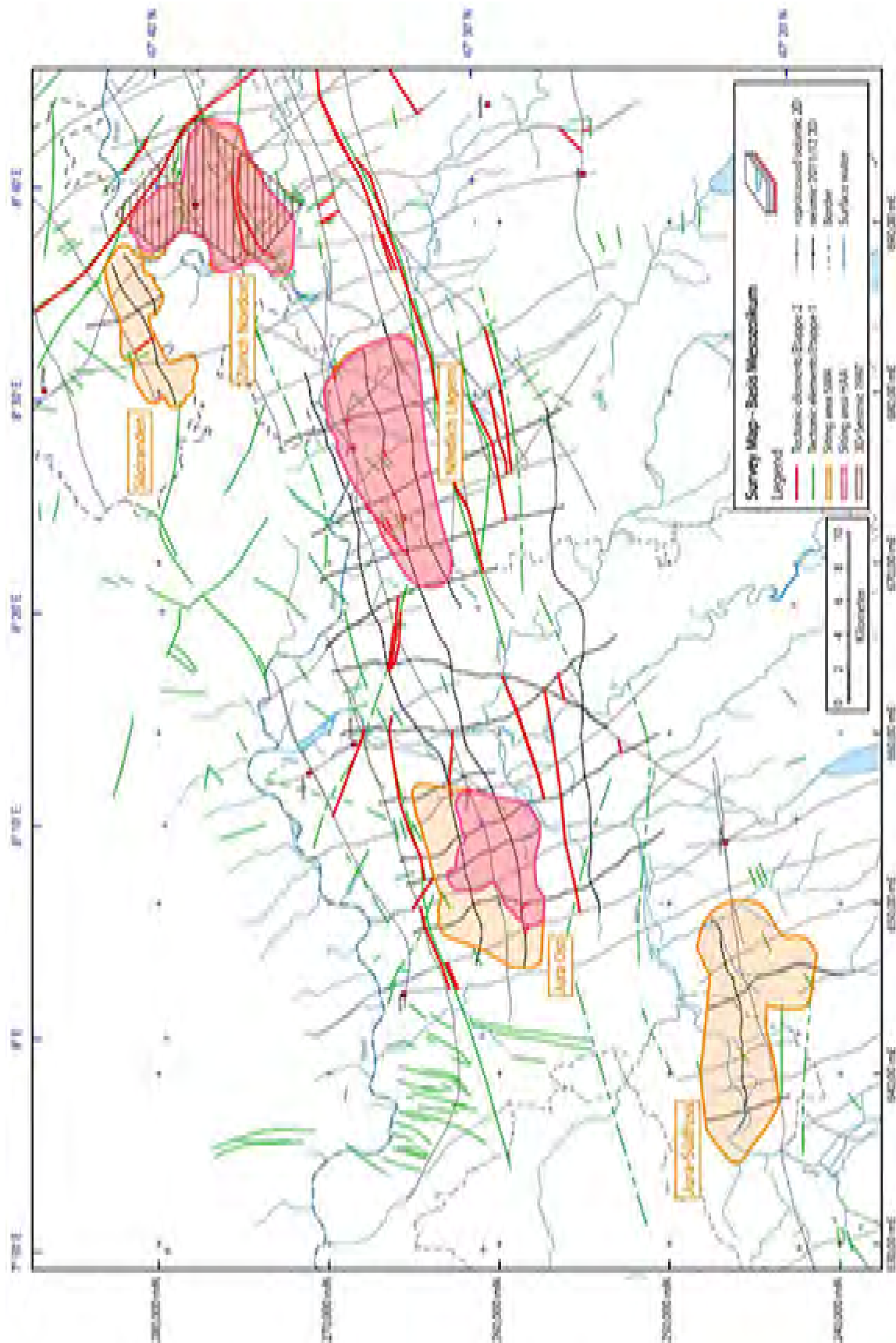


Figure 3-4: Comparison of tectonic elements Stage 1 vs. Stage 2 Survey Map – Base Mesozoic

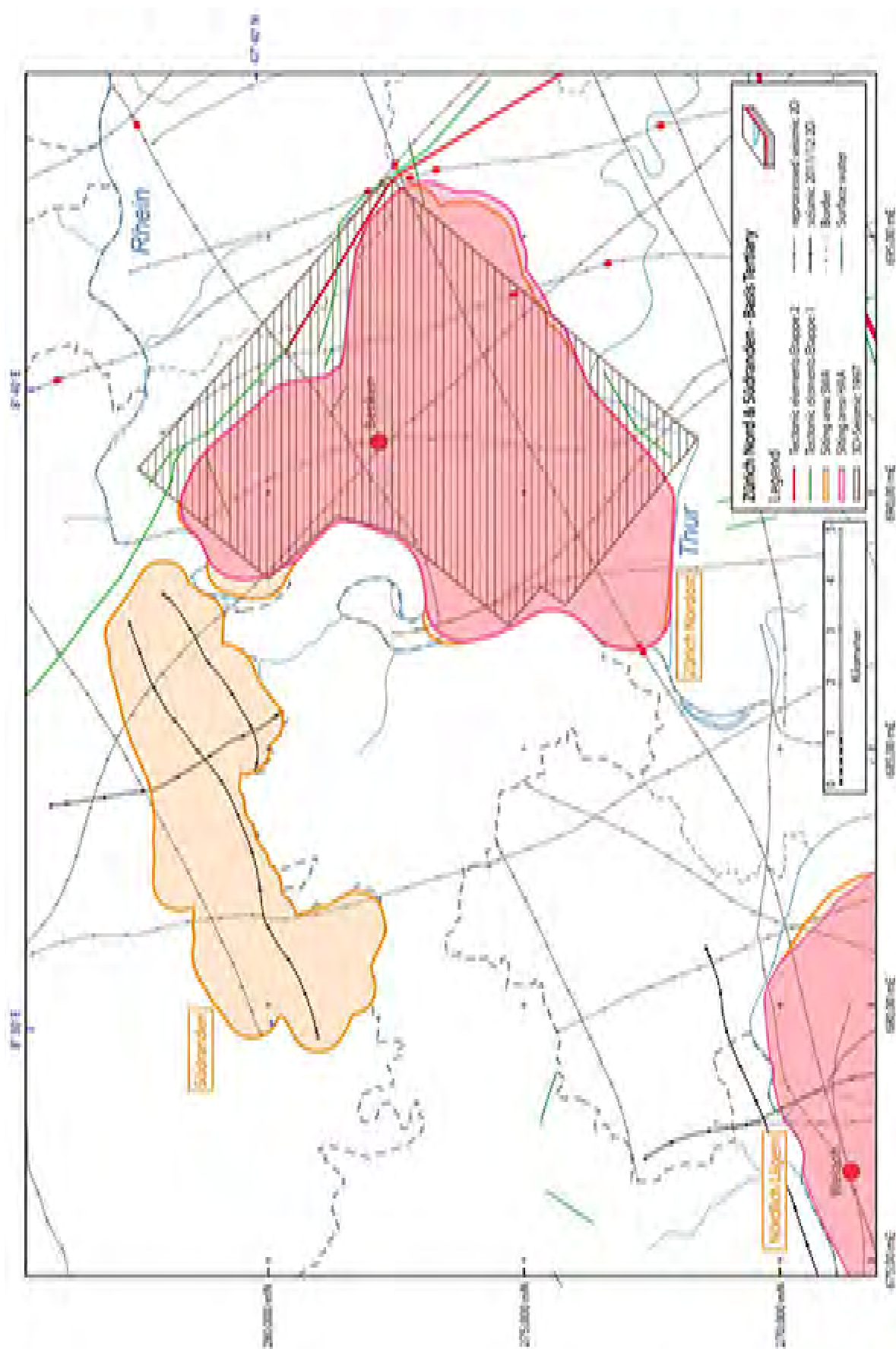


Figure 3-5: Comparison of tectonic elements Stage 1 vs. Stage 2 Zürich Nordost and Südstrichen – Base Tertiary

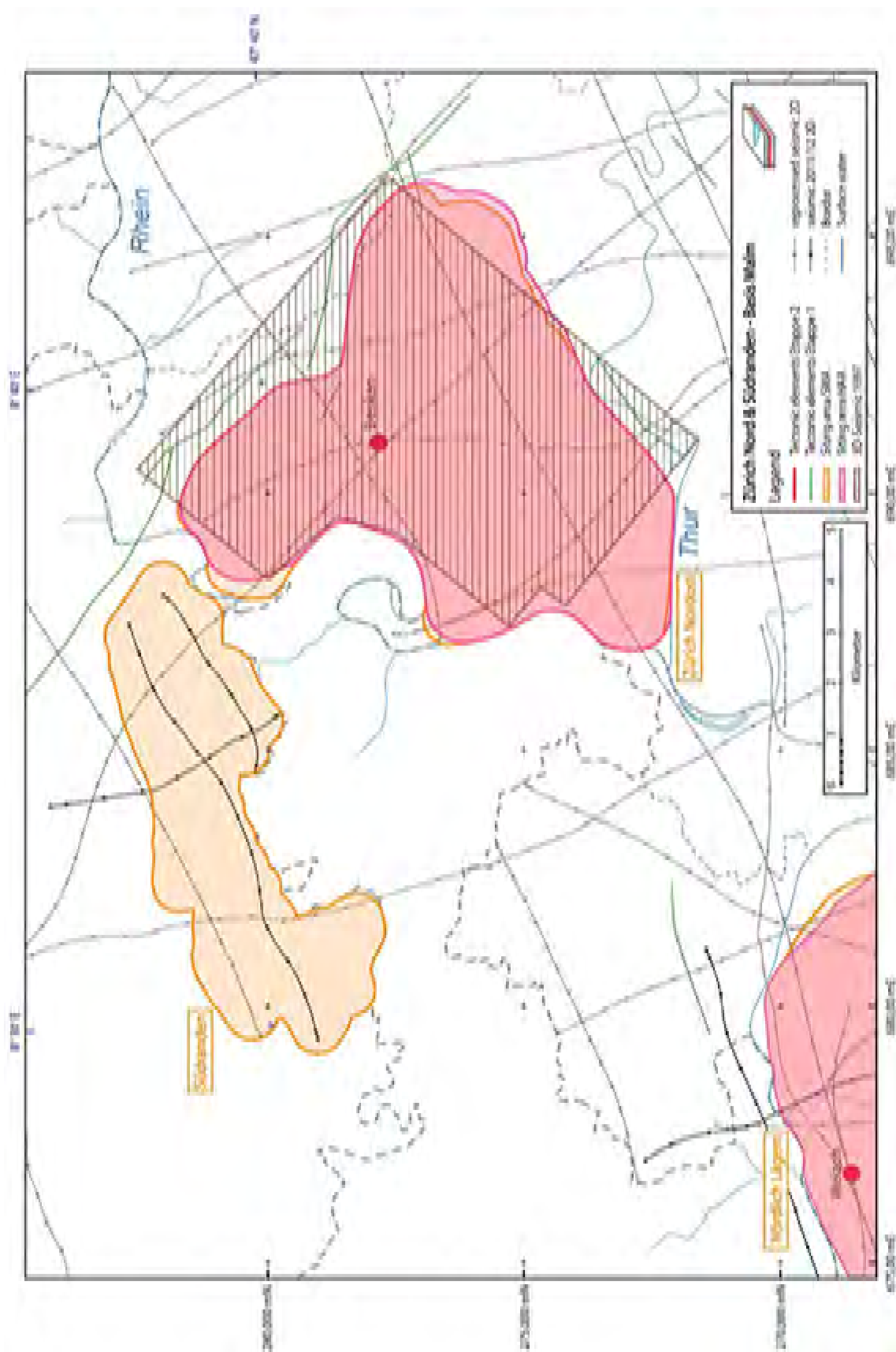


Figure 3-6: Comparison of tectonic elements Stage 1 vs. Stage 2 Zürich Nordost and Südranden – Base Malm

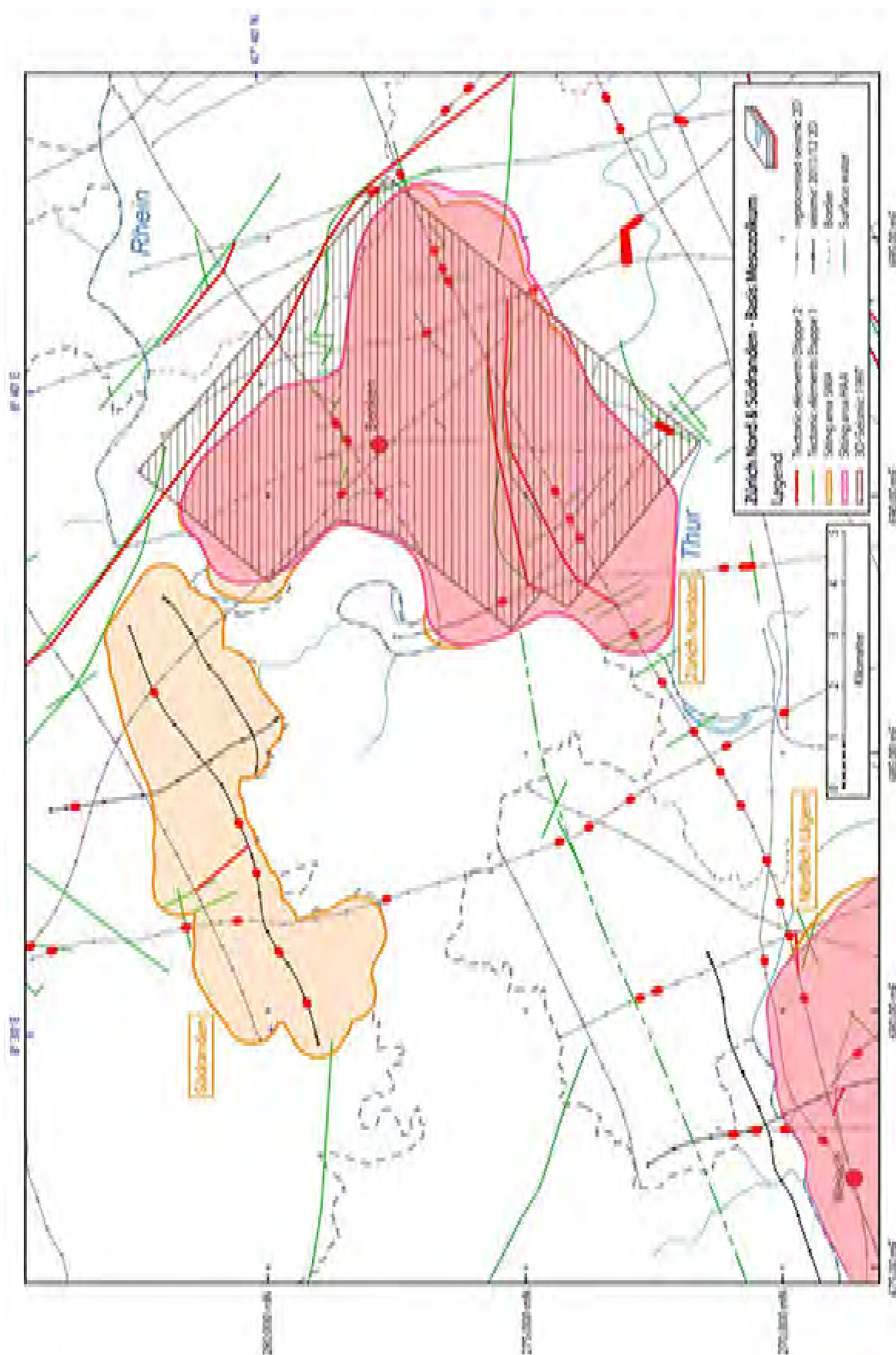


Figure 3-7: Comparison of tectonic elements Stage 1 vs. Stage 2 Zürich Nordost and Südanden – Base Mesozoic

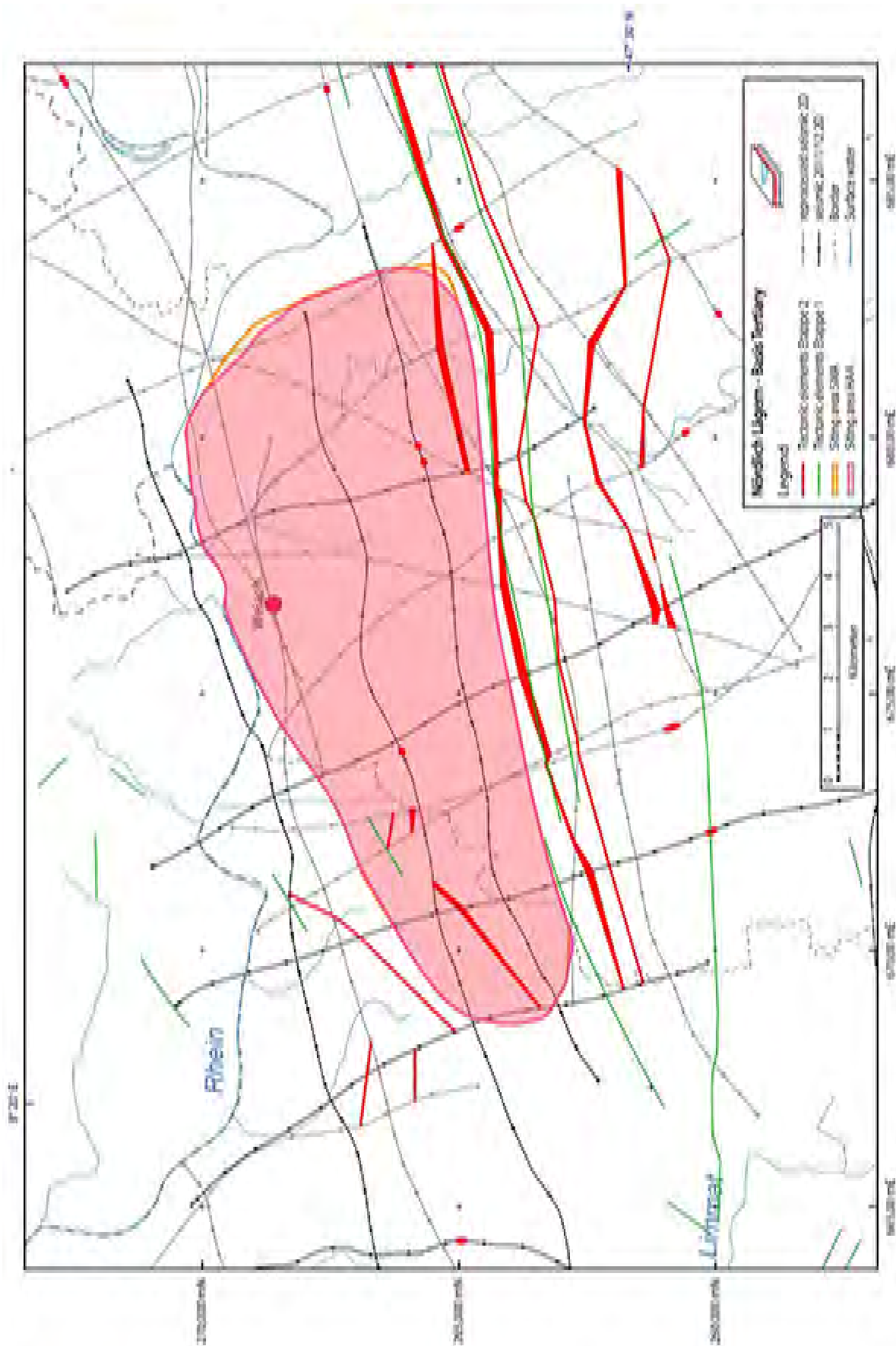


Figure 3-8: Comparison of tectonic elements Stage 1 vs. Stage 2 Nördlich Lägern – Base Tertiary

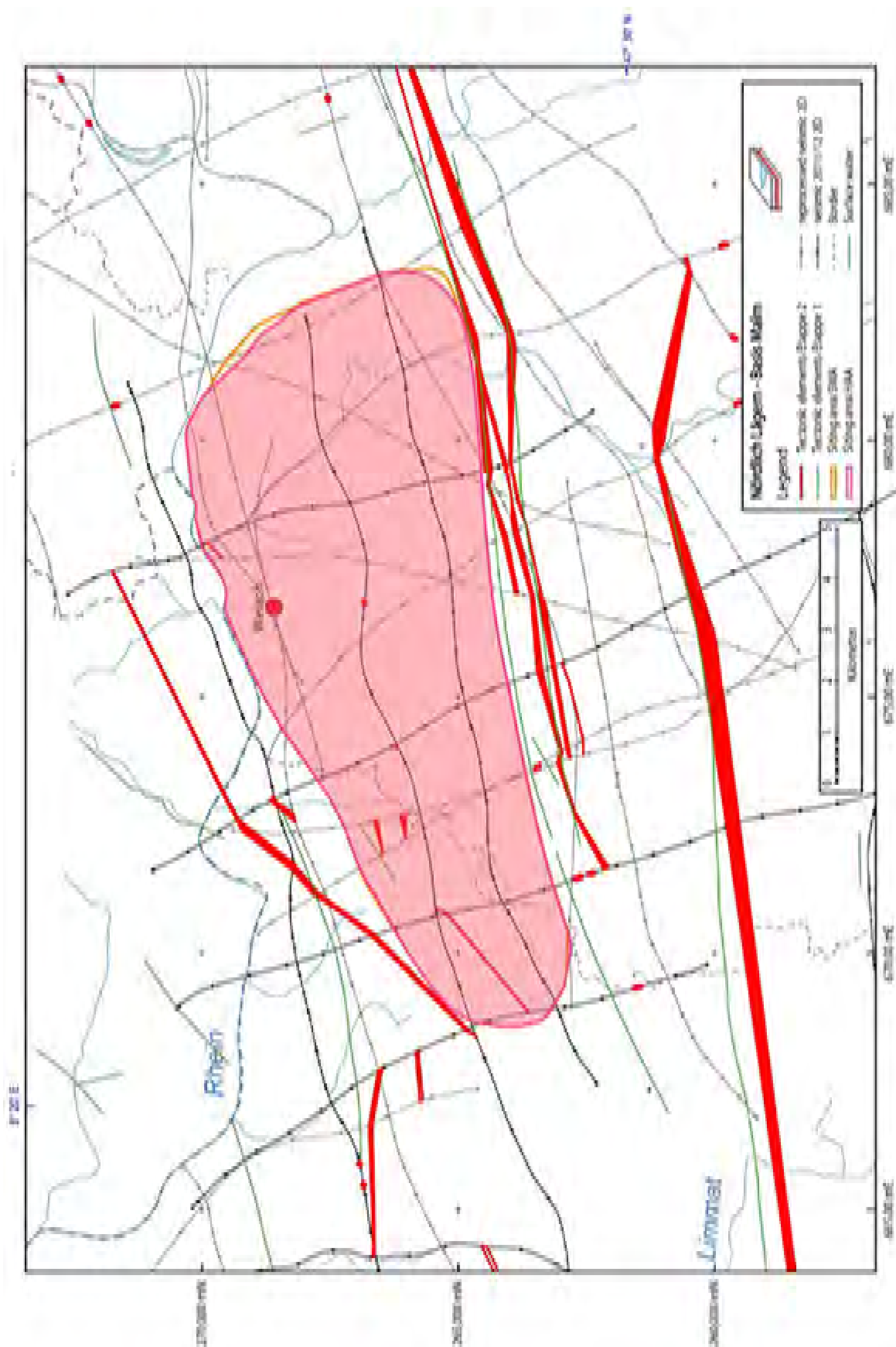


Figure 3-9: Comparison of tectonic elements Stage 1 vs. Stage 2 Nördlich Lägern – Base Malm

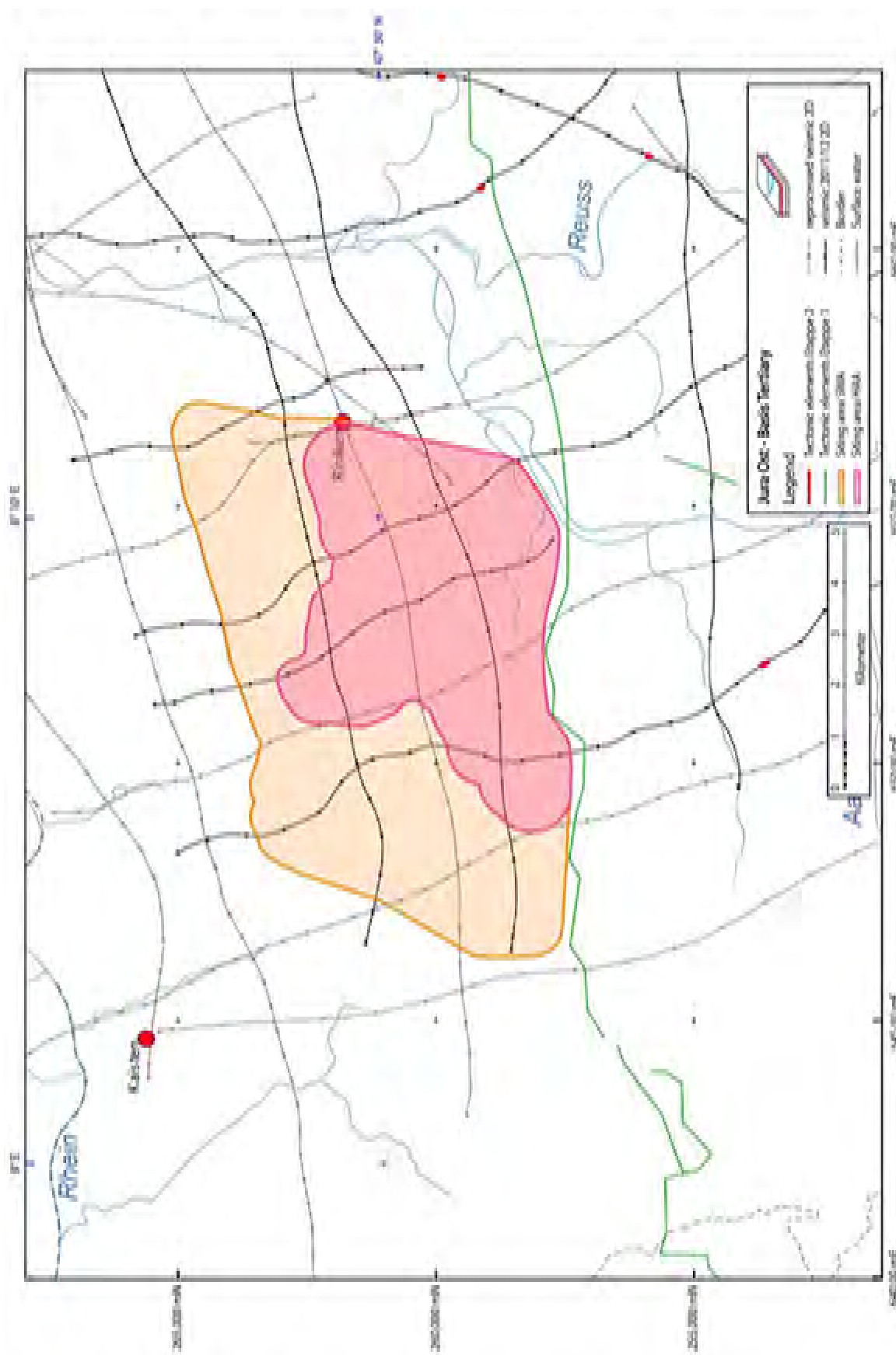


Figure 3-11: Comparison of tectonic elements Stage 1 vs. Stage 2 Jura Ost– Base Tertiary

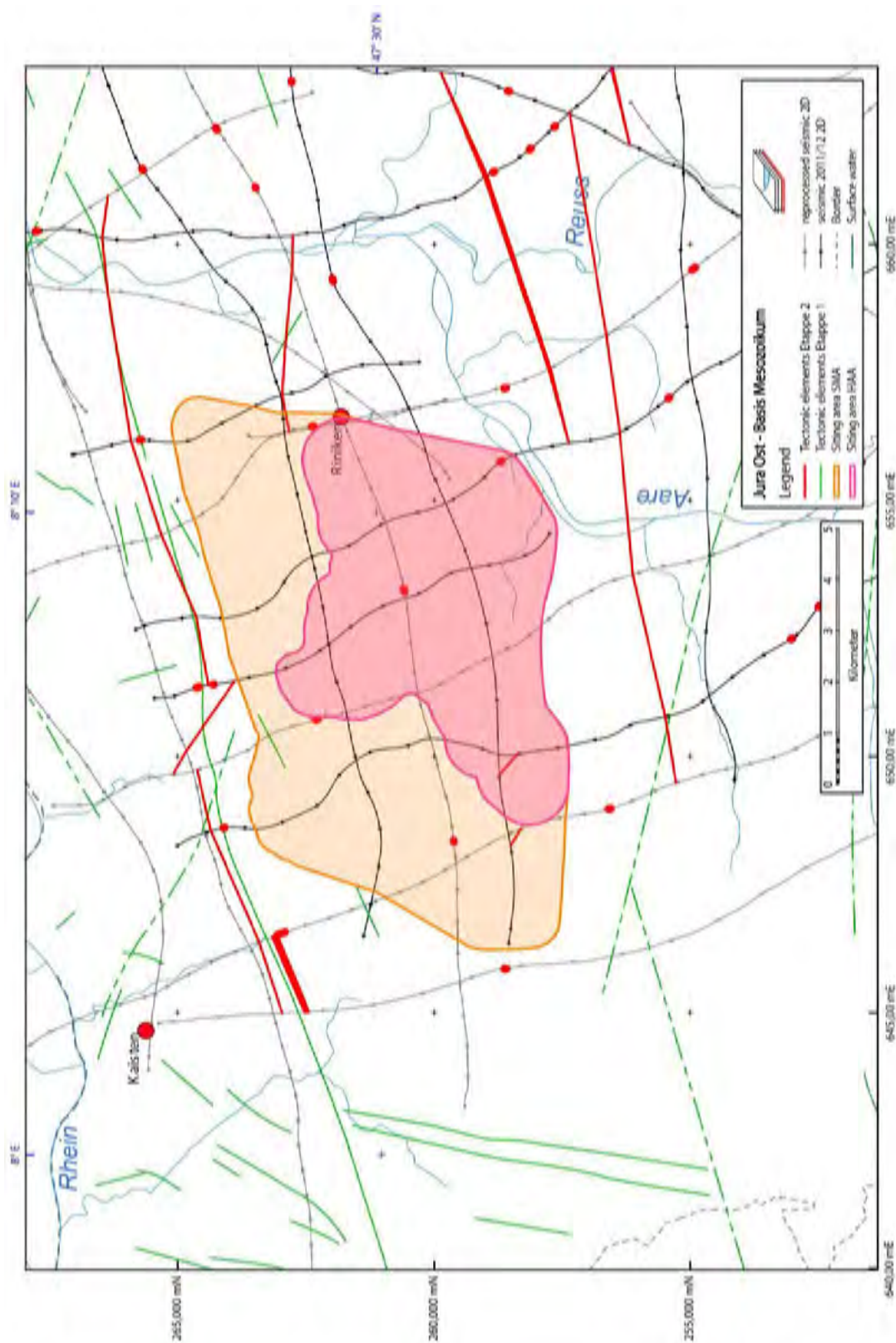


Figure 3-13: Comparison of tectonic elements Stage 1 vs. Stage 2 Jura Ost– Base Mesozoic

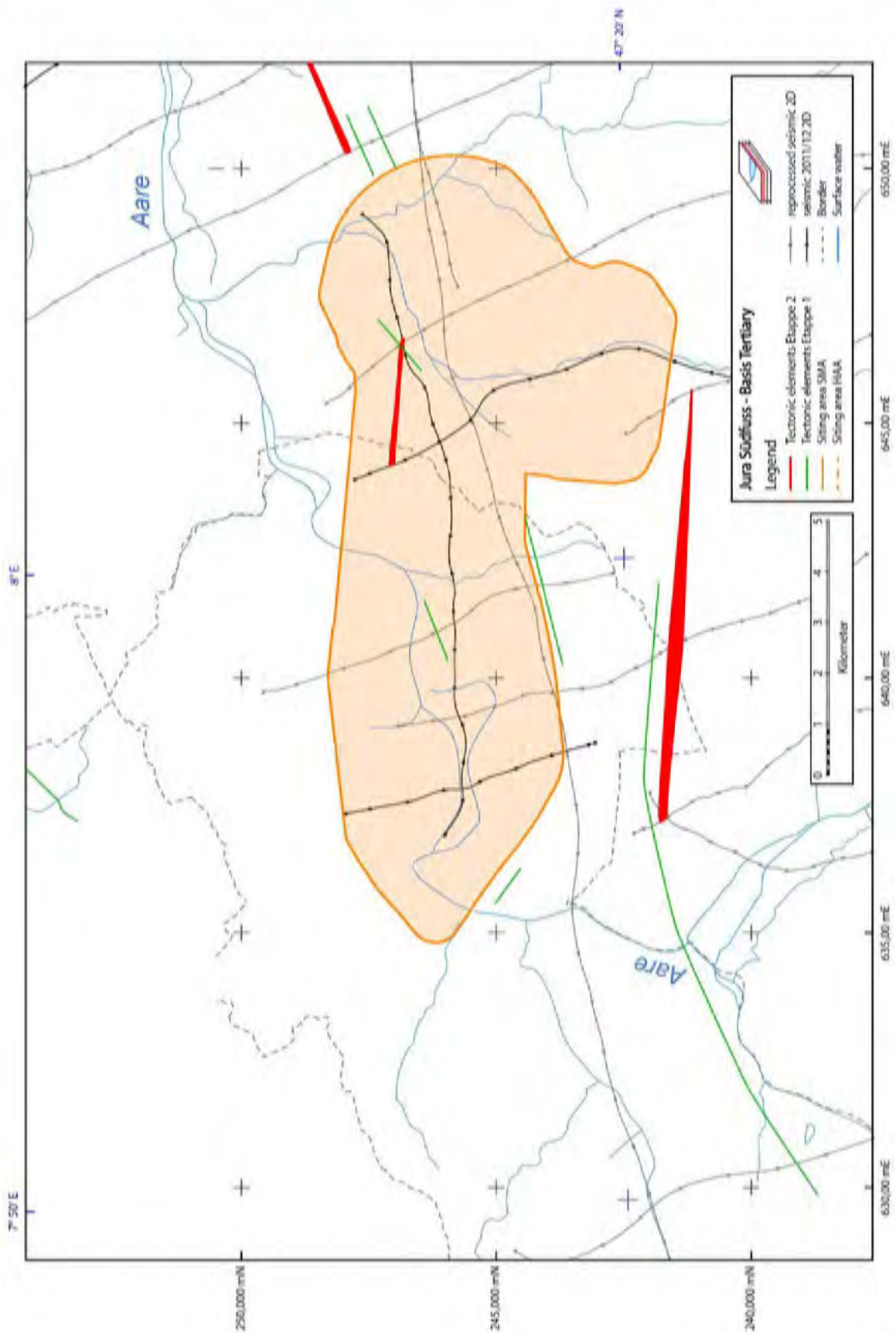


Figure 3-14: Comparison of tectonic elements Stage 1 vs. Stage 2 Jura Südfluss– Base Tertiary

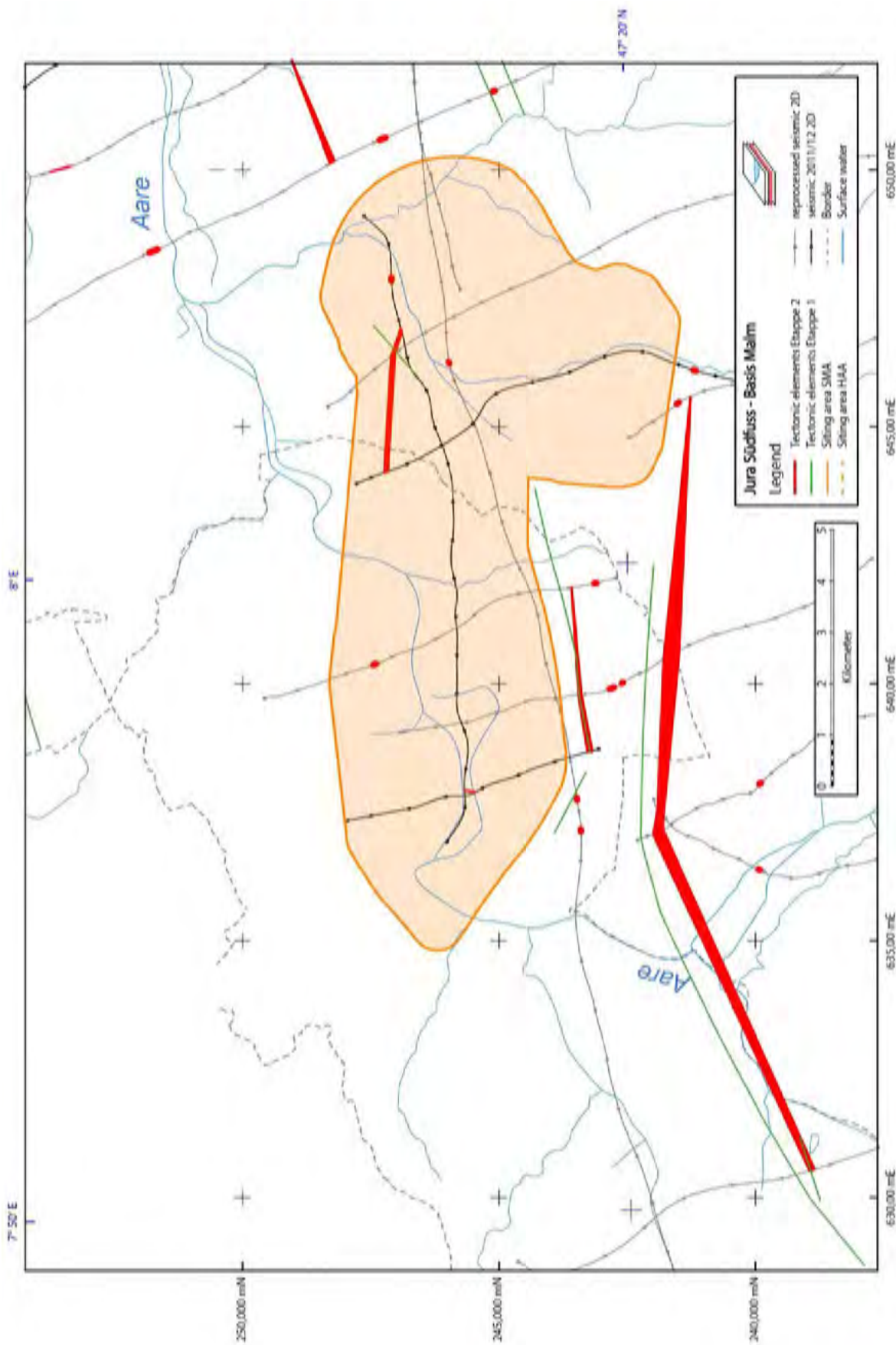


Figure 3-15: Comparison of tectonic elements Stage 1 vs. Stage 2 Jura Südfuss– Base Malm

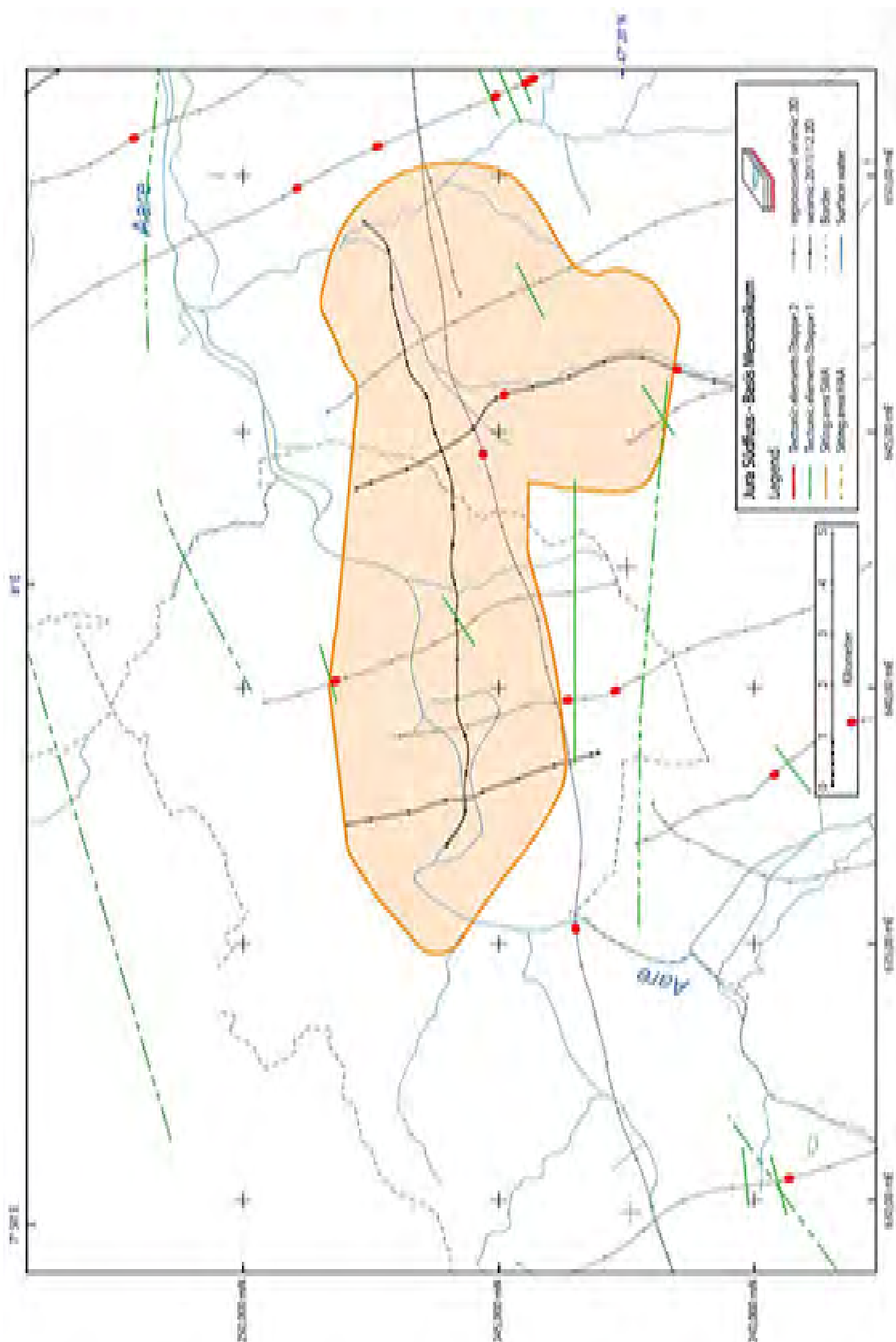


Figure 3-16: Comparison of tectonic elements Stage 1 vs. Stage 2 Jura Südfuss– Base Mesozoic

3.2 Tectonic map of northern Switzerland

The tectonic elements of northern Switzerland are described in great detail in Nagra's reports NTB 14-02 Dossier II, NAB 13-10 and in NAB-14-105. Two maps are of particular interest for our purpose: the tectonic map of northern Switzerland (Beilage 1-1 in NAB 14-105) and the tectonic map of top basement including the northern Permo-Carboniferous basin (Fig. 2-5 in NAB 14-105). These maps represent a compilation of the interpreted faults from 2D reflection seismic data.

Nagra carefully chose the five proposed potential siting regions (excluding the Wellenberg site) to be outside any major fault. Most of the siting regions are, however, bounded by these regional faults. Hence, their potential impact within the siting regions needs to be known. For these reasons we have focused our analysis on the regional-scale faults as compiled on the tectonic map of northern Switzerland (Figure 3-17). Dr. A. Sommaruga has investigated the local faults by checking this compilation against a detailed analysis of 2D seismic data (her full report is included here as Appendix 1).

First, it is important to decipher the multistage tectonic history of the region. Our approach consists in distinguishing the main fault trends. There are at least three major inherited faults trends: 1) WNW-ESW-striking faults ("Variscan" trend), 2) ENE-WSE-striking faults ("Permo-Carboniferous" trend), and 3) NNE-SSW-striking faults ("Rhenish" trend). The expression of the latest and youngest deformation (thin-skinned formation of the Jura fold-and-thrust belt), which affected the region of interest during the Late Miocene times, is characterised by a nearly E-W-oriented trend in northern Switzerland (Figure 3-18). For more details about the associated kinematics, the reader is referred to chapter 4. In the study area the shortening direction of the Late Miocene thin-skinned deformation was oriented nearly oriented N-S. We observe an angle between the ENE-trending basement fault associated with the Swiss Permo-Carboniferous trend and the E-W trend of the Jura main thrust. Numerous local NNE-SSW-striking faults accommodated differences in amount of thrust displacement with intensity decreasing towards the east (Figure 3-18).

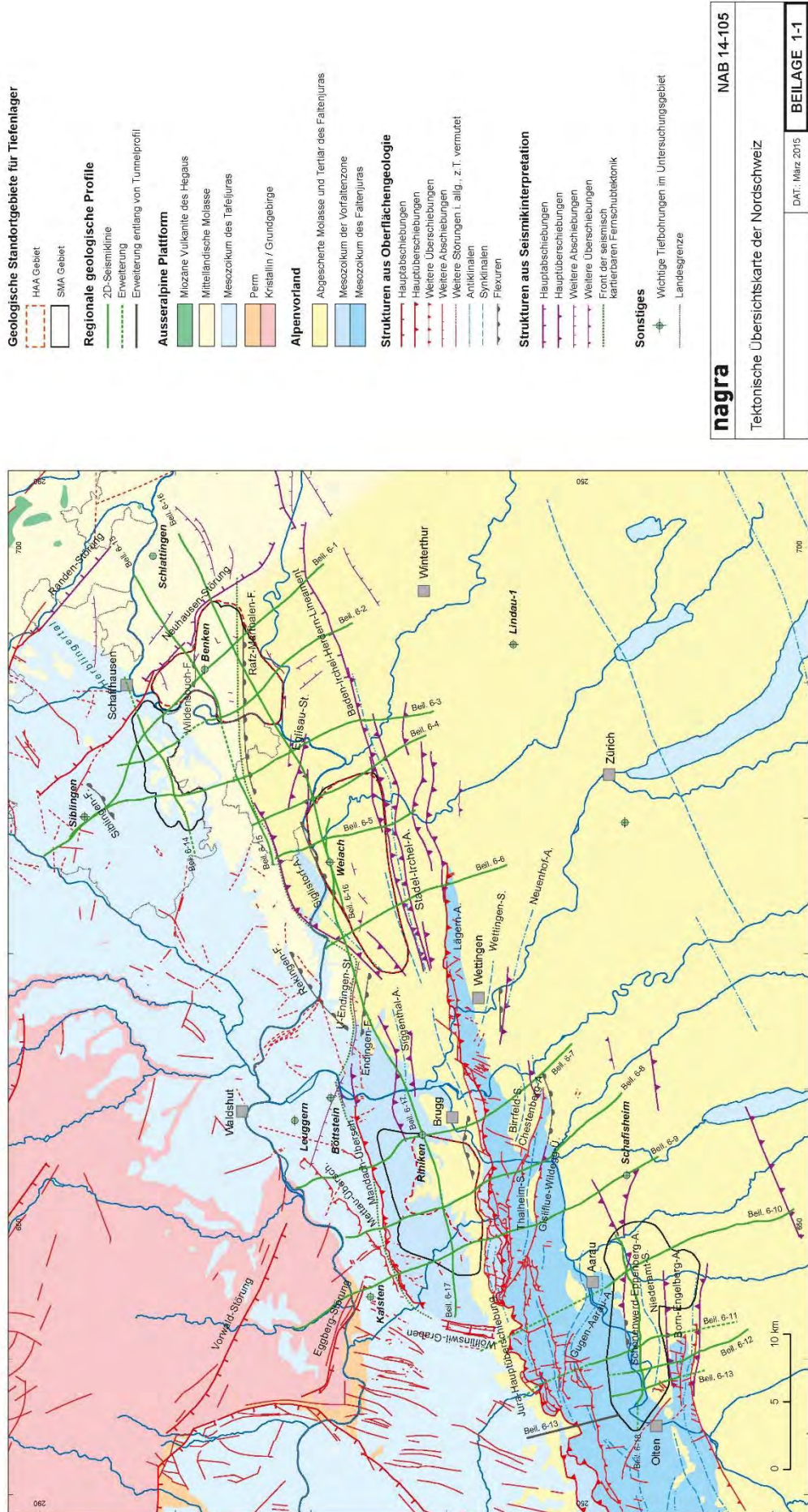


Figure 3-17: Tectonic map of northern Switzerland (from Nagra, NAB 14-105, Beilage 1-1).

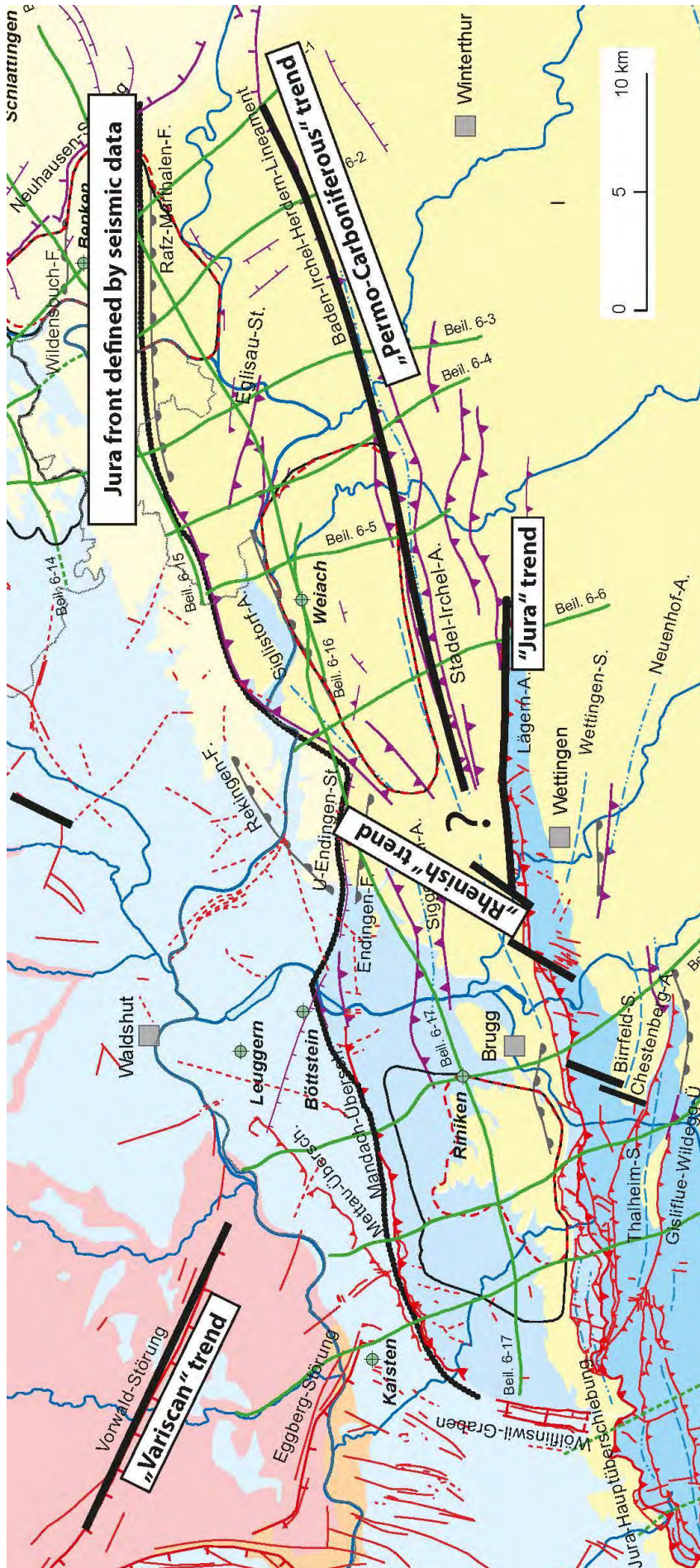


Figure 3-18: Tectonic map of northern Switzerland with the main fault trends: "Variscan" WNW-striking faults, "Permo-Carboniferous" ENE-striking faults, "Rhenish" NNE-striking faults and "Jura" E-W-striking faults (after Nagra, NAB 14-105, modified by C. Nussbaum, swisstopo)

3.3 Transfer zone

The “Vorfaltenzone” is separated from the “Tafeljura” by the distant-push (Fernschub) front of the Jura belt. This front, defined by the interpreted 2D-seismic data, is characterised by a bent shape “indenting” the northwestern edge of the Nördlich Lägern siting area (Figure 3-2). We attribute the non-cylindrical trend of the Jura front to the presence of a transfer zone. Looking at this region in detail (indicated by the rectangular box) in Figure 3-3, it is obvious that most of the thrusts and faults seem to be interrupted within the transfer zone. To the south, the Lägern-Anticline is displaced by sinistral strike-slip faults (red line in lower part of the transfer zone, Figure 3-3).

The transfer zone might be the cause for the change in orientation of the Siggenthal and Siglistorf Anticlines. In fact, both anticlines merge within the transfer zone (Figure 3-21). The ENE-WSW-striking Siggenthal-Anticline evolved as a pop-up-like structure to the east as the NE-trending Siglistorf-Anticline. It is even possible that the Siglistorf-Anticline corresponds to the eastern continuation of the Siggenthal-Anticline. As a consequence, the potential junction between both anticlines would be located within or very close to the western part of the siting region Nördlich Lägern.

The orientation change and shape of the Jura front looks as if it had been affected or deformed by an “indenter.” The transfer zone appears to coincide with the southern end of the Black Forest Massif at depth (Figure 3-5). Section 3.4 gives more details about this correlation.

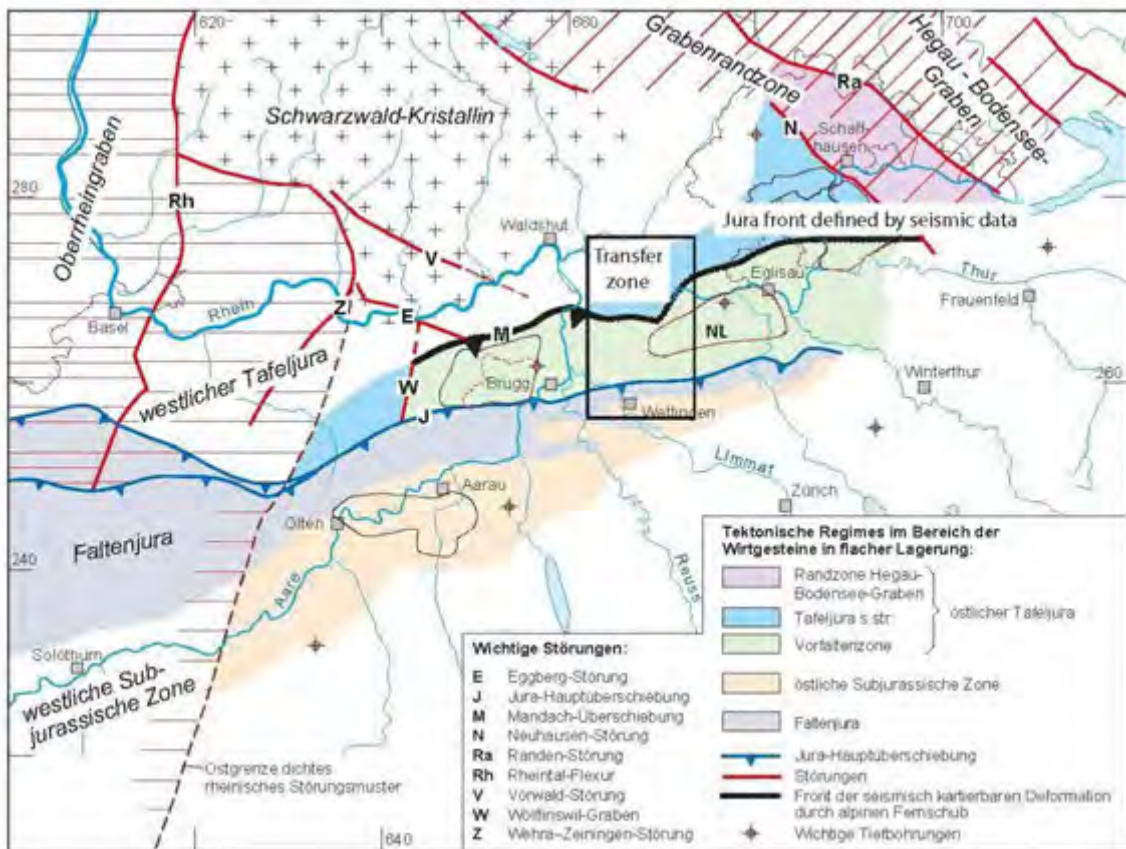


Figure 3-2: The Jura front is affected by a significant transfer zone located between the potential siting areas Jura Ost and Nördlich Lägern (NL). Note that the western edge of NL lies within the transfer zone (after Nagra, in NAB-14-105, modified by C. Nussbaum, swisstopo)

3.4 Role of inherited structures on present-day geometry

It has been well established by many authors (Laubscher, 1986, Diebold and Noack, 1997, Ustaszewski & Schmid, 2006) that the formation of the Jura fold-and-thrust belt has been largely affected by pre-existing basement-rooted structures, either as passive nucleation lines for new thrust ramps or as reactivated basement faults. The pre-existing structures largely influence localisation, structural characteristics, and kinematics of the thin-skinned thrust belt fronts. Prior to Late Miocene thin-skinned thrusting, the European Alpine foreland had already been affected by a multiphase tectonic history (Homburg et al., 2002, Dèzes et al., 2004, Ziegler 1992), resulting in a complex structural setting.

The complex tectonic pattern observed in Figure 3-3 is thought to be the surface expression of basement-rooted inherited structures at depth. Comparing the surface tectonic map (Figure 3-17) with the tectonic map of top basement (Figure 3-3) shows an obvious spatial relationship between folds (anticlines) and thrusts developed in the sedimentary cover and the top basement topography. The basement surface topography seems to have affected the fault and thrust nucleation and their orientation in the sedimentary cover that developed during the Late Miocene Jura contractional phase. In order to verify this working hypothesis, we tried to correlate faults identified on the available seismic lines (NAB 14-17) and reported on the top basement tectonic map (Figure 3-5) with the tectonic structures of the surface tectonic map (Figure 3-3). The complex tectonic evolution of northern Switzerland led to repeated basement-rooted faulting prior to the Late Miocene thin-skinned deformation of the Jura belt (see section 2.2). Reactivation of these faults at different geological times might have resulted in creation of a pronounced basement topography and related offsets of the overlying Muschelkalk detachment level. It is sometimes difficult to correlate thrusts in the cover with basement fault tips, especially for basement-rooted faults that run at a high angle to the belt (i.e. NNE-trending faults) and those that are poorly imaged on seismic dip lines. When the amount of shortening is larger, the basement fault tip does not match up with the thrust nucleation point in the cover due to this displacement.

Interestingly, the transfer zone is located at the southern edge of the Black Forest Massif. At large scale it seems to form a basement “sub-indenter” composed of two fault systems striking WNW-ESE and NNE-SSW, respectively. The sub-indenter shape of the Black Forest Massif is somewhat hidden beneath the northern part of the Permo-Carboniferous basin including the “Trograndzone Nord”. The WNW-striking fault system is composed of the Eggberg-Fault and Vorwald-Fault (Figure 3-5). We can also interpret the Unterendingen-Fault, shown on Figure 3-3, as a basement-rooted fault. This latter could be the eastern prolongation of the Vorwald Fault. The NNE-striking fault system is poorly identified probably because of its unfavourable orientation with respect to the seismic lines. The only NNE-striking fault of regional importance is the Siblingen-Fault further to the north (Figure 4-1). The sub-indenter appears to have affected the Jura seismic front. Further to the south, the Jura main thrust was affected by NNE-trending sinistral faults.

Basement topography played a dominant role in the nucleation and orientation of thrusts and related anticlines during the emplacement of the thin-skinned thrust belt front. Nevertheless, this does not mean that the Late Miocene deformation was thick-skinned. The sedimentary cover was detached above the Upper Triassic basal décollement.

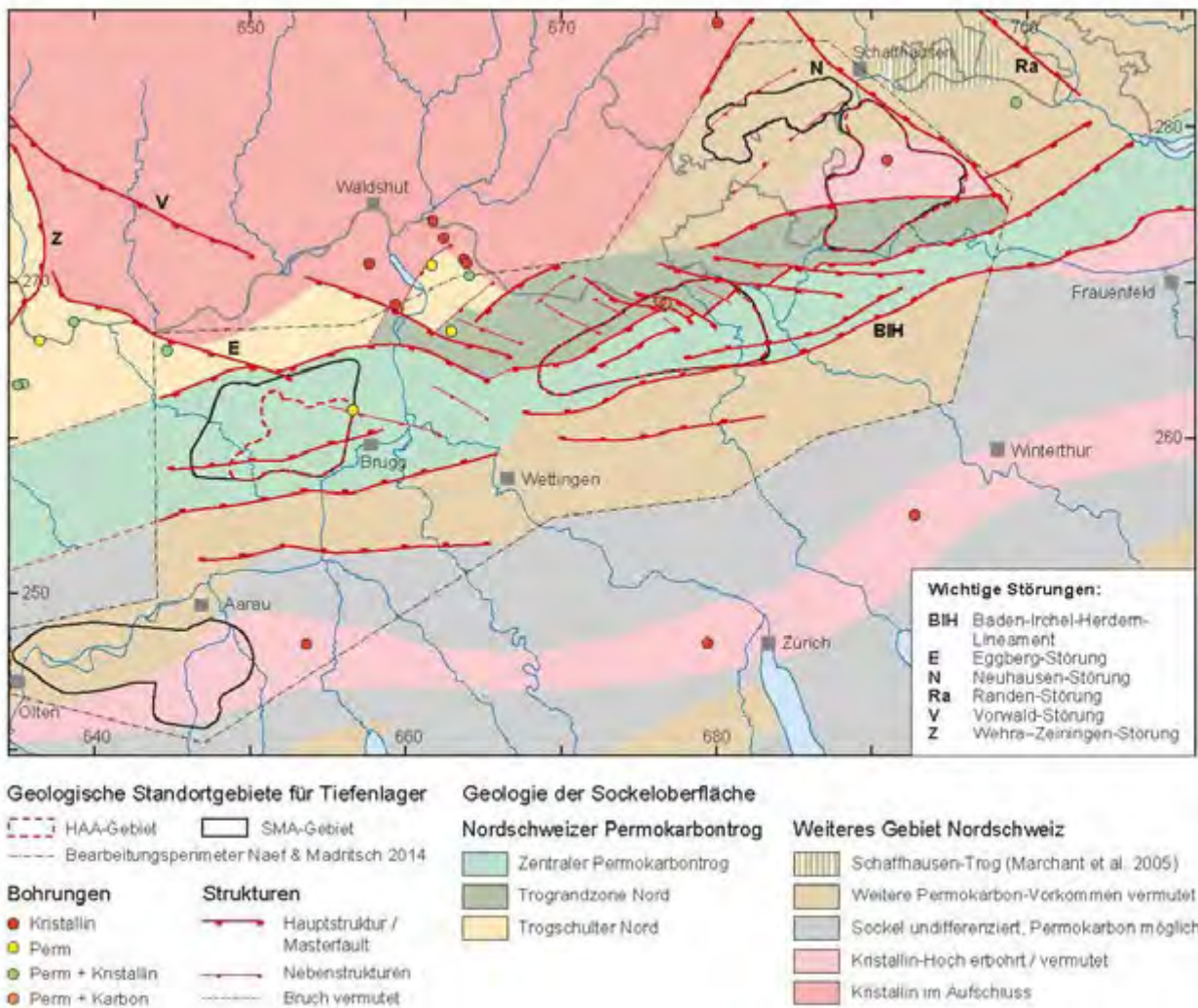


Figure 3-5: Tectonic map of top basement including the northern Swiss Permo-Carboniferous basin (after Nagra, NAB 14-105)

4 Tectonic history of northern Switzerland

To understand the complex present-day structural framework, we note that the region was affected by multiple phases of basement fault reactivation prior to the Late Miocene thin-skinned thrusting. At least three different inherited fault systems can be identified and traced: 1) WNW-ESE-striking faults (“Variscan” trend), 2) ENE-WSW-striking faults (“Permo-Carboniferous” trend), and 3) NNE-SSW-striking faults (“Rhenish” trend). This multiphase tectonic history is described in the literature provided to us (the reports listed in Table 1.1 and papers in Table 1.2). Nevertheless, sequential tectonic maps illustrating each deformation stage are missing. For more clarity in this regard, we present a tentative and non-exhaustive set of tectonic maps for some of the main tectonic stages.

4.1 Variscan inheritance and Late Palaeozoic wrench faulting

The investigated area was affected by the Variscan orogeny and subsequent post-orogenic transtension during Late Carboniferous and Permian times (Laubscher, 1986; Ziegler, 1992). In the Late Palaeozoic, pronounced wrench faulting led to the development of a 5-km deep WSW-ENE-striking Permo-Carboniferous basin. This tectonic phase is considered as the consequence of the Variscan orogeny characterised by WNW-ESE-striking faults (termed as “Variscan trend” faults in figures). Both sets of fault systems can be recognised in the study region as illustrated in Figure 4-1. It should be noted that these faults were not restored in the illustration.

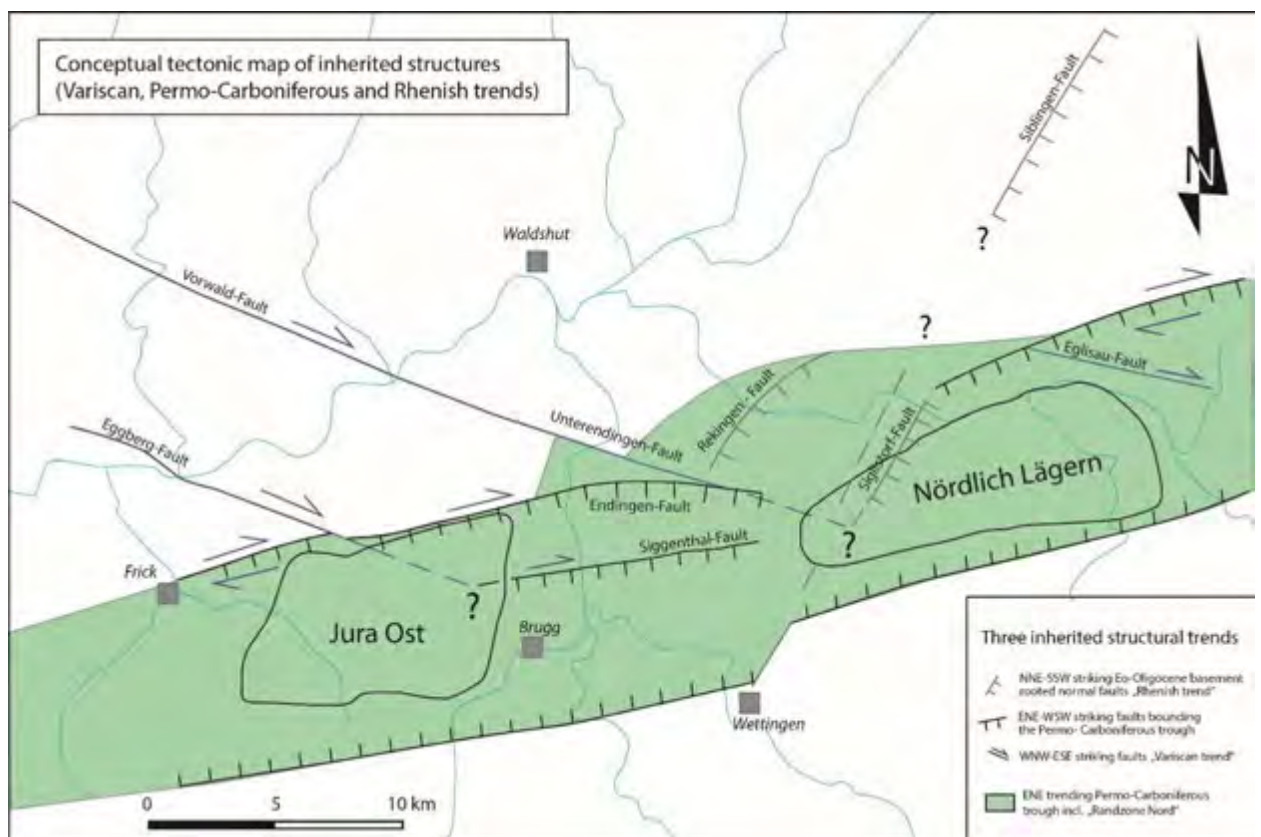


Figure 4-1: Conceptual tectonic map of inherited structures prior to Late Oligocene/Early Miocene uplift of the Black Forest Massif and subsidence of the Swiss Molasse Basin. At least three different inherited fault systems can be identified and traced: 1) WNW-ESE-striking faults (“Variscan” trend), 2) ENE-WSW-striking faults (“Permo-Carboniferous” trend), and 3) NNE-

SSW-striking faults (“Rhenish” trend). Note that the eastwards continuation of the Eggberg-Fault may eventually intersect the western part of the Siggenthal-Fault within the siting region Jura Ost (?). The Unterendingen-Fault may intersect the Siglistorf-Fault at the western part of the siting region Nördlich Lägern (?).

4.2 Jurassic basement-rooted fault reactivation

Interpreted seismic profiles suggest a mild reactivation of Late Palaeozoic structures during Jurassic time as attested by thickness changes and facies variations of the marine sediments (Gygi, 1986, Allenbach, 2001, Wetzel et al., 2003). Depending on the tectonic regime, differently oriented fault systems have been reactivated at different times during Early and Middle Jurassic.

During deposition of the Opalinus Clay Formation, Permo-Carboniferous ENE-WSW-trending faults were probably preferentially reactivated as indicated by thickening in the centre of the basin (Allenbach, 2001). At that time, the stress regime seems to have rotated. In fact, from middle Bajocian to middle Bathonian, epicontinental sediments were deposited in northwestern Switzerland (Gonzalez & Wetzel, 1996). They consisted of shallow-marine oolitic carbonates (Hauptrogenstein Formation, Celtic realm) and marly basinal deposits (Klingnau Formation, Swabian realm). The carbonate series of the Celtic realm, composed of three shallowing-upward successions each capped by a hardground, crop out west of the Aare River. In the basinal domain east of the present-day Aare River, the sequence above the Opalinus Clay is characterised by periodic sandy layers and oolitic hardgrounds. The facies belts within the Hauptrogenstein and Klingnau Formations suggest the evolution of a middle Jurassic N-S-trending, tidal-dominated oolitic barrier. Interestingly, the facies transition follows the N-S trend of the Aare River between Wildeggen and Waldshut. The isopach map between horizons “near-Top Opalinuston (nTOpa)” and “Base Malm (BMa)” shown in

Figure 4-2 confirms the thickening westwards where the carbonate series were deposited. These abrupt lateral changes in thickness and facies within the successions suggest local and regional patterns of differential subsidence, probably related to a mild tectonic reactivation of N-S basement-rooted faults. Nevertheless, there is poor evidence for fault propagation through the Mesozoic sedimentary cover. It is highly uncertain whether this tectonic event would have created the disruption of the Triassic decollement horizon.

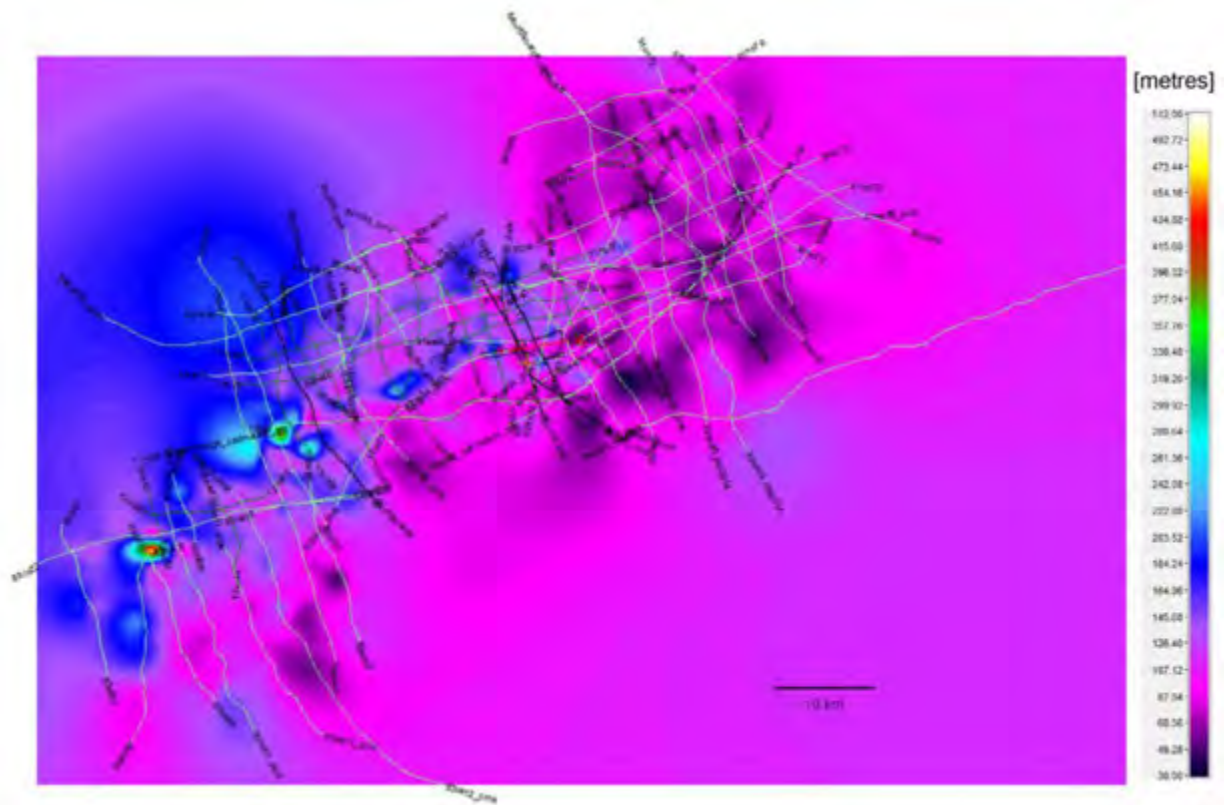


Figure 4-2: Isopach map of the “Dogger” interval between horizons nTOpa - BMa (map elaborated by R. Allenbach, swisstopo)

4.3 Paleogene extension (European Cenozoic rift system)

During the Eocene-Oligocene the European Alpine foreland was affected by an extensional tectonic regime with a WNW-ESE-oriented minimum principal stress σ_3 (i.e. Laubscher 2001). Even if the study region were situated further to the east of the Upper Rhine Graben, we would still expect NNE-striking, basement-rooted normal faults to have developed. Evidence for this is provided by NNE-trending normal faults bordering the eastern part of the Black Forest Massif basement (Figure 4-1), especially to the north. The Siblingen-Fault might be this kind of fault. Furthermore, we interpret the Siglistorf-Anticline, developed during Late Miocene thin-skinned thrusting, to be a consequence of a NNE-striking basement fault, called “Siglistorf-Fault” on Figure 4-1. This basement fault is supposed to have acted as a nucleation line for the Siglistorf fault-bend fold. Based on extensive outcrop-scale mapping, Madritsch (2015) has recently argued that indications for E-W extension are very rare in the sedimentary cover. According to Madritsch, the imprint of Upper Rhine Graben-related extension on the area of interest was minor. Stronger effect of E-W oriented extension related to the opening of the Southern Upper Rhine Graben are only observable to the west of the study area, beyond the Wölflinswil Graben (Figure 3-17, Figure 3-18). In conclusion, this Eo-Oligocene extension seems to have had only very local effect on the outcrop-scale fracture system, but we argue that it has indeed affected the regional large-scale basement faults.

4.4 Resulting tectonic setting of the three main inherited fault trends

Before the onset of the Late Oligocene/Early Miocene uplift of the Black Forest Massif and the subsidence of the Molasse Basin, the region of interest was characterised by a complex

tectonic setting resulting from the intersection of at least three major fault trends as described above in sections 4.1, and 4.3. These are: 1) WNW-ESE-striking faults (“Variscan” trend), 2) ENE-WSW-striking faults (“Permo-Carboniferous” trend), and 3) NNE-SSW-striking faults (“Rhenish” trend). Both siting regions Jura Ost and Nördlich Lägern may be crossed by such basement-rooted fault intersections. The eastwards continuation of the Eggberg-Fault may eventually intersect the western part of the Siggenthal-Fault within the siting region Jura Ost. The Unterendingen-Fault may intersect the Siglistorf-Fault within the western part of the siting region Nördlich Lägern. Both possible intersections are illustrated by a question mark in Figure 4-1.

4.5 Late Oligocene/ Early Miocene uplift of the Black Forest Massif and subsidence of the Molasse Basin

During Late Oligocene and Early Miocene, the study region was located at the northern rim of the north-western Molasse basin which is commonly considered to be a typical flexural foreland basin (e.g. Kuhlemann & Kempf, 2002, Kempf & Pfiffner, 2004). The subsidence of the southward adjacent Swiss Molasse Basin was contemporaneous with the uplift of the Black Forest Massif to the north. This uplift is associated with the Alpine forebulge described by Laubscher (2001). During Aquitanian times the influence of the Alpine contraction became discernible in the Alpine foreland. There is some evidence for this, e.g. the record of a flexure of that age covered unconformably by shallow marine Burdigalian sediments at the northern margin of the Molasse Basin, 50 km east of Basel (i.e. Isler & Pasquier, 1984). Associated with the forebulge phase, extensional faulting is also documented in the study region (Naef et al., 1995). This resulted in extensional reactivation of Late Palaeozoic basement-fault systems, well evidenced by seismic reflection analysis (Laubscher, 1986, Diebold & Noack, 1997). At least two different Late Palaeozoic fault systems are suspected to have been reactivated during this Eo-Oligocene extensional phase: 1) Variscan WNW-ESE-striking faults and 2) Permo-Carboniferous ENE-WSW-trending faults (Figure 4-3). Reactivation of these basement faults propagated through the entire Mesozoic and Cenozoic sedimentary sequence (i.e. Unterendingen-Fault in Figure 4-3). The case of the Unterendingen-Fault has been studied by Peter Bitterli on behalf of ENSI. Based on field arguments, Bitterli confirmed the extensional character of this fault with a vertical displacement of 55-60 m. Slickensides are purely vertical and do not show evidence of any dextral component (that would imply subsequent reactivation during the Late Miocene thrusting phase). The activity of the Unterendingen-Fault stopped before 18 Ma, as it is conformably overlain by Burdigalian OMM sediments. This Late Oligocene/Early Miocene extension reactivation may lead to local disruptions of the future Muschelkalk décollement horizon of the Jura fold-and-thrust belt and formed nucleation lines for the Late Miocene thrust ramps through the sedimentary cover (see section 4.5).

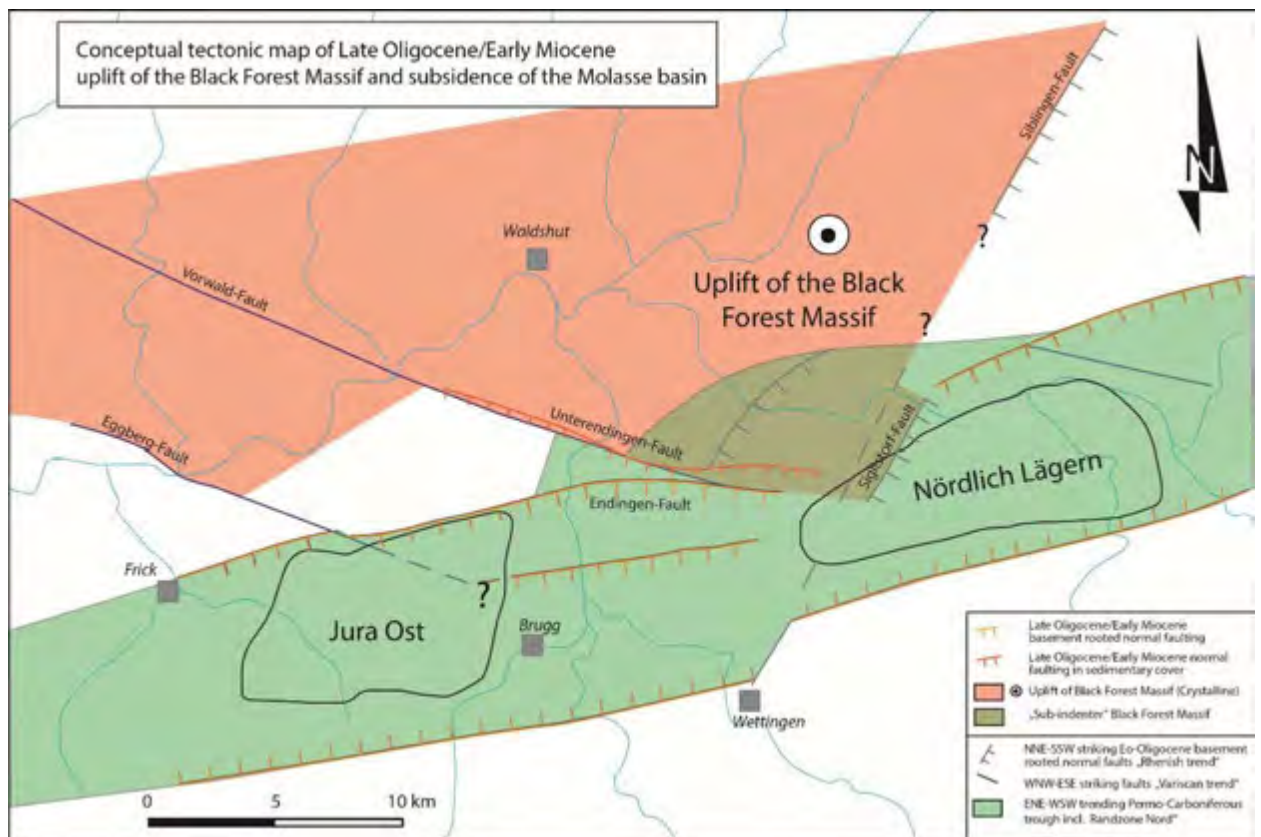


Figure 4-3: Conceptual map of tectonic elements after Late Oligocene/Early Miocene uplift of the Black Forest Massif and subsidence of the Swiss Molasse Basin. Both WNW-ESE-trending faults (“Variscan trend”) and ENE-WSW-trending faults (Permo-Carboniferous) were reactivated as normal faulting during uplift related to the Alpine forebulge

4.6 Late Miocene (Jura thin-skinned deformation)

As mentioned above, it is well established that the formation of the Jura fold-and-thrust belt has been largely affected by pre-existing basement-rooted structures, either as passive nucleation lines for new thrust ramps or as reactivated basement faults (e.g. Laubscher, 1986, Diebold and Noack, 1997, Ustaszewski & Schmid, 2006). Therefore, on the same map (Figure 4-4) we have superimposed the major inherited basement faults and the Late Miocene structures developed in the Mesozoic and Cenozoic sedimentary cover. Thrusting of the frontal Jura fold-and-thrust belt onto the autochthonous foreland in the eastern part did not begin before the Serravallian (10.5 Ma) (e.g. Becker, 2000). The Late Miocene thin-skinned deformation in the Jura is the result of Alpine distant-push (Fernschub). Basement-rooted inherited structures played a major role during this time: they formed nucleation lines for new ramp thrusts in the sedimentary cover above the Triassic décollement. Reactivation of basement-rooted faults during the Late Oligocene/Early Miocene extensional phase might have disrupted the Triassic décollement prior to the Late Miocene thrusting. Reactivated WNW-ESE-striking basement faults (“Variscan trend”) nucleated oblique ramps through the sedimentary cover with a dextral strike-slip component. NNE-SSW-striking basement faults (parallel to the east part of the Black Forest basement, “Rhenish trend”) formed oblique ramps associated with a sinistral strike-slip component, assuming a horizontal maximum stress directed NNW-SSE. Both reactivated fault systems form a kind of “sub-indenter” merging to the south, exactly within the transfer zone (as described in section 3.3). In contrast to the Southern Alps, here the basement is not

incorporated in the thrust sheets. Only the sedimentary sequence, which has been detached at the Upper Triassic décollement, is involved. The underlying basement remained largely unaffected during the Late Miocene phase, playing only a passive role (see Figure 4-4). Moreover, the edge of the “sub-indenter” is hidden beneath the Permo-Carboniferous trough and shoulder, making its identification more difficult.

The transfer zone described in section 3.3 comprises two differently oriented oblique thrust ramps that developed in the sedimentary cover: the Unterendingen-Fault to the west and the Siglistorf-Anticline to the east (Figure 4-5). This corresponds to the southern edge of the “sub-indenter.”

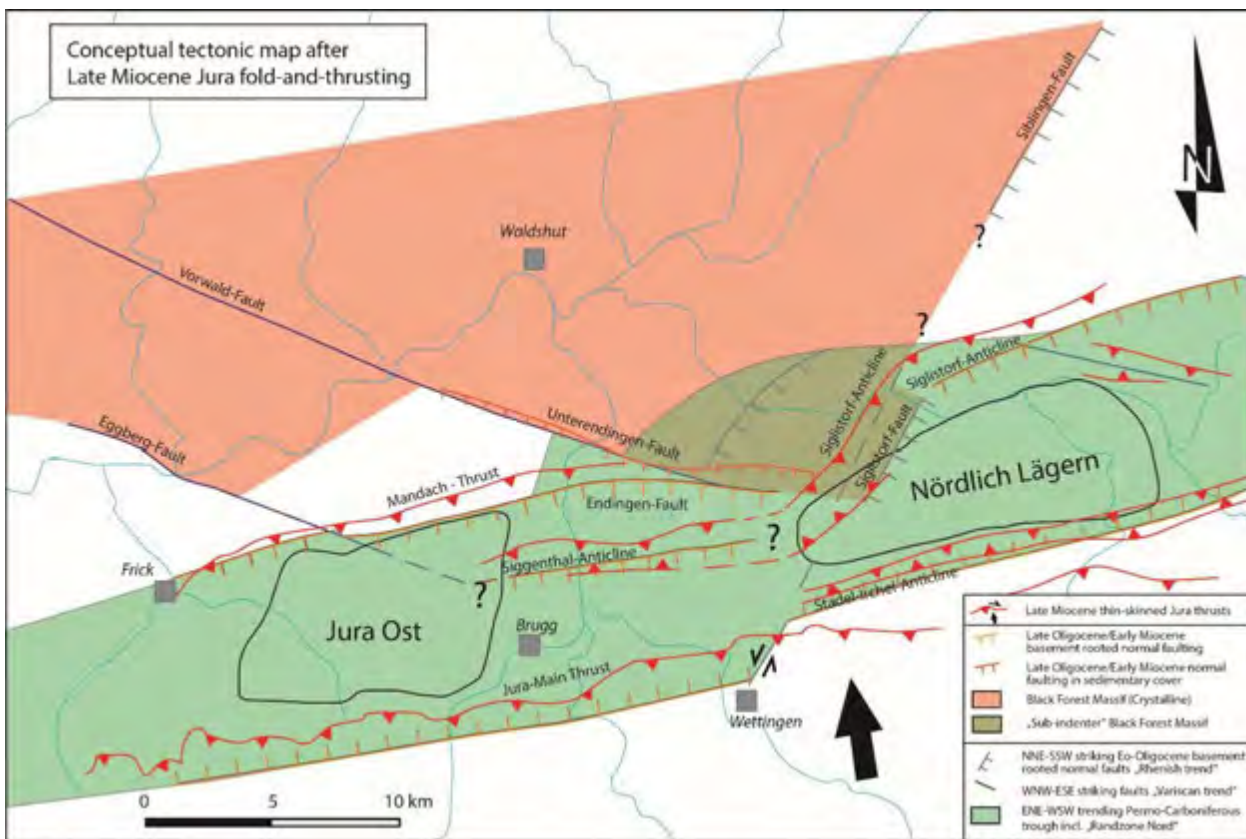


Figure 4-4: Conceptual tectonic map including the superposition of major top basement and surface tectonic elements after Late Miocene thin-skinned thrusting. The pronounced curvature of the Siglistorf-Anticline trending from ENE to NNE may be tentatively explained by a NNE-trending oblique ramp developed in the sedimentary cover as a result of basement-rooted fault having the same direction.

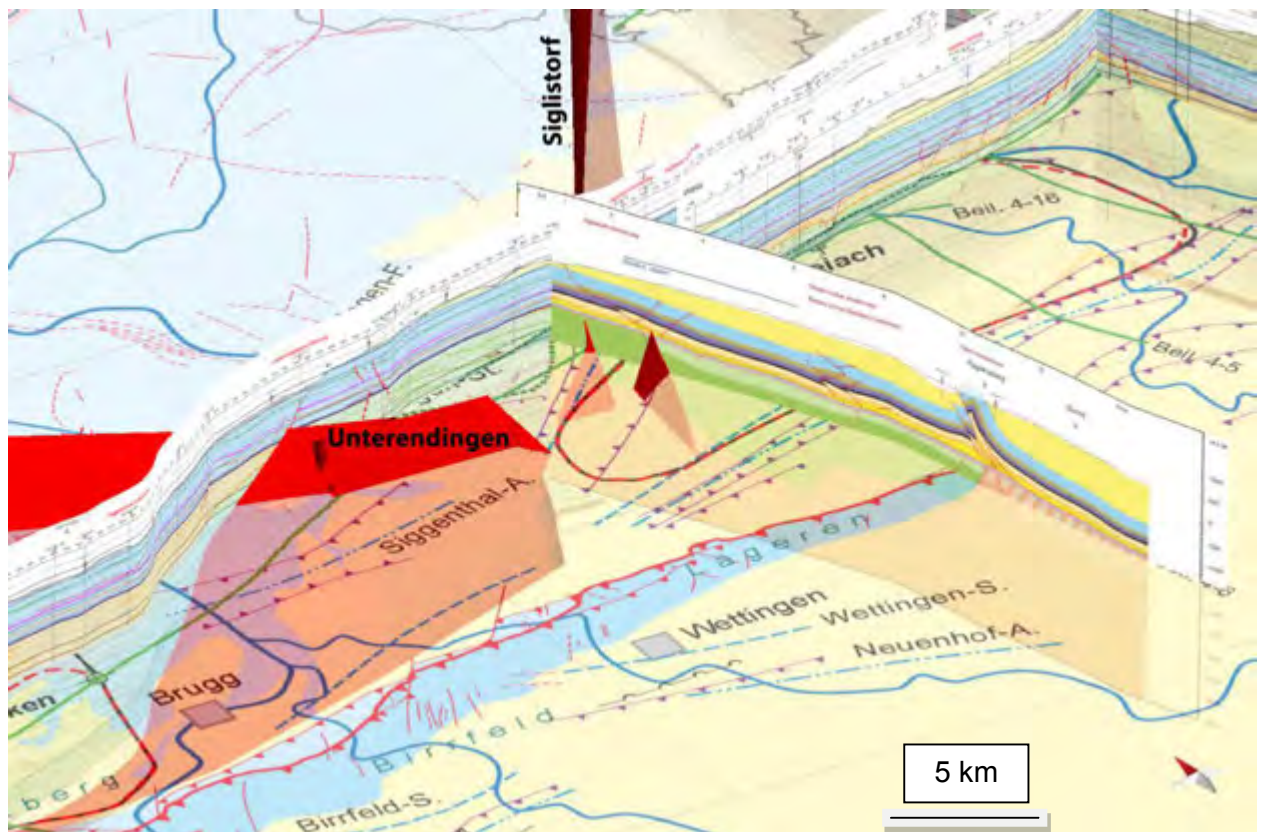


Figure 4-5: Tectonic map of northern Switzerland with Unterendingen dextral and Siglistorf sinistral oblique ramps propagating through the sedimentary sequence consequent to basement-rooted fault reactivation (image from 3D model *MOVE*, swisstopo).

5 Kinematic tectonic interpretation

The kinematic tectonic interpretation of northern Switzerland is the core of the expertise demanded by ENSI. Aware of the conceptual uncertainty facing geologists and seismologists involved with the seismic interpretation, Nagra has integrated cross-section restoration and balancing techniques in the seismic interpretation workflow. The result is documented in report NAB 14-105, which provides a compilation of the tectonic elements on maps and cross sections. This key report was available only at the end of May 2015. Moreover, the more pertinent kinematic considerations were not found in the huge documentation given to us in Nagra reports (NAB and NTB) but in two accepted papers in international journals by Malz et al. (2015) (Table 1-2). Both of these papers were available only at end of June 2015.

5.1 Balanced cross sections

The aims and benefits of constructing balanced cross sections are twofold: 1) elaborating geometrically viable and plausible 2D structural sections (present-day deformed sections) that can be restored to an initial state predating deformation (restored sections), and 2) quantifying deformation (shortening) along the balanced cross sections.

There are 18 cross sections appended to the report NAB 14-105. These profiles were balanced and restored in 2D using the *MOVE* software developed by Midland Valley. In a polyphase tectonic setting as in the Jura fold-and-thrust belt, a stepwise restoration of the balanced cross section enables us to study the relative timing and kinematics (backward modelling). Furthermore, we can test the consistency of balanced cross sections by forward kinematic modelling to check the deformation sequence (order of thrusts). In fact, the different deformation steps from the restored section to the deformed section must be documented and illustrated by forward modelling. Jordan et al. 2015 applied classical bed-length and area cross-section balancing methods to validate their interpretation. In a first approximation, all cross sections were balanced for horizons located above the regional décollement horizon, assuming the footwall units to be unaffected by the thin-skinned deformation. The forward kinematic modelling was, however, not part of report NAB 14-105. Only one attempt for the Jura Main Thrust is presented for one cross section. Moreover no *MOVE* files were provided for our review. Therefore, swisstopo has redrawn all sections in *MOVE*.

5.2 Discrepancy between balanced cross section and seismic interpretation

Despite extensive data reprocessing and significant improvement of data quality, the seismic images of the strongly deformed Folded Jura remain difficult to interpret because the seismic reflections cannot be followed continuously. One of the most significant examples is illustrated in Figure 5-1. The interpreted seismic profile shows a simpler thrust system than the corresponding balanced cross section. The internal structure of the Jura Main Thrust and the Chestenberg-Anticline has been improved in the balanced cross section by including geological information from geological maps, azimuth and dip values of relevant geological strata, and shallow boreholes. This example shows the complexity of properly imaging the core of anticlines.

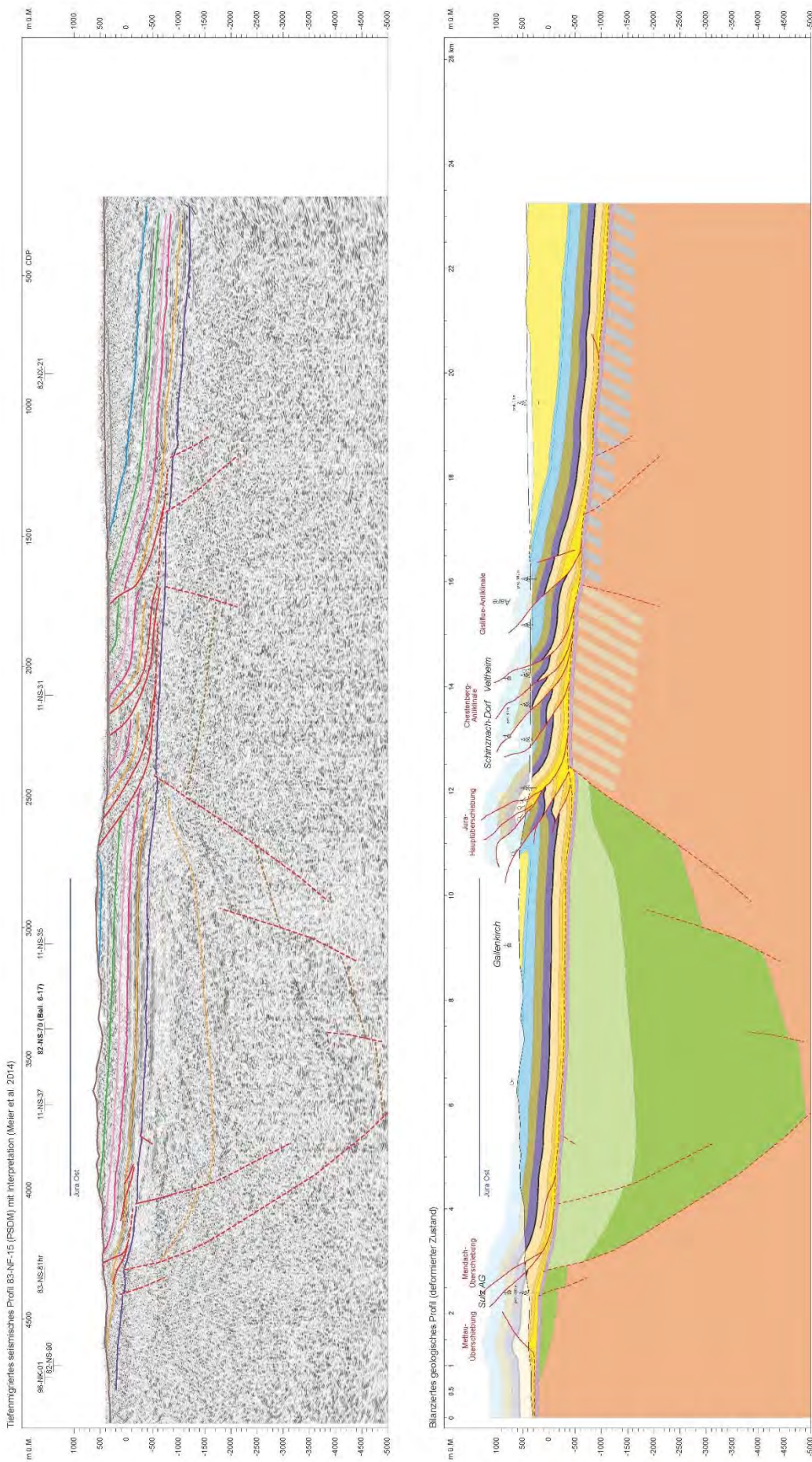


Figure 5-1: Interpretation of seismic profile 83-NF-15 (siting region Jura Ost). Comparison between interpreted structures by Meier et al., 2014 and balanced cross section by Jordan et al., 2015. Note the tectonic differences for the Jura Main Thrust and Chestenberg-Anticline

5.3 The kinematic evolution of the BIH triangle zone

One of the main results obtained by Jordan et al. (2015) and Malz et al. (2015) confirms that the balanced structural style is dictated by the mechanical properties of particular stratigraphic elements: with the main décollement, it is the Triassic evaporates; and with two subsidiary upper detachment levels, it is the base of Opalinus Clay and Effinger Schichten Formations. These upper detachments facilitate stacking of the main thrust and development of wedges, respectively. The Baden-Irchel-Herdern (BIH) triangle zone has been interpreted by the above authors as the result of a main basal décollement and subsidiary detachment in the Opalinus Clay. This interpretation is based on the images from seismic profiles. We find this solution very convincing. However, we present this example in order to show that the kinematic evolution of the BIH triangle zone may be interpreted in two different manners, both viable and restorable.

The BIH is interpreted as the southern border fault of the Permo-Carboniferous trough, a Palaeozoic normal fault, which can be traced for about 60 km with an ENE-WSW strike (Figure 3-16) (e.g. Malz et al., 2015). This inherited fault was reactivated in Early Miocene times in extension mode. Seismic data yield evidence for a normal reactivation of these border faults affecting Tertiary sediments (i.e. Bitterli et al., 2000). The reactivation led to disruption of the basal décollement within the Triassic evaporites. When the thin-skinned deformation front propagated northwards in Late Miocene times, a triangle zone developed above the reactivated extensional BIH Lineament. This triangle zone is composed of one major foreland-vergent thrust rooting in Triassic evaporites and a back-thrust rooting in the Opalinus Clay Formation. According to the kinematic hypothesis of Malz et al., (2015) the BIH triangle zone formed first. The deformation front then back-stepped to the SE to form the Lägern-Anticline and associated thrusts (Figure 5-1). The Siglistorf-Anticline and associated thrust NW of the BIH formed last.

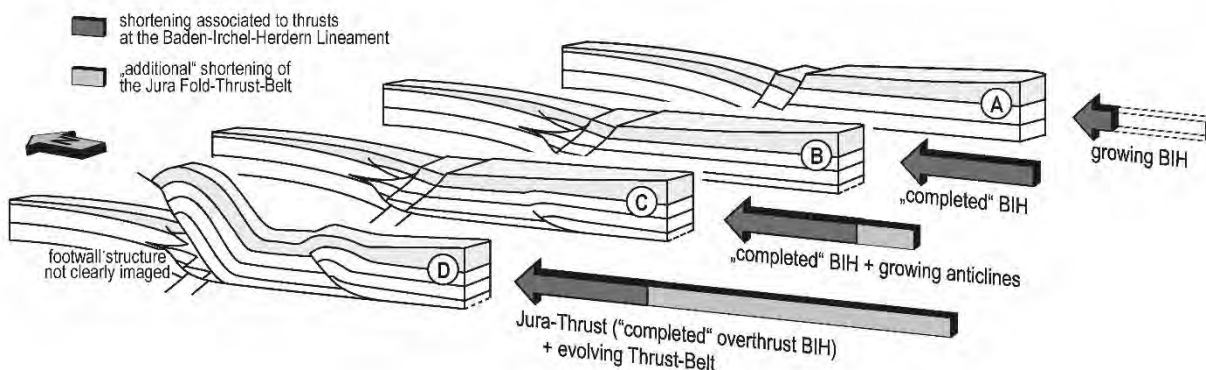


Figure 5-1: Proposed kinematic sketch from Malz et al., 2015 illustrating the evolution of the BIH triangle with respect to the Jura Main Thrust: A: initial state with less than 200 m shortening, the inherited normal faults are not affected by the shortening so far; B: Shortening of approximately 200m. The pre-existing normal fault is contractionally overprinted leading to the fully developed BIH triangle structure. C: shortening exceeds the maximum horizontal strain assimilated from the BIH triangle; on-going shortening results in the formation of new thrusts in the hinterland of the BIH; D: shortening strongly exceeds ~200 m; the stationary BIH triangle is overthrust by foreland propagating thrust-faults associated with the Jura belt. Inherited normal faults are completely cut by thrust-faults.

A. Kloppenburg proposed an alternative kinematic interpretation based on forward modelling of the section 91-NO-58 (Beilage 6-6 in NAB 14-105). A normal in-sequence order of thrusting is assumed, progressing from SSE to NNW (Figure 5-2). This order is allowable, i.e. geologically

and kinematically reasonable, but is not constrained by the geometry of thrusts as observed on the present-day section. Her detailed kinematic analysis is appended in Appendix 2.

In conclusion, there are no direct cross-cutting or kinematic constraints to prefer one interpretation over the other. Accordingly, both solutions are equally viable based on the constraints included in this study. This issue is not only of academic relevance. In the context of site selection it is important to know how the deformation front evolved in the past, where the present-day deformation front is located today, and how it will evolve in the near future. Both latter issues have been addressed by the mechanical approach (refer to section 6 and the full report in Appendix 3).

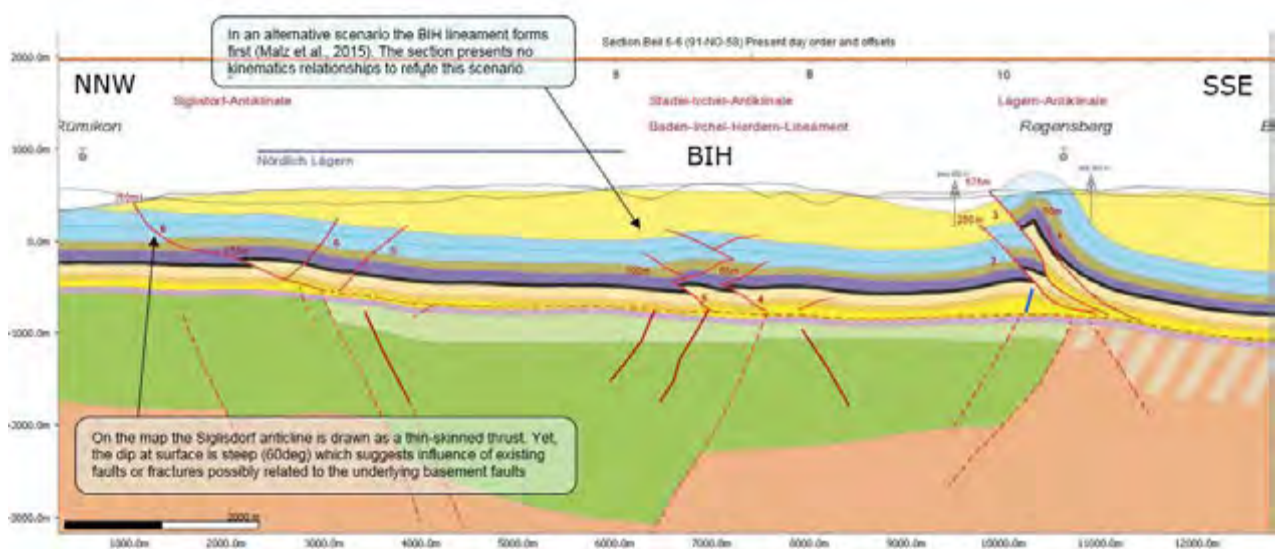


Figure 5-2: Alternative kinematic interpretation proposed by A. Kloppenburg by forward modelling (refer to Appendix 2) based on in-sequence thrusting and considering an alternative scenario for section 91-NO-58 (from Beilage 6-6 in NAB 14-105). Thrust faults are numbered according to their temporal sequence of activation. There are no direct constraints from cross-cutting relationships or kinematic considerations for the relative timing of the BIH and Läger-Anticline.

6 Present-day deformation front, future evolution, and recent thick-skinned tectonics

The present-day deformation front and the future evolution of northern Switzerland may be tentatively assessed by a mechanical approach. This task was commissioned to the University of Cergy-Pontoise. The reader is referred to Appendix 3 for the full description of the applied method and the obtained results. These authors have applied a simplified mechanical approach originally developed in Civil Engineering and called limit analysis (Salençon, 2002). The kinematic approach of limit analysis consists in calculating an upper bound of the tectonic force Q associated with a given distribution of deformation by accounting for mechanical equilibrium and maximum rock resistance, as described by the Coulomb criterion. By upper bound, we mean that, although the tectonic force is unknown, its exact value cannot be above the upper bound. An optimisation procedure then allows us to determine the distribution of deformation associated with the least upper bound.

6.1 Present-day deformation front

Caër et al., (Appendix 3) used the commercial software, *Optum G2*, to calculate the onset of deformation and stress fields resulting from horizontal compression. Rheological lithologies and weakness of existing faults are accounted for in their mechanical analysis. In a first approach, they assumed thin-skinned deformation: the rigid pushing wall extends from the surface down to the Muschelkalk décollement, and the basement below is considered fixed. The influence of the basement topography (see section 2.1) is expressed as local variations in the thickness of the Triassic décollement layer disrupted by inherited normal faults. The position of the present-day deformation front depends on the weakness of the Triassic décollement. A map of the deformation front has been drawn for a given set of rheological parameters spanning all physically realistic values. This map shows the areas that will likely remain undeformed in the near future (Figure 6-1). The key result is that the present-day deformation front may intersect the siting regions Jura-Südfuss and Nördlich Lägern, assuming a cohesion of 1 MPa and friction angles ranging from 0-10° for the décollement within the Triassic evaporites. These results are not significantly different for a lower cohesion value of 0.1 MPa. Dashed lines between the profiles indicate different fronts as we lack information there. The siting area Jura Ost is located outside and further north of the current position of the deformation front. The siting regions Zürich Nord-Ost and Südranden are not affected by the mechanical analysis as they lie outside the influence of the Triassic décollement. These results are not significantly different for a lower cohesion of 0.1 MPa.

6.2 Future evolution of the deformation?

We can assess the stability of the present-day deformation front (as shown in Figure 6-1) or, in other words, the new deformation front that may develop in the next million years, by applying the *SLAMTec G2* software. Parametric analysis suggests that, in the worst case, the current thrust ramps would remain active for at least 190 m of shortening before jumping to a new or another existing thrust ramp. Such a shortening would be reached after about 200,000 years, assuming a rapid convergence rate of 1 mm/year. This rate is considered to be an upper bound value; a rate of 0.1 mm/year would be more realistic, leading to fault stability for at least 2 myr. This duration is two times longer than the safety requirements of 1 myr for a deep geological disposal.

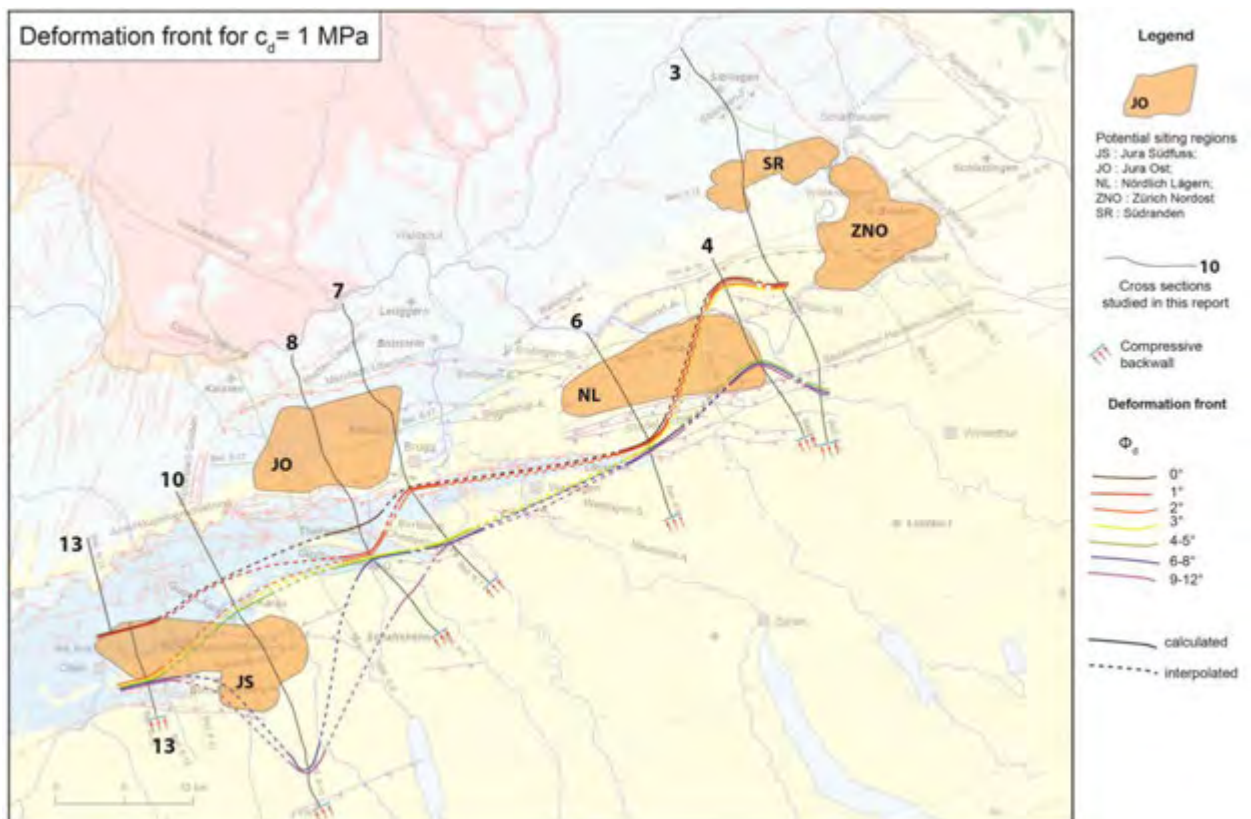


Figure 6-1: Synthetic map view of the present-day deformation front for various friction angles and assuming a cohesion on the Triassic décollement of 1 MPa (from Caër et al., see Appendix 3)

6.3 Recent / future thick-skinned tectonics (?)

To address the possibility of recent thick-skin tectonics, as postulated by an increasing number of authors, we refer to the paper of Malz et al. (2015). According to these authors, the BIH triangle zone may represent a major ENE-WSW-striking boundary separating regions with two different tectonic styles. On the basis of shortening considerations, these authors argue that the southern region seems to be dominated by thin-skinned tectonics and the northern side by thick-skinned deformation (Figure 6-2). To the north of the BIH triangle zone, the Siglistorf-Eglisau structure is located directly above the faults of the northern border of the Permo-Carboniferous trough. Since the BIH triangle zone is observed to have a fixed position in the hinterland, this is in contradiction to a pure thin-skinned deformation. Assuming thin-skinned thrusting, the BIH triangle zone should have been shifted northwards by passive thrusting on the Triassic décollement by a shortening equal to the distance accommodated by the Siglistorf-Eglisau structure. Thus, these authors conclude that the contractional deformation to the north of the BIH triangle zone cannot be explained by pure thin-skinned thrusting and at least part of it should be related to thick-skinned tectonics characterised by basement thrusts underneath the basal décollement that are able to compensate the shortening observed along the Siglistorf-Eglisau structure.

We compare these results obtained by Malz et al. (2015) with the mechanical analyses of Caër et al. (Appendix 3). The latter authors have simulated the possibility of recent or future thick-skin tectonics by applying a compressive force on a rigid wall placed in the Central Alps and extending vertically from the surface down to the upper-lower crust boundary. As a first major

result, the parametric analysis shows the mechanical possibility to have thick-skinned deformation associated with coeval slip on the Upper-Middle Triassic detachment in the eastern part of the Jura belt. The deformation uses the “mid-crustal” décollement (called D2) and evolves as a basement ramp to the north emerging either at the surface or connecting to the Triassic décollement (called D1). The authors find two main situations: for the highest friction values ($\Phi D2 = 10\text{-}30^\circ$), the crustal ramp emerges in the region of interest, potentially causing damage in this area. For lower friction values, the ramp emerges further north and the region is expected to be passively transported as part of the hanging wall of the ramp.

In a second stage, Caër et al. analysed deformation in the region of interest more precisely. The position of the basement ramp depends largely on the friction and cohesion values applied for the Triassic décollement D1. Low friction and/or cohesion values favour propagation of the basement ramp further to the north. As a second interesting result, the basement ramp emerges in all tested cases further north of the Jura Main Thrust, which coincides here with the BIH triangle zone (Figure 6-3). In fact, to the west the BIH triangle zone is re-thrusted and incorporated into the Jura Main Thrust. Thus, the mechanical results are not in contradiction with the interpretation by Malz et al. (2015) that postulate a thick-skin regime north of the BIH Lineament. Nevertheless, the potential position of the basement ramp differs between these interpretations. The mechanical analysis by Caër et al. shows that the ramp is never located directly beneath the Jura Main Thrust but always shifted to the north, its position depending on the friction and cohesion values assumed for both décollements D1 and D2. The southern border fault of the Permo-Carboniferous trough (BIH Lineament) does not play a major role here. We note that the analyses of Caër et al. concern a section further west (12-NS-42) intersecting with the siting area Jura Südfuss. Therefore, care should be taken when comparing theirs with the interpretation by Malz et al. (2015).

The present-day BIH may be considered as a lineament expressing the temporal evolution of the Jura Main Thrust from west to east. In the western part, the BIH has been completely incorporated and deformed by the Jura Main Thrust (Figure 5-1D). Towards east, the BIH has been inverted (triangle zone) (Figure 5-1B/C) and in the easternmost part, the BIH presents extensional faulting (Figure 5-1A). We argue that the easternmost part represents the less mature evolution of the structure, not yet affected by the Jura thrusting. It is uncertain if this part will be reached by the deformation front in the future. Other factors, such as significant decrease of the thickness of the Upper Triassic evaporite detachment level, may also control the tectonic style.

From Figure 3-2, it is likely that the BIH Lineament may intersect or merge with the Main Jura Thrust westwards as both run obliquely to one another. The possible intersection is located precisely within the transfer zone. The overall trend of the Jura Main Thrust seems to follow the southern border of the Permo-Carboniferous trough. Nevertheless, north of Wettingen, the Lägern-Anticline is oriented almost E-W. This E-W orientation corresponds to the expected “Jura” trend when not influenced by inherited structures (e.g. BIH Lineament, or more generally by the ENE-WSW striking southern border of the Permo-Carboniferous trough). Why does the orientation of the Jura Main Thrust deviate, to the north of Wettingen, from its general orientation controlled by the inherited southern border? A clue to an answer may be the presence of a local discontinuity at the southern border. Potential candidates for this disturbance might be the WNW-ESE-striking faults (“Variscan” trend). The “virtual” eastwards prolongation of the Eggberg-Fault would cross the city of Wettingen. On the local scale, a NNE-

SSW-striking fault seems to accommodate and transfer the shortening between the BIH Lineament and the Jura Main Thrust.

Based on mechanical analysis, cross section balancing, and shortening considerations, we conclude that there are several factors suggesting a possible recent thick-skinned deformation in the north of the Jura Main Thrust and the BIH Lineament.

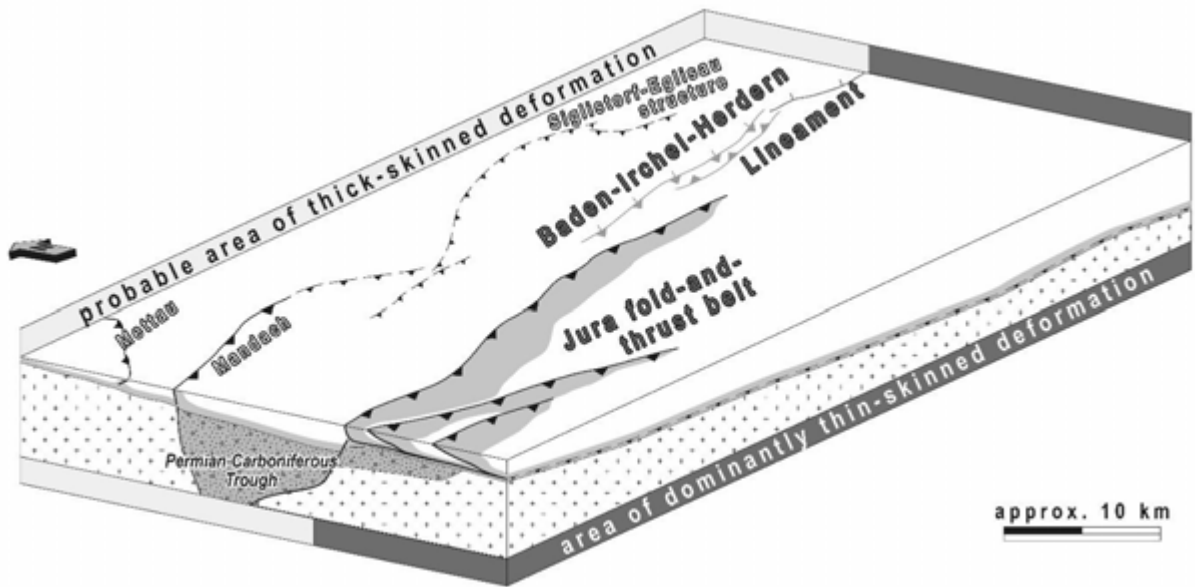


Figure 6-2: Conceptual sketch of the eastern end of the Jura fold-and-thrust belt illustrating the regional kinematic role of the Baden-Irchel-Herdern Lineament. This major tectonic structure is interpreted by Malz et al. (2015) to separate the study area into two regions characterised by different tectonic styles. The southern part being dominated by thin-skinned thrusting and the northern side by thick-skinned tectonics (figure from Malz et al., 2015).

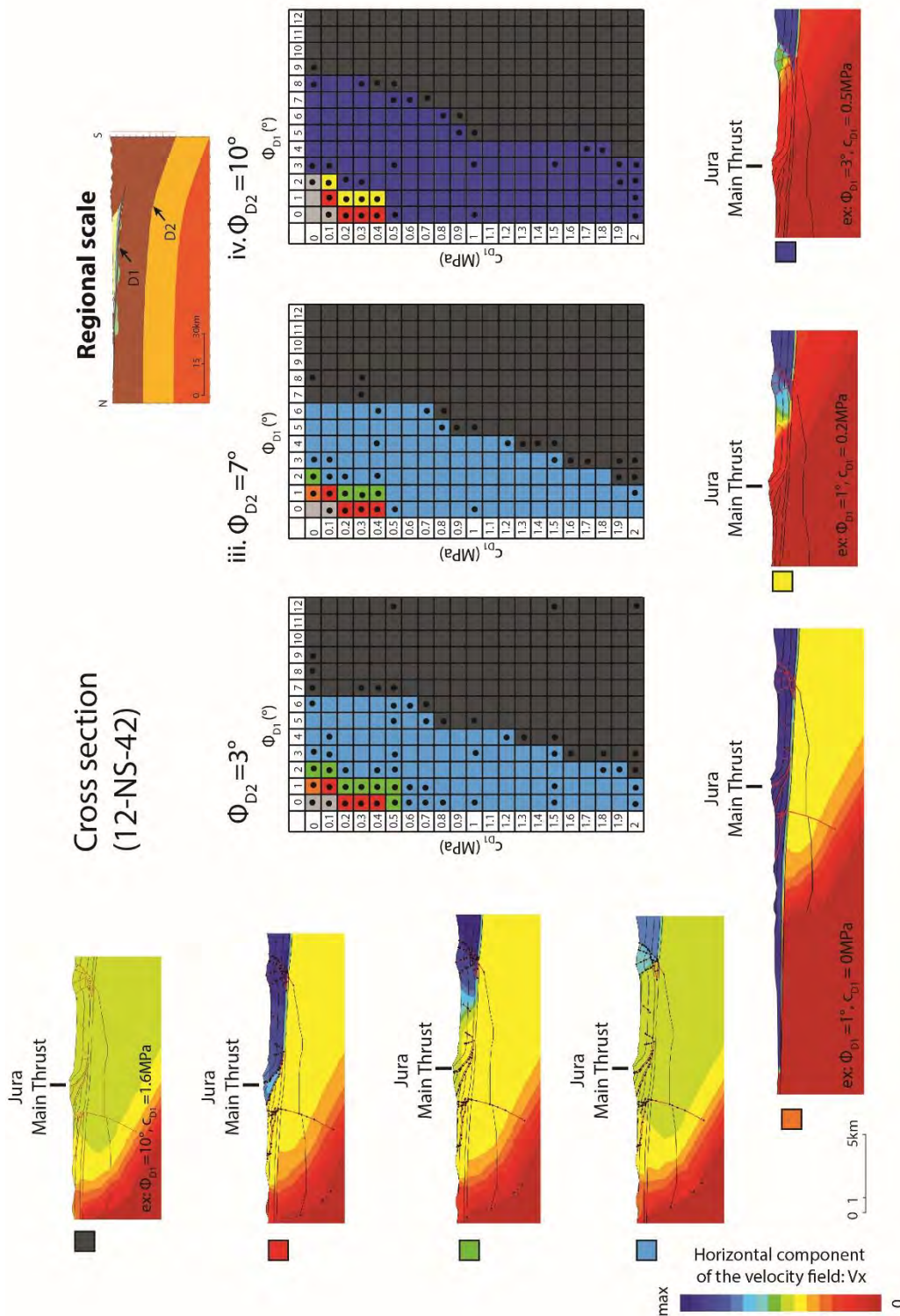


Figure 6-3: Results obtained with *Optum G2* for the thick-skin hypothesis tested on profile 12-NS-42 (siting area JS). Three cases for the lower décollement D2 were calculated: $C_{D2} = 0\text{MPa}$ fixed and $\Phi_{D2} = 3^\circ$, $\Phi_{D2} = 7^\circ$, $\Phi_{D2} = 10^\circ$. For the upper décollement D1, cohesion values ranging from 0 to 2 MPa and friction values from 0 to 12 ° are represented by a matrix. Calculated cases are represented by different square colours (from Caër et al., 2015, see details in Appendix 3)

6.4 Limitations of the applied mechanical approach

These predictions and conclusions are based on a simple mechanical and rheological description of materials and faults obeying the Coulomb criterion. On such a basis, it is not possible to predict in detail the deformation in a given tectonic region over a time scale of thousands of years. Too many effects have to be disregarded, such as fluid flow and its influence on friction parameters, surface transport (instabilities, erosion, sedimentation), and rate dependence of the rheology. In addition, the mechanical analysis by Caër et al. (Appendix 3) incorporates a series of assumptions. The upper crust is assumed to have homogenous properties, a significant simplification. Any differences in mechanical properties (e.g. existing faults, different trough geometries) may alter the model results. The present analysis aimed primarily at giving first-order predictions of the deformation and stresses to be expected from the interpreted seismic profiles and to help focus further studies on specific critical areas.

6.5 Neoseismicity

To check the present-day deformation front (Figure 6-1) and for any recently active faults, we combined the northern Switzerland seismicity dataset into our 3D *MOVE* model to check the correlation with regional faults. We integrated hypocenters of earthquakes recorded by the Swiss Seismological Service (SED) which monitors earthquakes in Switzerland and its neighbouring countries to assess Switzerland's seismic hazard. SED has catalogued all the earthquakes detected instrumentally since 1975 until 2008 in their database. This database is represented in digital format as the Earthquake Catalogue of Switzerland 2009 (ECOS-09). This catalogue also includes macroseismic and historical earthquakes since AD 250 based on the Macroseismic Earthquake Catalogue of Switzerland (MECOS). The earthquakes in the ECOS-09 are revised for their magnitudes and intensities and are listed with a homogeneous magnitude estimation based on the moment magnitude (M_w). ECOS-09 is available for download at <http://www.seismo.ethz.ch/prod/catalog>. Earthquakes from 2009 to 2015 are catalogued separately in the SED-database. These earthquakes are subject to future revision of their magnitude estimation. They are available for downloading through the Arclink Web-interface of the SED (<http://arclink.ethz.ch/webinterface/>).

The SED-database lists the hypocentral position (X, Y, and Z) and estimated magnitude for all known earthquakes from AD 250 until 2015. We imported the hypocentral position of the earthquakes in the targeted area into *MOVE* to yield the spatial distribution of these earthquakes. We can then compare these with geological and subsurface structure of the area. However, the existing catalogue does not provide well-defined geometrical aspects of the subsurface structure due to the sparse and scattered distribution of the earthquakes.

According to the ECOS-09 catalogue, there were 217 earthquakes from 1975 until 2008 with moment magnitudes (M_w) between 1.2 and 3.6 in northern Switzerland. On the basis of their cumulative event number during the period of 1975–2008 in this area, the catalogue has a magnitude completeness of $M_w = 1.5$. Lowering the magnitude completeness of the catalogue would increase the number of earthquakes with lower magnitudes detected in this area. Increasing the number of earthquakes detected would allow us to better define the geometrical aspects of subsurface structures.

The hypocentral position of the earthquakes is shown in the 3D model (Figure 6-3). It is difficult to draw any correlations with identified and interpreted faults of northern Switzerland. For this

reason, we suggest the implementation of a nanoseismic monitoring network (Joswig, 2008). Nanoseismic monitoring will allow us to lower the magnitude completeness by decreasing the detection threshold. The improved detection capabilities will make it possible to densify the results of existing datasets. Such projects may explore the potential and possibilities to detect and analyse existing records (see our recommendations in chapter 7).

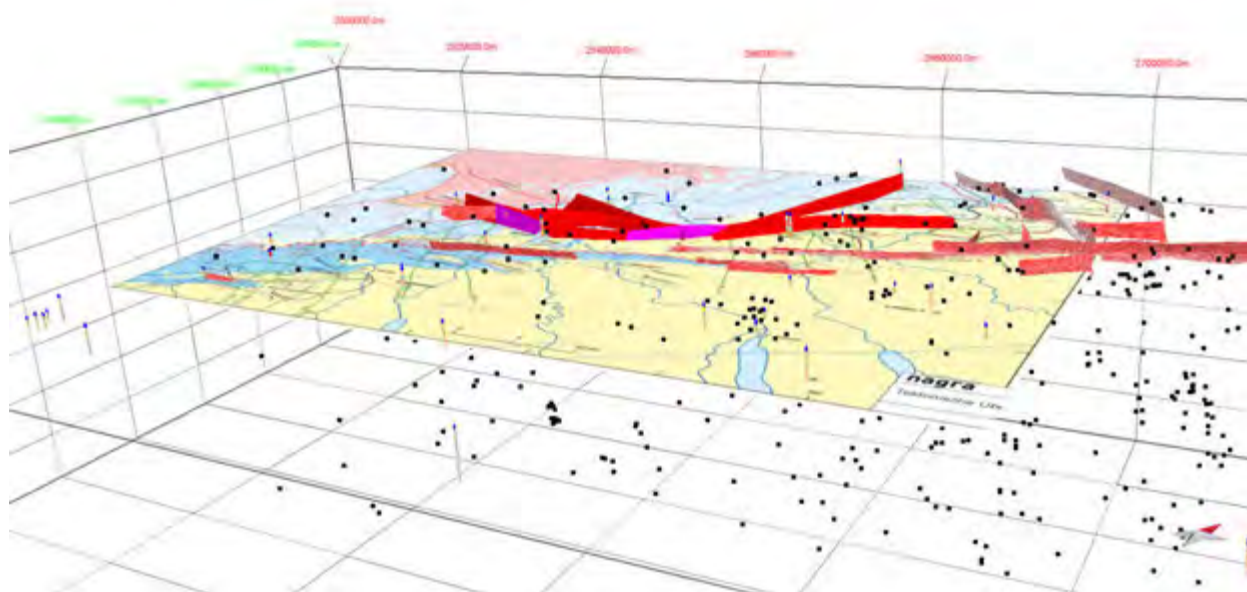


Figure 6-3: View of the 3D model including the hypocenters of 217 earthquakes published in the SED-database for the period between 1975 and 2008 (image by swisstopo). The tectonic map is from Nagra (Beilage 1-1, NAB 14-105).

7 Key outcomes and recommendations for further investigations

In this chapter we summarise the main results obtained by swisstopo (main text) and the external experts (Appendices 1, 2, and 3) in the course of the current review. This report discusses the role of inherited faults and their relationships with the resulting structures in the overlying detached sedimentary cover, hypotheses of past kinematic evolution of the study region, present-day deformation, and its future evolution. The potential of recent/future thick-skinned tectonics and recent seismicity are additional key issues to be investigated further.

7.1 Role of inherited faults and transfer zone

Our main criticism addresses the role of inherited basement faults on the area of interest. We believe that Nagra has not satisfactorily or clearly addressed the regional impact of these basement faults. It appears that Nagra has mainly concentrated its efforts on the interpretation of 2D-seismic data of faults in the sedimentary cover, detached above the Upper Triassic décollement. We understand that this effort focused on the sedimentary cover since the potential siting regions foresee a deep geological repository constructed within the Opalinus Clay. Our review of Nagra's kinematic interpretation of the tectonic structures in area indicates, however, that further investigation of the basement fault architecture would be welcome. In fact, basement-rooted inherited structures played a major role during the Late Miocene thin-skinned deformation. They formed nucleation lines for new ramp thrusts in the sedimentary cover above the Triassic décollement. We clearly observe a spatial and causal relationship between basement topography and initiation of thrusts at horst/graben contacts as well as for the thickness of the décollement composed of evaporites.

There are at least three major inherited fault trends in northern Switzerland: 1) WNW-ESW-striking faults ("Variscan" trend), 2) ENE-WSE-striking faults ("Permo-Carboniferous" trend), and 3) NNE-SSW-striking faults ("Rhenish" trend). The fold axes of the latest and youngest deformation (thin-skinned formation of the Jura fold-and-thrust belt), which affected the region of interest during the Late Miocene times, trend nearly E-W in northern Switzerland.

The significantly curved shape of the Jura front defined by seismic data (e.g. change of direction of the Siglistorf-Anticline) suggests the presence of a regional transfer zone intersecting the western edge of the siting area Nördlich Lägern (Figure 3-2). This transfer zone is located at the southern edge of the Black Forest Massif, at the junction between WNW-ESE-trending faults and NNE-SSW-striking faults (forming the eastern margin of the Black Forest Massif). Both fault systems form a kind of sub-indenter beneath the Triassic décollement. NNE-SSW-striking normal faults formed during the Eo-Oligocene rifting phase. The Late Oligocene/Early Miocene uplift of the Black Forest Massif is supposed to have reactivated the WNE-ESE-trending inherited faults in extensional mode, potentially disrupting the Triassic décollement. Hence, during the Late Miocene thin-skinned deformation, WNW-ESE-trending basement faults nucleated oblique ramps through the sedimentary cover associated with a dextral strike-slip component. NNE-SSW-striking basement faults formed oblique ramps associated with a sinistral strike-slip component, assuming a horizontal maximum stress directed N-S. It should be recalled that the underlying basement remained largely unaffected during the Late Miocene contractional phase since the sedimentary cover was detached above the Upper Triassic décollement.

We recommend a more detailed investigation of the junction of basement-rooted faults between the siting regions Jura Ost and Nördlich Lägern. The tectonic zone that should be avoided (Siglistorf-Anticline), may be part of a major regional fault zone. Basement faults like those related to the Siglistorf-Anticline run at high angle to the fold-and-thrust belt, consequently they are under-constrained in 2D seismic profiles. Construction of a 3D geometrical and kinematic model is the only way to better constrain the tectonic setting.

7.2 Kinematic evolution

We cannot unambiguously constrain the kinematic evolution of the tectonic framework. The proposed scenarios are non-unique and there is room for uncertainty and fine-tuning. Regarding the case of the tectonic evolution of the BIH triangle zone, Kloppenburg (Appendix 2) has tested the viability of the section 91-NO-58 intersecting the siting area Nördlich Lägern by forward modelling. She could demonstrate the plausibility of an in-sequence fault order, with new faults forming in the same direction as the transport direction. This result is required to match the steepness of structures found in this cross section. Her interpretation differs from the one proposed by Malz et al. (2015) who suggest that the BIH triangle zone developed at an early stage and the deformation front jumped backward to the south to form the Lägern-Anticline, implying out-of-sequence deformation. Kinematic modelling indicates that this interpretation is, in essence, also viable. To date there is no argument leading us to reject one or the other of these two interpretations.

In general, we strongly suggest testing the viability of all balanced cross sections presented in NAB 14-105 with 2D kinematic forward modelling in order to stepwise restore each section. Building a 3D geological model would be welcome, especially to predict the prolongation of tectonic structures in areas without any seismic data. Finally, 3D kinematic forward modelling of structures above the Triassic décollement is recommended to address the lateral changes in shortening amount and deformation style. The kinematic role of oblique ramps in the transfer zone can also be best explored by a 3D approach.

7.3 Present-day deformation front

The mechanical analysis conducted by Caër et al. (Appendix 3) enables us to draw in map view the position of the present-day deformation front for a given set of rheological parameters spanning all physically realistic values (Figure 6-1). The position of the front depends on the weakness of the Triassic décollement. This map shows the areas that will likely remain undeformed in the near future. The key result is that the present-day deformation front intersects the siting regions Jura-Südfuss and Nördlich Lägern. In contrast, the siting area Jura Ost is located outside and further north of the current position of the deformation front. The siting regions Zürich Nordost and Südranden also lie outside the influence of the Triassic décollement.

The stability of the present-day deformation front has been computed with the software package *SLAMTec G2*. Parametric analysis indicates that, in the worst case, the current thrust ramps would stay active for at least 190 m of shortening before jumping to a new or another existing thrust ramp. Assuming a rapid rate of 1 mm/year, such a shortening could be reached in about 200,000 years. A lower rate of 0.1 mm/year would be more probable, leading to fault stability over a period of at least 2 Ma. This duration is two times longer than the time span of 1 myr given by the safety requirements for a deep geological repository.

We emphasise that the present-day front deformation is located further to the south compared to the seismic deformation front formed by the most recent structures (i.e. Mandach Thrust, Siglistorf-Eglisau Fault) according to the kinematic evolution. Erosion affecting the Swiss Molasse basin situated to the south, and also within the Jura belt, can best explain this discrepancy. The mechanical analysis is very sensitive to the thickness of the wedge above the main basal décollement.

7.4 Recent and future thick-skinned tectonics?

The geoscience community largely accepts that the Jura Mountains formed during the Late Miocene in a thin-skinned fashion. Uncertainties concern the recent (e.g. Pleistocene, Holocene) and future evolution of the Jura fold-and-thrust belt. In this review, we applied the mechanical approach to explore this question (Caër et al., Appendix 3). Their mechanical analysis shows that recent/future thick-skin tectonics is mechanically possible in the eastern end of the Jura belt. Interestingly, thick-skinned deformation is found to be necessarily coeval with an activation of the Upper Triassic décollement (thin-skinned thrusting). Depending on the assumptions made for the Triassic décollement, the crustal ramp would emerge either significantly further north (e.g. Black Forest Massif) of the region of interest (for a weak décollement), or beneath the potential siting regions (for a stronger décollement) (Figure 6-3). The latter case might cause substantial deformation within or next to the siting regions. In the computed case (Jura Südfuss), the crustal ramp will always emerge to the north of the Main Jura Thrust. As there is at present a large uncertainty on the Coulomb parameters of the Triassic décollement, we recommend sampling the Triassic evaporites and conducting a series of laboratory experiments to determine the range of realistic friction values. This will be a first step in absence of direct in-situ measurements.

In addition, we recall that the thick-skin analysis has been performed only for the cross section intersecting the siting region Jura Südfuss (12-NS-42). We recommend that the same analysis should be repeated for the siting regions Jura Ost and Nördlich Lägern. Our preliminary results suggest that the easternmost part of the Jura belt may be currently affected by both thin- and thick-skinned tectonics. However, it should be recalled that clear field evidence is hard to find.

7.5 Nanoseismic monitoring

It is difficult to draw any correlations between the identified and interpreted faults with the recent seismicity of northern Switzerland. This can be explained by the fact that the earthquake catalogue of SED, from instrumental monitoring since 1975 until 2012, has a magnitude of completeness of $M_L = 1.5$ for the study area. In order to better understand the seismicity of northern Switzerland, lowering the magnitude completeness of the catalogue would be recommended to better define the scale and occurrence frequency of these events. Ongoing nanoseismic monitoring (Joswig, 2008, Sick et al., 2012) will yield a decrease in the magnitude completeness by lowering the detection threshold. In addition, improved detection capabilities will make it possible to densify the results of the existing datasets. Moreover, densification of the seismic network (i.e. increasing the number of stations) will lead to better hypocentre location accuracy.

Increasing the number of events detected using nanoseismic monitoring will improve isolation of single and possible clusters of events. These can be identified and further analysed by comparing and cross-correlating their waveforms to better understand their source

characteristics. Through waveform analysis, events which have a high cross-correlation factor can be relocated using the relative location methodology. This relative relocation technique will give a better view of the distribution of events and geometry of their seismogenic sources.

Optimisation of detection methods may yield a sufficient number of events for statistical analysis, such as frequency and b-value analysis, of the area. This analysis will improve our understanding of the probability of an event with a specific magnitude that might periodically repeat over time. Based on the b-value obtained for a targeted area, this will indicate the proportion of recurrence for lower and higher magnitude earthquakes in that area. Through this analysis, we can better assess the seismic hazard of the area.

An innovative workflow has been recently developed by Abednego et al. (2015) for calculating the focal mechanisms of low magnitude events. This requires a good knowledge of fault orientations obtained both from field data (including slip directions) and from 2D-seismic profiles. The present-day stress tensor could also be applied to these existing fault sets to compute focal mechanism models. Then, synthetic waveforms can be simulated at existing stations based on the computed focal mechanisms. These synthetic waveforms will be compared and correlated with existing records of stations to correlate best-fit computed focal mechanisms with the detected low magnitude events. A case study realised in and around the Mont Terri rock laboratory has shown the efficiency and potential of this method (Abednego et al., 2015).

7.6 Assessment on the siting areas

We base the following assessment of the siting areas only on tectonic considerations. All other criteria, such as technical construction feasibility, are not considered.

Of all potential sites, the siting areas Zürich-Nordost and Südranden present the most quiescent tectonic setting. There are still some uncertainties about the activation – or not – of a basal décollement within the Triassic evaporites in this most eastern part of the Jura belt and the potential impact of the neighbouring Hegau-Lake Constance Graben.

The siting area Jura Ost is located further to the west of the transfer zone and clearly beyond the present-day deformation front computed by the mechanical analysis. For this reason, its location seems to be more favourable than the one of Nördlich Lägern. However, this region lies in the continuation of “Variscan” inherited WNW-ESE-striking faults. In conclusion, the tectonic setting renders this siting area less appropriate for disposal than the site of Zürich-Nordost.

Analysis of regional faults and results of mechanical modelling indicate disadvantages for considering the siting area Nördlich Lägern for disposal. A nanoseismic monitoring (see section 7.5) would help determine whether the transfer zone (basement faults and associated Siglistorf-Anticline) in the western part of the siting area is still active or not. Furthermore, the mechanical approach suggests that the present-day deformation front may intersect with this siting area. Again, nanoseismic monitoring would help detect any recent seismicity along the supposed deformation front.

8 References

- Abednego, M., Blascheck, P., Mosar, J., Nussbaum, Ch., Joswig, M. & Bossart, P. (2015) : Focal Mechanism Analysis of Seismic Events from Microseismic Monitoring in Mont Terri Rock Laboratory, St-Ursanne (JU) : A Workflow, Swiss Geoscience Meeting 2015, Abstract volume, session 1, 22
- Allenbach, R. P. (2001): Synsedimentary tectonics in an epicontinental sea: A new interpretation of the Oxfordian basins of northern Switzerland, *Eclogae Geologicae Helveticae*, 94, 265–287.
- Becker, A. (2000): The Jura Mountains - an active foreland fold-and-thrust belt?, *Tectonophysics* 321, 381-406.
- Bitterli, T., Graf, H.R., Matousek, F. & Wanner, M. (2000): Geologischer Atlas der Schweiz 1:25'000, Blatt 1050 Zurzach, Erläuterungen. Landeshydrologie und - geologie, Bern, 89 S.
- Burkhard, M. (1990): Aspects of the large-scale Miocene deformation in the most external part of the Swiss Alps (Subalpine Molasse to Jura fold belt), *Eclogae Geologicae Helveticae*, 83, 559–583.
- Caër, T., Maillot, B., Souloumiac, P., Leturmy, P., Frizon de Lamotte, D. & Nussbaum, Ch. (2015) : Mechanical validation of balanced cross-sections: The case of the Mont Terri anticline at the Jura front (NW Switzerland), *Journal of Structural Geology*, 75, 32-48.
- Dèzes, P., Schmid, S. M. & Ziegler, P. A. (2004): Evolution of the European Cenozoic rift system: Interaction of the Alpine and Pyrenean orogens with their foreland lithosphere, *Tectonophysics*, 389, 1–33, doi: 10.1016/j.tecto.2004.06.011.
- Diebold, P. & Noack, T. (1997): Late Palaeozoic troughs and Tertiary structures in the eastern folded Jura, in O. A. Pfiffner, P. Lehner, P. Heitzmann, S. Mueller, and A. Steck, eds., *Deep structure of the Swiss Alps, Results from NRP 20*: Birkhäuser, 59–63.
- Gygi, R. A. (1986): Eustatic sea level changes of the Oxfordian (Late Jurassic) and their effect documented in sediments and fossil assemblages of an epicontinental sea, *Eclogae Geologicae Helveticae*, 79, 455–491.
- Gonzalez, R. & Wetzel, A. (1996): Stratigraphy and paleogeography of the Hauptrogenstein and Klingnau Formations (middle Bajocian to late Bathonian), northern Switzerland, *Eclogae Geologicae Helveticae*, 89/1, 695-720.
- Homberg, C., Bergerat, F., Philippe, Y., Lacombe, O. & Angelier, J. (2002): Structural inheritance and Cenozoic stress fields in the Jura fold-and-thrust belt (France), *Tectonophysics*, 357, 137–158, doi: 10.1016/S0040-1951(02)00366-9.
- Kuhlemann, J. & Kempf, O. (2002): Post-Eocene evolution of the North Alpine Foreland Basin and its response to Alpine tectonics. *Sedimentary Geology*, 152, 45-78.
- Isler, A. & Pasquier, F. (1984): Geologische Karte der zentralen Nordschweiz 1:100 000, mit angrenzenden Gebieten von Baden-Württemberg. Nagra and Schweiz, Geologische Kommission, Spezialkarte Nr. 131.
- Jordan, P., Malz, A., Heuberger, S., Pietsch, J., Kley, J. & Madritsch, H. (2015): Regionale geologische Profilschnitte durch die Nordschweiz und 2D-Bilanzierung der Fernschubdeformation im östlichen Faltenjura, Arbeitsbericht zu SGT-Etappe 2: NAB 14-105.

- Jordan, P., Noack, T. & Widmer, T. (1990): The evaporate shear zone of the Jura Boundary Thrust — New evidence from Wisen well (Switzerland), *Eclogae Geologicae Helvetiae*, 83, 525–542.
- Joswig, M. (2008): Nanoseismic monitoring fills the gap between microseismic networks and passive seismic, *First Break*, 26, 121-128.
- Kempf, O., & Pfiffner, O. A. (2004): Early Tertiary evolution of the North Alpine Foreland basin of the Swiss Alps and adjoining areas. *Basin Research*, 16, 549-567.
- Laubscher, H. (1961): Die Fernschubhypothese der Jurafaltung, *Eclogae Geologicae Helvetiae*, 54, 222–282.
- Laubscher, H. (1977): Fold development in the Jura, *Tectonophysics* 37, 337-362.
- Laubscher, H. (1986): The eastern Jura — Relations between thin-skinned and basement tectonics, local and regional, *Geologische Rundschau*, 75, 535–553, doi: 10.1007/BF01820630.
- Laubscher, H. (1987): Die tektonische Entwicklung der Nordschweiz, *Eclogae geol. Helv.* 80, 287-303.
- Laubscher, H. (2001): Plate interactions at the southern end of the Rhine graben, *Fachdokumentation Landesgeologie*, sep 746,19.
- Madritsch, H., Meier, B., Kuhn, P., Roth, P., Zingg, O., Heuberger, S., Naef, H. & Birkhäuser P. (2013): Regionale strukturgeologische Zeitinterpretation der Nagra 2D-Seismik 2011/12. Textband and Beilaganband, NAB 13-10.
- Madritsch, H., Schmid, S. M. & Fabbri, O. (2008): Interactions between thin- and thick-skinned tectonics at the northwestern front of the Jura fold-and-thrust belt (Eastern France), *Tectonics*, 27, TC5005, doi: 10.1029/2008TC002282.
- Madritsch, H. (2015): Outcrop-scale fracture systems in the Alpine foreland of central northern Switzerland: kinematics and tectonic context. *Swiss J Geosci*, doi 10.1007/s00015-015-0203-2.
- Malz, A., Madritsch, H. & Kley, J. (2015): Improving 2D-Seismic interpretation in challenging settings by integration of restoration techniques: A case study from the Jura fold-and thrust belt (Switzerland). *Interpretation Special Issue "Balancing, restoration, and palinspastic reconstruction"*, Manuscript ID: INT-2015-0012.
- Malz, A., Madritsch, H., Meier, B. Kley, J. (2015): An unusual triangle zone in the external northern Alpine foreland (Switzerland): Structural inheritance, kinematics and implications for the development of the adjacent Jura fold-and-thrust belt. *Tectonophysics* 670.
- Meier, B., Kuhn, P., Roth, P. & Madritsch, H. (2014): Tiefenkonvertierung der regionalen Strukturinterpretation der Nagra 2D-Seismik 2011/12, *Nagra Arbeitsbericht*.
- Naef, H., Birkhäuser, P., Roth, P. (1995): Interpretation der Reflexionsseismik im Gebiet Nördlich Lägern-Zürcher Weinland. *Nagra Technical Report NTB 94-14* (120 pp), Wettingen, Nagra.
- Naef, H. & Madritsch, H. (2014): Tektonische Karte des Nordschweizer Permokarbons: Aktualisierung basierend auf 2D-Seismik und Schwere-Daten, NAB 14-17.

- Nagra, NTB 14-02 (2014): SGT Etappe 2: Vorschlag weiter zu untersuchender geologischer Standortgebiete mit zugehörigen Standortarealen für die Oberflächenanlage, Geologische Grundlagen. Dossier II. Sedimentologische und tektonische Verhältnisse
- Salençon, J. (2002): De l'élasto-plasticité au calcul à la rupture. Ecole Polytechnique, Palaiseau, and Ellipses, Paris
- Sick, B., Walter, M. & Joswig, M. (2012): Visual Event Screening of Continuous Seismic Data by Superonograms, Pure and Applied Geophysics, SP Birkhäuser Verlag Basel, 1-11.
- Sommaruga, A., Eichenberger, U. & Mariller, F. (2012): Seismic Atlas of the Swiss Molasse Basin, Federal Office of Topography Swisstopo.
- Ustaszewski, K., & Schmid, S. M. (2006): Control of preexisting faults on the geometry and kinematics in the northernmost part of the Jura fold-and-thrust belt, Tectonics, 25, TC5003, doi: 10.1029/2005TC001915.
- Ustaszewski, K. & Schmid, S. M. (2007): Latest Pliocene to recent thick-skinned tectonics at the Upper Rhine Graben — Jura Mountains junction, Swiss Journal of Geosciences, 100, 293–312.
- Wetzel, A., Allenbach, R. & Allia, V. (2003): Reactivated basement structures affecting the sedimentary facies in a tectonically “quiescent” epicontinental basin: An example from NW Switzerland, Sedimentary Geology, 157, 153–172, doi: 10.1016/S0037-0738(02)00230-0.
- Willett, S. & Schlunegger, F. (2010): The last phase of deposition in the Swiss Molasse Basin: From foredeep to negative-alpha basin, Basin Research, 22, 623–639, doi: 10.1111/j.1365-2117.2009.00435.x.
- Ziegler, P. A. (1992): European Cenozoic rift system, Tectonophysics, 208, 91–111, doi: 10.1016/0040-1951(92)90338-7.



APPENDIX 1

Assessment report of 2D-seismic interpretation within Stage 2 of the Sectoral Plan for Deep Geological Repositories (SGT - E2) (northern Switzerland).

Author:

Dr. Anna Sommaruga (University of Fribourg)



Content:

Zusammenfassung	VIII
1 Introduction	9
1.1 Goal of the review	9
1.2 Questions to be addressed	10
1.2.1 Questions of “Schritt 1 von SGT - Etappe 2“	10
1.2.2 Questions of “Schritt 2 von SGT - Etappe 2“	10
1.2.3 Additional questions on specific seismic lines for siting regions	11
1.2.4 Additional questions concerning tectonic zones to be avoided and space requirement	12
1.3 Participation in meetings	12
1.4 Relevant Nagra reports for the assessment	13
2 Data	15
2.1 Critical overview on contents of Nagra reports	15
2.2 Seismic data	17
2.3 Well data	20
2.4 Depth conversion of seismic profiles	25
2.5 Seismic maps	25
3 Geological elements interpreted on seismic profiles	26
3.1 Seismic horizons	26
3.2 Classification of the reflection quality of interpreted seismic horizons	28
3.3 Fault definition	29
3.4 Classification of seismically interpreted faults	33
3.5 Interpretation of faults by Nagra	34
3.6 Geological structures	36
4 Discussion of geological features on seismic profiles in defined geological siting region	42
4.1 Südranden siting region	42
4.2 Zürich Nordost siting region	44
4.3 Nördlich Lägern siting region	51
4.4 Jura Ost siting region	58
4.5 Jura-Südfuss siting region	62
5 Answers to addressed questions	67
5.1 Answers to questions of “Schritt 1 von SGT - Etappe 2“	67
5.2 Answers to questions of “Schritt 2 von SGT - Etappe 2“	67
5.3 Answers to additional questions on specific seismic lines for siting regions	68
5.4 Answers to additional questions concerning tectonic zones to be avoided and space requirement	69
5.4.1 Tectonic zone to be avoided in the Nördlich Lägern siting region.	69
5.4.2 Space requirement	71
6 Statement	72
7 References	73
8 Appendices	76

Frage 28: Zu meidende tektonische Zonen	76
Frage 33: Geologische Entwicklung ZNO	87
Frage 63: Flexur	96

List of acronyms

Words in *italic* are written in German language.

§:	Chapter
ENSI:	Eidgenössisches Nuklearsicherheitsinspektorat
JO:	Jura Ost
JS:	Jura Südfuss
LDF:	Layout-determining faults
Mio:	Million
Nagra:	Nationale Genossenschaft für die Lagerung radioaktiver Abfälle
NL:	Nördlich Lägern
SGT – E1:	Sachplan geologisches Tiefenlager - Etappe 1 (SGT - Stage 1)
SGT - E2:	Sachplan geologisches Tiefenlager - Etappe 2 (SGT - Stage 2)
SGT – E3:	Sachplan geologisches Tiefenlager - Etappe 3 (SGT - Stage 3)
SR:	Südranden
TWT:	Two-way traveltime
ZNO:	Zürich Nordost

Legend of Nagra's figures has been kept in German.

List of appendices

Minutes/Protokoll of the meetings (these are added by ENSI)

Questions from Ensi addressed to Nagra and related answers.

- Frage 28: Zu meidende tektonische Zonen.
- Frage 33: Geologische Entwicklung ZNO.
- Frage 34: Anordnungsbedingte Störung Benken.
- Frage 35: Abgrenzung der Sicherheitsabstände um die regionalen Störungszonen in Etappe 2.
- Frage 63: Flexur.

List of Figures

Figure 2—1 : Location map of seismic profiles used by Nagra in SGT E2. The lines in red correspond to the new acquired (2011/2012) seismic data and the ones in black to the reprocessed old seismic lines. From NTB 14-01, Fig. 4.1-1.	18
Figure 2—2 : Comparison of the quality of reprocessed seismic lines of the 1982 (a) / 1991 (b) surveys with the new acquired (2011/12) seismic lines. TWT = Two-way travel Time. Modified from NAB 13-10, Fig. 2-3. For location see Beilage 2-1, NAB 13-10.	19
Figure 2—3 : Location map of wells (from NAB 14-34, Fig. 1-1). The Pfaffnau-1 well is located outside of the figure frame SW of the Schafisheim-1 well.	20
Figure 2—4: Synthetic seismogram from Benken-1 well in TWT. From NAB 13-10, Beilage 2-2.	22
Figure 2—5: Synthetic seismogram from Benken-1 well in depth. From NAB 14-34, Beilage 2-2.	23
Figure 3.1: Additionally seismic horizon interpretation in Weiach-1 well for the “Brauner Dogger”. Comparison of the sonic log with the seismic line 91-NO-75. From NAB 14-58, Fig. 8.	27
Figure 3.2: Description of the quality classes of the seismic horizons (on the left) and faults (on the right) as shown on the seismic lines. From NAB 13-10, Fig. 3-2.	29
Figure 3.3: Classification of geological/tectonic elements and their relevance concerning the layout of a geological repository at depth (modified from NAB 14-88, Fig. 2-1). a) Area-defining geological elements = regional faults (<i>regionale Störungen</i>); b) layout-determining geological elements = layout-determining faults (<i>anordnungsbestimmende Störungen</i>).	31
Figure 3.4 : Cross-section view of geological/tectonic elements and their relevance concerning the layout of a geological repository at depth (see Figure 3.3 for legend). Modified from NAB 14-88, Fig.2-2.	32
Figure 3.5: Location map of the regional fault zones and tectonic zones to be avoided (<i>zu meidende tektonische Zonen</i>) in northern Switzerland. From NAB 14-01, Fig. 4.4-1.	32
Figure 3.6 : Tectonic map of northern Switzerland. Additionally dashed thick red line corresponds to the Jura main thrust. Dashed thick blue line corresponds to the front of the Jura deformation taken from seismic lines. Modified from NTB 14-02, Beilage 4-1.	37
Figure 3.7 : Location of regional faults and related structures across the Top Liassic horizon TWT map. From NAB 13-10, Fig. 6-1.	38
Figure 3.8: Location of the Permo-Carboniferous troughs and the crystalline basement as interpreted in the NAB 14-17 report (Beilage 6-17). For remarks on wells, see also §2.3 well data)	40
Figure 4.1: Topography and quaternary filled channels in the Südranden siting region. EN: Enge; KR: Klettgau-Rinne; NH: Neuhauserwald-Rinne; RR: Rheinfall-Rinne; WA: Wagental. From NTB14-02, Dossier III, Fig. 4.4-10.	44
Figure 4.2: Map of the regional fault zones and tectonic zones to be avoided combined with the seismic location map for the Zürich Nordost siting region. Contours represent the Base Mesozoic horizon in depth (no precise depth value along the curve is indicated in Nagra’s figure, only intervals of 25m are mentioned in the caption). Compilation made by swisstopo from two maps of Nagra report figures (references indicated below the legend).	45
Figure 4.3: Location of the tectonic zone to be avoided (taken from Fig.4.4-4, NTB 14-02, Dossier II) in the Zürich Nordost siting area on the interpreted seismic line 83-SE-03 (from NAB 14-17, Beilage 6-12). According to Nagra, the tectonic zone to be avoided has been determined	

for this area on gravity data and on the Permo-Carboniferous through map. The interpretation of the Pre-Mesozoic units and faults of this TWT version line shows slight differences with the depth version presented in NTB 14-02 (Fig. 4.4-4). For location, see Figure 4.2. 46

Figure 4.4: Illustration of the eastern part of the seismic line 91-NO-75 in depth (on top) and in TWT below. Tectonic zone to be avoided, regional fault zone and *flexur* have been added according to the CMP location on the Figure 4.2. For legend for the bottom picture see Figure 4.3 and for location see Figure 4.2. 49

Figure 4.5: Illustration of the strike seismic line 91-NO-77 in TWT on top and converted to depth as a cross-section at the base. On the left, enlargement of the area in the blue rectangle on the seismic line. In the seismic section, the well name is Benken instead of Weiach (mistake on Nagra's figure). Regional fault zone and *flexur* have been added according to the CMP location on the Figure 4.2. For legend see Figure 4.3 and for location see Figure 4.2 51

Figure 4.6: Map of the regional fault zones and tectonic zones to be avoided combined with the seismic location map for the Nördlich Lägern siting region. Contours represent the Base Mesozoic horizon in depth (no precise depth value along the curve is indicated, only intervals of 25m are mentioned in the caption). Compilation made by swisstopo from two maps of Nagra reports (references indicated below the legend). 53

Figure 4.7: Interpretation of the faults (LDF) south of the Siglistorf anticline along three seismic lines in TWT. For reference of the figures, see below the lines. Black circles correspond to fault discussed in text. Tectonic zone to be avoided, regional fault zone and *flexur* have been added according to the CMP location on the Figure 4.2. For legend see Figure 4.3 and for location, see Figure 4.6. 56

Figure 4.8: Seismic line 11-NS-35 (PSDM version, scale in depth). On top non-interpreted and below interpreted seismic line (from A2-1-13, NAB 14-34). For arrows number 1, 2, 3, see explanations in text. Tectonic zone to be avoided has been added according to the CMP location from the Figure 4.2. For legend see Figure 4.4 and for location see Figure 4.6. 57

Figure 4.9: Map of the regional fault zones and tectonic zones to be avoided combined with the seismic location map for the Jura Ost siting region. Contours represent the Base Mesozoic horizon in depth (no precise depth value along the curve is indicated, only intervals of 25m are mentioned in the caption). Compilation made by swisstopo from two maps of Nagra reports (references indicated below the legend). 58

Figure 4.10: Southern part of the dip seismic line 11-NS-04 in depth (PSDM version). Tectonic zone to be avoided and *flexur* have been added according to the CMP location on the Figure 4.9. For legend see Figure 4.4 and for location see Figure 4.2. 60

Figure 4.11: Map of the regional fault zones and tectonic zones to be avoided combined with the seismic location map for the Jura Südfuss siting region. Contours represent the Base Mesozoic horizon in depth (no precise depth value along the curve is indicated, only intervals of 25m are mentioned in the caption). Compilation made by swisstopo from two maps of Nagra reports (references indicated below the legend). 63

Figure 4.12: Interpretation of the Born anticline on three different seismic lines or cross-section. Regional fault zone has been added according to the CMP location from the For legend see Figure 4.4, Figure 4.5 and Figure 4.7. For location map see 66

Figure 5.1: Alternative version of NTB 14-02 Dossier II Fig. 4.4-5 with contours of the Base Mesozoic horizon shown on top of the regional fault zone polygons. From Nagra, inserted in the answer at *Frage 63_Flexur*. 70

List of Tables

Table 1: Nagra's aims for the 2D-seismic evaluation in Stage 2 (SGT - E2). Presented by H. Madritsch in a meeting at ENSI (7.11.2014, ENSI 33/410 minutes).	10
Table 2 : List of the Nagra reports available for the review. Reports highlighted in grey have been evaluated in details.	14
Table 3: Well list with convention for picking of the seismic horizons. Wells are tied to old reprocessed seismic lines. BMz = Base Mesozoic; TMk = Top Muschelkalk, TLi = Top Liassic, BMa = Base Malm; BTe = Base Tertiary. From NAB 13-10, Tab. 2.....	24
Table 4 : Classification of the reflection quality on the interpreted seismic horizons. From NAB 13-10.	29
Table 5 : Description of the quality classes of the seismically determined faults (as shown on the seismic lines). From NAB 13-10, Tab. 5.....	34
Table 6: Seismic lines and related enclosures (<i>Beilagen/Anhänge – A-</i>) in reports for the Südranden geological siting region. In the last column are the specific questions from ENSI....	43
Table 7: Seismic lines and related enclosures (<i>Beilagen/Anhänge – A-</i>) in reports for the Zürich Nordost geological siting region. In the last column are the specific questions from ENSI.	45
Table 8: Seismic lines and related enclosures in reports for the Nördlich Lägern geological siting region. In the last column are the specific questions from ENSI.....	52
Table 9: Seismic lines and related enclosures in reports for the Jura Ost geological siting area. In the last column are the specific questions from ENSI.....	59
Table 10: Seismic lines and related enclosures in reports for the Jura-Sudfüss geological siting region. In the last column are the specific questions from ENSI.....	64

Zusammenfassung

Diese Auswertung beruht auf mehreren Nagra Berichten (die meisten davon öffentlich zugänglich) sowie auf Besprechungen betreffend der Interpretation von neu akquirierten (2011/2012) und alten re-prozessierten seismischen Linien aus der SGT-E2. Obwohl viele Berichte herangezogen wurden, enthalten nur drei Berichte die Interpretation der seismischen Profile (NAB 13-10, NAB 14-34, NAB 14-17) und ein separater Bericht (NAB 14-02, Dossier II) stellt die geologischen Strukturen vor, zusammen mit den regionalen Bruchzonen und den zu meidenden tektonischen Zonen. Ein abschliessender Bericht mit einer Synthese zur seismischen Interpretation fehlt jedoch.

Die 2D-seismischen Daten wurden von der NAGRA einwandfrei interpretiert. Die seismischen Horizonte wurden genau (exakt) an die Bohrungen angepasst und ihre Interpretation ist in der Nordschweiz meistens durchgehend genau. Der Top Opalinuston Horizont bleibt jedoch weitgehend konzeptuell und der Basis Mesozoikum Horizont zeigt eine ungleiche Qualität der Reflektoren im gesamten Gebiet. Die Interpretation der seismischen Horizonte innerhalb der regionalen Zone des Jurahauptüberschiebungsbruches hätte mit etwas mehr Details präsentiert werden können.

Die regionalen Störungszonen wurden von der NAGRA alle identifiziert und auf den seismischen Daten gut lokalisiert. Zusätzlich sind die Grenzen der zu meidenden tektonischen Zonen in den Standortgebieten auf den Karten hervorgehoben. Dieselben Zonen sind jedoch nur auf wenigen seismischen Profilen angezeigt. Das Herausstellen dieser Zonen ist dadurch gerechtfertigt dass die Anwesenheit von Brüchen oder Strukturen in den mesozoischen oder prä-mesozoischen Einheiten in den letzten 5 Millionen Jahren möglicherweise aktiv waren auch in Zukunft reaktiviert werden könnten. Erforschungen in der SGT3 sollten die genau Geometrie und den Versatz dieser Brüche genauer abklären. Betreffs den Aspekten der regionalen Bruchzonen und der zu meidenden tektonischen Zonen, hat die NAGRA Ihre Ziele (Identifizierung des geologischen Kontextes der regionalen Brüche und der zu meidenden tektonischen Zonen) erfolgreich erfüllt (erreicht) obwohl man in einigen Fällen genauere Darstellungen zu den verschiedenen Argumenten hätte präsentieren können.

Die Lage der anordnungsbestimmenden Störungen (Brüche ohne seitliche Korrelation) muss während der SGT Etappe 3 genauer bewertet werden um die Konturen der Lagerperimeter der SMA und HAA Lager zu verfeinern. Die Umriss der Brüche die die Basis Mesozoikum am Rande des Permo-Karbonbeckens durchbrechen sind auf der 2D-Seismik nicht sehr gut (unzureichend) definiert. Auf dieser 2D-Seismik bleibt der genaue Standort des Permo-Karbondrogens zum Teil spekulativ. Das Verständnis der Entwicklung des Permo-Karbon Grabens war für die Nagra in der Interpretation der Etappe SGT - E2 nicht ein Hauptobjektiv. Im nächsten Schritt (Etappe 3), sollten zwei Aspekte zur Verfeinerung der Umriss der Standorte eine wesentliche Rolle spielen: ein 3D-Seismik Kampagne und ein kinematisches Model des Lagergebietes um somit das Verständnis zur geologischen Entwicklung des Permo-Karbondrogens zu verfeinern. Verbesserte genauestens auf geophysikalischen Daten basierende bilanzierte Profile durch das in SGT - E2 erforschte Gebiet sollten erstellt und integriert werden. Sogar Details in den Bruchzonen – als nicht relevant für die Lager betrachtet – sollten präzise dargestellt werden. Andernfalls könnte ein Problem der Glaubwürdigkeit auftreten. Basierend auf dieses neuen Modellen könnte die NAGRA das Risiko einer Reaktivierung von Brüchen einschätzen/abwägen.

1 Introduction

1.1 Goal of the review

This review is done in the frame of a mandate by swisstopo (project contract: FL403-SGT-2 of the 31.01.2014 with extension on the 30.04.2015) to assess the tectonic interpretation from Nagra on the 2D-seismic data in northern Switzerland during Stage 2 of the SGT. This report is exhaustive with figures, tables and descriptions upon request of swisstopo.

This swisstopo mandate is included in a mandate from ENSI (Swiss Federal Nuclear Safety Inspectorate) on the assessment of the 2D-seismic data of Stage 2 (SGT – E2, Sachplan geologisches Tiefenlager - Etappe 2) elaborated by Nagra which is in charge to propose sites to host a repository for radioactive waste. The Stage 2 aims at selecting at least two potential geological siting regions for each repository type for further investigation in SGT - Stage 3. For this assessment, ENSI established an expert team focusing on the processing of the seismic data and on the geological and tectonic interpretation of the seismic data respectively.

In Stage 1 (SGT – E1), Nagra selected five geological siting regions in Northern Switzerland to be investigated for disposal of low and intermediate level waste (L/ILW, respectively in German: SMA), while a repository for high level waste (HLW, respectively in German: HAA) was only considered suitable in three of the five siting regions (ZNO, NL and JO). The major aim of Nagra's work (Table 1) for the geological part in the 2D-seismic interpretation in the Stage 2 (SGT – E2) is to identify the geological settings (faults and structures), especially regional faults, tectonic zones to be avoided and the layout-determining faults. It was also estimated if these features could be reactivated during a period of 1 Mio years considered the lifetime of a radioactive waste repositories. Minor aims from Nagra are listed in Table 1 (e.g. better understanding of the Permo-Carboniferous troughs). Table 1: Nagra's aims for the 2D-seismic evaluation in Stage 2 (SGT - E2). Presented by H. Madritsch in a meeting at ENSI (7.11.2014, ENSI 33/410 minutes).

ENSI addressed specific questions to each expert, which were subdivided into two steps (Schritt 1 and Schritt 2) for the review process. Questions are addressed in §1.2.1, §1.2.2 and §1.2.4 and answered in §5.1, §5.2 and §5.4 respectively. For the author, additional questions on specific seismic lines are addressed in §1.2.3 for each siting region and answered in sub-chapter from §4.1 to §4.5. Upon invitation by ENSI, several meetings (§1.3) with the different experts fostered discussion on the addressed questions. Nagra and Proseis AG collaborators attended a couple of these meetings to answer questions and clarify facts.

Ziele der 2D-Seismik Auswertung

Hauptziele:

1. Verifikation & Präzisierung des Verlaufs von regionalen Störungszonen
2. Information zu anordnungsbestimmenden Störungen innerhalb der Standortgebiete
3. Vertiefung des regionalen kinematisch-tektonischen Verständnisses um die HAA-Gebiete Bözberg und Nördlich Lägern im Hinblick auf SGT- Etappe 3

Nebenziele:

- Input zu Ungewissheiten Tiefenlage & Mächtigkeit Wirtsgesteine
- Verifikation von Verlauf & Tiefe der wichtigsten quartären Felsrinnen
- Identifikation von Faziesübergängen (z.B. im Braunen Dogger)
- Besseres Verständnis des Permokarbons
- Feldparameter tests für zukünftige 3D-Seismik-Kampagnen

2 Mhh / 7.11.2014 2D-Seismik-Auswertung SGT-E2: ENSI-Review Schritt 2

nagra.

Table 1: Nagra's aims for the 2D-seismic evaluation in Stage 2 (SGT - E2). Presented by H. Madritsch in a meeting at ENSI (7.11.2014, ENSI 33/410 minutes).

1.2 Questions to be addressed

The questions were presented in German by ENSI in the contract (H-101002) and in meetings, and are not translated in English. The answers of the questions are discussed in Chapters 4 and 5.

1.2.1 Questions of "Schritt 1 von SGT - Etappe 2"

- A. Sind die Interpretationen der Strukturen der seismischen Linien nachvollziehbar?
- B. Wurde bei der seismischen Interpretation der durch die geophysikalische Datenverarbeitung u.U. entstandenen Mehrdeutigkeit der Modelle genügend Beachtung geschenkt?

1.2.2 Questions of "Schritt 2 von SGT - Etappe 2"

- C. Sind Lokation und Verlauf von regionalen Störungszonen, von anordnungsbestimmenden Störungen und von konzeptionell zu meidenden tektonischen Zonen nachvollziehbar?
- D. Ist die geologisch-tektonische Interpretation der seismischen Linien vollständig?
- E. Wurde bei der geologisch-tektonischen Interpretation der durch die geophysikalische Datenverarbeitung u.U. entstandenen Mehrdeutigkeit der Modelle genügend Beachtung geschenkt?

1.2.3 Additional questions on specific seismic lines for siting regions

Five investigated geological siting regions were considered in this review: (1) Südranden (SR), (2) Zürich Nordost (ZNO), (3) Nördlich Lägern (NL), (4) Jura Ost (JO) and (5) Jura-Südfuss (JS).

Südranden siting region (1)

12-NS-66: Das ENSI wünscht sich für dieses Profil eine Aussage zur generellen Betrachtung von Multiplen im Grundgebirge.

12-NS-75: Zu diesem Profil hat das ENSI keine Detailfragen.

12-NS-77: Das ENSI stellt sich die Frage, wie gut die Neuhauserwald-Rinne (CMP 4550 bis 4850) und damit einhergehende mögliche tektonische Störungen im Grundgebirge (Rand eines Permokarbon-Troges?) erkennbar sind.

Zürich Nordost siting region (2)

91-N0-77: Zu diesem Profil hat das ENSI keine Detailfragen.

91-N0-68: Zu diesem Profil hat das ENSI keine Detailfragen.

Nördlich Lägern siting region (3)

11-NS-18: Wie gut ist die Datengrundlage für die eingezeichneten Störungen im Grundgebirge? Sind diese belastbar? Bei diesem Profil geht es generell um die Belastbarkeit bei der Interpretation des Grundgebirges.

11-NS-20: Die Nagra klassifiziert die nördliche Zone im Standortgebiet als tektonisch zu meidende Zone. Grund dafür sind die Trogränder des Permokarbondroges und Störungen in der Trias und des Juras. Frage: Wie belastbar sind dazu die Erkenntnisse aus der 2D-Seismik in diesem Profil? (CMP 4200 bis 5200).

11-NS-35: Die Nagra schlägt für Nördlich Lägern einen Lagerperimeter im östlichen Teil des Standortgebietes vor. Frage: Wie belastbar sind die interpretierten Störungen im Grundgebirge und im Jura und in der Trias zwischen CMP 7200 und 8200? Gibt es andere Interpretationsvarianten?

Jura Ost siting region (4)

11-NS-04: Das Profil zeigt ruhige Lagerungsverhältnisse, einzig zwischen CMP 2900 bis 3000 ist im Tiefenbereich der Trias eine Variation in der Mächtigkeit zu beobachten. Ist diese Variation ein Artefakt (z. B. Geschwindigkeitsmodell) oder möglicherweise ein Effekt der Tektonik?

11-NS-06: Dieses Profil zeigt Ähnlichkeiten mit dem Profil 11-NS-04. Wie kann die Anomalie (Verdickung) bei CMP 5800 bis 5900 im Bereich des Muschelkalks interpretiert werden? Existieren ähnliche Strukturen auf der Nachbarlinie 11-NS-04?

11-NS-35: Zu diesem Profil hat das ENSI keine Detailfragen.

Jura-Südfuss siting region (5)

12-NS-42: Der Fokus der Beurteilung in diesem Profil liegt generell auf dem OPA. Spezifische Frage: Wie belastbar ist die Interpretation der Störung bei CMP 3050 bis 3150 im Bereich des OPA? Wie signifikant ist die potentielle Verdickung in der Trias im Teil des Profils süd-südöstlich CMP 2500?

12-NS-44: Der Fokus der Beurteilung in diesem Profil liegt auf den Effinger-Schichten und der Fortsetzung der Born-Engelberg-Struktur in dieses Gebiet. Welche Auswirkungen hat die Verdickung der Trias (duktilen Verhalten) auf die sich spröde verhaltenden Kalkbänke der Effinger-Schichten?

12-NS-53: Im Grundgebirge sind starke Reflexionsbündel zu erkennen. Handelt es sich hier um Permokarbon (zwischen CMP 3600 und 5200)?

1.2.4 Additional questions concerning tectonic zones to be avoided and space requirement

1.1.1.1 Ist der Zusammenhang zwischen dem Rand des Nordschweizer Permokarbontrogs, der Flexur (see NTB 14-02, Dossier II, Fig 4.4-3) und den Störungsbild aus der 3D-Seismik im Zürcher Weinland belastbar?

1.1.1.2 Wie aussagekräftig sind die Neigungskarten des Top Lias?

1.1.1.3 Ist die von der Nagra auf Basis der 2D-Seismik ausgewiesene Flexur am nördlichen Rand des Standortgebiets NL nachvollziehbar und belastbar?

1.1.1.4 Kann aufgrund der Erfahrungen aus dem Standortgebiet ZNO (Hinweis auf Zusammenhang zwischen Permokarbontrug, Flexur und Strukturzone) für das Standortgebiet NL eine potentielle Strukturzone antizipiert werden?

1.1.1.5 Ist es fachlich nachvollziehbar und gerechtfertigt, eine unterschiedliche Anzahl an anordnungsbestimmenden Störungen in den Lagerperimeter der Standortgebiete anzunehmen (zum Beispiel dass für die Standortgebiet NL und JS die Anzahl der Störungszonen viel grösser ist als für die anderen)? Wenn ja, was ist die Datengrundlage für diese Annahme?

1.3 Participation in meetings

My participation in meetings started in August 2013. The ENSI expert team had earlier meetings where I was not involved at that time. Presentations given by Nagra or Nagra-Proseis AG team and ENSI collaborators during the below listed meetings gave supplementary information not included in the reports relevant for this review, but certainly in prior reports (Table 2).

19.08.2013: Brugg, ENSI office. Kick-off Meeting der ENSI-Experten für den Review der 2D-Seismik der Nagra im Rahmen von Etappe 2 SGT. Minutes elaborated by ENSI (29.10.2013, ENSI 33/314).

22.11.2013: Zürich-Oerlikon, Proseis AG office. Review Interpretation 2D-Seismik: Meeting bei Proseis AG Zürich. Discussion on the NAB 13-10. Minutes elaborated by ENSI (17.01.2014, ENSI 33/332).

17.03.2014: Fribourg, University, Anna's office. Presence of T. van Stiphout and Ch. Nussbaum. Presentation of my review on the NAB 13-10. No minutes (see intermediary report).

31.03.2014: Brugg, ENSI office. Workshop: Diskussion der Beurteilungs-ergebnisse 2D-Seismik-Review Schritt 1. Minutes elaborated by ENSI (03.06.2014, ENSI

- 33/359). I could not participate (Entschuldigt in Protokoll). Christophe Nussbaum presented my review.
- 07.11.2014: Brugg, ENSI office. Beurteilung 2D-Seismik der Nagra im Rahmen der SGT Etappe 2 Meeting zu Review Schritt 2. Minutes elaborated by ENSI (05.01.2015, ENSI 33/410).
- 10.03.2015: Brugg, ENSI office (morning). Koordinations-Meeting swisstopo-Sommaruga. Minutes elaborated by ENSI (14.04.2015, ENSI 33/426).
- 10.03.2015: Zürich-Oerlikon, Proseis AG office (afternoon). Fachgespräch zur Interpretation der 2D-Seismik SGT Etappe 2. Discussion on the NAB 14-34. Minutes elaborated by ENSI (02.06.2015, ENSI 33/430).
- 16.03.2015: Bern, swisstopo (afternoon). Mechanical analysis of the eastern end of the Jura (NE Switzerland): role of basement ramps and inherited fault. Minutes elaborated by swisstopo, Christophe Nussbaum (27.03.2015).
- 27.04.2015: Brugg, ENSI office. Workshop: Beurteilungsergebnisse 2D-Seismik-Review SGT Etappe 2. Minutes elaborated by ENSI (09.07.2015, ENSI 33/436). Presentation of my review.
- 22.05.2015: Brugg, ENSI office. Workshop: Fachsitzung zur Interpretation der 2D-Seismik der Nagra. Minutes elaborated by ENSI. Presentation of my review.
- 25.08.2015: Bern, swisstopo. Meeting zur kinematischen Modellierung geologischer Profile. Minutes elaborated by ENSI (10.09.2015, ENSI 33/450).

In addition to afore listed meetings, several informal meetings were organized at Fribourg University with Christophe Nussbaum (person in charge of this review at swisstopo) in order to organize the administrative part of this review (contracts, planning with ENSI) and to discuss scientific issues.

After the last scientific meeting (22.05.2015), ENSI asked me to address questions to Nagra regarding few discussed topic. Two questions (Frage 33 and Frage 34 in Appendices) have been sent to ENSI a couple of days after (29.05.2015). Nagra answered in June (21.06.2015); see questions and answers in Appendices and discussion in §4.2.

More recently a series of questions (Frage 63 in Appendices) addressed to Nagra has been sent to ENSI (1.10.2015); these questions regarding Flexur are related to the additional questions from ENSI on the tectonic zones to be avoided and flexures (additional questions in §1.2.4 and discussion in §3.6).

1.4 Relevant Nagra reports for the assessment

Many reports were available for this review. Table 2 shows the list of reports that were considered for this assessment. The highlighted (in grey) reports were evaluated with special attention. Short critical overview on contents of specific Nagra reports is given in §2.1.

Nagra reference	Title	Authors	Date
NAB 13-10	Regionale strukturgeologische Zeitinterpretation der Nagra 2D-Seismik 2011/12. Textband and Beilagenband.	H. Madritsch, B. Meier, P. Kuhn, Ph. Roth, O. Zingg, S. Heuberger, H. Naef, Ph. Birkhäuser	Juni 2013
NAB 13-40	Gravity Data in Northern Switzerland and Southern Germany.	A.G. Green, K. Merz, U. Marti, T. Spillmann	July 2013
NTB 14-01 Anhang	Sicherheitstechnischer Vergleich und Vorschlag der in Etappe 3 weiter zu untersuchenden geologischen Standortgebiete	Nagra	Dezember 2014
NTB 14-02 - Dossier I	SGT Etappe 2: Vorschlag weiter zu untersuchender geologischer Standortgebiete mit zugehörigen Standortarealen für die Oberflächenanlage. Geologische Grundlagen. Dossier I. Einleitung.	Nagra	Dezember 2014
NTB 14-02 - Dossier II Anhang	SGT Etappe 2: Vorschlag weiter zu untersuchender geologischer Standortgebiete mit zugehörigen Standortarealen für die Oberflächenanlage. Geologische Grundlagen. Dossier II. Sedimentologische und tektonische Verhältnisse.	Nagra	Dezember 2014
NTB 14-02 - Dossier III Anhang	SGT Etappe 2: Vorschlag weiter zu untersuchender geologischer Standortgebiete mit zugehörigen Standortarealen für die Oberflächenanlage. Geologische Grundlagen. Dossier III. Geologische Langzeitenentwicklung.	Nagra	Dezember 2014
NTB 14-02 - Dossier VII	SGT Etappe 2: Vorschlag weiter zu untersuchender geologischer Standortgebiete mit zugehörigen Standortarealen für die Oberflächenanlage. Geologische Grundlagen. Dossier VII. Nutzungskonflikte.	Nagra	Dezember 2014
NTB 14-02 - Dossier VIII	SGT Etappe 2: Vorschlag weiter zu untersuchender geologischer Standortgebiete mit zugehörigen Standortarealen für die Oberflächenanlage. Geologische Grundlagen. Dossier VIII. Charakterisierbarkeit und Explorierbarkeit.	Nagra	Dezember 2014
NAB 14-17	Tektonische Karte des Nordschweizer Permokarbons: Aktualisierung basierend auf 2D-Seismik und Schwere-Daten.	H. Naef, H. Madritsch	Dezember 2014
NAB 14-34	Tiefenkonvertierung der regionalen Strukturinterpretation der Nagra 2D-Seismik 2011-12. Textband, Beilagen, Anhangen	B. Meier, P. Kuhn, S. Muff, P. Roth, H. Madritsch	September 2014
NAB 14-57	Reflexionsseismische Analyse der Effinger Schichten	B. Meier, G. Deplazes	Oktober 2014
NAB 14-58	Vorabdruck_ Reflexionsseismische Analyse des „Braunen Doggers“	B. Meier, G. Deplazes	Dezember 2014
NAB 14-88	Simulation of layout-determining fault networks based on 2D-seismic interpretations: Implications for sub-surface space reserves in geological siting regions in northern Switzerland	G.W. Lanyon, H. Madritsch	December 2014
NAB 14-105	Regionale geologische Profilschnitte durch die Nordschweiz und 2D-Bilanzierung der Ferschubdeformation im östlichen Faltenjura: Arbeitsbericht zu SGT-Etappe 2.	P. Jordan, A. Malz, S. Heuberger, J. Pietsch, J. Kley, H. Madritsch.	März 2015 (available as expert since 27.04.2015)

Table 2 : List of the Nagra reports available for the review. Reports highlighted in grey have been evaluated in details.

2 Data

2.1 Critical overview on contents of Nagra reports

Information on the structures and the faults was included in two main reports (NAB 13-10 and NAB 14-34) concerning the geological interpretation of the seismic profiles from Northern Switzerland. Additional important information or details in order to understand the geological setting, the tectonic zones to be avoided, and the parameters defining the geological siting region were obtained from other reports (see list in Table 2).

Each Nagra (NAB or NTB) report provides a wealth of important information. A noteworthy effort has been done in presenting interpreted and non-interpreted versions of the seismic lines. Some reports are elaborated by Nagra's contractors and are written in parallel by different authors. This leads to some inconsistencies in linking work from one report to another one. A synthesis of the seismic interpretation reports which includes all processing versions (PSTM, DTConv, PSDM) for the Mesozoic layers combined with the interpretation of the Permo-Carboniferous trough is missing. The reader has to go through all the reports to find documents related to a specific seismic line (e.g. Table 6 to Table 10) and then search for explanations in text – especially if there are inconsistencies from one version to another one. In the 10.03.2015 meeting, Nagra suggested to use all the versions for the review (excerpt from Minutes, ENSI 33/426: "Für die Betrachtung bittet die Nagra alle Versionen (PSTM, PSDM und DTconv) zu nutzen. Bei Unklarheiten betreffend Störungen wird die Nagra auf Rückfrage klar Position beziehen, welche Interpretation relevant ist. ").

Several maps (seismic location map, geological map, TWT/Depthing/Velocity/Thickness map for horizons) and seismic lines are presented in Appendices (Beilagen –B– /Anhänge –A–). These are helpful for understanding the work. The updated tectonic map discussed in NAB 13-10 was available only in NTB 14-02 (Beilage 4-1, NTB 14-02, Dossier II). This tectonic map should have been combined with the CMP seismic location map. This is missing as well as a map with location of seismic lines (with CMP) on top of regional fault zones and tectonic zones to be avoided. This would help the reader to localize these zones on the seismic lines. This type of map (e.g. Figure 4.2) has been created by swisstopo for its experts in order to facilitate the review.

NAB 13-10

This *Arbeitsbericht*, referred also as Madritsch et al. 2013, presents the seismic interpretation in time domain of the new acquired (2011/2012) seismic profiles. The location and the trend of the regional faults and the small-scale faults are mapped. The regional fault zones, the tectonic zones to be avoided and the layout-determining faults are not shown on the profiles and not discussed. Links between field structure observations and seismic data interpretation are explained. An updated tectonic map is missing in this report. This report is one of the main reports for this evaluation.

NTB 14-01

This *Technischer Bericht* has not to be reviewed by the 2D-seismic reviewer, but was provided as additional information. In this *Technischer Bericht*, we only considered a couple of figures (e.g. Fig. 4.4-1) regarding the limit of the repository perimeter (*Lagerperimeter*), to be able to

focus on relevant target regions or locations.

NTB 14-02 Dossier II

This *Technischer Bericht* (Dossier II: Sedimentological and geological settings) acts as a kind of synthesis report on the geological outcome of the 2D-Seismic interpretation. It includes some geological fundamentals, few partially balanced cross-sections (without description) based on the 2D-seismic interpretation and the location of the regional fault zones and the tectonic zones to be avoided for each siting region. The updated tectonic map of North Switzerland is enclosed and shows the lateral extend of the main geological structures. However, a seismic location map with CMP on top this tectonic zone map (see discussion above) is missing. The geological interpretation of the sections in this report refers to Jordan et al. 2015 report, which was not available at the time of the main phase of the review and therefore not considered.

NTB 14-02 Dossier III

This *Technischer Bericht* (Dossier III: Evolution of the long-term geology) consists of the description of the recent and long-term geology: neotectonics and erosion. In this technical report, we only considered figures (e.g. Figure 4.4-10).

NAB 14-17

This *Arbeitsbericht* presents the geological interpretation of the Permo-Carboniferous troughs with a major update of the tectonic map of the Permo-Carboniferous troughs from northern Switzerland. The location of the troughs is modeled based on the gravity anomaly map (Green et al. 2013). The authors distinguish between three seismic facies within the central graben. This report is one of the relevant reports for this evaluation.

NAB 14-34

This report completes the NAB 13-10 report and both reports are main reports for this evaluation. It presents the depth conversion of the geological interpretation of the Nagra 2D-seismic survey 2011/2012 and of the older seismic lines. The interpretation of the Near Top Opalinuston horizon is new (not included in the other reports). There is a discussion on the evaluation and differences of the structures (faults) in depth domains. It includes a short description of the layer/thickness model and estimation of the uncertainties of the depth/thickness values for the seismic horizons and for the host rocks.

NAB 14-57

This *Arbeitsbericht*, referred also as Meier & Deplazes (2014a), presents a seismic facies analysis of the “*Effinger Schichten*” layers; we only considered figures (Figs. 10 and 13, NAB 14-57) and *Beilagen* (Beilage 6, Beilage 7, Beilage 8).

NAB 14-58

This *Arbeitsbericht*, referred also as Meier & Deplazes (2014b), presents a seismic facies analysis of the “*Braune Dogger*” layers; we only considered figures (Fig. 8, Fig. 9, Fig. 11 from NAB 14-58) and *Beilagen* (Beilage 3, Beilage 6).

NAB 14-88

This *Arbeitsbericht* discusses how potentially the layout-determining fault could tectonically

affect the different geological siting regions and what the implications are. This study, based on few data, is mainly modelling and conceptual and therefore the practical use of the results remains questionable.

NAB 14-105

This *Arbeitsbericht*, referred also as Jordan et al. 2015, presents geological balanced cross-sections from Northern Switzerland. Several authors have elaborated these sections. This report has unfortunately been received too late in the review process and could not be evaluated here. Some cross-sections are already known through reading of the NTB 14-02, Dossier II report.

2.2 Seismic data

Seismic data available for this review consist of two sets (Figure 2—1):

- 33 old reprocessed 2D-seismic reflection profiles acquired by Nagra between 1982-1992;
- 20 new acquired (2011/2012) 2D-seismic reflection profiles.

A third set of seismic data was used by Nagra for the seismic interpretation. It consists of 19 confidential seismic lines (acquired between 1979-1990) owned by SEAG and reprocessed by Nagra (NAB 13-10). These seismic lines are inserted neither in the NAB 13-10 nor in NAB 14-34 reports. Only one profile (83-SE-03, Beilage 6-12, NAB 14-17) of these SEAG seismic profiles is included in the report NAB 14-17. All SEAG lines could be consulted at Proseis AG office if necessary.

The location of the new seismic survey filled the gap between the old seismic lines recorded by Nagra or by the petroleum industry (mainly SEAG) (Figure 2—1). Both sets provide enough 2D-seismic reflection data to localize the regional geological faults and the tectonic zones to be avoided in the selection process of the radioactive waste repository.

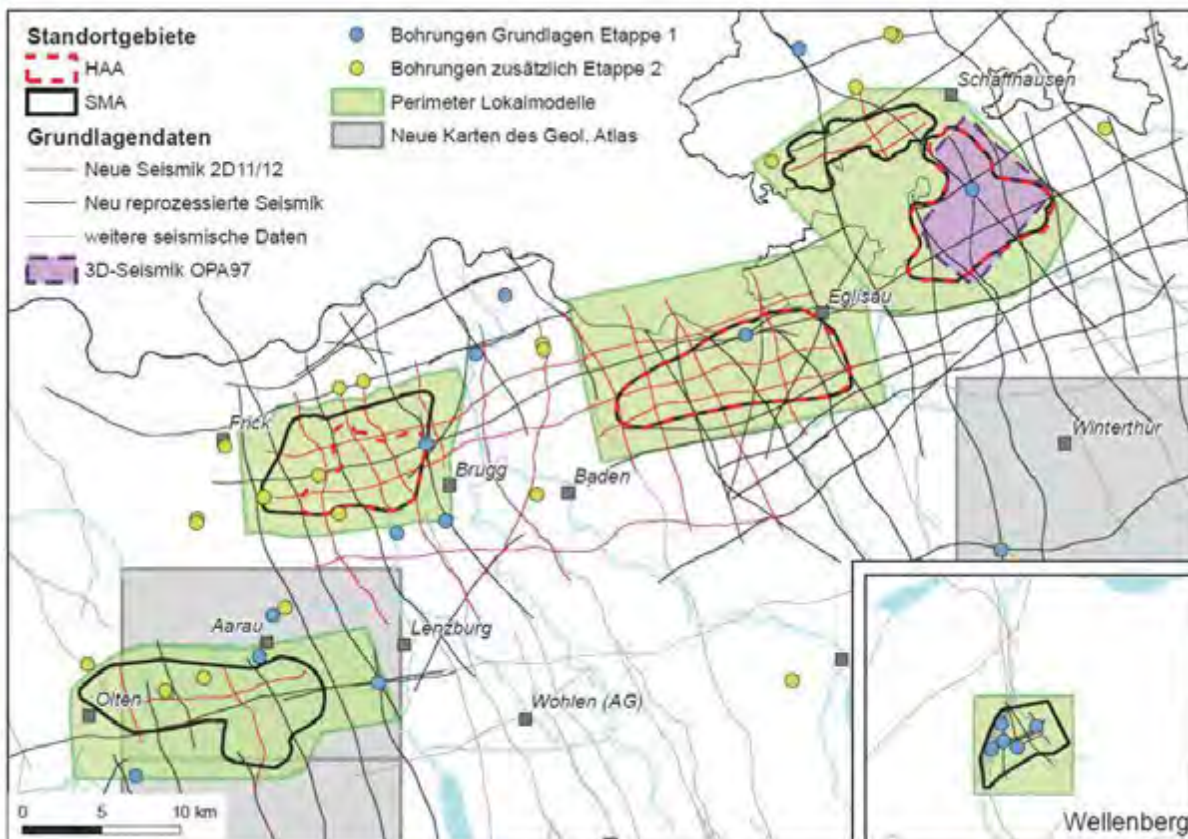


Figure 2—1 : Location map of seismic profiles used by Nagra in SGT E2. The lines in red correspond to the new acquired (2011/2012) seismic data and the ones in black to the reprocessed old seismic lines. From NTB 14-01, Fig. 4.1-1.

The reprocessing of the older lines has yielded in quality with higher resolution of the seismic image and a better lateral continuity of the reflections (Figure 2—2). The quality of the old seismic lines was variable; the reprocessing has produced a homogenous set of data with the same processing parameters representing reliable and high quality images of the subsurface. The new acquired seismic data have been processed in a good way that the resulting seismic images are reliable.

In Figure 2—2, the horizontal scale is missing (it is not shown on the original figure in the NAB 13-10 report) and we assume that the horizontal scale is the same for the fourth lines. Nagra compares the seismic data quality of two seismic lines, which do not have the same direction. Directions have been added for the assessment on top of the Figure: a) strike line WSW-ENE versus dip line, NW-SE and b) two dip lines with a different direction (NNE-SSW, NNW-SSE). Although this is not an optimal way to compare the seismic quality of the lines, we can see an improvement of the seismic image from the old to the new acquired seismic surveys. Supposedly the line in the middle of the Figure 2—2 a and b corresponds to the intersection line between the two lines.

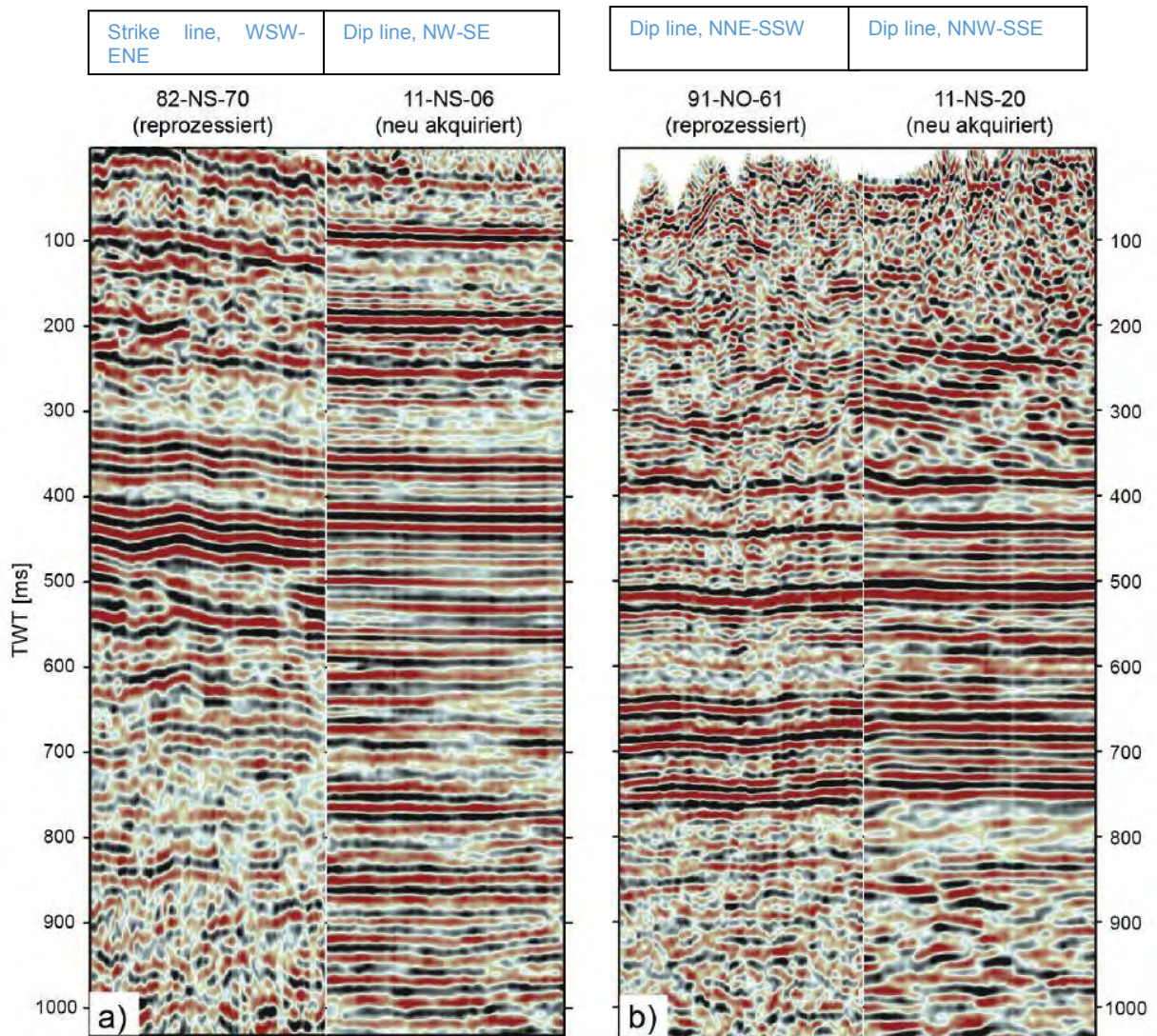


Figure 2—2 : Comparison of the quality of reprocessed seismic lines of the 1982 (a) / 1991 (b) surveys with the new acquired (2011/12) seismic lines. TWT = Two-way travel Time. Modified from NAB 13-10, Fig. 2-3. For location see Beilage 2-1, NAB 13-10.

Both sets of seismic data (old reprocessed and new acquired) include high quality seismic lines, which are suitable for a geological interpretation of the structures within the geological siting region. According to reports for Schritt 1 of the “Data processing” expert team (M. Riede and F. Wenzel), the processing of the seismic data has followed an optimal procedure resulting in a high quality seismic image.

The NAB 13-10 report includes in its *Beilagen* a profile of each of the new acquired seismic line at a 1:50'000 scale. The old reprocessed seismic data are in the Appendix (of NAB 13-10) at the same scale. The datum plane is not indicated on these plates, but we suppose 500m = 0ms TWT. As mentioned in the report NAB 13-10 (p.4), Nagra applies a single Datum Plane to all the seismic lines, which is a logic procedure. On the seismic horizon map derived from the seismic interpretation of the lines (included in the *Beilage* of the same report), the Datum Plane (DP) is 500m (*Bezugsniveau*).

Precise location maps with CMP points along the trace of the seismic lines are included in various reports. Regrettably, this type of seismic location map has not been provided as a layer on top of the tectonic map including the five investigation geological siting regions or on top of the map with the “tectonic zones to be avoided” (see also discussion in §2.1). This makes detailed review and location of structures tedious and difficult.

2.3 Well data

About 10 deep wells are available in northern Switzerland for calibrating the seismic data (Figure 2—3). They were drilled for radioactive waste purpose (Nagra), for search of oil, or for geothermal purposes during different periods, but most of them in 1980's.

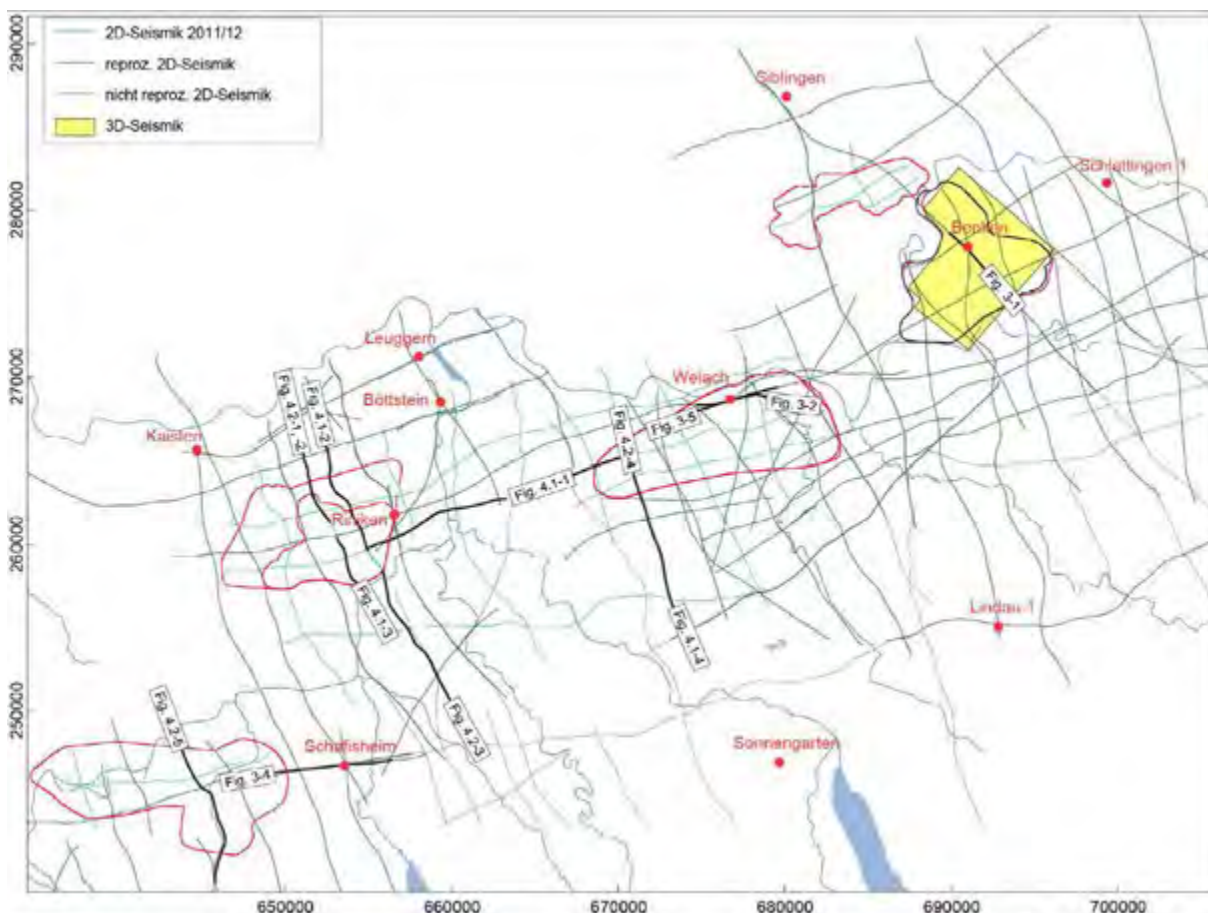


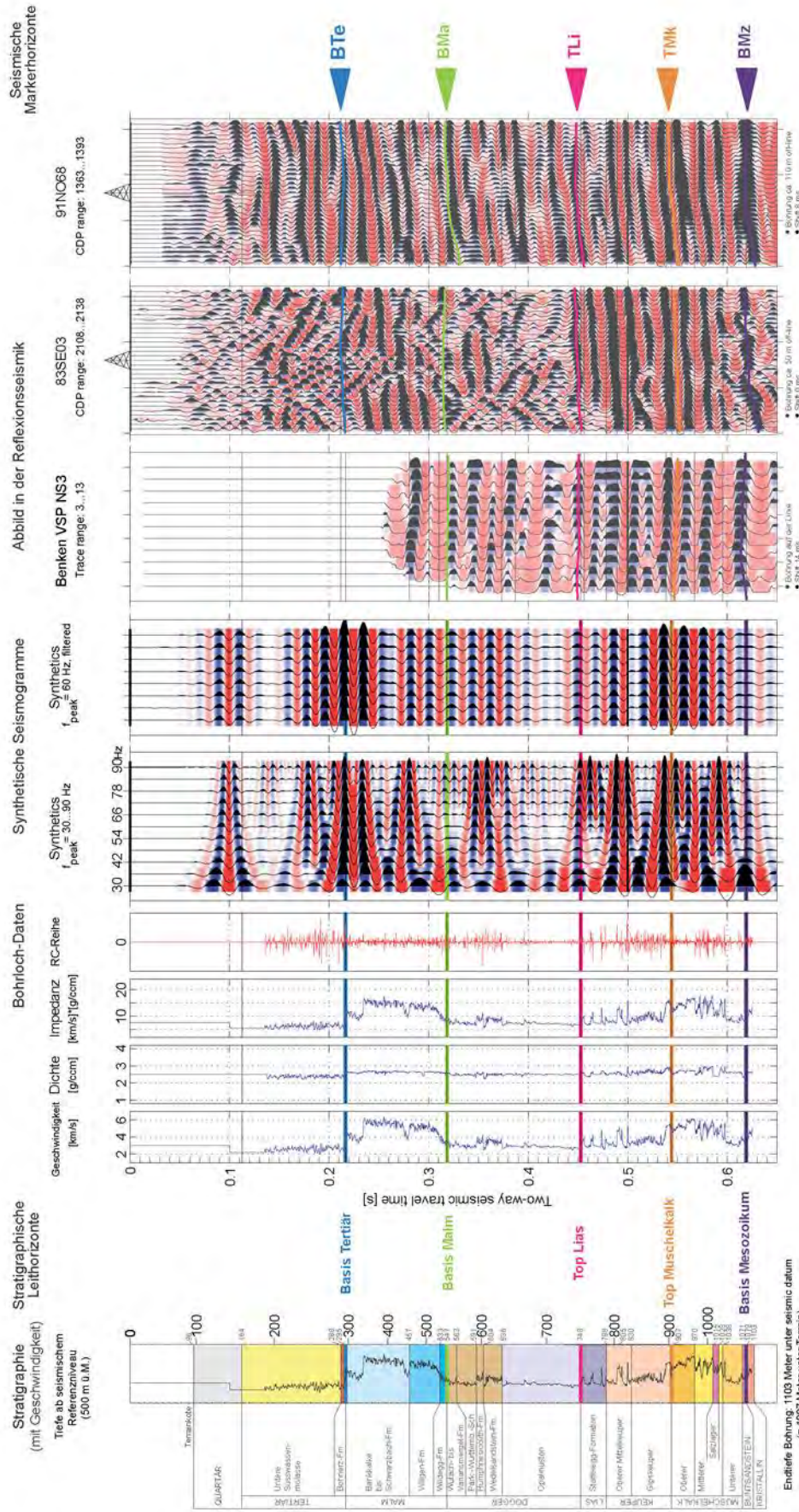
Figure 2—3 : Location map of wells (from NAB 14-34, Fig. 1-1). The Pfaffnau-1 well is located outside of the figure frame SW of the Schafisheim-1 well.

In the NAB 13-10 report, Nagra presented the correlation and seismograms in time for 9 wells (Weiach-1, Riniken-1, Schafisheim-1, Lindau-1, Leuggern-1, Böttstein-1, Pfaffnau-1, Benken-1 –Figure 2.4-, Siblingen-1). Additionally log data from Kaisten-1, Sonnengarten-1 and Schlattingen-1 have been mentioned in other reports (e.g. NAB 14-58). Five horizons have been calibrated and interpreted: Base Tertiary, Base Malm, Top Liassic, Top Muschelkalk and Base Mesozoic.

As explained by Nagra's collaborator during a meeting (22.11.2013), the new seismic survey has been land out with the objective to fill the gap between the old seismic grid rather than to

better correlate the existing wells and seismic lines. Therefore, the new acquired seismic data are not tied to the wells (Table 3). In view of the good quality of the reprocessed seismic lines, we can support this decision.

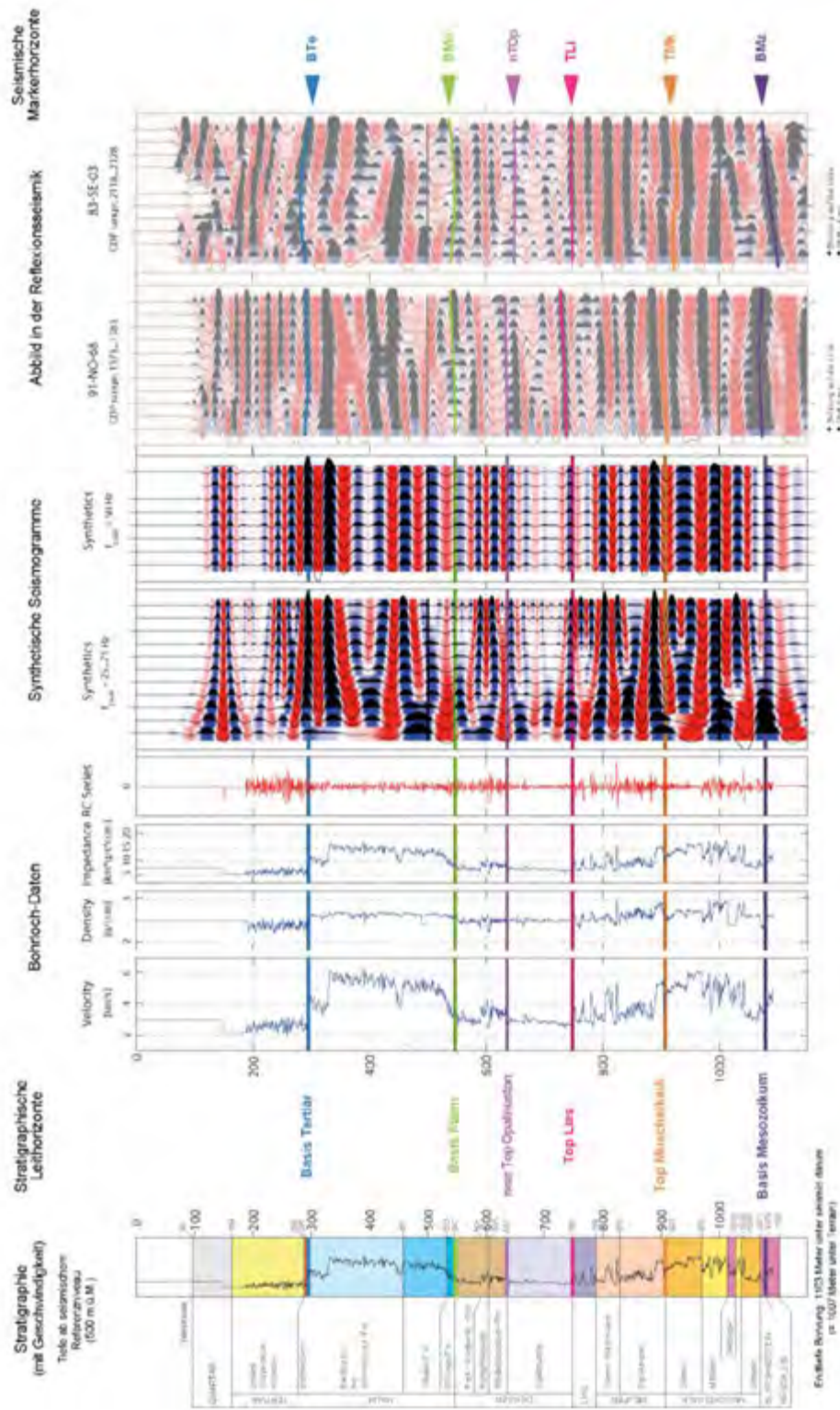
Proseis AG together with Nagra's collaborators have done the interpretation of the well log data and the seismic data. From the boreholes, synthetic seismograms have been generated derived from the acoustic log and the density log data. The correlation and the synthetic seismograms are precise and well done. Even if reflectors are not always of the highest quality, a good correlation could be achieved. In the NAB 14-34 report, seismograms in depth of six wells are presented (Benken-1 – see Figure 2—4, Lindau-1, Pfaffnau-1, Riniken-1, Schafisheim-1, Weiach-1). In addition to the above mentioned horizons, the Near Top Opalinuston reflector is also described.



nagra	
Synthetische Seismogramme Bohrung Benken	
Zeitinterpretation 2D-Seismik 2011/12	DAT.: Juni 2013
BEILAGE 2.2	

NAB 13-10

Figure 2—5: Synthetic seismogram from Benken-1 well in TWT. From NAB 13-10, Beilage 2-2.



nagra NAB 14-34

Synthetisches Seismogramm Bohrung Benken in Tiefe

Tiefenkonvertierung 2D-Seismik 2011/12 DAT. Sep. 2014 BEILAGE 2.2

Figure 2—6: Synthetic seismogram from Benken-1 well in depth. From NAB 14-34, Beilage 2-2.

	Bohrung	Profil	Linien-Offset [m]	Shift [ms]	BMz	TMk	TLi	BMa	BTe
1	Weiach	82-NS-70	0	20	trough	trough	peak	zero→+	peak
		91-NO-75	0	8	trough	trough	peak	zero→+	peak
2	Riniken	82-NS-70	17	0	trough	trough	peak	peak	
		82-NF-30	63	0	trough	trough	peak	peak	
3	Schafisheim	83-SE-07	65	0	peak	trough	peak	zero+→	peak
		82-NF-10	65	8	peak	trough	peak	zero+→	peak
		83-NS-22	79	12	peak	trough	peak	zero+→	peak
		82-NS-20	81	8	peak	trough	peak	zero+→	peak
4	Lindau-1	79-SE-46	21	0	peak	peak	peak	zero→+	peak
		84-SE-05	125	0	peak	peak	peak	zero→+	peak
5	Leuggern	82-NF-50	64	0	peak				
6	Böttstein	82-NX-40	77	0	zero→+	trough			
		82-NF-50	26	0	zero→+	trough			
7	Pfaffnau-1	83-NF-02	40	8	peak	peak	peak	peak	peak
8	Benken	91-NO-68	109	8	peak	trough	peak	zero→+	peak
		83-SE-03	52	0	peak	trough	peak	zero→+	peak
9	Siblingen	91-NO-68	380	0	peak	zero→+			

Table 3: Well list with convention for picking of the seismic horizons. Wells are tied to old reprocessed seismic lines. BMz = Base Mesozoic; TMk = Top Muschelkalk, TLi = Top Liassic, BMa = Base Malm; BTe = Base Tertiary. From NAB 13-10, Tab. 2.

As general remark (especially in reports – *Text und Beilagen*- NAB 13-10 and 14-34): the well names are not defined clearly in the reports and not referred exactly on the maps (Figures, *Beilagen*). Industry (oil or geothermal) well names have a number after the name (e.g. -1, -2) which informs on the number of wells at the same location. In Nagra's reports, the number has been added rarely only and not in a consistent way. As an example in Weiach there are two wells (-1, -2) and the number should be mentioned when referring to this well. The same remark is applicable for the Schlattigen wells. Although Sonnengarten-1 well is mentioned, it is however not described in the text.

Two wells discussed in the reports show imprecise data:

- In the *Beilagen* of reports NAB 13-10 and 14-34, Nagra presents Pfaffnau-1 well with Permo-Carboniferous sediments. When reconsidering the analyses of the samples of the well, Matter et al. (1987) mentions that the Permo-Carboniferous unit is not present in the well. The latter unit corresponds to Buntsandstein sediments. In a meeting (10.03.2015), Nagra mentioned that they know this paper, but they rather refer to other papers. Minutes of the 10.03.2015 meeting (ENSI 33/426): „Die Angaben von Buchi wurden sowohl in der regionalen Kompilation von Kämpfe 1984 (Institut für Geologie und Paläontologie, Universität Stuttgart) als auch der Kompilation von H. Naef in NAB 06-26 («Permocarboniferous?») übernommen.“ However, report NAB 06-26 doesn't seem to mention it.

- The Schlattingen-1 well reaches the crystalline basement beneath the Permian sediments (circa 50m?). *Beilage* 6-17 of NAB 14-17 report shows a yellow circle for the Schlattingen-1 drill hole (Figure 3.9), meaning presence of Permian sediments only despite drilled crystalline basement, which is an error. The circle should be filled by green color (*Perm + Kristallin* in the legend).

The depth values of the stratigraphic horizon in the wells are the only reliable and precise depth values that exist. The seismic tie to well gives a difference of +/- 20m already at the well location. For example, the Near Top Opalinuston horizon is not well defined in the wells.

2.4 Depth conversion of seismic profiles

The NAB 14-34 report presents the PSDM version (PSDM depthing, *Pre-Stack Tiefenmigration*) of the seismic lines. The methodology used for the depth conversion and the velocity model is beyond the scope of this geological review and is evaluated by M. Riede and F. Wenzel.

The PSDM profiles should be compared to the PSTM version (Pre Stack Time Migration, *Pre Stack Zeitmigration*) or the DTConv version (Depth-Time conversion), which is considered as an end product (NAB 14-34, Rybarczyk 2012).

The PSDM version is presented in the Appendix 2 of NAB 14-34 report for each seismic line (reprocessed and new acquired surveys) at the 1:50'000 scale. For the new seismic survey, a comparison between the PSTM, DTconv, PSDM (included the velocity model) is presented in Appendix 1 of NAB 14-34 for each seismic line. Profiles are vertically exaggerated (not to scale).

The horizon seismic interpretation on the PSDM version of the seismic lines is taken from NAB 13-10 report. The seismic interpretation of the Near Top Opalinuston horizon is included in the PSDM version, which was not the case in the NAB 13-10 report. Almost all the faults that were interpreted on the PSTM version were transferred on the PSDM version. According to Nagra, the PSDM version shows a better image, so in my opinion a reinterpretation of some fault zones should have been done by Nagra. Few critical cases are discussed in the NAB 14-34 report. An assessment on these cases (e.g. Fig. 4.3, NAB 14-34) is given in §3.5 which discuss the fault interpretation by Nagra.

2.5 Seismic maps

Structural maps at scale 1:100'000 in TWT for each seismic horizon are included in the NAB 13-10 report. Enlargements of the maps at 1:50'000 are presented for each geological siting region. Depthing structural maps for each seismic horizon are presented in report NAB 14-34 at 100'000 scale. These maps have not been evaluated in detail, but were useful for correlation and location of structures/faults.

3 Geological elements interpreted on seismic profiles

3.1 Seismic horizons

A general characterization of seismic horizons is difficult due to the change of the geological setting, of the sedimentological facies change and of the geophysical parameters of the lines. Interpretation has been made mostly in a careful way by the Nagra and Proseis AG team. Seismic horizons have been followed on seismic profiles in closed loops, starting from the wells (seismic tie to well, §2.3).

Five major seismic horizons have been interpreted on all the seismic lines and both sets of seismic data (NAB 13-10): Base Tertairy (BTe), Base Malm (BMa), Top Liassic (TLi), Top Muschelkalk (TMK), Base Mesozoic (BMz). In the NAB 14-34 report, the Near Top Opalinuston horizon is added (Figure 3—1).

In the first step of this evaluation (*Schritt 1*, NAB 13-10), I asked (22.11.2013 meeting, ENSI 33/332 minutes) why Nagra has not interpreted more seismic horizons, e.g. Top Triassic and Top Opalinuston? H. Madritsch's (Nagra) answer was that "The five seismically interpreted horizons included in the NAB 13-10 report (Figure 3—4) are those that were defined during the Stage 1 of Nagra's investigations and seismic interpretation. The choice of the interpreted seismic horizons was made on the quality of the reflectors and the lateral continuity rather than on the stratigraphic unit limits. These seismic horizons are named Base or Top of the concerned stratigraphic limit. Additionally more horizons are already picked in the computer work station on the seismic lines (Near Top Effinger Schichten, Near Top Opalinuston). These horizons are labelled with the prefix "Near" due to the difficulty in picking the reflector. In a later meeting (7.11.2014, ENSI 33/410 minutes, discussion on the NAB 14-34 report), Ph. Birkhäuser (Nagra) mentioned that the Near Top Opalinuston horizon quality is meant to be conceptual (see detail in §3.2).

In the NAB 14-57 and 14-58 reports, additional seismic horizons have been presented in order to demonstrate the change of facies thickness (Effinger Schichten layer and Brauner Dogger layer) (Figure 3.2).

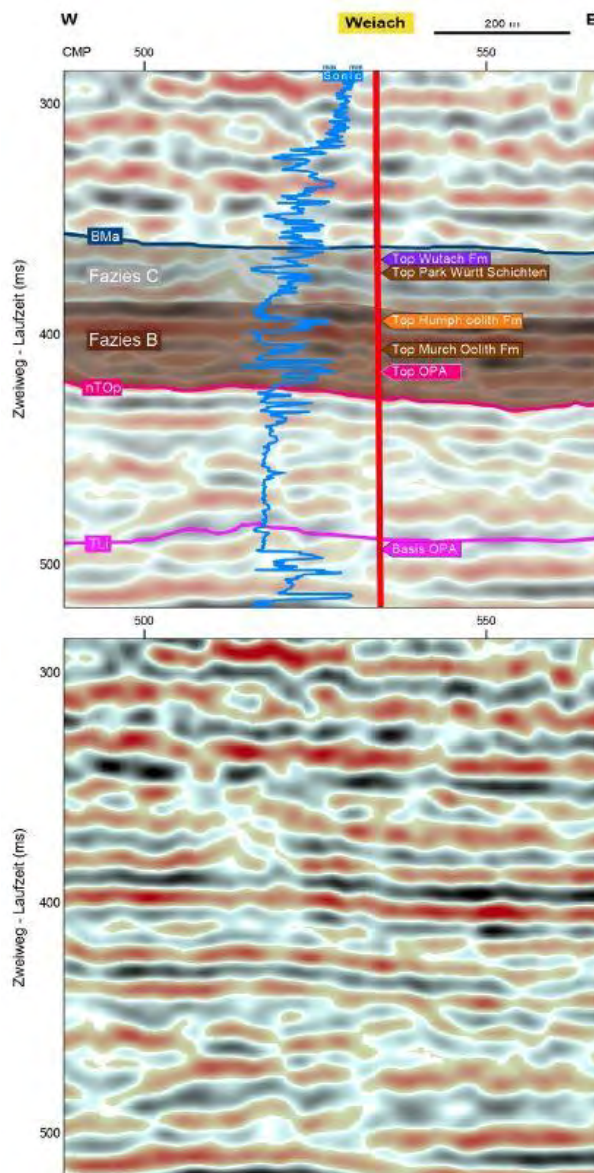


Figure 3.2: Additionally seismic horizon interpretation in Weiach-1 well for the “Brauner Dogger”. Comparison of the sonic log with the seismic line 91-NO-75. From NAB 14-58, Fig. 8.

Base Tertiary, Base Malm /Top Dogger

No comments.

Near Top Opalinuston

This seismic horizon is very difficult to interpret, because it is a non-reflective horizon. The Opalinuston layer is a clay rich horizon, which will appear as a transparent unit (non-reflective facies). The lateral continuity is not visible on seismic lines. The Opalinuston bed thickness is based mainly on the wells, because it is too imprecise to calculate it from seismic interpretation.

Top Liassic /Base Opalinuston, Top Muschelkalk

No comment.

Base Mesozoic

This seismic horizon corresponds to the beginning of a new sedimentary cycle on top of the Paleozoic sediments or crystalline metamorphic rocks. This horizon is important for the geological context and especially also for the understanding of the Permo-Carboniferous through edges. As it is mentioned in the NAB 13-10 report, it is difficult to interpret reflections below Base Mesozoic horizon, because the presence of reflections does not mean the presence of Permo-Carboniferous sediments (e.g. discussion on Benken-1 well, Fig. 3-3, NAB 13-10).

3.2 Classification of the reflection quality of interpreted seismic horizons

A classification of the reflector quality (Table 4, Figure 3.3) has been established by Nagra in comparison to the one from Sommaruga et al. (2012). It depends on the quality of the reflectors and on the certainty of the interpretation (lateral continuity of the reflector, tectonic setting). The quality class of seismic horizon is interpreted in the NAB 13-10 report, but it has not been applied to the depth converted version (PSDM) in report NAB 14-34.

Three quality classes of the seismic horizons were assigned (1 – *gut definiert*-, 2 – *ausreichend definiert*-, 3 – *schlecht definiert/konzeptionell*-). The quality was evaluated by Nagra-Proseis AG team on the strength and the lateral continuity of the seismic reflection, correlation with geological outcrops and on the confidence in the interpretation of a specific seismic reflector. This may explain why in some cases low strength and lateral continuity reflections could be assigned in class 2 or 1. This issue has been discussed with the Nagra –Proseis AG team at the 22.11.2013 meeting.

The quality class attributions by Nagra-Proseis AG team together to horizons in report NAB 13-10 is mostly logic, but in some cases it could be reconsidered and given a higher class number (lower quality). The Base Mesozoic horizon (BMz) is often represented by a class 1 quality horizon ("*gut definiert Qualität des interpretierten Markerhorizonts*"); class 2 or 3 would be more appropriate for the strength of the reflection. I suppose the confidence of the interpreter knowing the geological context has pushed to attribute a better class. It would have been more appropriate to remain conservative.

Near Top Opalinuston horizon is not included in the NAB 13-10 report and therefore no quality class are attributed to it. It is very difficult to map it, and sometimes impossible. As has been discussed in the 10.03.2015 meeting, Nagra mentioned that this horizon is conceptual. From the minutes (ENSI 33/430) of the meeting: „*P. Birkhäuser hält abschliessend fest: Wäre der Hilfshorizont nTop in der Zeitinterpretation (NAB 13-10) dargestellt worden, wäre er als gepunktete Linie, sprich konzeptionell, eingezeichnet worden*“. In my opinion, Nagra should have done the exercise to interpret the Near Top Opalinuston horizon on the PSTM version for consistency reason. I agree that in many places the quality class of this seismic horizon would be conceptual, but certainly not everywhere (e.g. on the seismic line 11-NS-16, CMP 5150-4950). If Nagra's comment is justified, it brings the question on the confidence in mapping the Near Top Opalinuston horizon and the depth of this horizon.

Qualitätsklassifizierung Markerhorizonte		Qualitätsklassifizierung Störungen	
————	gut definiert	————	robust
- - - - -	ausreichend definiert	- - - - -	ungewiss
.....	schlecht definiert / konzeptionell	konzeptionell

Figure 3.3: Description of the quality classes of the seismic horizons (on the left) and faults (on the right) as shown on the seismic lines. From NAB 13-10, Fig. 3-2.

Reflexions-qualität	Interpretations-gewissheit	Qualität des interpretierten Markerhorizonts	Klasse	Situationsbeispiel
sehr gut	gross	gut definiert	1	sehr deutliche & kontinuierliche Reflexionen in nur geringfügig tektonisch beanspruchtem Bereich und/oder nahe einer Tiefbohrung bzw. geologischen Aufschlüssen
sehr gut	gering	ausreichend gut definiert	2	sehr deutliche & kontinuierliche Reflexionen in tektonisch stark beanspruchtem Bereich abseits von Tiefbohrungen bzw. geologischen Aufschlüssen
gut	gross	ausreichend gut definiert	2	deutliche & weitgehend kontinuierliche Reflexionen in nur geringfügig tektonisch beanspruchtem Bereich und/oder nahe einer Tiefbohrung bzw. geologischen Aufschlüssen
gut	gering	schlecht definiert	3	deutliche & weitgehend kontinuierliche Reflexionen in tektonisch stark beanspruchtem Bereich abseits von Tiefbohrungen bzw. geologischen Aufschlüssen
schlecht	gross	ausreichend gut definiert	2	undeutliche & wenig kontinuierliche Reflexionen in nur geringfügig tektonisch beanspruchtem Bereich und/oder nahe einer Tiefbohrung bzw. geologischen Aufschlüssen
schlecht	gering	konzeptionell	3	undeutliche & wenig kontinuierliche Reflexionen in tektonisch stärker beanspruchtem Bereich abseits von Tiefbohrungen bzw. geologischen Aufschlüssen

Table 4 : Classification of the reflection quality on the interpreted seismic horizons. From NAB 13-10.

3.3 Fault definition

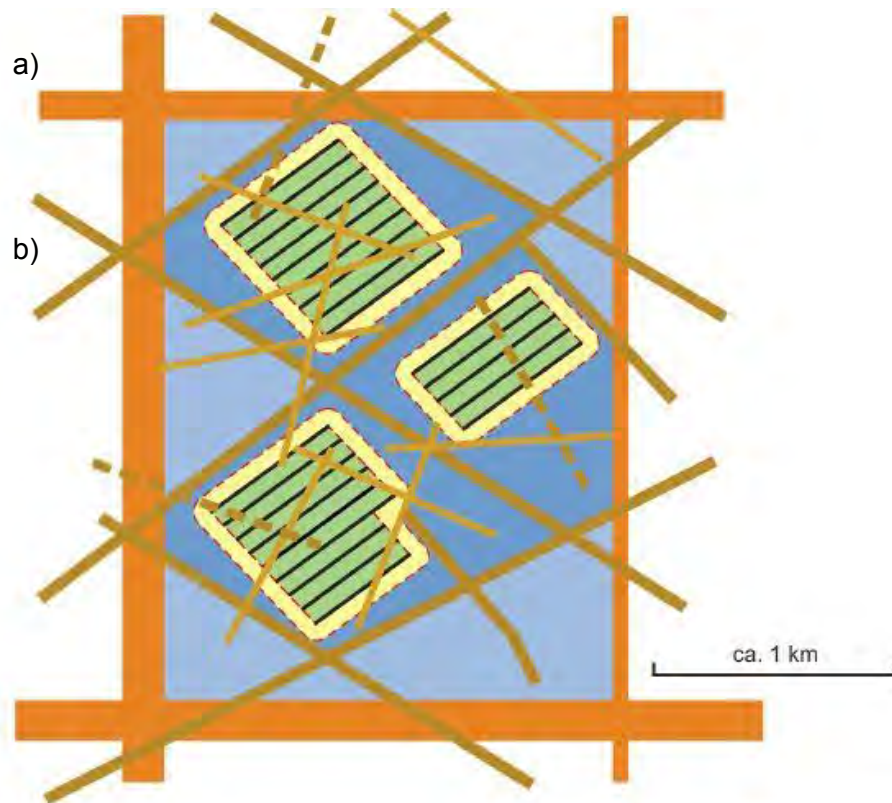
The identification of the geological faults is one of the important parts of the 2D-seismic interpretation work. The following explanations are based on the NAB 13-10 report.

On the seismic profiles, faults with a vertical offset > 10 ms in TWT displacing a stack of reflection were interpreted by Nagra-Proseis team. Considering a high average seismic velocity (4000 m/s for Jura Südfuss siting region in Table 4 from NAB 13-10) between the Base Malm – Top Liassic interval, the 10 ms offset corresponds to a vertical displacement of circa 25 +/-

10 meters. Vertical offsets < 10 m were not systematically interpreted, because in many cases it was not clear if the feature was a real geological structure or a seismic processing artefact. The resolution of 2D-seismic lines within the Opalinuston unit is close to 20 m. This minimum has been critical in the elaboration of the fault element classification (Figure 3.4). Fault offsets > 20 m within a 50 – 100 m thick geological unit (e.g. Opalinuston) planned as a radioactive waste host rock, are considered problematic for a repository. See also discussion in §3.4.

Nagra's concept on faults is related to the relevance of the faults within a geological siting repository. This concept has been developed with civil engineers, taking into account mechanical problems of the rocks (*Wirtgesteine* and *Rahmengesteine*) within the repository and has resulted in a classification with different types of geological elements (Figure 3.4, Figure 3.5). Two of them are fundamental for this review (see also description of point a) and b) in the Figure 3.4):

- a) Geological elements defining siting region boundaries including **regional faults** (*regionale Störungen*) and tectonic zones to be avoided (*zu meidende tektonische Zonen*)
- b) Geological elements defining layout of disposal area including layout-determining geological elements (*anordnungsbestimmende Störungen*).






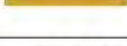
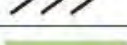



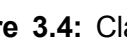
Symbol	Description	Significance
	a) area-defining geological elements	defining siting region
	b) layout-determining geological elements	defining usable disposal zone and layout of disposal area
	emplacement-determining geological elements	defining emplacement within the disposal room area
	small scale geological elements	taken into account during safety analysis
	disposal room	–
	disposal room area	–
	disposal area	–
	usable disposal zone	–
	non-usable disposal zone	–

Figure 3.4: Classification of geological/tectonic elements and their relevance concerning the layout of a geological repository at depth (modified from NAB 14-88, Fig. 2-1). a) Area-defining geological elements = regional faults (*regionale Störungen*); b) layout-determining geological elements = layout-determining faults (*anordnungsbestimmende Störungen*).

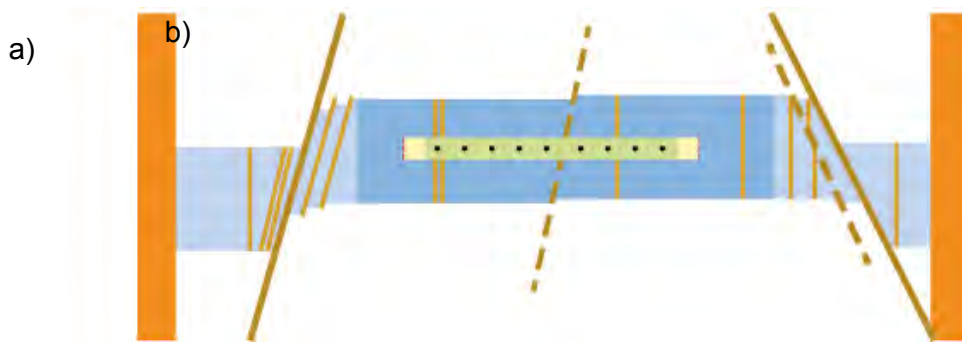


Figure 3.5 : Cross-section view of geological/tectonic elements and their relevance concerning the layout of a geological repository at depth (see Figure 3.4 for legend). Modified from NAB 14-88, Fig.2-2.

Additionally, the following type of faults or zones have been presented by Nagra during the 22.11.2013 meeting (see minutes ENSI 33/332):

Regional fault area (regionale Störungszone)

This area is determined by faults which have been interpreted on several seismic profiles and have a km long lateral extension. It limits small-scale fault areas. The regional faults are taken from the seismic interpretation in the NAB 13-10 report. Minimal displacement of these faults is circa 20 m (see above). These regional faults (thrust or normal faults) have been mapped by Nagra and are shown in red on the general map of Figure 3.6.

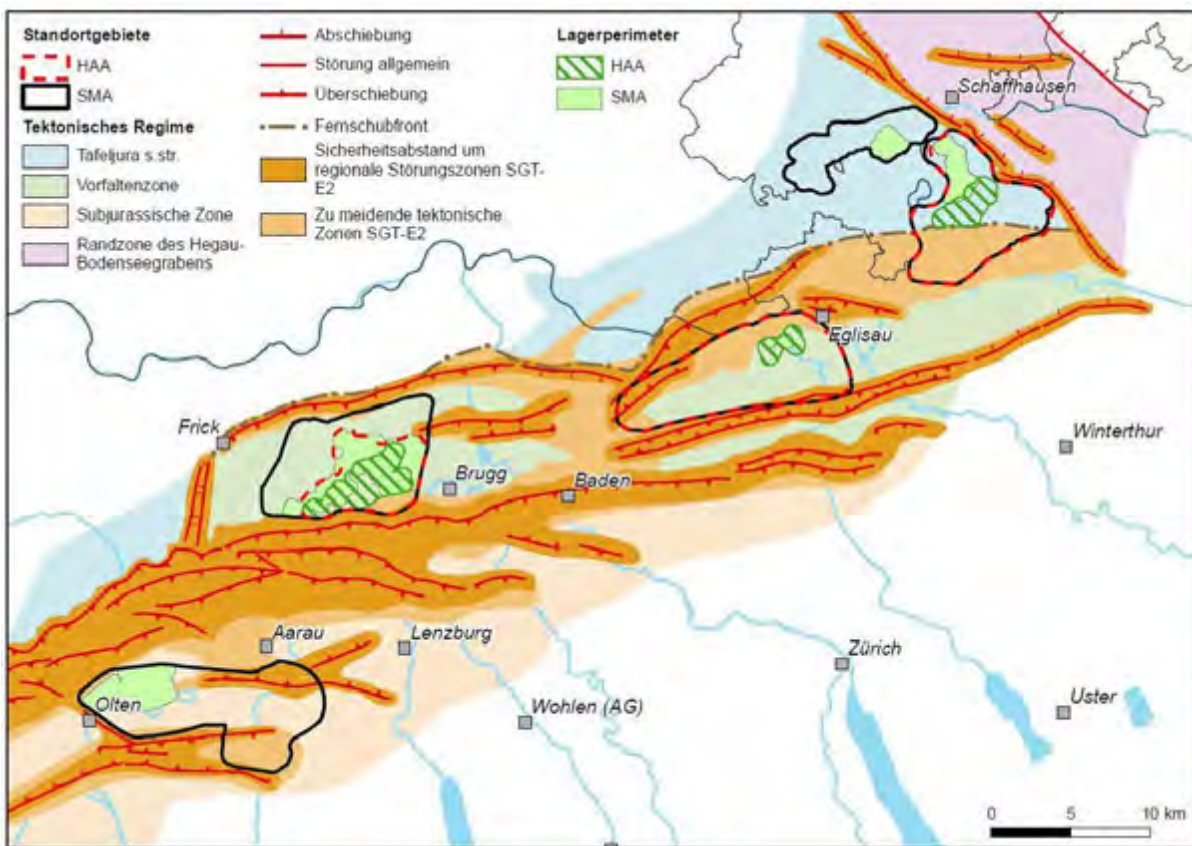


Figure 3.6: Location map of the regional fault zones and tectonic zones to be avoided (*zu meidende tektonische Zonen*) in northern Switzerland. From NAB 14-01, Fig. 4.4-1.

Tectonic zones to be avoided (zu meidende tektonische Zonen)

These zones were introduced in the Stage 2 (*SGT – E2*) by Nagra in order to refine or optimize the potential siting area in the underground for the nuclear waste repository (*Lagerperimeter*). In Stage 2 (*SGT - E2*) Nagra has to exclude areas, not suitable for the construction of a repository (Figure 3.6). These zones have been defined on the presence of faults or folds, which show indications of late Cenozoic reactivation. The limit of these zones is based on the seismic interpretation of the profiles. The NAB 13-10 report is considered by Nagra as a *Rohdaten* report for this issue.

These important zones used by Nagra to refine the repository perimeter are regrettably not mapped on the seismic location maps showing CMP (see §6.2.1 and §6.4) neither on the seismic profiles of the NAB 13-10 or NAB 14-34 reports.

Layout-determining faults (anordnungsbestimmende Störungen)

These faults are defined by Nagra from an engineering perspective, where the vertical offset is close to the limit of the 2D-seismic resolution (>20 m). No correlation from one seismic line to another can be made. This type of faults has been interpreted on one seismic line only, as local structure and does not have a clear geological extent over a long distance. These faults are from the interpretation of the NAB 13-10 report. This type of faults will be considered more carefully in Stage 3 (*SGT – E3*) with the availability of 3D-seismic surveys. They are not used to define the limits of the repository of the geological siting region. The concept of the LDF faults has been discussed in the NAB 14-88 report (Simulation of layout-determining fault networks based on 2D-seismic interpretations: Implications for sub-surface space reserves in geological siting regions in northern Switzerland). They are almost not discussed in the other reports, making it difficult to assess them.

Small-scale geological elements

Small-scale geological elements have a vertical offset <20 m. These small elements are considered during the safety analysis (Figure 3.4). Faults and folds that are best defined as being of second-order importance for *SGT – E2* have not been marked on the interpreted sections.

It is important to note, that faults showing smaller vertical offsets (small-scale faults) may also be relevant for *Lagerperimeter* of the repository for other reasons (hydrogeology, long-term safety etc.). In NAB 14-88 report, it is mentioned that in an assessment of space reserves at depth from an engineering perspective, these kinds of small-scale tectonic faults and associated issues are not addressed.

In my opinion, layout-determining faults, small-scale elements and their geological meaning have to be analyzed carefully during Stage 3 (*SGT - E3*). In Stage 2 (*SGT – E2*), it is difficult to assess these mentioned elements because they were not really discussed by Nagra in the reports.

3.4 Classification of seismically interpreted faults

The classification of quality for the interpreted faults (Figure 3.3) is similar to that proposed for the seismic horizons (see also Sommaruga et al. 2012). The class quality of faults is interpreted in the NAB 13-10 report, but it has not been done on the depth converted version (PSDM) in

report NAB 14-34.

Three quality classes were assigned (1 - *robust*-, 2 - *ungewiss*-, 3 - *konzeptionell*-) (Table 5, Figure 3.3). The quality was evaluated on the offset of reflection and the reflection related quality class.

Beurteilungskriterium	Beurteilung der Störungsinterpretation	Klasse
Verstellung eines seismischen Markerhorizonts der Qualitätsklasse 1 oder 2	robust	1
Verstellung eines seismischen Markerhorizonts der Qualitätsklasse 3	ungewiss	2
Basierend auf regionalgeologischen Konzepten oder aufgrund der Verstellung eines Markerhorizonts der Qualitätsklasse 4	konzeptionell	3
Gemäss in geologischen Karten publiziertem Oberflächenaufschluss	geologisch beobachtet	1

Table 5 : Description of the quality classes of the seismically determined faults (as shown on the seismic lines). From NAB 13-10, Tab. 5.

In the NAB 13-10 report, there is no description of the correlation on the maps between fault quality classes. It would have been interesting to add a symbol for the faults on the seismic horizon TWT maps (which are included in the *Beilagen* of the NAB 13-10 report), which illustrates the class quality of the faults (similar to Figure 3.3). A single fault could have a different seismic expression from one line to another. Therefore, it is not necessary to correlate the same quality class for a single fault (lateral variation), but at least this information should be shown on the map.

3.5 Interpretation of faults by Nagra

In the 22.11.2013 meeting (ENSI 33/332 minutes), the experts discussed the interpretation of the faults on the seismic lines and also asked the Nagra - Proseis AG collaborators why some rather obvious faults on the seismic profiles had not been interpreted. The answer was that these faults were usually part of broad fault zones (regional fault zones), which would not be considered as potential nuclear waste repository in the SGT - E2. For consistency reasons, Nagra should have interpreted also these faults.

In the NAB 14-34 report (see §4.1.1, *Übertragung und Anpassung der Zeitinterpretation*), Nagra discusses the transfer of the interpretation from the PSTM/DTConv seismic line version to the PSDM (depth converted) version. Almost all the faults that were interpreted in the NAB 13-10 report were kept. As an example, they show the seismic line 11-NS-04 (Fig. 4-3, NAB 14-34). On the PSTM version from NAB 13-10, no real offset was shown for this line. Nagra, in its report, writes that the PSDM version shows a better image, and in this case, we have continuous reflections. Therefore, it would have been more comprehensible to remove the fault. Nagra's answer to my comments (see minutes ENSI 33/426) during the meeting of the 10.03.2015 in Proseis AG office:

„Laut Nagra wurden generell die Brüche aus den Profilen der PSTM in den Profilen der PSDM und DTconv beibehalten. Es gibt jedoch einige Ausnahmen wie z.B. in Seismiklinie 11-NS-16 bei CMP 4200. Die Nagra hält fest, dass grundsätzlich die Interpretation aus der PSTM beibehalten wurde und, wo dies nicht der Fall ist, die Änderungen im Bericht NAB 14-34 vermerkt wurden. Für die Betrachtung bittet die Nagra alle Versionen (PSTM, PSDM und DTconv) zu nutzen. Bei Unklarheiten betreffend Störungen wird die Nagra auf Rückfrage klar Position beziehen, welche Interpretation relevant ist.“

Although a small number of faults are not included on the maps and some minor faults are not marked on the interpreted 2D-seismic sections, Nagra emphasized that these features would be considered during the development of regional tectonic and dynamic models. In the Stage 3 (SGT – E3), based on 3D-seismic data, Nagra will reconsider these faults and reassess them. To avoid discussions and misunderstanding for the experts and for reasons of “Nachvollziehbarkeit”, it would have been clearer to interpret all the faults (major and minor) on the 2D-seismic data and mark them on the horizon maps.

The maximum length of a fault that could be missed in Nagra’s maps is determined by the space between the seismic lines. The maximal distance between two neighbour and parallel seismic lines depends on the profile coverage for a considered area.

The interpretation of the Base Mesozoic horizon beneath the Jura main décollement zone has not been done accurately. This topic has been debated in the 10.03.2015 meeting in Proseis AG office. Below an excerpt from the minutes (ENSI 33/426) is shown.

Question III.3: “Beneath the main Jura thrust, we observe in your interpretation on the PSDM Version a sag structure for the Base Mesozoic horizon. This sag structure is due to a velocity problem under the Jura anticline and is not a real structure in my opinion (e.g. line 11-NS-16 in Fig. 4-4, NAB 14-34). On the TWT version, the interpretation should follow the reflections, which often shift upwards under the "anticline". This change in interpretation on the TWT version would result in a different image on the depth-converted version. Did you consider to go back to change the interpretation for this horizon?”

„Die Nagra erläutert, dass sie dieses Phänomen detailliert analysiert und im Bericht NAB 14-34 adressiert und diskutiert hat (siehe Beilage 2). A. Sommaruga betont, dass der von ihr beobachtete Effekt in mehreren Profilen mit der Jura-Hauptüberschiebung zu sehen ist. Die Nagra hält den Vorschlag von A. Sommaruga die Interpretation in Zeit nachträglich zu ändern, um diesem Phänomen entgegen zu wirken, letztendlich für nicht sinnvoll (auch aus Transparenzgründen). Viel eher schiene es ihr sinnvoll, dass das der Tiefenkonversion zugrundeliegende Geschwindigkeitsmodell auf Basis einer z.B. durch Bilanzierung verifizierten Strukturinterpretation (siehe NAB 14-105) geologisch zu plausibilisieren und die Tiefenkonversion anschliessend noch mal durchzuführen wäre. Für SGT - E2, in welcher derartig grosse Störungszonen grossräumig abgegrenzt werden, erscheint ihr ein derartig iteratives Vorgehen aber nicht stufengerecht.“

According to me, this iterative exercise would have been useful in order to constrain better the geological/balanced cross-sections.

Some complex faulted and/or folded zones identified on the seismic sections could be interpreted in terms of different structural models. The Stadel-Irchel anticline is a very good

example of these zones. Two alternative models are well illustrated and discussed by Nagra in NAB 13-10 on Fig. 6-3 (see also discussion in §6.4.3). This type of presentation and discussion could have been applied for other structures e.g. Born anticline (see also discussion in §6.4.5).

3.6 Geological structures

Four geological siting regions are located in the Molasse basin and the Jura foreland fold-and-thrust belt (Figure 3.7). A fifth geological siting region, Südranden, is located entirely in the Tabular Jura, north of the seismic front of the Jura deformed zone. Structural elements seen on the seismic lines are folds, thrust faults, reverse faults, normal faults and structures associated to these elements.

Anticlines and lineaments

Identification of the anticlines and lineaments (the latter term is used by Nagra, but not clearly defined) in northern Switzerland has already started in Stage 1 (*SGT - E1*) and has further been investigated in details in Stage 2. Thanks to the new acquired and the old reprocessed 2D-seismic data, faults could be correlated laterally with more confidence. Nagra has given local names to anticlines and lineaments, which are seen in the Figure 3.8. Some of these structures are discussed in Chapter 4, where specific seismic profiles are discussed. The Schönenwerd-Eppenwerd anticline is a structure newly identified in Stage 2.

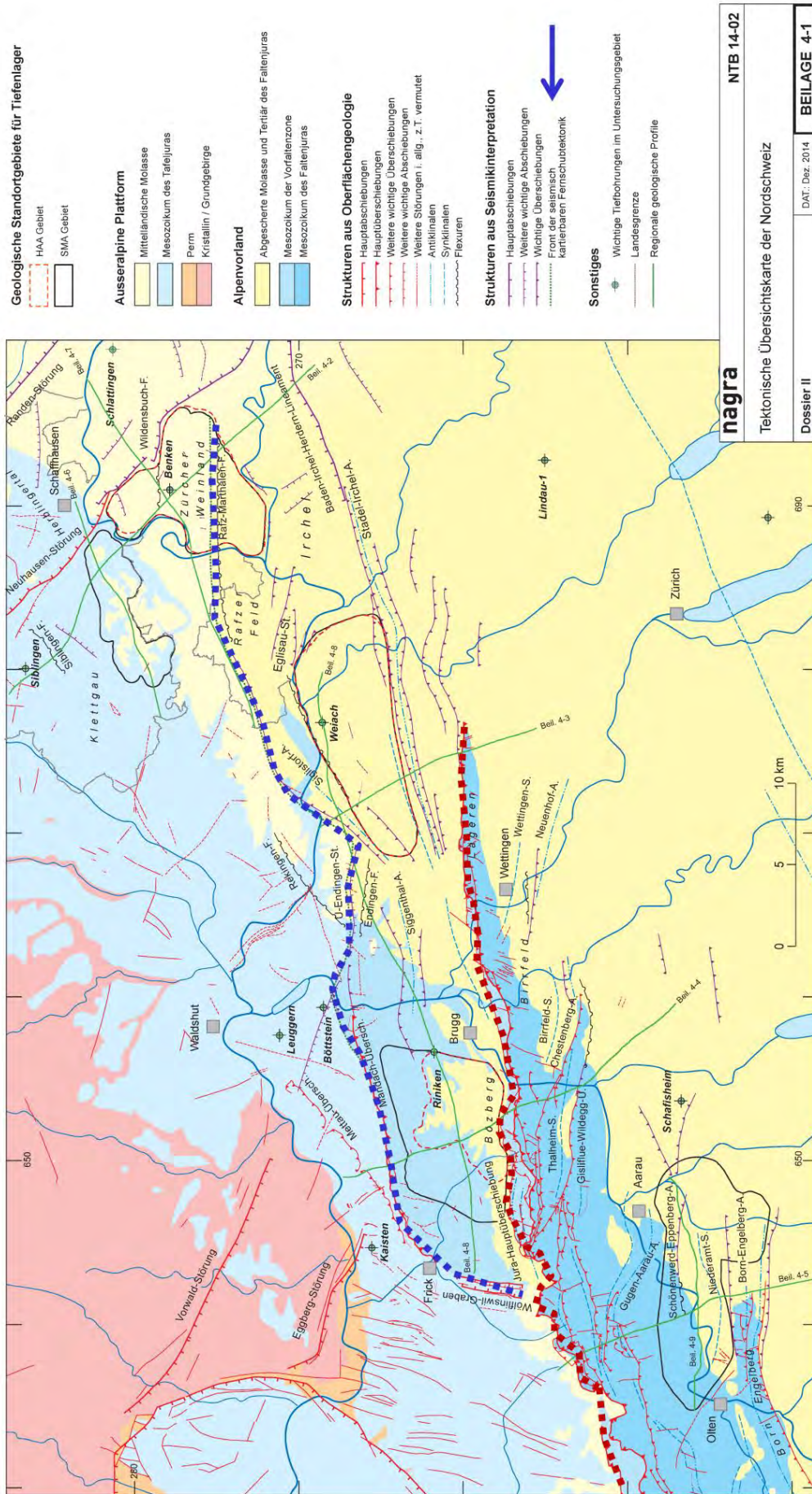


Figure 3.7 : Tectonic map of northern Switzerland. Additionally dashed thick red line corresponds to the Jura main thrust. Dashed thick blue line corresponds to the front of the Jura deformation taken from seismic lines. Modified from NTB 14-02, Beilage 4-1.

Since Nagra's work, the seismically mapped front of the Jura décollement has been moved north to include the "Vorfallenzzone" into the Jura deformation zone (Figure 3.7). Geological siting regions (*Standortgebiete*) are located south of the Jura front deformation, except Südranden and the northern part of Zürich Nordost siting regions. According to several studies in northern Switzerland (Mosar 1999, Madritsch et al. 2008, Madritsch et al. 2010, Ustaszewski et al. 2007), deformation and tectonic activity along the main Jura thrust were present until recently (2 Mio years) in the Mesozoic cover and also in the basement (inversion of Permo-Carboniferous trough?).

Several fault orientations exist in northern Switzerland: NW-SE, WSW-ENE, NS. They have different period of activity and different types of movements (compression, extension and transtension. For the major faults, an important component of transtension should not be neglected in addition to normal movement (see also Dooley & Schreurs, 2012).

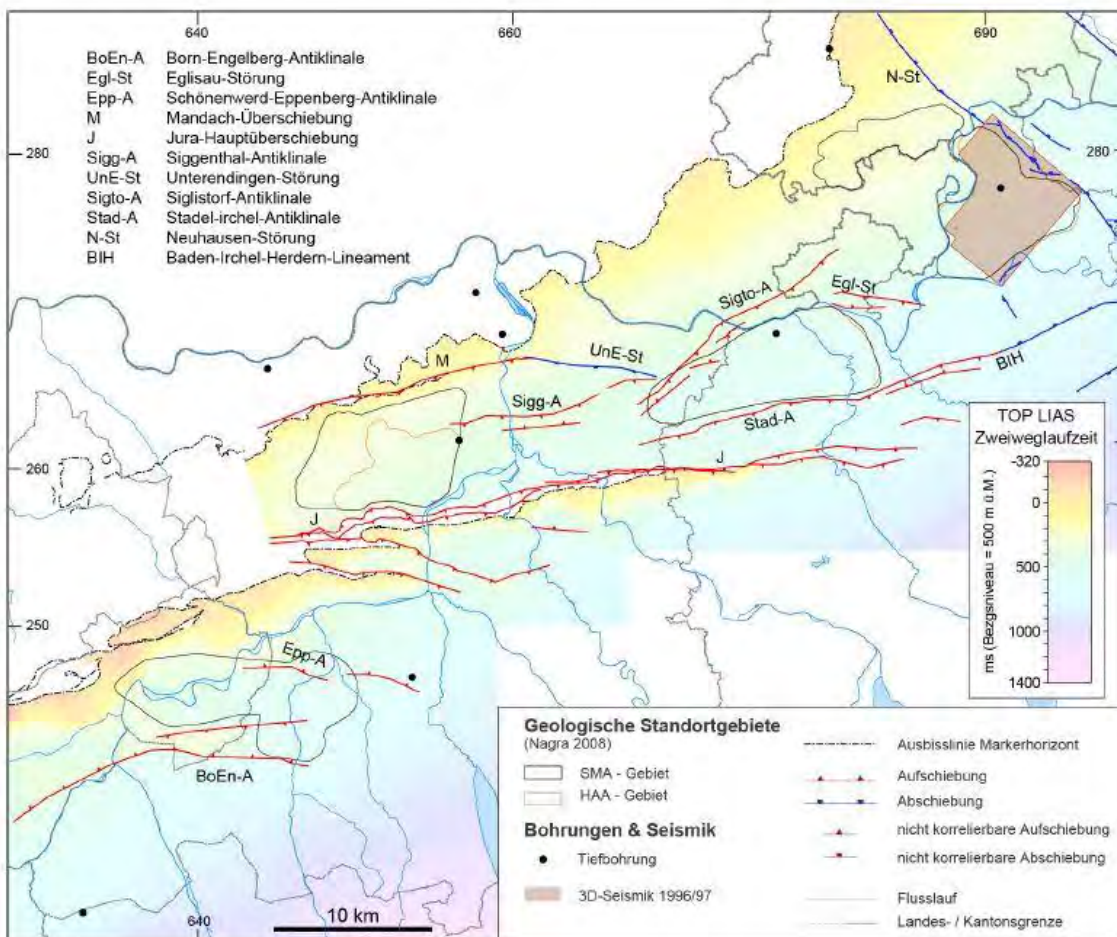


Figure 3.8 : Location of regional faults and related structures across the Top Liassic horizon TWT map. From NAB 13-10, Fig. 6-1.

Permo-Carboniferous troughs

Deep drilling in northern Switzerland by Nagra has proven the presence of Permo-Carboniferous troughs and opened the discussion on this topic (Matter et al. 1987). Permian and Carboniferous sediments were identified only in the Weiach-1 well (Matter et al. 1988) and in the Weiach-2 well (Forest Oil – SEAG, Reinicke 2011); some other deep wells reach the

Permian sediments only and/or crystalline rocks (Figure 3.9). The identification of the troughs on the new acquired 2D-seismic data or on the old reprocessed seismic lines remains challenging because the reflections below the Base Mesozoic horizon are discontinuous and of low amplitude. The location of the Permo-Carboniferous troughs (NAB 14-17) is also based on the new gravity map of northern Switzerland (Green et al. 2013). The interpretation of the Pre-Mesozoic units is based on seismic facies correlation and discordances between reflection stacks. Three seismic facies were recognized by Nagra in the *Zentraler Permokarbondrog* especially in the Jura Ost geological siting area. From older to younger: the *Untere Trog* filling (UT) which consists of the Carboniferous sediments with high amplitude series continuous on short distances; the *Mittlere Trog* (MT) filling, which is a thick series (>1s TWT, about > 2km) with numerous discordances and waved reflections; the *Obere Trog* filling (OT) beneath the Mesozoic units with parallel to sub-parallel reflections up to Base Mesozoic horizon.

Interpretation and understanding of the grabens in the NAB 14-17 has been improved based on models (Burg et al. 1994) and results from the 2D- and 3D- surveys (Marchant et al. 2005). Major faults bounding the half-grabens are distinguishable (can be deduced), but many minor faults are not clearly identifiable and remain conceptual or speculative. In my opinion, faults in the basement could be faults, which are potentially active (recent tectonics). The risk of reactivation of these faults has to be evaluated and discussed by Nagra in more details also considering the displacement of the Mesozoic cover above the main décollement level in Triassic layers.

Interpretation of the seismic lines in the Pre-Mesozoic units has been done mainly by one author (H. Naef), which gives consistency to the interpretation of the seismic facies. Given the low quality of the seismic reflections in this domain, this leads the interpreter to a large part of subjectivity. Therefore, the question arises if another author would obtain the same results.

The “Flexur” symbols shown in the mentioned figures/maps do not represent the precise traces of flexures (e.g. the “Flexur-Achse” in the sense of Murawski & Meier (1998) which is the line that follows the hinge of the bended layers) but have an illustrative character to roughly show the flexure’s along-strike orientation (similar to the shown red traces of regional fault zones; compare answer to ENSI question 35). The polygons marking flexure – related “Tektonisch zu meidende Zonen” (see Fig. 4.4.1 and polygon outlines in Figs. 4.4.4, 4.4.5 & 4.4.6) cover the entire bended/flexured sediment package.

From my point of view, and in order to have a better comprehension of this topic (*Nachvollziehbarkeit*), flexures and their axial surfaces should first have been interpreted clearly on each seismic profile (only part of them are illustrated, see Figure 4.7, where the word *Flexur* in red has been added by the reviewer). Then, Nagra should have illustrated them precisely on the maps as a trace (there are two axial surface traces in a flexure) for each seismic horizon. The location of the axial surface trace changes from one seismic horizon to another. In that case, we would have had a precise limit of the flexure and a clear lateral correlation. Therefore, the maps shown in the NTB 14-02 (e.g. Fig. 4.4.-4 and others) are too synthetic.

Nagra’s answer to further questions from ENSI (*Frage 63* in Appendices) is as follow:

“It is correctly noted by the reviewer that the location of flexures is a key criterion to delimit the tectonic zones to be avoided. In our earlier reply to the reviewer’s initial sub-question number 3 (see above) we did not state that the mapping of these flexures is only rough. What was stated is that the symbol used in the addressed NTB figures only roughly sketches the flexures along the strike orientation. As was explained, it is the shown polygon outlines that delimit the tectonic zones to be avoided, e.g. the flexure zones.

The question raised by the reviewer is still rectified to some extent as the precision of this delimitation is of course affected by uncertainties, in this case stemming from the seismic data density but also the structural geological mapping approach/concept (e.g. expert view). The sensitivity /significance of this uncertainty for the size of the potential disposal perimeters in the various siting regions but in particular Nördlich Lägern was tested in the course of Nagra’s evaluation.”

4 Discussion of geological features on seismic profiles in defined geological siting region

For the five geological siting areas, ENSI has formulated questions on specific seismic lines. For each siting region (*Standortgebiet*), we propose a table with the main seismic lines and the related *Beilagen/Anhänge*/Figures included in reports and the questions addressed by ENSI. Discussion is based on Nagra's figures (maps and seismic interpreted lines) to which minor modifications (explained in the caption) have been made.

The general recommendation of ENSI for this part of the review is as follows: „*Generell soll bei der Beurteilung der Fokus auf denjenigen Profil-Sektionen liegen, welche einerseits im Standortgebiet liegen oder einen Einfluss auf das Standortgebiet haben, andererseits die Ergebnisse der Einengung konservativ in Frage stellen konnten. Ist das Inventar an Störungen vollständig, oder mussten Anzeichen von potentiellen Störungen mitberücksichtigt werden (Konservativität)?*“

4.1 Südranden siting region

This geological siting region is located in the autochthonous Tabular Jura, NE of the Jura frontal thrust, and is in an extensional tectonic context. Three new seismic lines have been acquired, two strike lines and one dip line (Figure 4.2). No well is located in this siting region.

No regional fault is located in this geological siting region. The Neuhausen fault (Figure 3.8) is located to the eastern edge of the siting region and is visible only on the old reprocessed seismic line (91-NO-79), in the absence of other data across this structure. No tectonic zone to be avoided is located in this siting region.

Line name	NAB 13-10, Beilage	NAB 14-34	NTB 14-02	NAB 14-17	Questions from ENSI
12-NS-66	Beilage 5-18	A2-1-18	A1-7	-	<i>Das ENSI wünscht sich für dieses Profil eine Aussage zur generellen Betrachtung von Multiplen im Grundgebirge.</i>
12-NS-75	Beilage 5-19	A2-1-19	A1-7	-	<i>Zu diesem Profil hat das ENSI keine Detailfragen.</i>
12-NS-77	Beilage 5-20	A2-1-20	Beilage 4-6, A1-7	-	<i>Das ENSI stellt sich die Frage, wie gut die Neuhauserwald-Rinne (CMP 4550 bis 4850) und damit einhergehende mögliche tektonische Störungen im Grundgebirge (Rand eines Permokarbon-Troges?) erkennbar sind.</i>
91-NO-68	A-26	A2-2-26	Beilage 4-2, Beilage A1-8	Fig. 5-3	-

Additional lines					
91-NO-79	A-32	A2-2-32		Beilage 6-16	-
84-NF-65	A-19	A2-2-19		Beilage 6-11	-

Table 6: Seismic lines and related enclosures (*Beilagen/Anhänge – A-*) in reports for the Südranden geological siting region. In the last column are the specific questions from ENSI.

12-NS-66

The interpretation of the Pre-Mesozoic units in the Südranden siting area is not trivial. Nagra did not interpret (in the NAB 14-17 report) in the SR siting region, the Pre-Mesozoic units on the new acquired seismic lines (Table 6). The relationships between reflections in the Pre-Mesozoic unit on the depth (PSDM) version of the 12-NS-66 seismic line (A 2-1-18 in NAB 14-34) look quite different from the TWT (PSTM) version (Beilage 5-18, NAB 13-10). On the depth version, the reflections are sub-parallel resembling more to multiples. On the TWT version, reflections are discontinuous and not sub-parallel with possible internal onlaps. On the 84-NF-65 seismic line (parallel dip line located western), Nagra in collaboration with H. Naef suppose a Permo-Carboniferous through on the TWT version (Beilage 6-11, NAB 14-17). Continuous parallel reflections close to the intersection with the 12-NS-77 strike line (but not visible on that line) resemble the ones in the *Obere Trogfüllung* unit. However, the presence of the Klettgau through remains difficult to assess.

12-NS-77

The interpretation of this strike seismic line presents three faults, probably layout-determining faults, at CMP 2550, 3750, 4650 across the Mesozoic layers. No clear offset of reflections, even of Base Mesozoic horizon can be seen. The last fault at CMP 4650 is not seen (no offset of reflections) on the intersecting dip seismic line 91-NO-68. On the PSDM version of the line 12-NS-77, which should be a better image, the reflections are wavy but continuous without offset. A slight thickening is visible in the Triassic unit. Northward, the interpretation on the parallel seismic line 91-NO-79 (Beilage 6-16, NAB 14-17) does not show any fault. Reflections are continuous without offset. Accordingly, the presence of these faults is questionable.

ENSI questions the influence of the *Neuhauserwald-Rinne* or channel (NH in Figure 4.1) on the reflections within the Mesozoic or Pre-Mesozoic units and on the interpretation of the structures. This channel filled with quaternary sediments is located on top of the “last” fault (CMP 4650) discussed in the paragraph above. The channel is recognizable on the depth version (A2-1-20, NAB 14-34). An influence of the channel on the data processing cannot be excluded. The reflections within the many Mesozoic layers are continuous even if they are wavy. No major structure can be observed. We cannot exclude a normal fault dipping toward East with a very small offset. This type of fault would be small-scale element, with no lateral correlation.

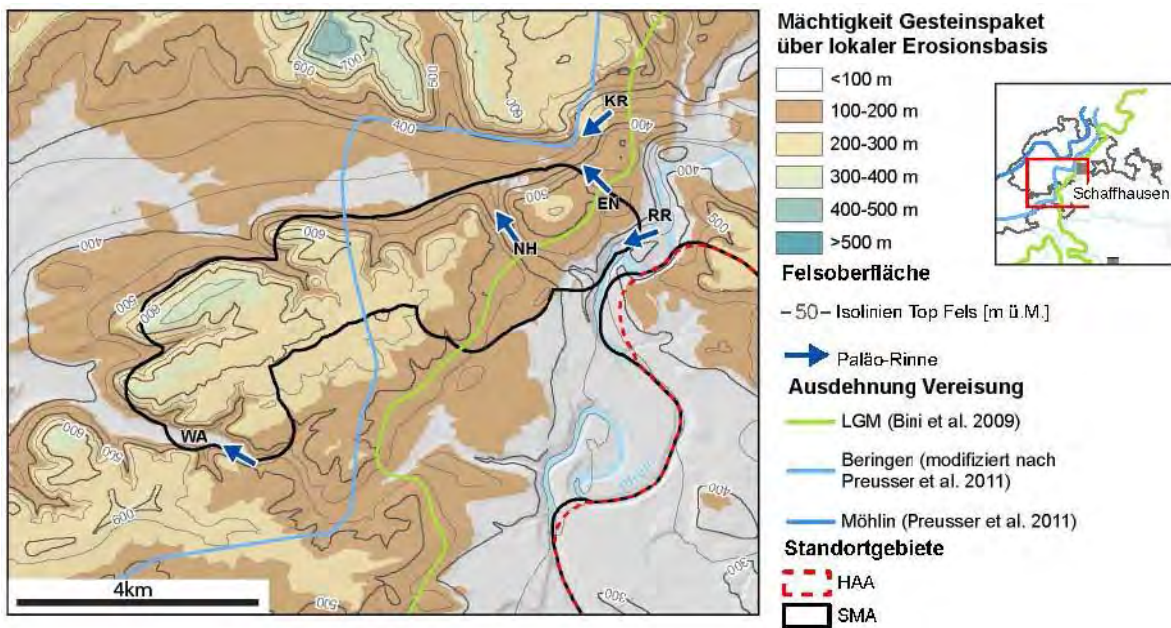


Figure 4.1: Topography and quaternary filled channels in the Südranden siting region. EN: Enge; KR: Klettgau-Rinne; NH: Neuhauserwald-Rinne; RR: Rheinfall-Rinne; WA: Wagental. From NTB14-02, Dossier III, Fig. 4.4-10.

4.2 Zürich Nordost siting region

The northern part of this geological siting region is located north of the Jura thrust front (Figure 3.7) in the autochthonous Tabular Jura. The southern part is located in the *Vorfaltenzone*, which is part of the detached Jura cover. The Benken-1 well, reaching crystalline rocks, is located in the centre of this siting region.

No new seismic line (2011/2012) has been acquired in this siting region. Only reprocessed seismic lines were available in the reports. Some seismic lines are SEAG (named SE) seismic lines, which for confidential reasons are not included in the reports (NAB 13-10 and NAB 14-34). However, the possibility to consult the lines at Proseis AG office was offered (this has not been done since 83-SE-03 seismic profile is included in the NAB 14-17 report) (Table 7). The seismic profiles have different vertical scales (TWT, depth) in the reports and Pre-Mesozoic units are not interpreted on each version.

Line name	NAB 13-10, Beilage (TWT)	NAB 14-34 (PSDM)	NTB 14-02 (Depth)	NAB 14-17 (TWT)	NAB 14-58 (TWT)	Questions from ENSI
91-NO-68	A-26, Fig. 3.3	A2-2-26	Beilage 4-2, Beilage A1-8	Fig. 5-3	Beilage 6, Fig.9	Zu diesem Profil hat das ENSI keine Detailfragen.
91-NO-77	A-31	A2-2-31	Beilage 4-7, Beilage A1-8			Zu diesem Profil hat das ENSI keine Detailfragen.

Additional lines						
91-NO-75	A-30	A2-2-30	Beilage A1-8	Beilage 6-14		-
83-SE-03	-	-	Fig. 4.4-4	Beilage 6-12		-

Table 7: Seismic lines and related enclosures (*Beilagen/Anhänge – A-*) in reports for the Zürich Nordost geological siting region. In the last column are the specific questions from ENSI.

The Neuhausen fault (Figure 3.8, Figure 4.2) is the major regional fault delimiting the northeastern part of the geological siting region. This normal fault has an offset ~70m (~50ms) affecting all the seismic horizons (Base Mesozoic included) and is oriented NW-SE, parallel to major faults in the Schwarzwald basement. This fault was certainly active in the Tertiary time and most probably already during Mesozoic and Pre-Mesozoic times. Activity post-dating the main Jura phase of folding is not excluded (see discussion in NTB 14-02, Dossier II p.67 and Dossier III p.13).

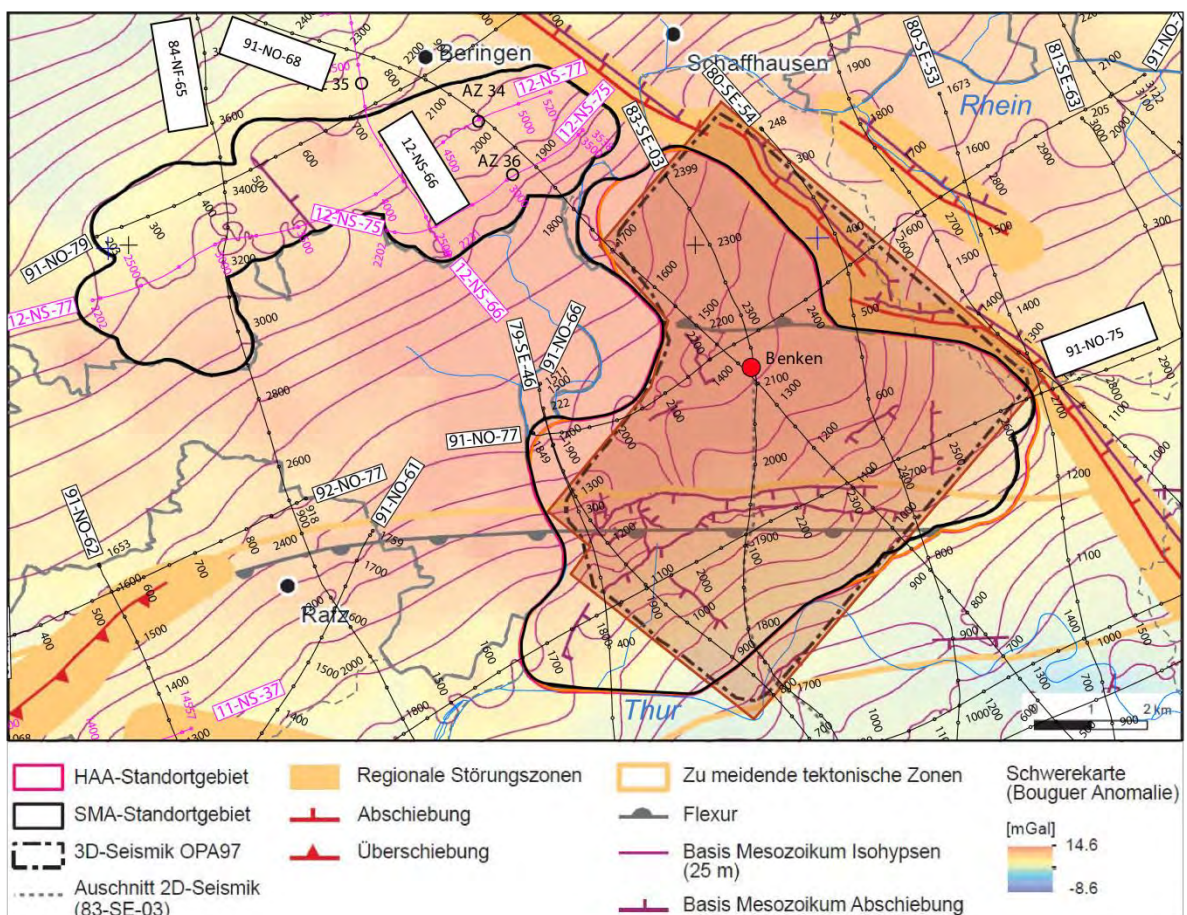


Figure 4.2: Map of the regional fault zones and tectonic zones to be avoided combined with the seismic location map for the Zürich Nordost siting region. Contours represent the Base Mesozoic horizon in depth (no precise depth value along the curve is indicated in Nagra’s figure, only intervals of 25m are mentioned in the caption). Compilation made by swisstopo from two maps of Nagra report figures (references indicated below the legend).

In this geological siting region, the southern area has been defined by Nagra as a tectonic zone to be avoided (Figure 4.2). The northern orange limit line (tectonic zone to be avoided) is located along a fault (labelled Q on Figure 3.9 and Figure 4.3) which offsets only the Base Mesozoic horizon. This steep normal fault (which could, from my point of view, have a transpressive component), borders the northern part of the Randzone Nord trough and is located about 500 m north of the *Rafz-Marthalen Flexur* (Figure 4.3, dip seismic line 83-SE-03). On the seismic profiles, Nagra does not indicate the axial surfaces in the flexure of Rafz-Marthalen and Andelfingen. This indication would have helped the reader to visualize the flexures. On this seismic line, the s-shape deformation of the Mesozoic/Cenozoic reflection packages is slightly visible above the Q fault and above the H fault. According to the definition of flexure (see §3.6 and *Frage 63* in Appendices), the movement along the fault in the Pre-Mesozoic units is thought to cause the deformation.

The western extension of the Rafz-Marthalen structure is not clear from the seismic data. The tectonic style of the Siglistorf anticline shows a more deformed structure as the Rafz-Marthalen flexure. More detailed geological (including mapping) studies in the area between ZN and NL siting regions would be necessary to make a link between the geological structures and faults.

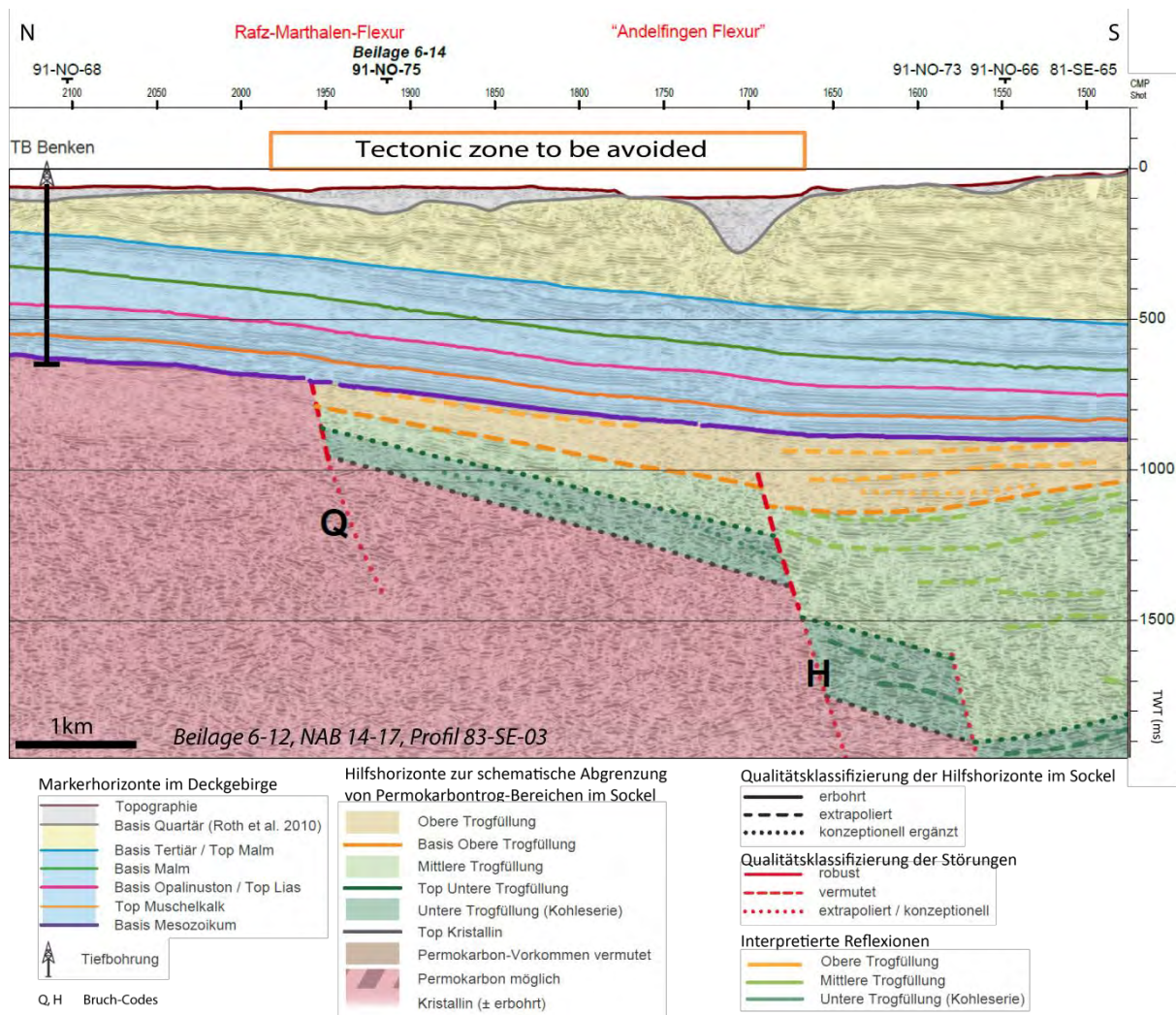


Figure 4.3: Location of the tectonic zone to be avoided (taken from Fig.4.4-4, NTB 14-02, Dossier II) in the Zürich Nordost siting area on the interpreted seismic line 83-SE-03 (from NAB 14-17, Beilage 6-12). According to Nagra, the tectonic zone to be avoided has been determined

for this area on gravity data and on the Permo-Carboniferous through map. The interpretation of the Pre-Mesozoic units and faults of this TWT version line shows slight differences with the depth version presented in NTB 14-02 (Fig. 4.4-4). For location, see Figure 4.2.

91-NO-75

On the strike seismic line 91-NO-75 (Figure 4.4) a large scale anticline located west of the Neuhausen fault is recognizable on the TWT version and on the depth section (CMP 2500-2680). All the units from Base Mesozoic horizon to the Tertiary unit are gently folded and parallel. Given the fact that this structure is seen also on the depth-converted version, we suggest that it is not related to a velocity problem, but rather to tectonics. This horst-like structure in the basement is presumably of Pre-Mesozoic age (possibly Hercynian or Permo-Carboniferous). No clear onlap of Mesozoic series on Base Mesozoic horizon is visible. On top, we see also a folded structure of presumably Tertiary age since Cenozoic layers seem folded too. Do we have one single structure from the Pre-Mesozoic to the Tertiary unit? Most likely yes, but I do not have an explanation for this structure, but one could think of neotectonic (recent) activity in relation with the Neuhausen fault. See below Nagra's explanation on this topic.

Nagra's answer to Frage 33:

"The Benken Horst is interpreted to reflect a Late Paleozoic structure in the first place, whose bounding faults were repeatedly reactivated later on (e.g. during Mesozoic and Cenozoic times). A neotectonic and possibly recent activity of these faults is not obvious, but cannot be entirely excluded (see conclusion in NTB 14-02 Dossier III chapter 3.8). This is one of the reasons why the "Rafz-Marthalen Flexur" (southern border fault of the Benken horst mildly reactivated in Post-Paleozoic times), which can be traced over several 2D-seismic profiles, was defined as "zu meidende tektonische Zone" and avoided as part of delineating the Lagerperimeters for the "Sicherheitstechnische Vergleich", as was the "Neuhausen Störung" (presumed eastern border fault of the horst with clear signs for Late Tertiary activity) regarded as "Regionale Störungszone" (see NTB 14-02 Dossier II, Kap. 4.5.2).

The other presumed border faults of the Benken Horst are the "Strukturzone von Niderholz" to the West and the "Wildensbacher Flexur" to the North. Both structures have a comparably local character and could only be mapped in detail with the help of 3D-seismic data. Nagra is aware, that similar structures may not yet be detected in other siting regions, where no 3D-seismic data are available in SGT-E2. In order to treat all siting regions equally in the course of the "Sicherheitstechnische Vergleich" of SGT-E2, these "3D-seismic scale structures" were not treated as regional tectonic elements and avoided straight away, but taken into account as "anordnungsbestimmende Störungszonen" (see NTB 14-02, Dossier II, Kap. 4.5.2).

The structure addressed by the ENSI question and visible on profile 91-NO-75 is not considered to stem from a velocity problem. It is known as the "Antiklinale von Trüllikon" and was analysed in detail with the help of 3D-seismic data (see NTB 00-03 by Birkhäuser et al. 2001, sections 4.6.2 page 90). While not directly linkable with a border fault of the Benken Horst, it does show signs for post-Paleozoic (Mesozoic and Cenozoic) activity. Most importantly, the "Antiklinale von Trüllikon" is not traceable over several 2D-seismic profiles (like the above mentioned "Rafz-Marthalen Flexur") and as such, similar to the "Wildensbacher Flexur" and the "Strukturzone von Niderholz" a "3D-seismic scale structure". For this reason it was not regarded as regional tectonic element, but as an "anordnungsbestimmende Störungszone".

In NTB 14-02, a cross-section has been drawn along the 91-NO-75 seismic line (A 1-8, NTB 14-

02, Dossier II). West of the village of Oerlingen (CMP 2300), the décollement level (frontal Jura thrust) has been omitted in the Triassic layers of the figure. According to Nagra's tectonic map of the area (Figure 3.7), the frontal Jura thrust is located here and this means that this area has been deformed during the Miocene time, possibly also later. From my point of view, this detail is important for the understanding of the geological evolution of the area.

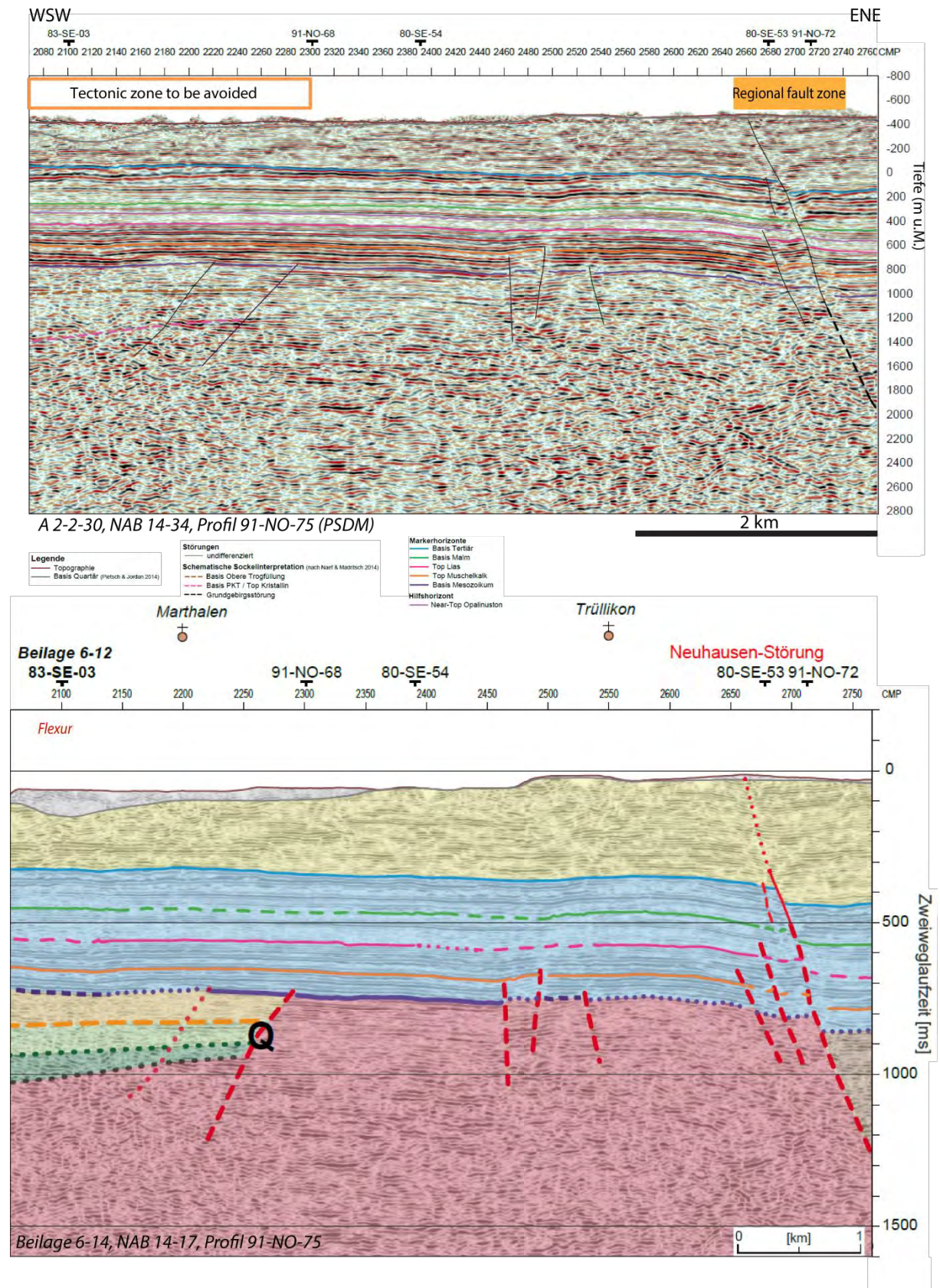


Figure 4.4: Illustration of the eastern part of the seismic line 91-NO-75 in depth (on top) and in TWT below. Tectonic zone to be avoided, regional fault zone and *flexur* have been added according to the CMP location on the Figure 4.2. For legend for the bottom picture see Figure 4.3 and for location see Figure 4.2.

91-NO-77

Recent movement on normal faults should also be considered beneath the Benken village. A fault (certainly layout-determining fault) has been drawn on the cross-section along the strike seismic line 91-NO-77 (Figure 4.5 below). This fault is not present on the seismic interpretation (Figure 4.5, A-31, NAB 13-10). We can see on the enlargement (left side in the Figure 4.5) a bending of the layers but not a discrete offset (along the fault). Deeper layers are more bended than upper layers suggesting more activity in the Triassic and Early Jurassic time. What is Nagra's reason to put this fault on the depth section and when is this fault active? This question is part of the *Frage 34* addressed to Nagra (see Appendices). Nagra's answer is as follows:

"The mentioned fault underneath the Benken village, which is visible on profile A1-8 of NTB 14-02, Dossier II, is associated with the "Wildensbucher Flexur". As notified by ENSI this fault is actually not visible on the 2D-seismic profile 91-NO-77. In the geological profile along this seismic section the structural interpretation was complemented according to the interpretation of the 3D-seismic data by Birkhäuser et al. (2001; NTB 00-03), which covers this area (see outline on profile construction by Jordan et al. 2014, NAB 14-105 page 54, 3rd paragraph).

As already outlined in the answer for ENSI Frage 33, the fact that the "Wildensbucher Flexur" could only be fully identified with the help of 3D-seismic data speaks against its classification as "Regionales tektonisches Element" in order to keep up with the SGT-requirement to treat all siting regions equally in the course of the "Sicherheitstechnische Vergleich". The structure is treated as "anordnungsbestimmende Störungszone".

The "Wildensbucher Flexur" was analysed in detail by Birkhäuser et al. (2001, NTB 00-03). It is inferred to be inherited from a Late Paleozoic basement fault (possibly constituting to the northern border of Benken Horst west of profile 91-NO-77). Within the Mesozoic and Cenozoic sedimentary stack it is constituted by an en echelon array of several minor normal faults. The 3D-seismic data suggests a kinematic link with the "Neuhausen Fault". As such the fault was definitely active during Cenozoic times. A neotectonic or even recent activity of the latter regional fault zone is not obvious, but cannot be entirely excluded (see conclusions in NTB 14-02 Dossier III chapter 3.8)."

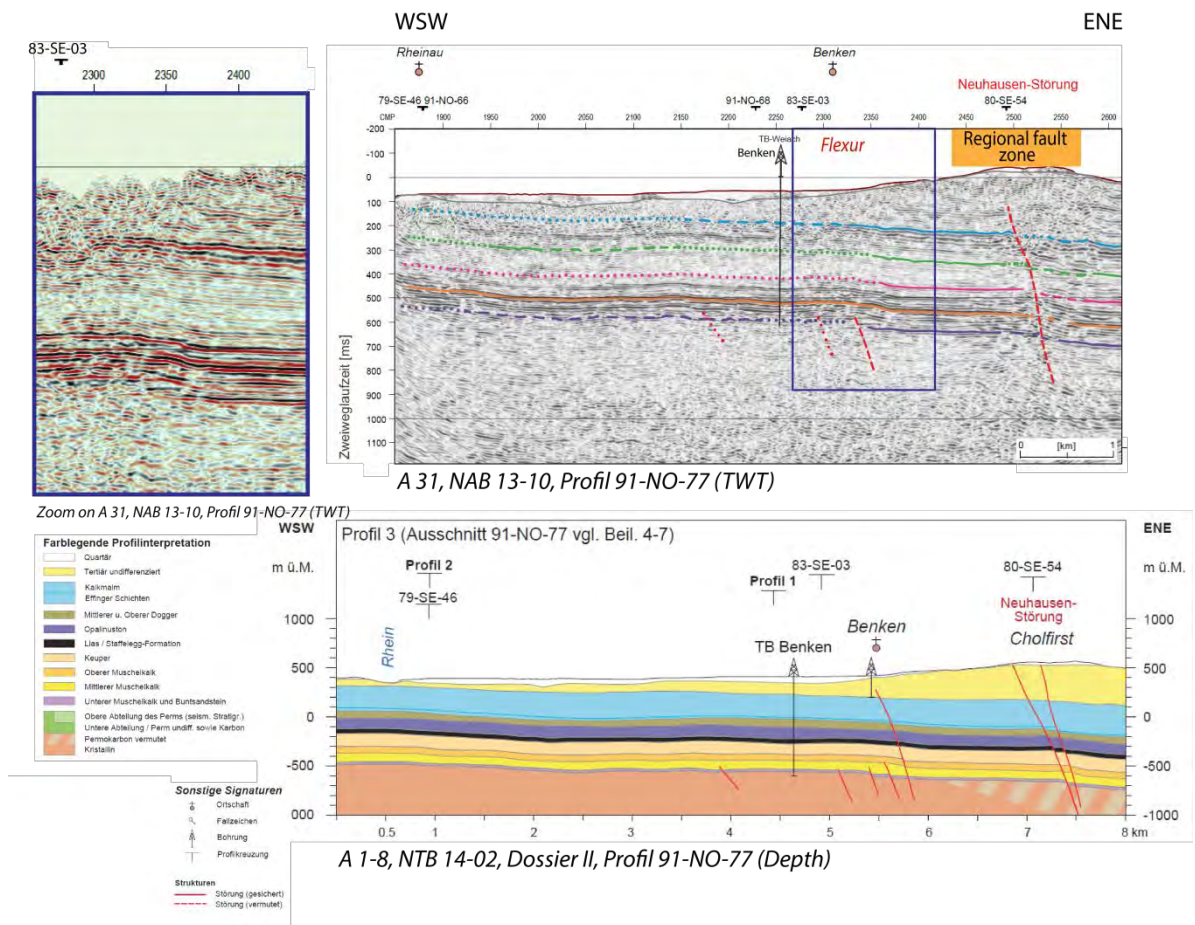


Figure 4.5: Illustration of the strike seismic line 91-NO-77 in TWT on top and converted to depth as a cross-section at the base. On the left, enlargement of the area in the blue rectangle on the seismic line. In the seismic section, the well name is Benken instead of Weiach (mistake on Nagra’s figure). Regional fault zone and *flexur* have been added according to the CMP location on the Figure 4.2. For legend see Figure 4.3 and for location see Figure 4.2

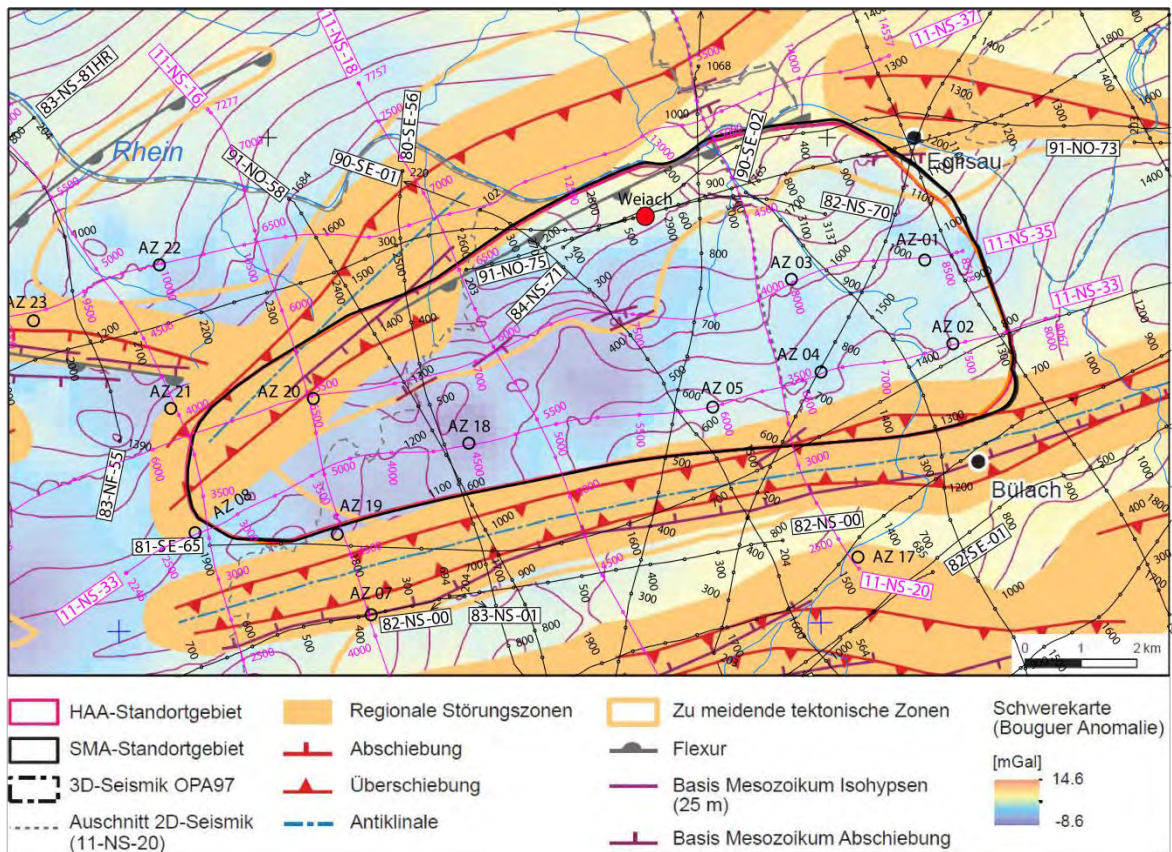
4.3 Nördlich Lägern siting region

The Nördlich Lägern geological siting region is located south of the Jura frontal thrust in the area called *Vorfaltenzone* (Figure 3.6). It is surrounded by three regional fault/fold zones (Figure 3.8 and Figure 4.6): the Siglistorf anticline to the North, the Eglisau fault to the NE edge and the Stadel-Irchel anticline (with lateral extension to the East into the Baden-Irchel-Herdern lineament). These zones are clearly visible on the seismic lines. In this siting region, Nagra has determined the southern area along the Siglistorf anticline as a tectonic zone to be avoided (Figure 4.6).

Numerous seismic data cover this siting region (Table 8): five newly acquired seismic lines and more than five old reprocessed seismic lines (either Nagra data or SEAG data). Weiach-1 well is located in the northern part of the siting region, and has reached Permian and Carboniferous sediments and even crystalline rocks beneath the Paleozoic sediments.

Line name	NAB 13-10- Beilage (TWT)	NAB 14-34 (PSDM)	NTB 14-02 (Depth)	NAB 14-17 (TWT)	NAB 14-58 (TWT)	Questions from ENSI
11-NS-18	Beilage 5-9	A2-1-9		Beilage 6-9		<i>Wie gut ist die Datengrundlage für die eingezeichneten Störungen im Grundgebirge? Sind diese belastbar? Bei diesem Profil geht es generell um die Belastbarkeit bei der Interpretation des Grundgebirges.</i>
11-NS-20	Beilage 5-10	A2-1-10		Beilage 6-10		<i>Die Nagra klassifiziert die nördliche Zone im Standortgebiet als tektonisch zu meidende Zone. Grund dafür sind die Trogränder des Permokarbondrogens und Störungen in der Trias und des Juras. Frage: Wie belastbar sind dazu die Erkenntnisse aus der 2D-Seismik in diesem Profil? (CMP 4200 bis 5200)</i>
11-NS-35 (E part)	Beilage 5-13	A2-1-13	A2-5	Beilage 6-13	Beilage 3, Fig.11	<i>Die Nagra schlägt für Nördlich Lägern einen Lagerperimeter im östlichen Teil des Standortgebietes vor. Frage: Wie belastbar sind die interpretierten Störungen im Grundgebirge und im Jura und in der Trias zwischen CMP 7200 und 8200? Gibt es andere Interpretation-svarianten?</i>
Additional lines						
11-NS-16	Beilage 5-8	A2-1-8		Fig. 5.2		-
91-NO-58	A-22	A2-2-22	Beilage 4-3,A2-5			-
82-NS-70	A-06	A2-2-6	Beilage 4-8, A2-5	Beilage 6-1		-

Table 8: Seismic lines and related enclosures in reports for the Nördlich Lägern geological siting region. In the last column are the specific questions from ENSI.



Seismic survey from Beilage 2-1, NAB 14-34; Regional fault zones/tectonic zones to be avoided from NTB 14-02, Dossier II, Fig. 4.4-5

Figure 4.6: Map of the regional fault zones and tectonic zones to be avoided combined with the seismic location map for the Nördlich Lägern siting region. Contours represent the Base Mesozoic horizon in depth (no precise depth value along the curve is indicated, only intervals of 25m are mentioned in the caption). Compilation made by swisstopo from two maps of Nagra reports (references indicated below the legend).

11-NS-16

This dip seismic line images the two regional structures: the Siglistdorf anticline and the Stadel-Irchel anticline (Figure 4.7). The distance between the two zones is short, maximum 2 km. The depth conversion of this line (PSDM A2-1-8, NAB 14-34) has given good results, with a better imaging than the TWT image. As a consequence, north of the Stadel-Irchel anticline a fault has been removed on the PSDM version (A2-1-8, NAB 14-34) and on the DTconv version (Fig. 4-8, NAB 14-34). In this case, this action looks comprehensible (nachvollziehbar), as explained in NAB 14-34 (Fig.4-8, p.34, caption of the figure): „Das markant verbesserte Abbild der DTconv-Version der Linie 11-NS-16 gegenüber der PSTM-Version machte bei erhöhter Kontinuität der Reflexionen auf dem Niveau der Trias und des Lias nördlich und südlich der Stadel-Irchel-Struktur Horizont- und Strukturanpassungen notwendig. Besonders nördlich der Stadel-Irchel-Struktur hatte sich das Reflexionsbild derart verändert, dass die ursprünglich interpretierten Über- und Aufschiebungen nicht mehr haltbar wurden“

11-NS-18

This dip seismic line crosses the two regional fault zones. The Stadel-Irchel anticline has been studied in detail by Nagra and coworkers resulting in a new model with fish-tail structures in the

Cenozoic and Mesozoic layers. This new alternative integrates old synsedimentary faults, change in thickness of units, change in thrust vergence, multiple décollement levels and shallow fault angles. This interpretation has been validated by classical evaluation of bed-length and area in cross-sections presented in a submitted paper by Malz *et al.* (Nagra's team co-authors). The "old" alternative, a flower structure model, is presented for comparison in the NAB 13-10 (see Fig. 6-3 of NAB 13-10). The Base Mesozoic horizon is offset by a normal fault named BIH (Baden-Irchel-Herdern lineament). This fault rooting in the basement could suggest another interpretation of the deformed layers (flower structure with in situ deformation?), but less plausible in the regional context (see legend Fig. 6-3, NAB 13-10). Nagra's work is exemplar for the understanding of Stadel-Irchel anticline showing how to find a solution accommodating all the structural elements.

On the TWT version (Beilage 5-9, NAB 13-10) at CMP 6300-5900 (Figure 4.7), three faults have been interpreted in the Mesozoic and one crosses the Base Mesozoic horizon (1 km south of the Siglistdorf anticline). These faults, apparently layout-determining fault, are located at the southern limit of the tectonic zone to be avoided (Figure 4.7). The lateral extension of this structure could be found on the dip parallel line 11-NS-20 located to the East.

ENSI's question on this line focusses on the interpretation of the basement or the Permo-Carboniferous troughs. Nagra's interpretation is convincing for the location of the faults D and N beneath the Mesozoic units (Beilage 6-09, NAB 14-17) and for the *Zentraler Permokarbondrog*, but less convincing for the location of fault E. As a proof of the presence of Permo-Carboniferous sediments in this area, there is the Weiach-1 (-2) well which is located only a few kilometres further NE (see also discussion on the Permo-Carboniferous troughs in §3.6).

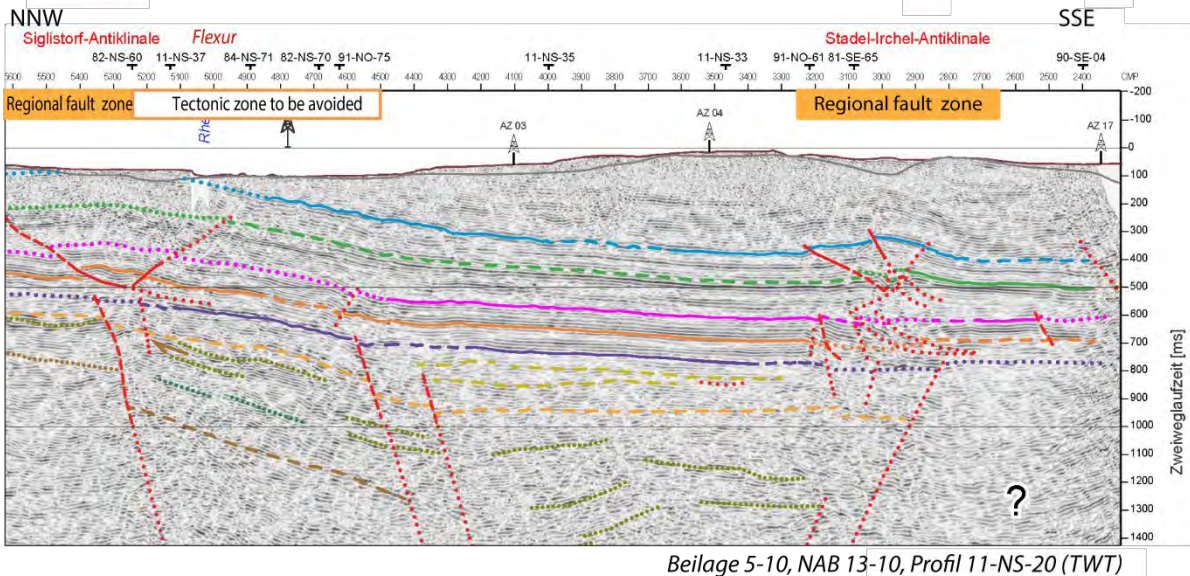
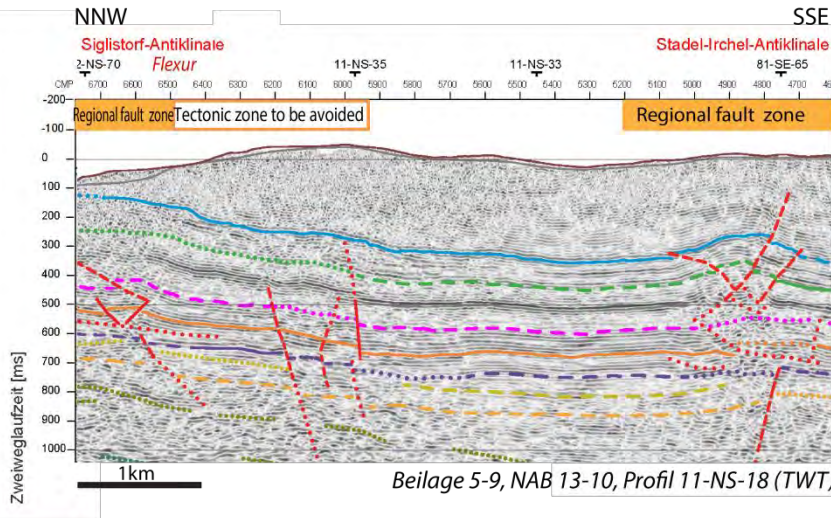
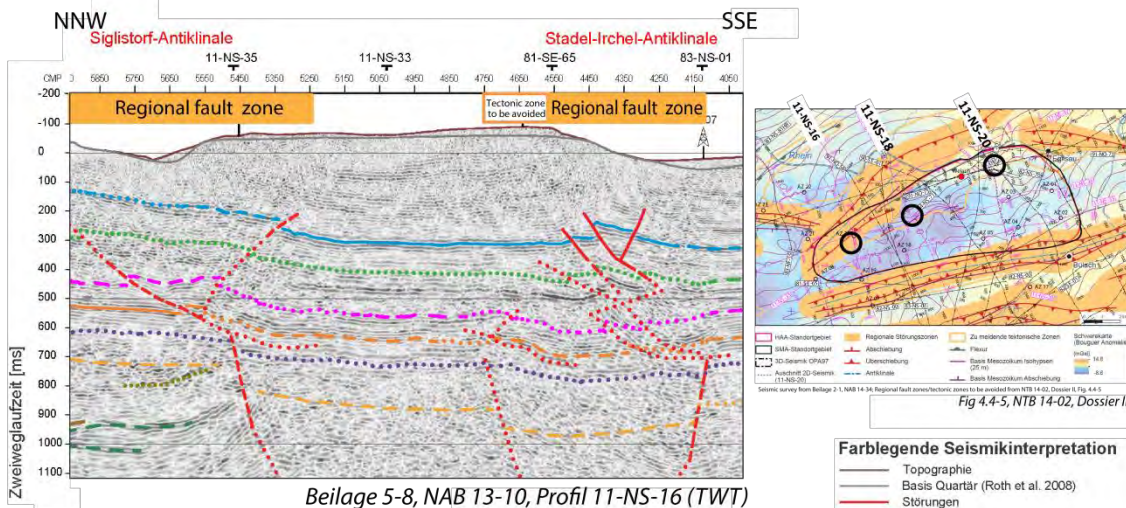
Based on this seismic profile and other parallel profiles, Nagra interprets a flexure south of the regional fault zone (see map Figure 4.6) along the northern border of the NL siting region. The location of this flexure has been transferred on the Figure 4.7 of the seismic line (see *Flexur* written in red), which should allow to better understand what Nagra considers a flexure to be. We notice the s-shape deformation of the Mesozoic layers between 6500 and 6400 CMP, which can be considered as a flexure. A movement of the underlying tectonic blocks should cause the flexure and so certainly, a reactivation of the fault across Base Mesozoic horizon at CMP 6600 would be the cause. The flexure is not well discussed and described by Nagra: mapping of the axial surfaces of the flexure interpreted on the seismic line would render the interpretation of the flexure more credible (see discussion §3.6). The quality of Base Mesozoic horizon is attributed to class 1 or 2. Considering the reflection quality, I would attribute rather class 2 to 3.

11-NS-20

This dip seismic line shows one layout-determining fault in the Mesozoic layers between CMP 4200 and 5200, south of the Siglistorf anticline. Nagra's interpretation of the structure is not fully clear. Interpretations vary laterally from West to East (from line 11-NS-16 to 11-NS-20, Figure 4.7). In the line discussed herein, one could alternatively suggest an early phase of a fish-tail structure (e.g. Stadel-Irchel), with alternation of forward and backward thrusts. Nagra classifies faults in the basement from "conceptual to uncertain". Seismic data show disturbed reflections and small offsets, which highlight the presence of a structure. The quality class 1 of Base Mesozoic horizon, as given by Nagra, in the tectonic zone to be avoided does not correspond to

the reflection quality. In the southern part of this zone, we should give a class quality 2. At CMP 5000 circa, Nagra interprets a flexure, which is not obvious to see on the seismic line (Figure 4.7).

As discussed above on the seismic line 11-NS-18, the formation of the Siglistorf anticline structure is not well understood yet. The link between this anticline and a reactivated fault crossing Base Mesozoic (D fault on Beilage 6-09, NAB 14-17) is not clear, but could be suspected. This area needs to be studied more carefully during the Stage 3. Additional studies would probably elucidate this structure (type of faults and age of deformation) located in the *Vorfaltenzone*, which is the zone with most recent and possibly ongoing deformation (tectonics). By including this zone into the tectonic zone to be avoided, Nagra supposes reactivation of the basement faults. This is certainly right, but to be sure, we would need more arguments and a 3D-survey.



Farbliegende Seismikinterpretation

- Topographie
- Basis Quartär (Roth et al. 2008)
- Störungen

Mesozoikum

Markerhorizonte und Strukturen

- Basis Tertiär / Top Malm
- Basis Malm
- Basis Opalinuston / Top Lias
- Top Muschelkalk
- Basis Mesozoikum

Paläozoikum

Schematische Abgrenzung der Trogbereiche

- Basis Obere Trogfüllung
- Basis PKT / Top Kristallin

Interpretierte Reflexionen

- Obere Trogfüllung
- Untere Trogfüllung
- Karbon (Kohle?)

Qualitätsklassifizierung Horizonte

- gut definiert
- ausreichend definiert
- schlecht definiert / konzeptionell

Qualitätsklassifizierung Störungen

- robust
- ungewiss
- konzeptionell

Sonstige Signaturen

- Ortschaft
- Ausbiss Markerhorizont (mit/ohne Schichtfallen)
- Aufzeitbohrung / Tiefbohrung

Figure 4.7: Interpretation of the faults (LDF) south of the Siglistorf anticline along three seismic lines in TWT. For reference of the figures, see below the lines. Black circles correspond to fault discussed in text. Tectonic zone to be avoided, regional fault zone and flexur have been added according to the CMP location on the Figure 4.2. For legend see Figure 4.3 and for location, see Figure 4.6.

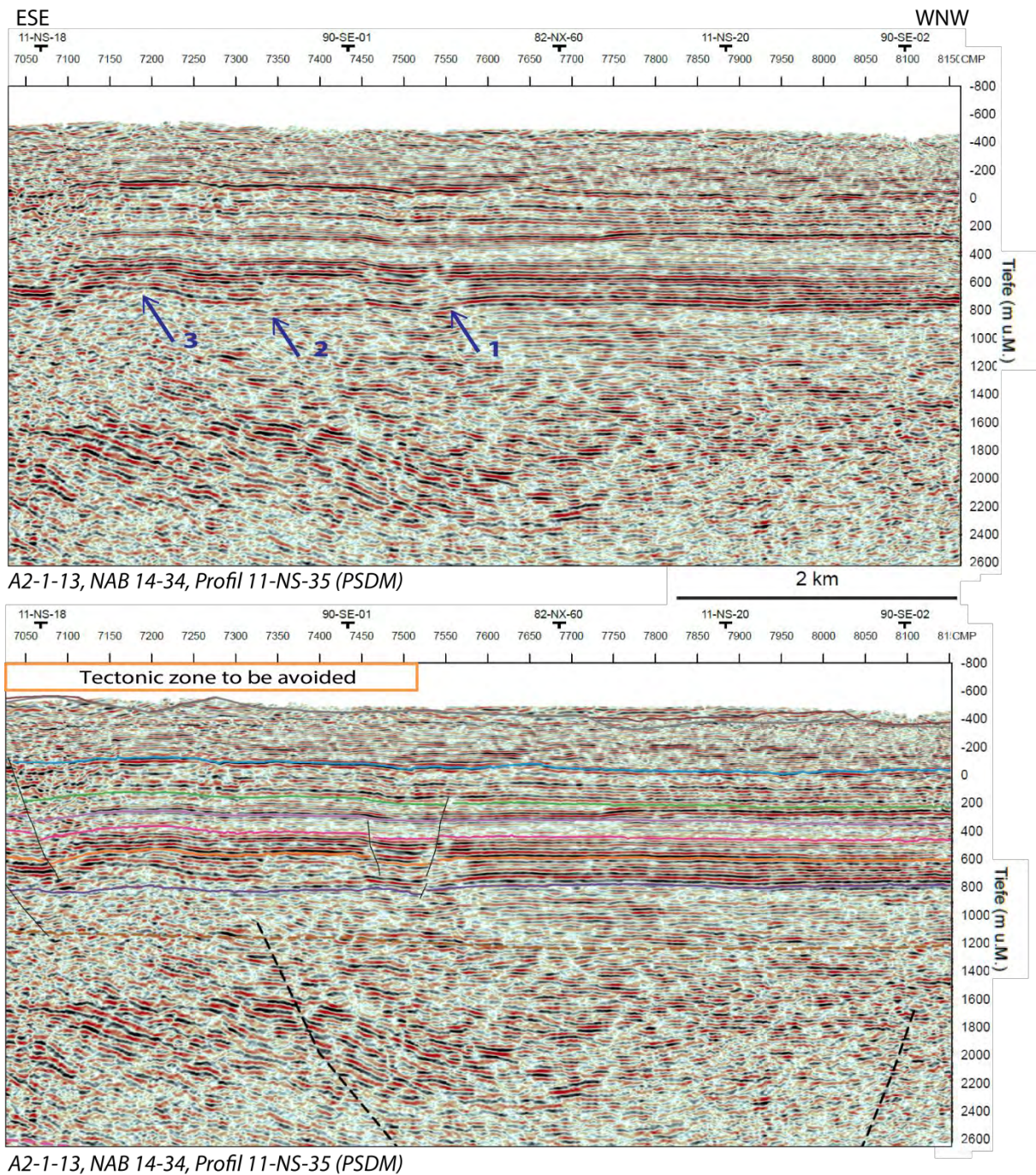


Figure 4.8: Seismic line 11-NS-35 (PSDM version, scale in depth). On top non-interpreted and below interpreted seismic line (from A2-1-13, NAB 14-34). For arrows number 1, 2, 3, see explanations in text. Tectonic zone to be avoided has been added according to the CMP location from the Figure 4.2. For legend see Figure 4.4 and for location see Figure 4.6.

11-NS-35

ENSI's question concerns the interpretation beneath the Mesozoic layers. The number 1 fault on this strike line (Figure 4.8) offsets the Base Mesozoic horizon. This normal fault in Nagra's interpretation is the only one offsetting the Base Mesozoic horizon here. Reflections show also an offset where the arrow number 2 points. Base Mesozoic horizon is probably not as smooth as interpreted. Number 3 points at a feature with oblique reflections and change of thickness

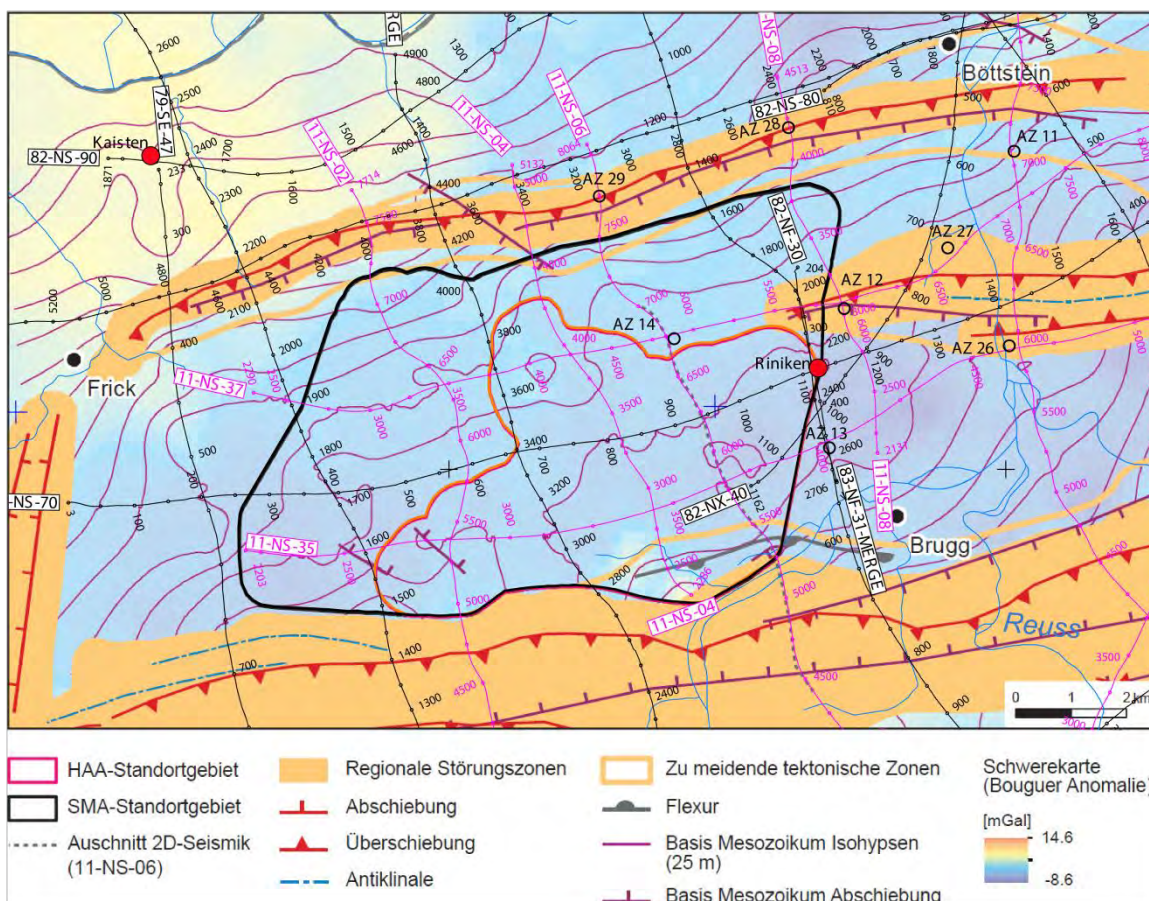
within the Triassic layers. It remains unclear whether this feature is only due to facies change.

In my opinion, sedimentary seismic facies of the Permo-Carboniferous trough filling are more easily recognizable than the faults, which remain conceptual on this seismic line (see also Beilage 6-13, NAB 14-17).

4.4 Jura Ost siting region

The Jura Ost geological siting region is located in the *Vorfaltenzone* (Figure 3.7), between the Jura frontal thrust as mapped from seismic lines (Mandach thrust fault) and the main Jura thrust (*Jura-Hauptüberschiebung*) (Figure 3.8). They are two regional fault zones, located mainly outside along the geological siting region limit (Figure 4.9). To the East, the Siggenthal anticline ends at the border of this siting region. The Jura Ost siting region lies above the *Zentraler Permokarbondrog* (Figure 3.9).

Numerous seismic data cross this siting region (Table 9): six new seismic lines and more than four old reprocessed seismic lines (either Nagra or SEAG lines). Riniken-1 well, which reaches the Permian sediments, is located at the eastern border of the geological siting region.

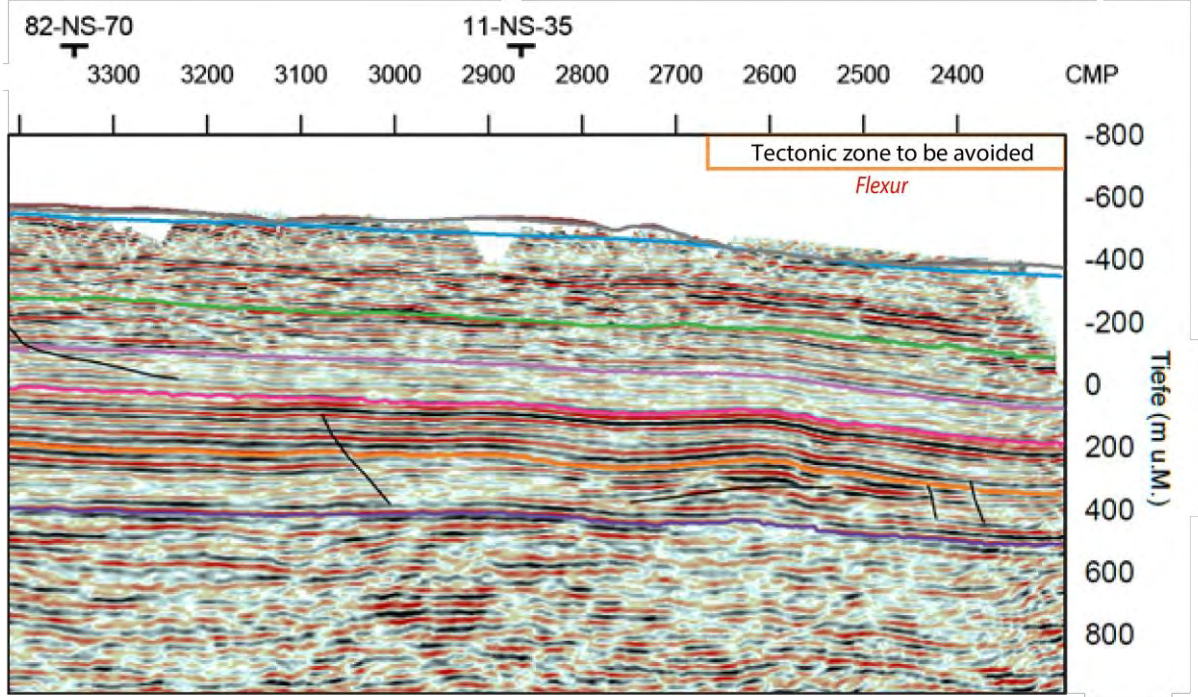
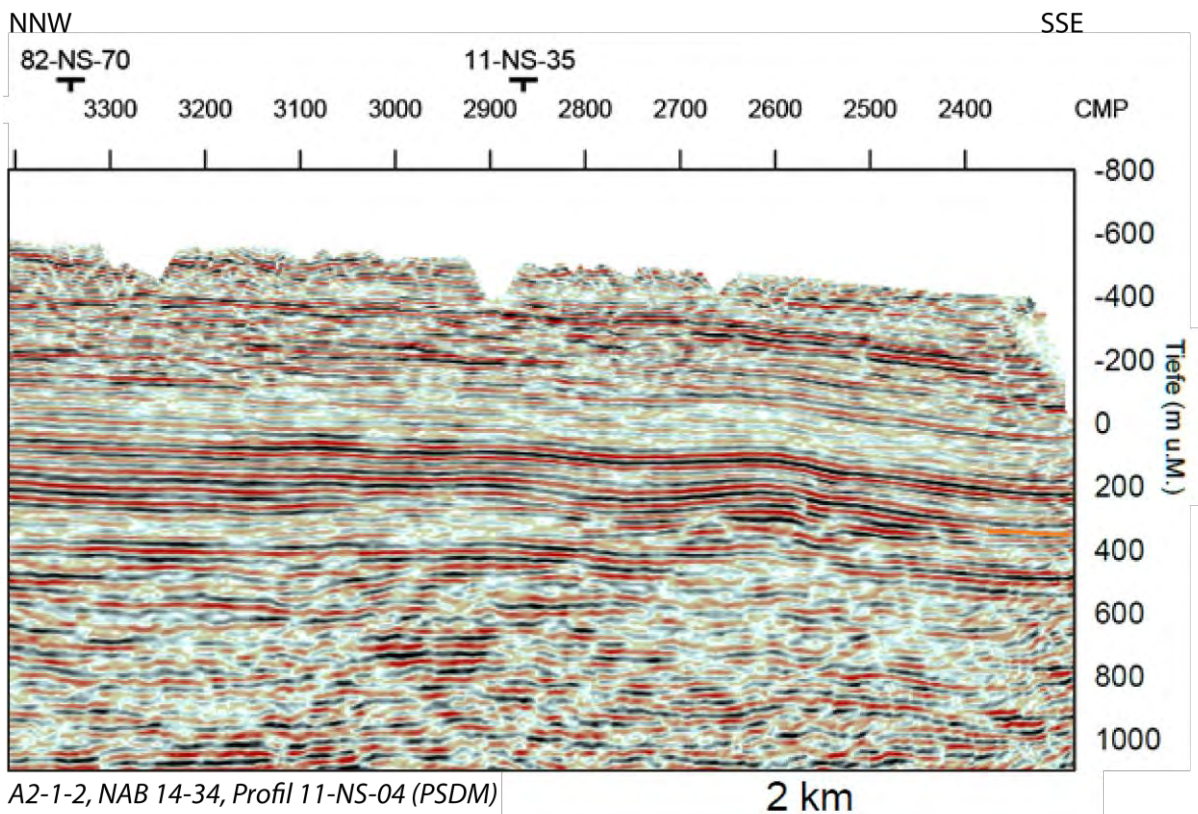


Seismic survey from Beilage 2-1, NAB 14-34; Regional fault zones/tectonic zones to be avoided from NTB 14-02, Dossier II, Fig. 4.4-6

Figure 4.9: Map of the regional fault zones and tectonic zones to be avoided combined with the seismic location map for the Jura Ost siting region. Contours represent the Base Mesozoic horizon in depth (no precise depth value along the curve is indicated, only intervals of 25m are mentioned in the caption). Compilation made by swisstopo from two maps of Nagra reports (references indicated below the legend).

Line name	NAB 13-10-Beilage (TWT)	NAB 14-34 (PSDM)	NTB 14-02 (Depth)	NAB 14-17 (TWT)	NAB 14-57 (Effi) (TWT)	NAB 14-58 (BD (TWT))	Questions from ENSI
11-NS-04	Beilage 5-2	A2-1-2					<i>Das Profil zeigt ruhige Lagerungsverhältnisse, einzig zwischen CMP 2900 bis 3000 ist im Tiefenbereich der Trias eine Variation in der Mächtigkeit zu beobachten. Ist diese Variation ein Artefakt (z. B. Geschwindigkeitsmodell) oder möglicherweise ein Effekt der Tektonik?()</i>
11-NS-06	Beilage 5-3	A2-1-3		Beilage 6-5 Fig. 5-1			<i>Dieses Profil zeigt Ähnlichkeiten mit dem Profil 11-NS-04. Wie kann die Anomalie (Verdickung) bei CMP 5800 bis 5900 im Bereich des Muschelkalks interpretiert werden? Existieren ähnliche Strukturen auf der Nachbarlinie 11-NS-04?</i>
11-NS-35 (W part)	Beilage 5-13	A2-1-13	A3-5	Beilage 6-13	Fig 10	Beilage 3	<i>Zu diesem Profil hat das ENSI keine Detailfragen</i>
Additional lines							
83-NF-15	A-13	A2-2-13	Beilage 4-4, A2-5	Beilage 6-4			-
82-NS-70	A-06	A2-2-6	Beilage 4-8, A2-5	Beilage 6-1			-

Table 9: Seismic lines and related enclosures in reports for the Jura Ost geological siting area. In the last column are the specific questions from ENSI.



A2-1-2, NAB 14-34, Profil 11-NS-04 (PSDM)

2 km

A2-1-2, NAB 14-34, Profil 11-NS-04 (PSDM)

Figure 4.10: Southern part of the dip seismic line 11-NS-04 in depth (PSDM version). Tectonic zone to be avoided and *flexur* have been added according to the CMP location on the Figure 4.9. For legend see Figure 4.4 and for location see Figure 4.2.

11-NS-04

This dip seismic line is located in the middle of the siting region. This line shows the deformed Mesozoic layers associated with the Mandach thrust. The interpretation of the Base Mesozoic

horizon and the related faults is rather complicate. In contrast, south of this thrust, the layers are little deformed (Herznach-Bözberg *Tafel*). The southernmost part of this seismic line (CMP 3000-2350) is well illustrated in the NAB 14-34 (Fig. 4-3, p. 24) showing better continuity of the reflectors. This is also the case in the PSDM version as illustrated here in the Figure 4.10. The fault interpreted at CMP 3100 on the PSTM version is taken over on the PSDM version, even if reflections are continuous. This is questionable, because interpretation should rely on the seismic image. Below an excerpt of the caption of Fig. 4-3 from NAB 14-34 (p. 24), which explains the position of Nagra:

“Der Vergleich der PSTM- gegenüber der DTconv-Version der Linie 11-NS-04 zeigt letztere mit einem besonders oberhalb des Top Lias allgemein kontinuierlichen Reflexionsbild. Einige der in der PSTM-Version noch deutlich erkennbaren Störungen sind in der DTconv-Version nicht mehr so deutlich oder gar nicht mehr erkennbar. Diese Strukturen wurden bei der Interpretation in Tiefe trotzdem weiter mitgeführt. „

ENSI asks if the change of thickness within the Triassic unit is due to velocity problem or to a related structure. We do not have convincing arguments to decide. Between CMP 2900 and 2400 on the PSDM version (Figure 4.10), two Mesozoic horizons (Top Muschelkalk and Top Liassic horizons) are wavy, while the Base Mesozoic horizon below is sub-horizontal. This leads to conclude that there is a lateral change of thickness within the Triassic unit (Muschelkalk layers). On the PSTM version, this lateral change of thickness does not appear clearly around CMP 3000, but is clearer around CMP 2600 at the southern end of the line. The zone between CMP 2650 and 2286 is considered by Nagra as a tectonic zone to be avoided; it includes a flexure. This flexure is not very clear on this interpretation. Nagra should have shown in a clearer way what is considered as flexure on this seismic line. The flexure is much clearer on the 11-NS-06 parallel seismic line. This zone, located at the frontal part of the Jura main thrust anticline (Figure 3.7), should be studied in details in Stage 3.

11-NS-06

This dip profile is quite similar to the profile 11-NS-04, but extends farther to the South and therefore crosses the main Jura thrust (*Jura-Hauptüberschiebung*). Beneath the main Jura thrust, we observe a sag structure in the Base Mesozoic horizon in Nagra's interpretation (PSDM version). From my point of view, the sag structure is a velocity artefact (velocity pull-down?) (e.g. Fig.4-4, NAB 14-34). Otherwise, on the time version, the interpretation (e.g. Base Mesozoic horizon) should follow the reflections, which is not the case on this line. This type of change in the interpretation of the time (TWT) version, would yield a different interpretation when shown on a depth-converted profile.

ENSI's question concerns the interpretation of the thickening (CMP 5800-5900) within the Triassic beds. In this zone, we do not see a thickening in the Triassic beds, but rather discontinuities of the reflections within the Triassic beds. Base Mesozoic and Top Liassic horizons are sub-horizontal. A decreasing of the Triassic unit thickness starts at CMP 5550 and continues progressively toward the South up to CMP 5100. This change of thickness in the Triassic unit can be interpreted as sedimentary or salt flowage. If we compare with seismic line 11-NS-04, where we are on both seismic lines in the same structural position (north of the major Jura thrust), we would therefore expect to have the same features in the Triassic layers. However, we observe a minor difference. The presence of the flexure is clearer on this seismic line than on the 11-NS-04.

To the North, the lateral extension of the Siggenthal anticline - determined with a fault across Top Muschelkalk and Top Liassic horizons on seismic line 11-NS-08 - is recognizable with a small thickening in the Triassic beds (CMP 7300 and 6700). This supports that the anticline structure ends here.

The 11-NS-06 profile is the key line for the interpretation of the three Permo-Carboniferous facies in the troughs; the seismic facies are well defined on this line, which was used for their definition (see Fig. 6-3 in NAB 14-17). The line crosses the *Zentraler Permokarbondrog*. However, the fault system in the basement (e.g. K and L fault in Beilage 6-5, NAB 14-17) is interpreted differently on the Appendices (*Beilagen*) of various reports (compare with B5-3, NAB 13-10 and A2-1-3). This shows that Nagra's interpretation of the minor faults in the basement is rather speculative and not consistent.

According to the regional fault zone map of Jura Ost siting area (Figure 4.9), the area (CMP 5250-5500) north of the main Jura thrust is considered as tectonic zone to be avoided. On this line, this is justified with the poorly defined seismic reflections in the Mesozoic units and the location of a flexure (which is recognizable on the seismic line). In addition, a potential reactivation of the faults across the Base Mesozoic horizon is possible, although the faults are qualified uncertain.

4.5 Jura-Südfuss siting region

The Jura-Südfuss siting region is located half in the Jura fold-and-thrust belt and half in the Molasse Basin (Figure 3.7). It is surrounded by three regional faults: to the North-East by the Schönenwerd-Eppenberg anticline, to the North-West by the Jura main thrust (*Hauenstein-Dottenberg Überschiebung*), to the South by the Born-Engelberg anticline (Figure 3.8). The Mesozoic layers have been detached from the basement and have been displaced toward the North by several km.

Numerous seismic lines cross this siting region (Table 10): three new seismic lines were acquired and five old reprocessed seismic lines were used (Figure 4.11). One recent well data exist within this siting region, the Gösgen SB-4 well and two wells are located outside of the siting region: the Schafisheim-1 well is located 5 km to the East and Oftringen-1 well 5 km to the SW.

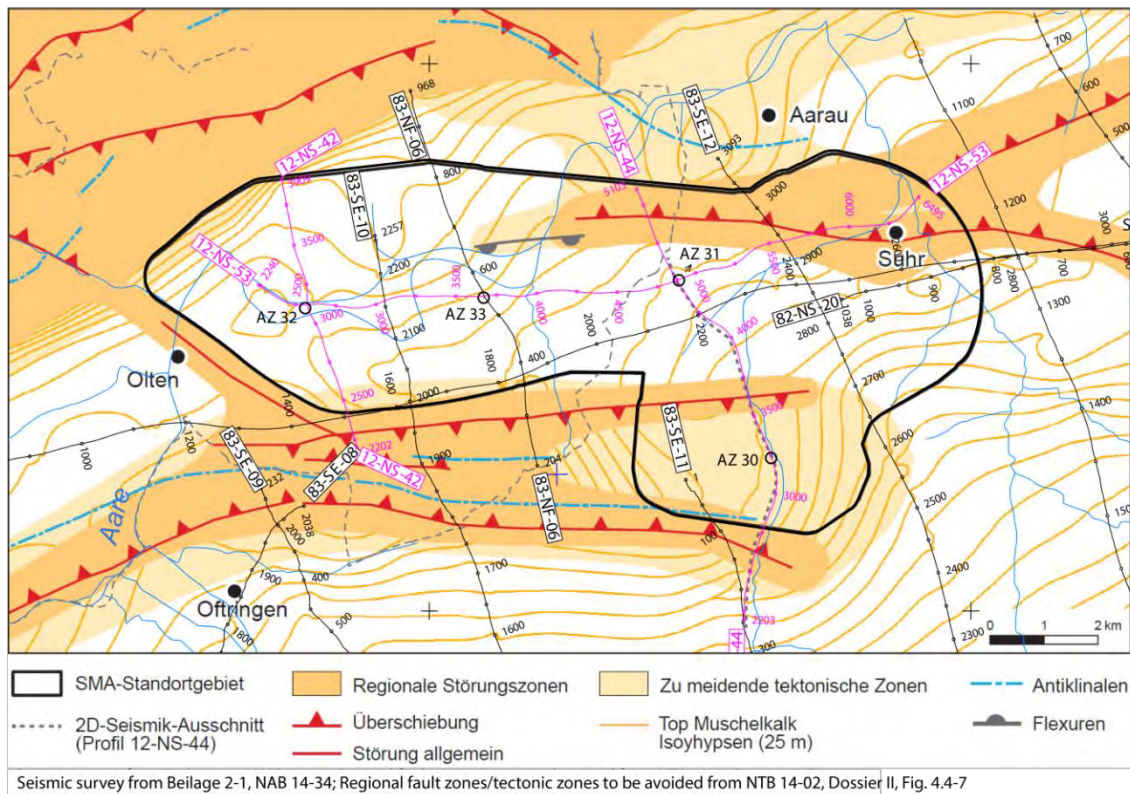


Figure 4.11: Map of the regional fault zones and tectonic zones to be avoided combined with the seismic location map for the Jura Südfuss siting region. Contours represent the Base Mesozoic horizon in depth (no precise depth value along the curve is indicated, only intervals of 25m are mentioned in the caption). Compilation made by swisstopo from two maps of Nagra reports (references indicated below the legend).

Line name	NAB 13-10-Beilage (TWT)	NAB 14-34 (PSDM)	NTB 14-02 (Depth)	NAB 14-17 (TWT)	NAB 14-57 (Effi)	Questions from ENSI
12-NS-42	Beilage 5-15	A2-1-15	A4-5		Beilage 6	<i>Der Fokus der Beurteilung in diesem Profil liegt generell auf dem OPA. Spezifische Frage: Wie belastbar ist die Interpretation der Störung bei CMP 3050 bis 3150 im Bereich des OPA? Wie signifikant ist die potentielle Verdickung in der Trias im Teil des Profils süd-südöstlich CMP 2500?</i>
12-NS-44	Beilage 5-16	A2-1-16			Beilage 7	<i>Der Fokus der Beurteilung in diesem Profil liegt auf den Effinger-Schichten und der Fortsetzung der Born-Engelberg-Struktur in dieses Gebiet. Welche Auswirkungen hat die Verdickung der Trias (duktiles Verhalten) auf die sich spröde verhaltenden Kalkbänke der Effinger-Schichten?</i>

12-NS-53	Beilage 5-17	A2-1-17	B4-9, A4-5	Beilage 6-15	Beilage 8, Fig. 13	<i>Im Grundgebirge sind starke Reflexionsbündel zu erkennen. Handelt es sich hier um Permokarbon (zwischen CMP 3600 und 5200)?</i>
Additional lines						
83-NF-06		A2-2-12	Beilage 4-5, A4-5			

Table 10: Seismic lines and related enclosures in reports for the Jura-Sudfuss geological siting region. In the last column are the specific questions from ENSI.

12-NS-42

Three faults (layout-determining faults) are interpreted along this dip line (Figure 4.12). The presence of the southern fault (CMP 3050-3150) is questionable; there is little evidence on the seismic line to interpret this fault. At the southern end of the seismic line, we can observe a thickening within the Triassic layers. The Nagra-Proseis AG team interpreted this structure as an evaporite-filled pillow, which makes sense. This thickening is related to the development of the Born-Engelberg anticline. On the parallel line, the 83-NF-06, the seismic facies of this thickening looks different and one could interpret other sediments than Triassic layers (Permian?) to be present. In the NAB 14-02 (Dossier II, A4-5 Profiles 2 and 3), geological sections across the Born anticline present an imbricate of Permian layers beneath the Born anticline. This new alternative interpretation (different from the one on the seismic sections) should be discussed in more detail. A Permian imbrication has consequences on the shortening not only on the Born anticline, but also on the layers in the whole geological siting region. This interpretation is a completely new model, which has kinematic implications on the formation of the Jura fold-and-thrust belt (thin-skin versus thick skin models discussed in the literature). The Born anticline is surrounded by Tertiary sediments (Molasse) and represents the first fold in the eastern area. A comparison with the Hermrigen fold in Canton Bern (Sommaruga et al. 2012, Encl. 6) or Trecovagnes high in Canton Vaud (Sommaruga 1997), which are also first folds of the Jura belt should be included in this broad study. As a conclusion, the Born anticline interpretation should be looked at in more detail.

12-NS-44

The focus of this dip seismic line is, as the 12-NS-42 line, on the interpretation of the Born anticline. The interpretation of the Base Mesozoic horizon does not follow the reflections, which leads to an incomprehensible interpretation. Discussion on this anticline is the same as the one given above for the 12-NS-42 line.

ENSI questions on the deformation of the *Effinger Schichten* lying on top of the Triassic thickening. The thickening of the Triassic beds can lead to internal deformation on the above layers. Discontinuous reflections are visible on the line, but it is difficult to assess if they represent internal deformation within the *Effinger Schichten*.

12-NS-53

ENSI's question on this line concerns the reflections in the basement. Indeed, there is a series

of good reflections and I would suppose Permo-Carboniferous sediments to be present, even if we cannot recognize the three series of seismic facies (*Obere Trogfüllung*, *Mittlere Trogfüllung*, *Untere Trogfüllung UT / "Kohleserie"*) which are explained in the NAB 14-17 (Fig. 5-1).

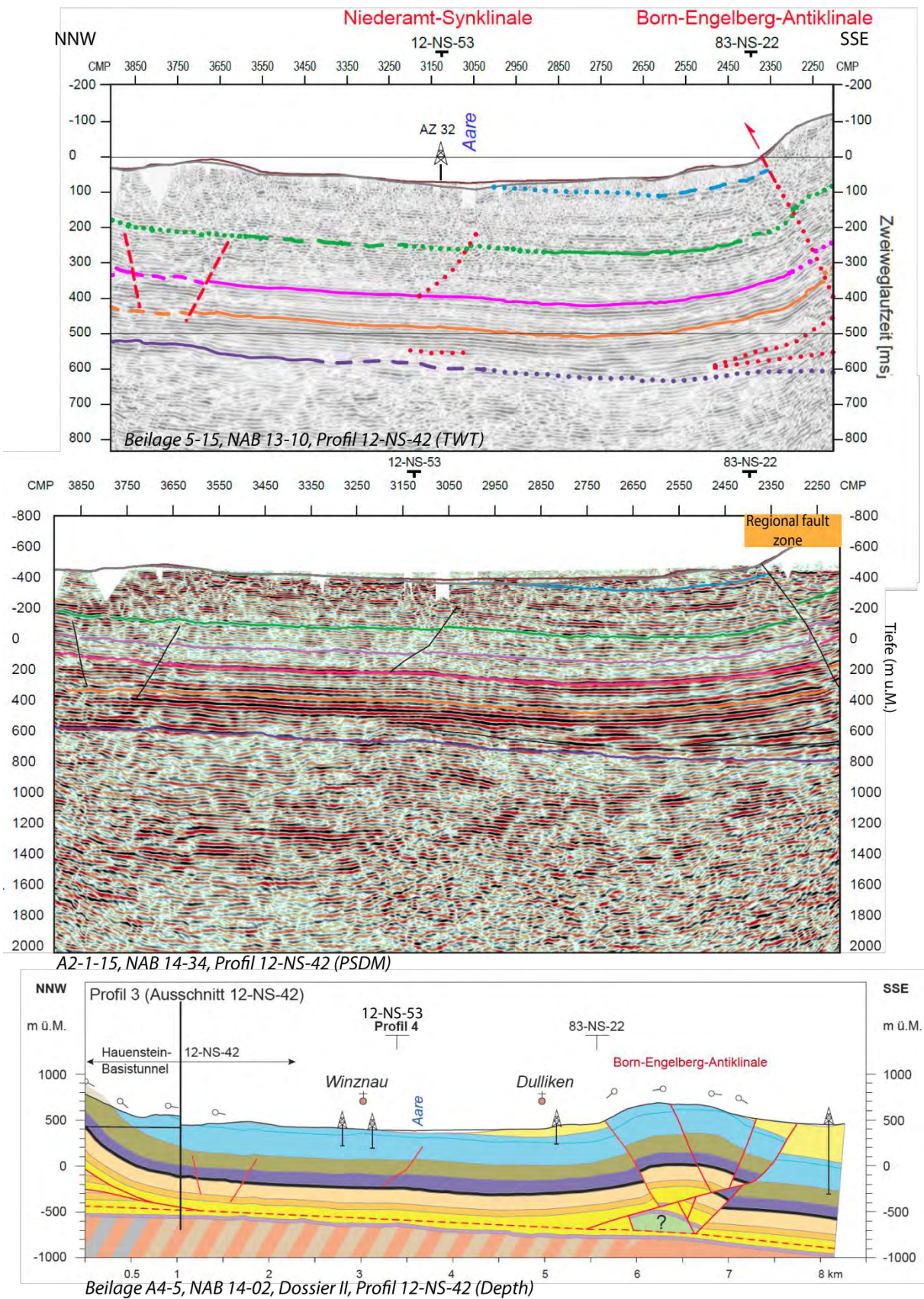


Figure 4.12: Interpretation of the Born anticline on three different seismic lines or cross-section. Regional fault zone has been added according to the CMP location. For legend see Figure 4.4, Figure 4.5 and Figure 4.7. For location map see .

5 Answers to addressed questions

5.1 Answers to questions of “*Schritt 1 von SGT - Etappe 2*“

A. Sind die Interpretationen der Strukturen der seismischen Linien nachvollziehbar?

New acquired and old reprocessed seismic lines are of good quality allowing an interpretation of the structures in the Mesozoic and Cenozoic layers. Seismic line quality is appropriate to determine the major faults and the tectonically disturbed zones. All regional fault zones have been localized and interpreted. Few minor faults proposed by Nagra are at this step not comprehensible.

B. Wurde bei der seismischen Interpretation der durch die geophysikalische Datenverarbeitung u.U. entstandenen Mehrdeutigkeit der Modelle genügend Beachtung geschenkt?

In most cases yes: the authors discussed in the text two interpretations when it was necessary and they even showed an alternative model for one specific structure. They also used low quality classes for horizons and faults to present their uncertainties. In a few cases, I would have expected more caution at this step of the procedure, especially in the interpretation of the Base Mesozoic horizon (poorer quality class).

5.2 Answers to questions of “*Schritt 2 von SGT - Etappe 2*“

C. Sind Lokation und Verlauf von regionalen Störungszonen, von anordnungsbestimmenden Störungen und von zu meidenden tektonischen Zonen nachvollziehbar?

Regionale Störungszonen

The location and the outline of the regional fault zones have been well defined and well interpreted on the 2D-seismic data. The regional faults can be seen on the seismic data. Most of the regional faults were already known from former Nagra studies, but the new acquired 2D-seismic data and the reprocessed old seismic lines helped to refine the location, the shape and to link fault segments. All regional fault zones have been detected. The location of these zones on the depth converted seismic lines is similar to the one on the TWT data.

However, the interpretation of the seismic horizons within regional fault zones should be discussed in more detail in the next stage SGT – E3. The interpretation and the depth conversion of the seismic horizons (especially the Base Mesozoic horizon) beneath the Jura main thrust fault should have been made with detail (see discussion in §3.5). The structure of the Born anticline with a Permian sediment imbrication (see §4.5, line 12-NS-42) which comes as a surprise needs also a detailed discussion. Further studies would improve the comprehension of the investigated area.

Anordnungsbestimmende Störungen

This type of faults (LDF) is poorly discussed on the interpreted seismic lines or in the two related reports (NAB 13-10, NAB 14-34). The vertical offset of these faults is close to the 2D-seismic resolution and they do not have any lateral correlation from one line to another one, which is why their direction is only loosely constrained. These faults are considered in a

separate report (NAB 14-88), but from a more theoretical/statistical point of view. The presence of these faults is uncertain, because some of them are not seen on all seismic line versions for a specific line (TWT version, depth-converted version).

Zu meidende tektonische Zonen

The tectonic zones to be avoided are defined on maps, but unfortunately not shown on all relevant seismic lines. These zones cover areas, where there are structures affecting the Mesozoic layers or where there is supposed reactivation of Permo-Carboniferous through faults. Nagra includes also flexures of Mesozoic-Cenozoic layers caused by movement along faults in the basement. These zones are well located in each siting region. In Zürich Nordost, we raise the question if not to enlarge this zone towards the Southeast of Benken-1 well, because of the presence of a large amplitude fold (called by Nagra as Trüllikon anticline, see answer from Nagra to question 1 in §4.2) which is not fully understood.

D. Ist die geologisch-tektonische Interpretation der seismischen Linien vollständig?

The geological interpretation of the seismic lines is mainly complete in the siting regions, although we miss some explanations or discussions on the evolution/age of some structures, especially since different deformational events are known in northern Switzerland (NAB 14-02, Fig. 1.3-2).

Outside the geological repository perimeter, regional structures are identified, but are not interpreted in detail. Although considered irrelevant by Nagra, we believe that Nagra should present also detailed interpretation (TWT and depth) for these zones (see §3.5) - often located at both edges of the repository emplacement - in order to give credibility to their entire work and to add to the understanding of age and evolution of these faults. Places of interference between two faults, even not located in or near the siting regions, may well serve to identify their age relationship and kinematics, which are regionally relevant.

The additional horizon Top Opalinuston – even if it is mostly conceptual - on the depth version (PSDM) has completed the set of horizons necessary for this kind of work.

E. Wurde bei der geologisch-tektonischen Interpretation der durch die geophysikalische Datenverarbeitung u.U. entstandenen Mehrdeutigkeit der Modelle genügend Beachtung geschenkt?

The interpretation on the depth converted seismic lines (PSDM version) is mainly imported from the interpretation in TWT. In most of the seismic lines, this makes good sense, because the imaging of the reflections is very close. In some cases, the imaging in DTconv version is better and the seismic reflections are different (more continuous). In their reports Nagra highlighted these cases (especially faults), but decided to keep the version from the TWT interpretation (e.g. line 11-NS-04 in Fig. 4-3, NAB-14-34). This conservatism is questionable, for example beneath the major anticlines (located in regional fault zones), where interpretation in time leads to inappropriate structures on the depth-converted lines (e.g. line 11-NS-16 in Fig. 4-4, NAB 14-34).

5.3 Answers to additional questions on specific seismic lines for siting regions

The answers to these questions addressed by ENSI are placed in § 4.1 to §4.5 with the

discussion on the specific siting region (SR, ZN, NL, JO and JS).

5.4 Answers to additional questions concerning tectonic zones to be avoided and space requirement

ENSI questions (written below in §5.4.1 to 5.4.2) addressed to the 2D- seismic experts are related to the limits of the tectonic zones to be avoided established by Nagra.

5.4.1 Tectonic zone to be avoided in the Nördlich Lägern siting region.

5.4.1.1 *Ist der Zusammenhang zwischen dem Rand des Nordschweizer Permokarbondrogs, der Flexur (see NTB 14-02, Dossier II, Fig 4.4-3) und den Störungsbild aus der 3D-Seismik im Zürcher Weinland belastbar?*

The question concerns the relevance of the link between the location of the Permo-Carboniferous troughs, the flexures and the basement faults seen on the 3D-seismic in the Zurich Nordost siting region.

The observation from the seismic data have been discussed in §4.2 regarding the ZN geological siting region. The 3D-seismic survey has helped to link laterally the individual basement faults. To determine the presence of Permo-Carboniferous sediments on the seismic lines, it is necessary to see reflections beneath the Base Mesozoic horizon. This is a case on the Figure 4.4-3 from NTB 14-02 (Dossier II), where we see high amplitude reflectors contrasting with non-reflective areas. The location of the faults is not well constrained by the reflectors in the supposed Permo-Carboniferous sediments, while in the Triassic unit, it appears better constrained. To link the faults from Triassic to Pre-Mesozoic unit seems coherent according to the geological evolution of the area, even if it is not clear from the seismic data. The location of the flexure is not very well illustrated.

A link between all these structural elements identified by Nagra certainly exists, but Nagra does not convince the reviewer in its reports (Nagra should assemble all the arguments on one or two figures). A mapping of the flexures (axial surface traces) on top of the contour map of the main marker seismic horizons (e.g. Base Tertiary, Top Liassic, Base Mesozoic) would allow to follow all the criteria.

5.4.1.2 *Wie aussagekräftig sind die Neigungskarten des Top Lias?*

The dip maps of the Top Liassic presented by Nagra (included in the answer to Frage 28) are based on the contour depth maps of the Base Opalinuston horizon. The latter maps presented in *Beilagen* of NTB 14-02 (Dossier II) cannot be considered by the reviewer in the assessment of the regional fault zones, because the contours are covered by fault zone polygons (e.g. A2-8, NTB 14-02, Dossier II).

The scale of the dip maps is ranging from 1° to 10°. One degree of change in dip represents 10% on the scale of dip. Nagra uses these dip maps, among other data, to determine the tectonic zones to be avoided. These maps show areas where the dip is higher and I agree that we can consider higher dip as one of the criterion to determine the tectonic zone to be avoided. In that sense, the amount in degree of dip to include in tectonic zones to be avoided should have been indicated and applied systemically. It looks like this criterion of high degree in dip to include some areas is not applied systemically in an objective way (e.g. in NL, south of Eglisau

and in ZN, SE of Benken). In my opinion, these maps are not meaningful by themselves, but they could contribute to evaluate the critical zones (e.g. tectonic zones to be avoided, regional fault zones).

5.4.1.3 Ist die von der Nagra auf Basis der 2D-Seismik ausgewiesene Flexur am nördlichen Rand des Standortgebiets NL nachvollziehbar und belastbar?

The term of flexure has not been discussed and defined in the recent reports by Nagra. Flexures are used in the reports as a criterion to determine the tectonic zones to be avoided, and so I would have expected a clearer definition and a precise mapping related to observations on the seismic lines. This is not case, as highlighted in the answers from Nagra to the related questions on flexures (see questions and Nagra's answers in §3.6 Flexures). The flexure location in the NL siting region is illustrated on the map of Figure 4.6. The new acquired seismic lines 11-NS-18 and 11-NS-20 cross the flexure (Figure 4.7), but Nagra does not located it on the seismic interpreted lines (*Flexur* word in red has been added for this review, see caption of the figure). I suppose that Nagra interprets as flexure on the 11-NS-18 seismic profile, the s-shape deformation of the Mesozoic layers between 6500 and 6400 CMP (see discussion in §4.3). A movement of the underlying tectonic blocks should cause the flexure and so I suppose that a reactivation of the fault across Base Mesozoic horizon at CMP 6600 would be the cause. On the parallel seismic line 11-NS-20, the flexure is mapped by Nagra around 5000 CMP, but it does not appear so clearly on the seismic line. The Base Mesozoic contour map does not indicate clear changes in dip along the mapped flexure trace (Figure 5.1). The tectonic zone to be avoided is located on the steeper part of the Base Mesozoic horizon. Here the mapping of axial surface trace would have helped to convince the reviewer and to make it more comprehensible.

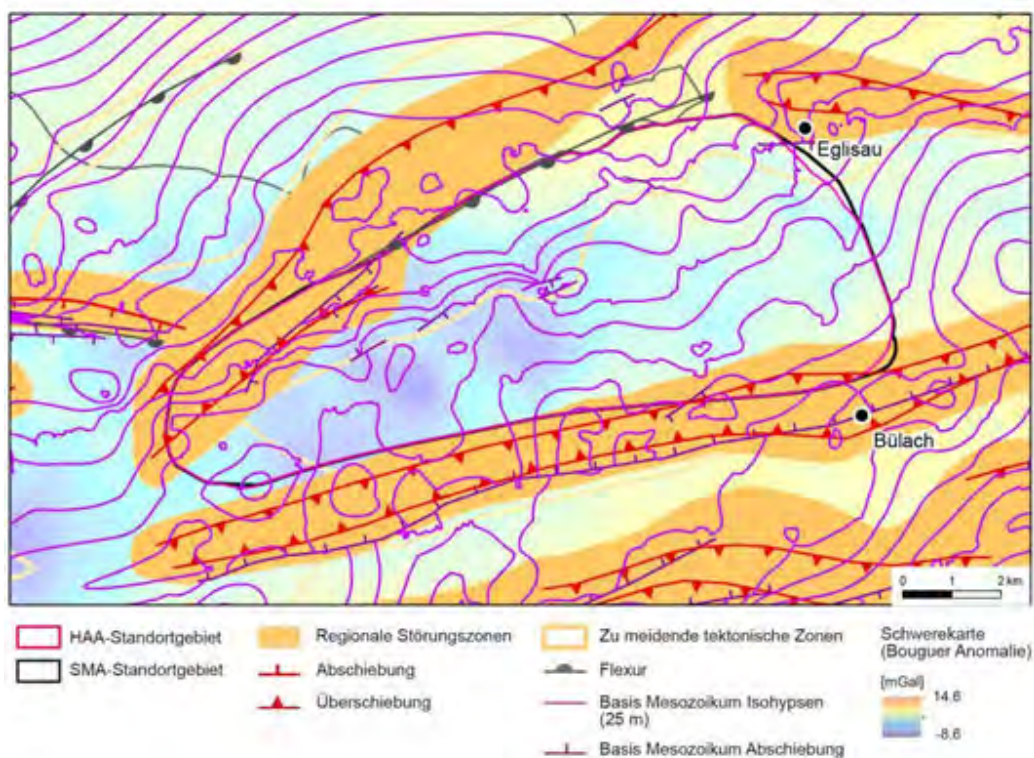


Figure 5.1: Alternative version of NTB 14-02 Dossier II Fig. 4.4-5 with contours of the Base Mesozoic horizon shown on top of the regional fault zone polygons. From Nagra, inserted in the

answer at *Frage 63_Flexur*.

5.4.1.4 Kann aufgrund der Erfahrungen aus dem Standortgebiet ZNO (Hinweis auf Zusammenhang zwischen Permokarbontrug, Flexur und Strukturzone) für das Standortgebiet NL eine potentielle Strukturzone antizipiert werden?

There are similar issues in ZNO and NL geological sitting region: edge of Permo-Carboniferous through, interaction with Mesozoic and Cenozoic layers, possible fault reactivation. So far, the structures along the northern part of the NL sitting region are not well understood yet and especially a correlation from one dip seismic line to the next one is not clear. This is discussed in §4.3, where we described the structural elements of the seismic lines. A 3D-survey would be necessary and certainly would allow to better understand this area. Nagra should illustrate precisely all the structures on contour maps and seismic profiles.

5.4.2 Space requirement

5.4.2.1 Ist es fachlich nachvollziehbar und gerechtfertigt, eine unterschiedliche Anzahl an anordnungsbestimmenden Störungen in den Lagerperimeter der Standortgebiete anzunehmen (zum Beispiel dass für die Standortgebiet NL und JS die Anzahl der Störungszonen viel grösser ist als für die anderen)? Wenn ja, was ist die Datengrundlage für diese Annahme?

The layout-determining faults (LDF) are defined (§3.3) from an engineering perspective, where the vertical offset is close to the limit of the 2D-seismic resolution (>20 m). No correlation from one seismic line to another seismic line can be made and on 2D-seismic data, they do not have a clear geological extent. The number of faults is based on seismic data. Nagra has certainly interpreted all the LDF faults visible on the 2D-seismic data, but we cannot exclude that a LDF has not been interpreted by Nagra. 3D-seismic data will constrain the interpretation of this type of faults. These LDF are almost not discussed in the seismic reports.

The number of faults is a convincing argument if you take into account the lateral extension of the faults, the type of offset and in which lithology they are located. Here, we do not have all these elements. In that sense, it is justified to have a different amount of LDF faults in each area.

6 Statement

This evaluation is based on several Nagra reports (mostly reports publically available) and meetings concerning the interpretation of the new acquired (2011/2012) and old reprocessed seismic lines included in the SGT – E2. Although many reports were consulted, three main reports include the seismic interpretation of the profiles (NAB 13-10, NAB 14-34, NAB 14-17) and one separate report (NAB 14-02, Dossier II) present the geological structures with the regional fault zones and the tectonic area to be avoided. However, a final synthesis report on the seismic interpretation is missing.

The 2D-seismic data have been correctly interpreted by Nagra. Seismic horizons have been tied accurately to the wells and their interpretation is mostly precise across all of northern Switzerland. However, the Top Opalinuston horizon remains mainly conceptual and the Base Mesozoic horizon shows a variable quality of reflections across the whole area. The interpretation of the seismic horizons within the Jura main thrust fault regional zone could have been presented in more detail.

Regional fault zones (*Regionale Störungszonen*) are well located on the seismic data and Nagra has identified all regional fault zones. Additionally, limits of tectonically disturbed zones named tectonic zones to be avoided (*Zu meidende tektonische Zonen*) within the geological siting regions are highlighted on maps, but only on few seismic lines. The outline of these zones is mainly justified, because of the presence of faults or structures in the Mesozoic or Pre-Mesozoic units, which could have been active in the last 5 Mio years and could be reactivated in the future. Next Stage 3 should clarify more precisely the geometry and the offset of the faults. For the aspects of regional fault zones and tectonic zones to be avoided, Nagra has answered with success to its major aims (identify the geological settings of regional faults and tectonic zones to be avoided) even if we would have expected in some cases more precise illustration of its arguments.

The location of the local-determining faults (faults with no lateral correlation) has to be evaluated in more detail during Stage 3 (SGT – E3) in order to refine the outline (*Lagerperimeter*) of the L/ILW and HLW repositories. Outlines of the faults across the Base Mesozoic horizon located at the edge of a Permo-Carboniferous trough are not very well defined on the 2D-seismic data. On this 2D-seismic data, the location of the Permo-Carboniferous remains partly speculative. The understanding of the geological evolution of the Permo-Carboniferous troughs was for Nagra not a major aim in the interpretation in Stage 2 (SGT - E2). In the next Stage (SGT – E3), in order to refine the outline of the repositories in the selected siting regions, some aspects should become prime goals: a 3D survey in order to refine the understanding of the geological evolution of the Permo-Carboniferous troughs together with the kinematic model of the siting regions. Refined balanced cross-sections across the area investigated in Stage 2 (including regional fault zones) and based closely on the geophysical data should be integrated. Even details within these regional fault zones – considered irrelevant for the repositories - should be represented accurately. Otherwise, a problem of credibility may arise. Based on these new elaborated models, Nagra could evaluate the risk of the reactivation of the faults in the future.

7 References

- Bini, A., Buoncristiani, J.-F., Couterrand, S., Ellwanger, D., Felber, M., Florineth, D., Graf, H.R., Keller, O., Kelly, M., Schlüchter, C. & Schoeneich, P. (2009): Die Schweiz während des letzteiszeitlichen Maximums (LGM). Karte 1:500'000. Bundesamt für Landestopografie swisstopo.
- Burg, J.P., van den Driessche, J. & Brun, J.-P. (1994): Syn- to post-thickening extension in the Variscan Belt of Western Europe: modes and structural consequences. *Géologie de la France* 3, 33-51
- Dooley T.P. and Schreurs G. (2012): Analogue modelling of intraplate strike-slip tectonics: A review and new experimental results. *Tectonophysics* 574–575, 1–71.
- Green, A.G., Merz, K., Marti, U. & Spillmann, T. (2013): Gravity data in Northern Switzerland and Southern Germany. *Nagra Arbeitsber. NAB 13-40*, Wettingen.
- Jordan, P., Graf, H.R., Eberhard, M., Jost, J., Kälin, D. & Bitterli-Dreher, P. (2011): Geologischer Atlas der Schweiz 1:25'000, Blatt 1089 Aarau (Atlasblatt 135), Erläuterungen. Bundesamt für Landestopografie swisstopo, Wabern (Bern).
- Jordan, P., Malz, A., Heuberger, S., Pietsch, J., Kley, J. & Madritsch, H. (2015): Regionale geologische Profile durch die Nordschweiz und 2D-Bilanzierung der Fernschubdeformation im östlichen Faltenjura: Arbeitsbericht zu SGT Etappe 2. *Nagra Arbeitsber. NAB 14-105*.
- Madritsch, H., Schmid, S.M. & Fabbri, O. (2008): Interactions between thin- and thick-skinned tectonics at the northwestern front of the Jura fold-and-thrust belt (eastern France). *Tectonics* 27, TC5005, doi:10.1029/2008TC002282.
- Madritsch, H., Preusser, F., Fabbri, O., Bichet, V., Schlunegger, F. & Schmid, S.M. (2010): Late Quaternary folding in the Jura Mountains: evidence from syn-erosional deformation of fluvial meanders. *Terra Nova* 22, 147-154.
- Madritsch, H., Meier, B., Kuhn, P., Roth, P., Zingg, O., Heuberger, S., Naef, H. & Birkhäuser, P. (2013): Regionale strukturgeologische Zeitinterpretation der Nagra 2D-Seismik 2011/12. *Nagra Arbeitsber. NAB 13-10*.
- Malz, A., Madritsch, H. & Meier, B. (submitted): Triangle zone formation and associated thrust front development in thin-skinned foreland fold belts: a case study from the Eastern Jura Mountains. *Tectonophysics*.
- Marchant, R., Ringgenberg, Y., Stampfli, G., Birkhäuser, P., Roth, P. & Meier, B. (2005): Paleotectonic evolution of the Zürcher Weinland (northern Switzerland), based on 2D- and 3D-seismic data. *Eclogae geol. Helv.* 98, 345-362.
- Matter, A. (1987): Faziesanalyse und Ablagerungsmilieus des Permokarbons im Nordschweizer Trog. *Eclogae geol. Helv.* 80/2, 345-368.
- Matter, A., Peters, Tj., Bläsi, H.-R., Meyer, J., Ischi, H. & Meyer, Ch. (1988): Sondierbohrung Weiach – Geologie. Text- und Beilagenband. *Nagra Tech. Ber. NTB 86-01*.
- Meier, B. & Deplazes, G. (2014a): Reflexionsseismische Analyse der Effinger Schichten. *Nagra Arbeitsber. NAB 14-57*.
- Meier, B. & Deplazes, G. (2014b): Reflexionsseismische Analyse des 'Braunen Doggers'. *Nagra Arbeitsber. NAB 14-58*
- Mosar, J. (1999): Present-day and future tectonic underplating in the western Swiss Alps: reconciliation of basement/wrench-faulting and décollement folding of the Jura and Molasse basin in the Alpine foreland. *Earth Planet. Sci. Lett.* 73, 143-155.
- Murawski, H. & Meyer Wilhelm (1998): *Geologisches Wörterbuch*. 10. Auflage, Enke Verlag, Stuttgart, 278 p.

- NAB 06-26: Stratigrafie, Mächtigkeit und Lithofazies der mesozoischen Formationen in der Nordschweiz. Eine Kompilation von Bohrungen, Übersichts- und Aufschlussprofilen. H. Naef. Nagra. Dezember 2008.
- NAB 13-10: Regionale strukturgeologische Zeitinterpretation der Nagra 2D-Seismik 2011/12. Textband and Beilagenband. H. Madritsch, B. Meier, P. Kuhn, Ph. Roth, O. Zingg, S. Heuberger, H. Naef, Ph. Birkhäuser. Nagra. Juni 2013.
- NAB 13-40: Gravity data in Northern Switzerland and Southern Germany. Text and Enclosures. Green, A.G., Merz, K., Marti, U. & Spillmann, T. Nagra, Wettingen. July 2013.
- NAB 14-17: Tektonische Karte des Nordschweizer Permokarbondrogs: Aktualisierung basierend auf 2D-Seismik und Schwere-Daten. H. Naef, H. Madritsch. Nagra. Dezember 2014.
- NAB 14-34: Tiefenkonvertierung der regionalen Strukturinterpretation der Nagra 2D-Seismik 2011-12. Textband, Beilagen, Anhangen B. Meier, P. Kuhn, S. Muff, P. Roth, H. Madritsch. Nagra. September 2014.
- NAB 14-57: Reflexionsseismische Analyse der Effinger Schichten B. Meier, G. Deplazes. Nagra. Oktober 2014.
- NAB 14-58 Vorabdruck_Reflexionsseismische Analyse des „Braunen Doggers“ B. Meier, G. Deplazes. Nagra. Dezember 2014.
- NAB 14-88: Simulation of layout-determining fault networks based on 2D-seismic interpretations: Implications for sub-surface space reserves in geological siting regions in northern Switzerland G.W. Lanyon, H. Madritsch. Nagra. December 2014.
- NAB 14-105: Regionale geologische Profilschnitte durch die Nordschweiz und 2D-Bilanzierung der Ferschubdeformation im östlichen Faltenjura: Arbeitsbericht zu SGT-Etappe 2. P. Jordan, A. Malz, S. Heuberger, J. Pietsch, J. Kley, H. Madritsch. Nagra. März 2015.
- NTB 00-03: 3D-Seismik: Räumliche Erkundung der mesozoischen Sedimentschichten im Zürcher Weinland. Ph. Birkhäuser, Ph. Roth, B. Meier, H. Naef. Nagra. August 2001.
- NTB 14-01: SGT Etappe 2: Vorschlag weiter zu untersuchender geologischer Standortgebiete mit zugehörigen Standortarealen für die Oberflächenanlage. Sicherheitstechnischer Vergleich und Vorschlag der in Etappe 3 weiter zu untersuchenden geologischen Standortgebiete. Nagra. Dezember 2014
- NTB 14-02: Dossier I. SGT Etappe 2: Vorschlag weiter zu untersuchender geologischer Standortgebiete mit zugehörigen Standortarealen für die Oberflächenanlage. Geologische Grundlagen. Dossier I. Einleitung. Nagra. Dezember 2014.
- NTB 14-02: Dossier II. SGT Etappe 2: Vorschlag weiter zu untersuchender geologischer Standortgebiete mit zugehörigen Standortarealen für die Oberflächenanlage. Geologische Grundlagen. Sedimentologische und tektonische Verhältnisse. Nagra Dezember 2014.
- NTB 14-02: Dossier III. SGT Etappe 2: Vorschlag weiter zu untersuchender geologischer Standortgebiete mit zugehörigen Standortarealen für die Oberflächenanlage. Geologische Grundlagen. Geologische Langzeitenentwicklung. Nagra. Dezember 2014.
- NTB 14-02: Dossier VII SGT Etappe 2: Vorschlag weiter zu untersuchender geologischer Standortgebiete mit zugehörigen Standortarealen für die Oberflächenanlage. Geologische Grundlagen. Nutzungskonflikte. Nagra. Dezember 2014.
- NTB 14-02: Dossier VIII SGT Etappe 2: Vorschlag weiter zu untersuchender geologischer Standortgebiete mit zugehörigen Standortarealen für die Oberflächenanlage. Geologische Grundlagen. Dossier VIII. Charakterisierbarkeit und Explorierbarkeit. Nagra Dezember 2014.
- Preusser, F. & Graf, H.R. (2002): Erste Ergebnisse von Lumineszenzdatierungen eiszeitlicher Ablagerungen der Nordschweiz. Jber. Mitt. Oberrhein. Geol. Ver., N.F. 84, 419-438. Roth, Ph., Naef, H. & Schnellmann, M. (2010): Kompilation und Interpretation der

- Reflexionsseismik im Tafeljura und Molassebecken der Zentral- und Nordostschweiz. Unpubl. Nagra Interner Bericht NIB 08-10.
- Reinicke, K.M. (2011): Unkonventionelles Gas – Wo liegen die Herausforderungen? Erdöl Erdgas Kohle 127/10, 340-342.
- Rybarczyk, G. (2012): Abschlussbericht des Reprozessings der regionalen seismischen Profildaten in der Nordschweiz. Unpubl. Nagra Interner Ber.
- Rybarczyk, G. (2013): Seismische Datenverarbeitung der Nagra 2D-Seismik 2011/12 in Zeit. Nagra Arbeitsber. NAB 13-09.
- Sommaruga, A. (1997): Geology of the Central Jura and the Molasse Basin: new insight into an evaporite-based foreland fold and thrust belt. – Mém. soc. neuchâteloise sci. nat. 12, 176.
- Sommaruga, A., Eichenberger, U. & Marillier, F. (2012): Seismic Atlas of the Swiss Molasse Basin. Text Volume. Edited by the Swiss Geophysical Commission. Matér. Géol. Géophys. 44, swisstopo, Wabern.
- Ustaszewski, K. & Schmid, S.M. (2007): Latest Pliocene to recent thick-skinned tectonics at the Upper Rhine Graben – Jura Mountains junction. Swiss J. Geosci. 100, 293-312.

8 Appendices

Frage 28: Zu meidende tektonische Zonen

Versandt am 28.05.2015, Antwort erhalten am 21.06.2015.

Betrifft: NTB 14-01, Fig. 4.1-2 und weitere Figuren zu den tektonischen Elementen der Nordschweiz

Wie definiert die Nagra die Ränder der zu meidenden tektonischen Zonen? Wie wird z.B. die Einbuchtung des Südrandes der im Norden des Standortgebietes NL durchziehenden zu meidenden tektonischen Zone vorgenommen? Im zentralen Bereich des Standortgebietes NL gibt es zwei kleinere tektonische Strukturen (ca. 2 km südlich der Bohrung Weiach, vgl. Beilage A2-8 in NTB 14-02). Um diese herum zieht sich der Südrand der zu meidenden tektonischen Zone und biegt dann nach Nordosten in einem Bogen bis zur nächsten tektonischen Struktur, die ca. 2 km östlich von Weiach liegt. Wie wurde die Krümmung dieses Bogens festgelegt? Man könnte alternativ die Bucht bis zum Rand des Standortgebietes ausweiten und damit das Gebiet um die Bohrung Weiach als ausserhalb der zu meidenden tektonischen Zone erklären.

Antwort der Nagra vom 21.06.2015:

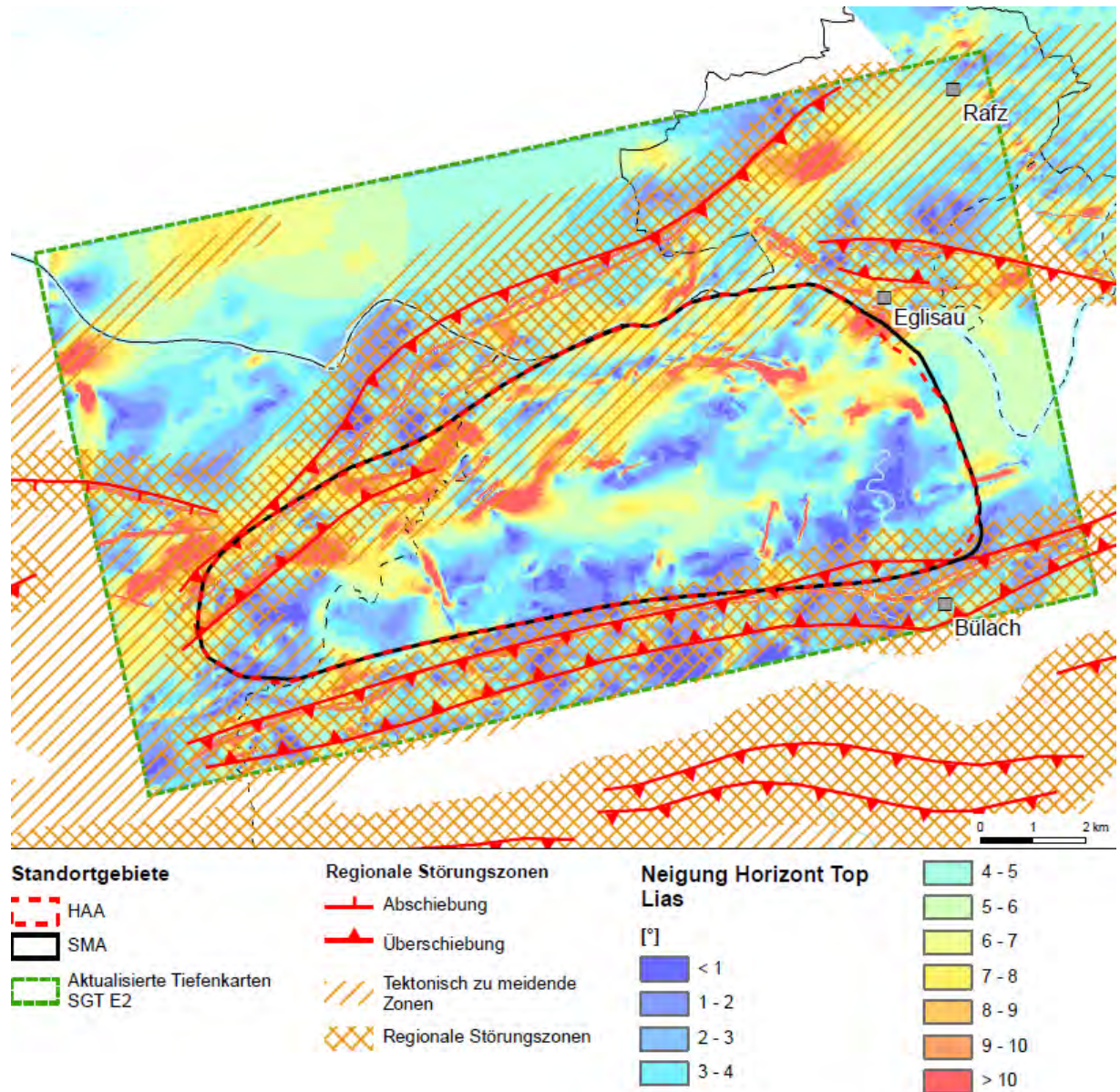
Die Abgrenzung der zu meidenden tektonischen Zonen ist in NTB 14-02 Dossier II Kap. 4 beschrieben. Generell wird in Kap. 4.4.2 (S. 72) und für das Standortgebiet Nördlich Lägern im Speziellen nochmals in Kap. 4.5.3 (S. 84) darauf eingegangen.

Die angesprochene zu meidende tektonische Zone im Gebiet NL betrifft post-paläozoisch reaktivierte Grundgebirgsstörungen am Nordrand des Nordschweizer Permokarbondrogs. Die generellen Kriterien für deren Abgrenzung sind im oben genannten Bericht wie folgt beschrieben (vgl. Absatz 3 auf S.75): *„Indikativ für die von derartigen regionalen tektonischen Elementen betroffenen Bereiche sind deutliche, über mehrere Kilometer verfolgbare Flexuren des mesozoisch-känozoischen Sedimentstapels über an der Basis Mesozoikum kartierbaren Störungen (s. Naef & Madritsch 2014). Die post-paläozoisch reaktivierten Grundgebirgsstörungen zeichnen sich neben ihrer direkten Abbildung in den 2D-Seismikprofilen ausserdem deutlich in den Isohypsenkarten der verschiedenen mesozoischen, seismischen Markerhorizonte ab; im Falle der Randstörungen des zentralen Nordschweizer Permokarbondrogs häufig auch durch markante Gradienten in den regionalen Schwerekarten (s. Fig. 2.3-1)“.*

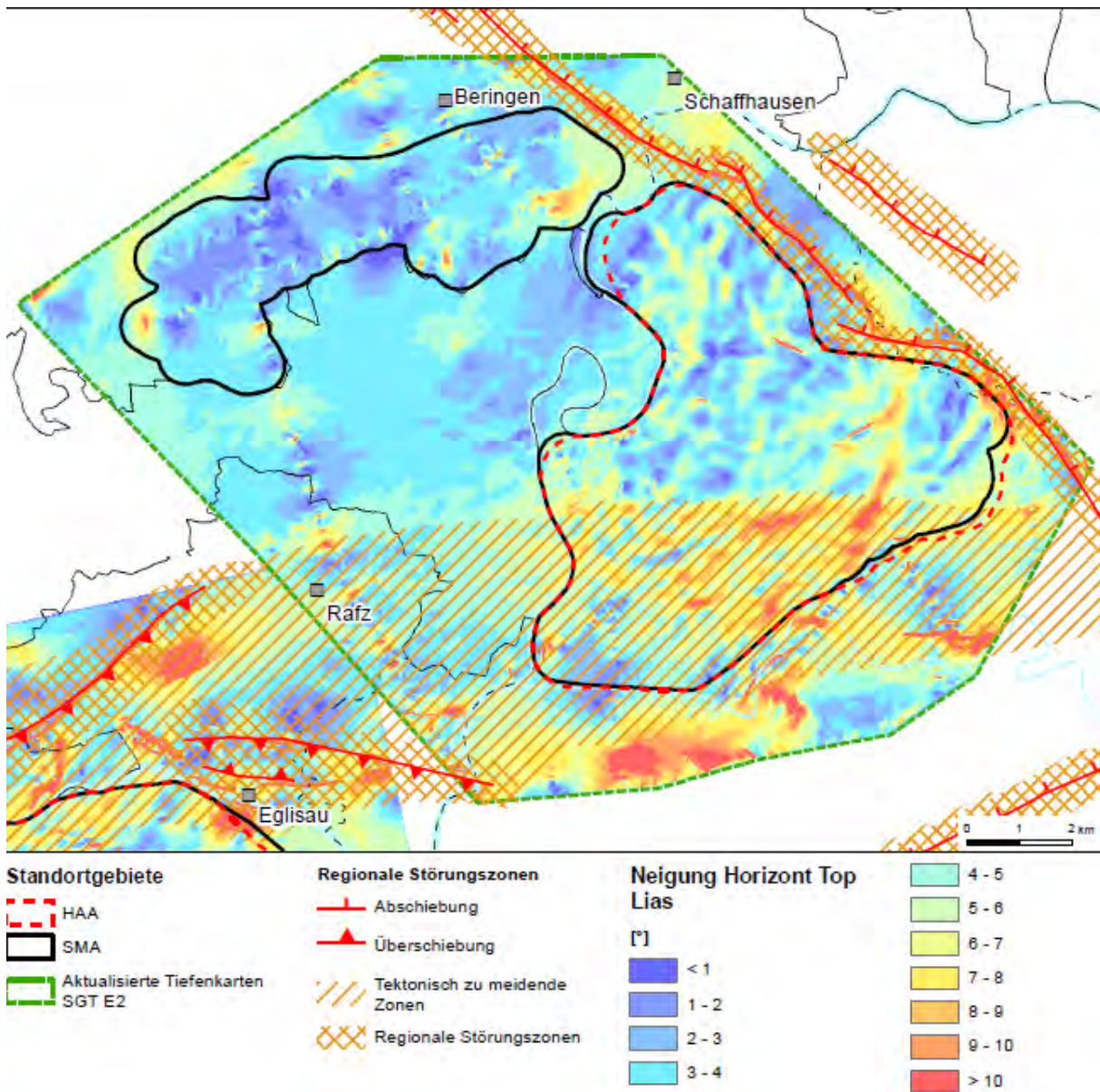
Die zu meidende tektonische Zone im Gebiet Nördlich Lägern und insbesondere deren Südbegrenzung wird also nicht nur durch die in der ENSI-Frage adressierten, meist nicht lateral korrelierbaren Strukturen auf einzelnen 2D-Seismiklinien definiert, sondern vor allem aufgrund der Analyse des Verlaufs der Isohypsen der diversen mesozoischen Markerhorizonte (vgl. S. 85 Absatz 2). In Fig. 4.4-5 des oben genannten Berichts sind nur die Isohypsen der Basis Mesozoikum dargestellt (für weitere Horizonte wird hier auf NAB 13-10 verwiesen). Diese zeigen deutlich eine grossräumig verfolgbare Flexur ab Nordrand des Standortgebiets NL, welche die zu meidende tektonische Zone repräsentiert.

Zur zusätzlichen Veranschaulichung derselben wird hier eine weitere Figur beigelegt, welche eine Neigungskarte der Basis Opalinuston (entspricht dem seismischen Markerhorizont Top Lias)

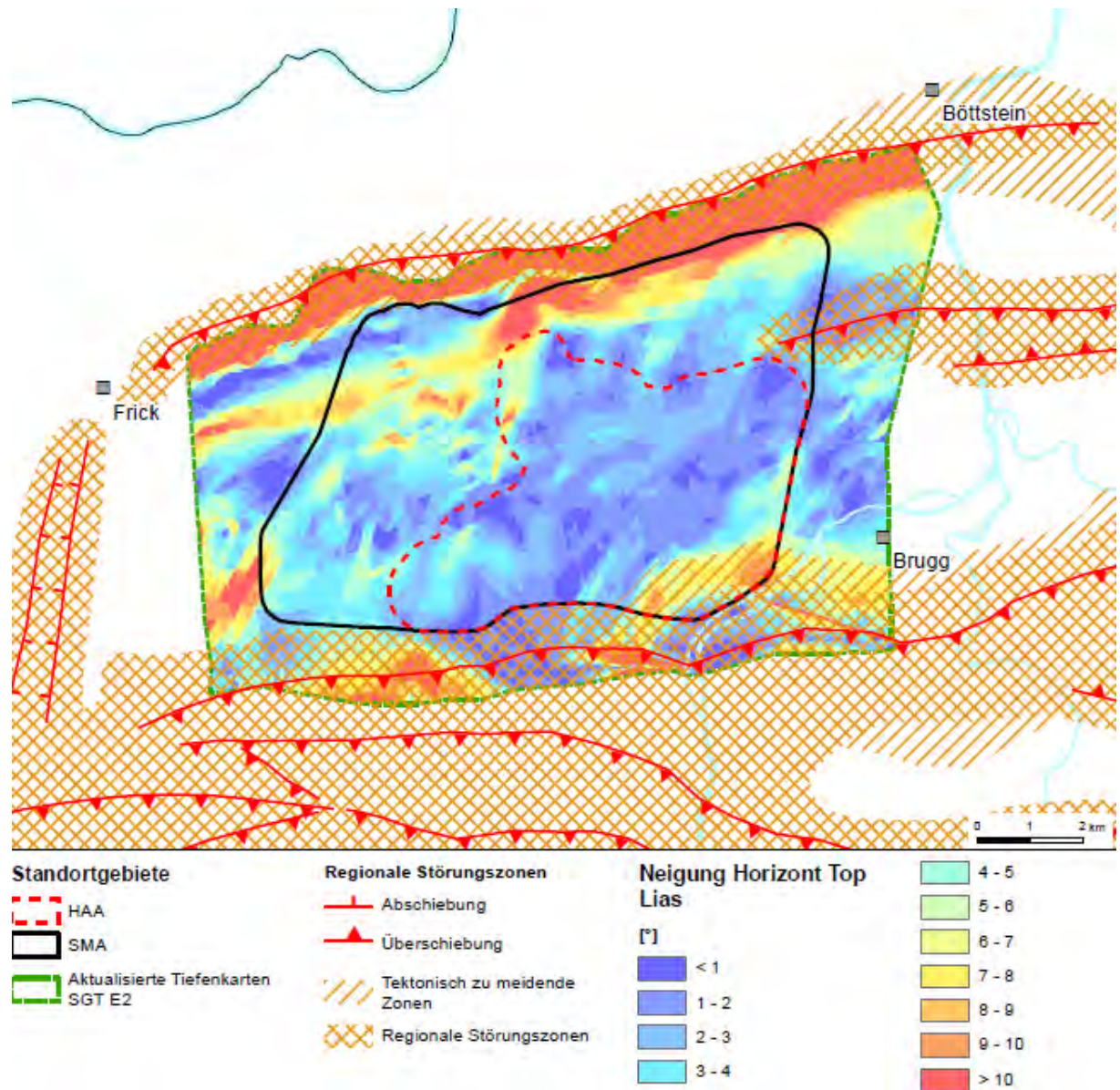
zeigt, anhand derer die gewählte Südbegrenzung für die zu meidende tektonische Zone noch deutlicher nachvollzogen werden kann. Der Vollständigkeit halber werden auch entsprechende Karten für die Standortgebiete Zürich Nordost und Jura Ost hinzugefügt, welche von gleichartigen zu meidenden tektonischen Zonen betroffen sind.



Frage 28: Abb. 1: Neigungskarte des geologisch modellierten seismischen Markerhorizonts Top Lias im Standortgebiet Nördlich Lägern mit überlagerten „regionalen Störungszonen“ und „zu meidenden tektonischen Zonen“ gemäss NTB 14-01 (siehe Diskussion im Text).



Frage 28: Abb. 2: Neigungskarte des geologisch modellierten seismischen Markerhorizonts Top Lias im Standortgebiet Zürich Nordost mit überlagerten „regionalen Störungszonen“ und „zu meidenden tektonischen Zonen“ gemäss NTB 14-01



Frage 28: Abb. 3: Neigungskarte des geologisch modellierten seismischen Markerhorizonts Top Lias im Standortgebiet Jura Ost mit überlagerten „regionalen Störungszonen“ und „zu meidenden tektonischen Zonen“

Rückfrage des ENSI vom 14.07.2015:

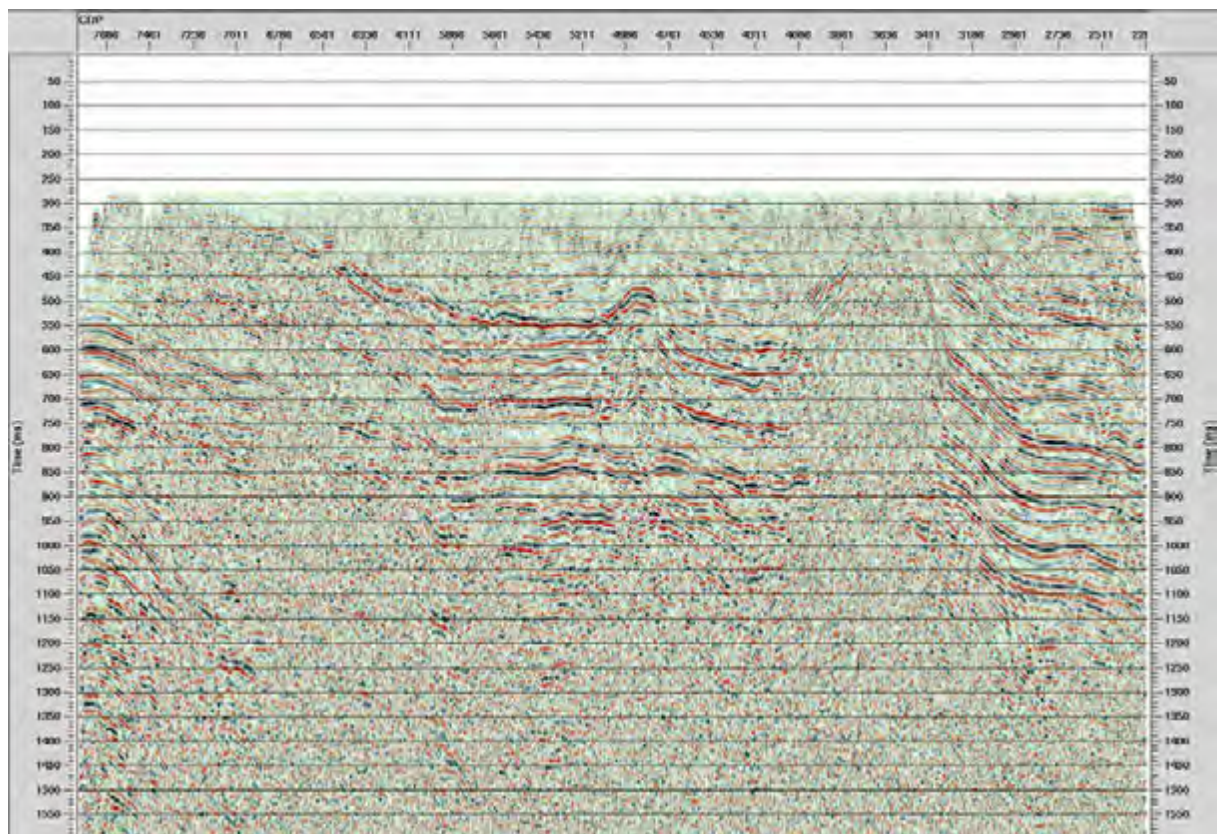
1. Die Nagra zeigt in der Antwort zur Frage 28 hochauflösende Neigungskarten für die Gebiet NL, ZNO und JO. Die Karten zeigen die Neigung des modellierten seismischen Horizontes Top Lias. Das ENSI wünscht sich präzisierend Erläuterungen bzgl. der Datengrundlage und Auflösungsgenauigkeit der Karten? Z.B. wie genau sind diese Angaben abseits der seismischen Profile in JO und NL?

Antwort Nagra: Wie das ENSI richtig feststellt, leiten sich die hier gezeigten Neigungskarten aus den modellierten Tiefenkarten der Basis Opalinuston ab, welche in Nagra (2014) für alle Standortgebiete gezeigt werden (vgl. Beilagen A1-11, A2-8, A3-8 und A4-9). Die Berechnung der Neigungskarten anhand der Tiefenkarten erfolgte mittels ArcMap (Funktion Slope).

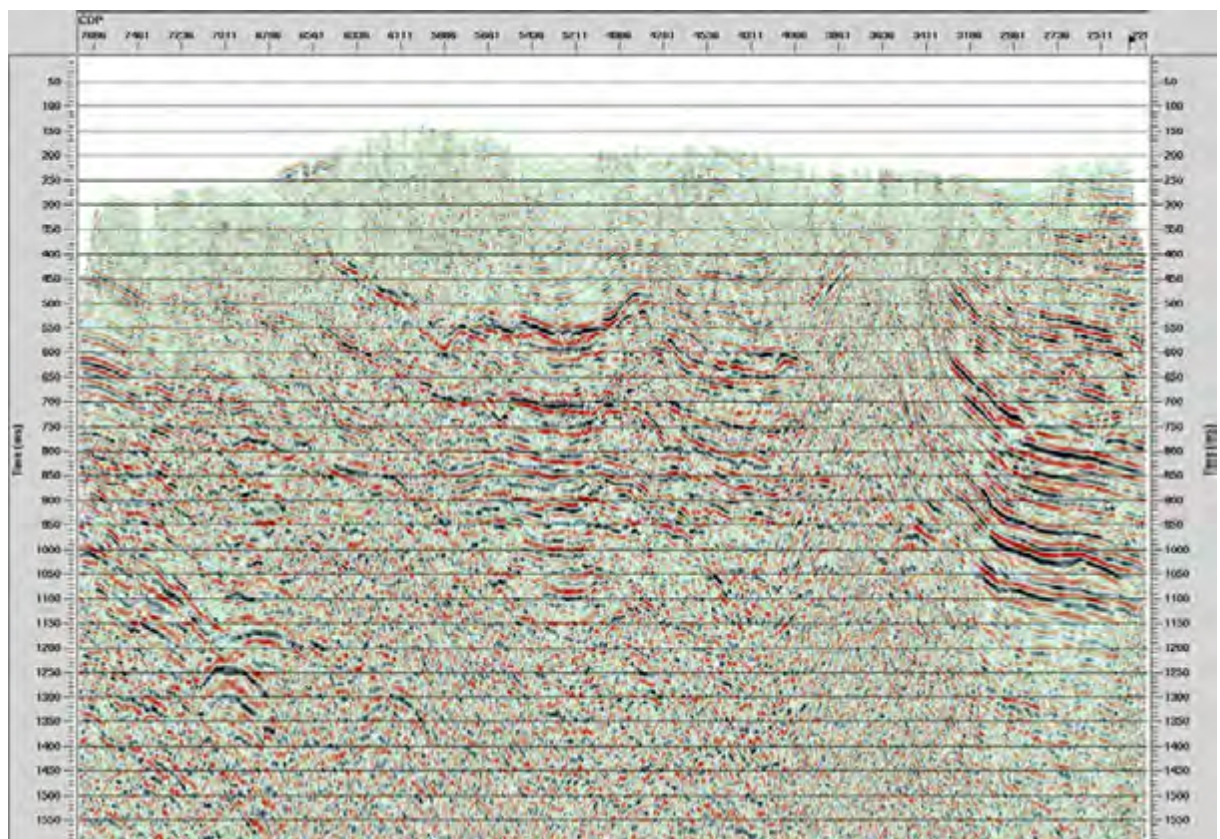
Die Auflösungsgenauigkeit der den Neigungskarten zugrundeliegenden Rasterdaten entspricht jenen der Tiefenkarten (vgl. Nagra 2014, Becker et al. 2015) und beträgt 25 m. Beachtet werden muss hierbei, dass das 2D-Raster in der Umgebung der Störungen die 3D-Situation nur bedingt abbilden kann. So werden an Abschiebungen die fehlenden Zellen eines Horizonts entlang der Störungsfläche interpoliert, während an Aufschiebungen nur die hangende Scholle im Neigungsraaster abgebildet wird.

Die Ungewissheiten der Rasterinformationen in den Neigungskarten sind grundsätzlich an die Ungewissheiten der Tiefenlage des modellierten Horizonts gekoppelt. Letztere wurde in Nagra (2014) grob abgeschätzt (vgl. Beilagen A1-14, A2-11, A3-10, A4-12). Rein qualitativ kann in Analogie dazu zunächst für die Ungewissheiten der Neigungsangaben festgehalten werden, dass diese abseits der Seismiklinien grösser sind als entlang derselben. Entlang der Seismiklinien kommen theoretisch dieselben Aspekte zum Tragen, wie sie von Meier et al. (2014) für die Ungewissheit in der Tiefenlage seismisch interpretierter geologischer Horizonte adressiert wurden (Statik-Korrektur, Picking des Seismik-Interpreten, Geschwindigkeitsmodell). Anstelle einer mathematischen Quantifizierung der Ungewissheiten für die hier gezeigten, aber nicht publizierten Neigungsangaben wird hier im Sinne eines qualitativen Evaluationsansatzes auf die Berichte zur seismischen Datenverarbeitung von Rybarczyk (2012, 2013 und 2014) verwiesen. In diesen Berichten werden frühe Stapel-Versionen der verschiedenen Seismiklinien gezeigt und gegenüberstellt (e.g. Profile vor und nach Statik- und Misfit-Korrekten, sowie vor und nach Tiefenwandlung, vgl. Abbildung 4). Diese Gegenüberstellungen zeigen deutlich, dass die im vorliegenden Dokument gezeigten Neigungskarten den generellen geologischen Schichtverlauf so nachzeichnen, wie er bereits aus nur rudimentär prozessierten seismischen Daten hervorgeht. Qualitativ betrachtet kann deshalb davon ausgegangen werden, dass die durchaus vorhandenen Ungewissheiten der Neigungskarten den generellen Schichtneigungstrend, wie er innerhalb der interessierenden Gebiete entlang mehrerer Seismikprofile gleichartig in Erscheinung tritt und sich in weiterer Folge auf die inter- bzw. extrapolierten Rasterdatensätze überträgt, nicht in Frage stellen. Im Falle des Standortgebiets Nördlich Lägern beispielsweise gibt es mehrere unabhängige Hinweise auf ein steileres Einfallen der Schichtfolge am Nordrand des Gebiets (vgl. Ausführungen zu Abbildung 4).

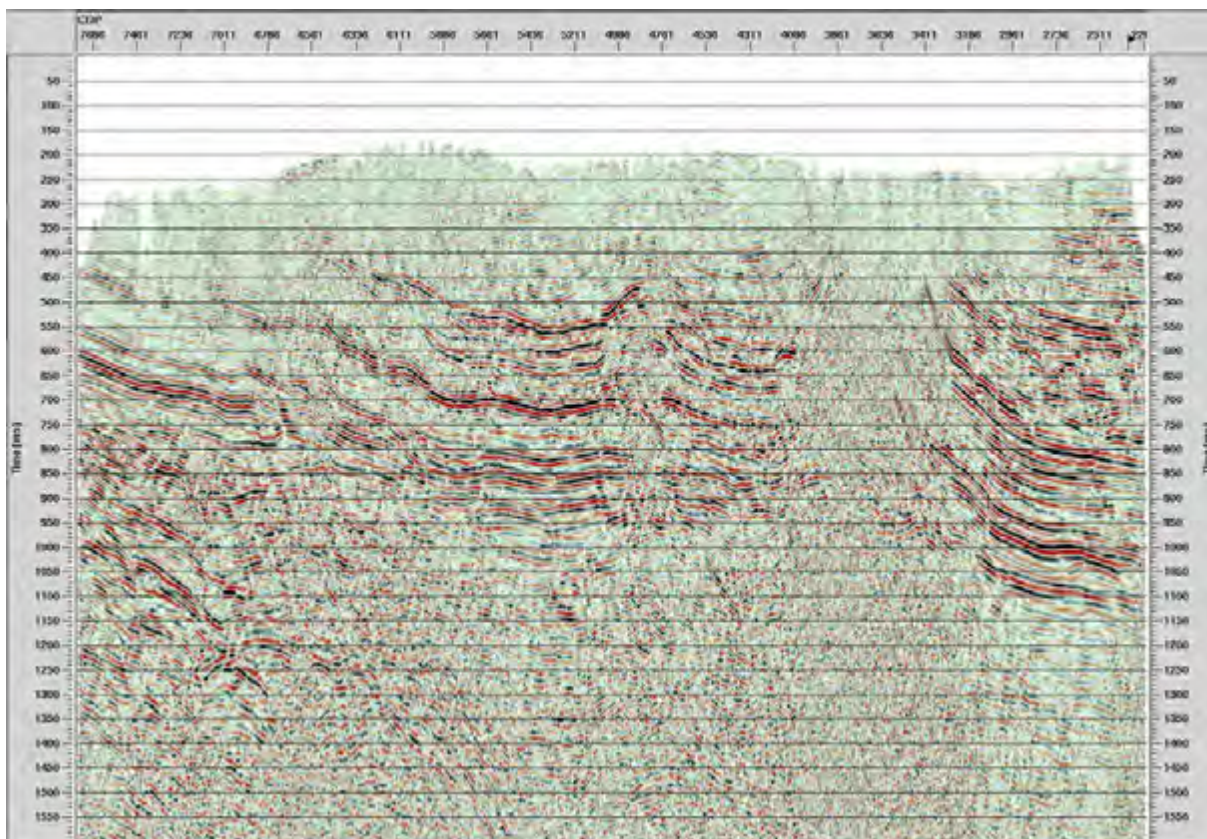
Frage 28: Abb. 4: Gegenüberstellung von verschiedenen Versionen des seismischen Profils 11-NS-18 (zusammengestellt aus den Berichten von Rybarczyk 2013 & 2014). Sie zeigt, dass der generelle, sich aus dem Seismikprofil ergebende Schichtneigungstrend, wie er auch in den hier gezeigten Neigungskarten in Erscheinung tritt, bereits in einem sehr frühen Stadium der Bearbeitung der seismischen Daten in Erscheinung tritt und ungeachtet der verschiedenen Bearbeitungsschritte erhalten bleibt. Entlang der seismischen Profile wird dieser Trend daher qualitativ als robustes Charakteristikum für die geologische Interpretation erachtet. Im Falle des hier beispielhaft illustrierten Querprofils durch das Standortgebiet Nördlich Lägern betrifft dies insbesondere das deutlich steilere Einfallen des geologischen Schichtstapels am Nordrand des Profils (in den Abbildungen ca. links von CDP 5800) gegenüber dem zentralen Profilabschnitt. Eine deutliche Flexur, welche auch in den Schichtneigungskarten angedeutet wird und von Nagra (2014) als zu meidende tektonische Zone ausgewiesen wurde, zeichnet sich bereits nach den reststatischen Korrekturen deutlich in den seismischen Daten ab (Abb. 4c).



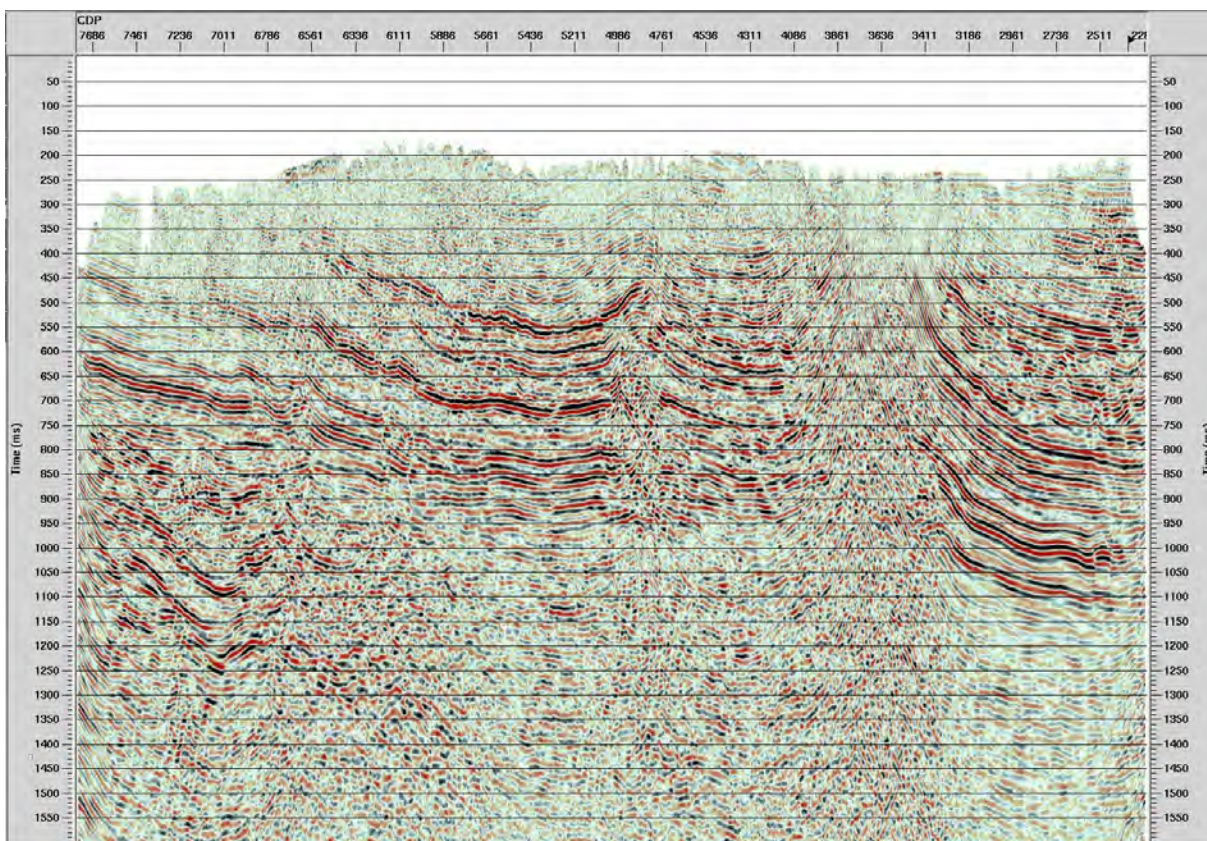
a) 11-NS-18 Feldstapelung



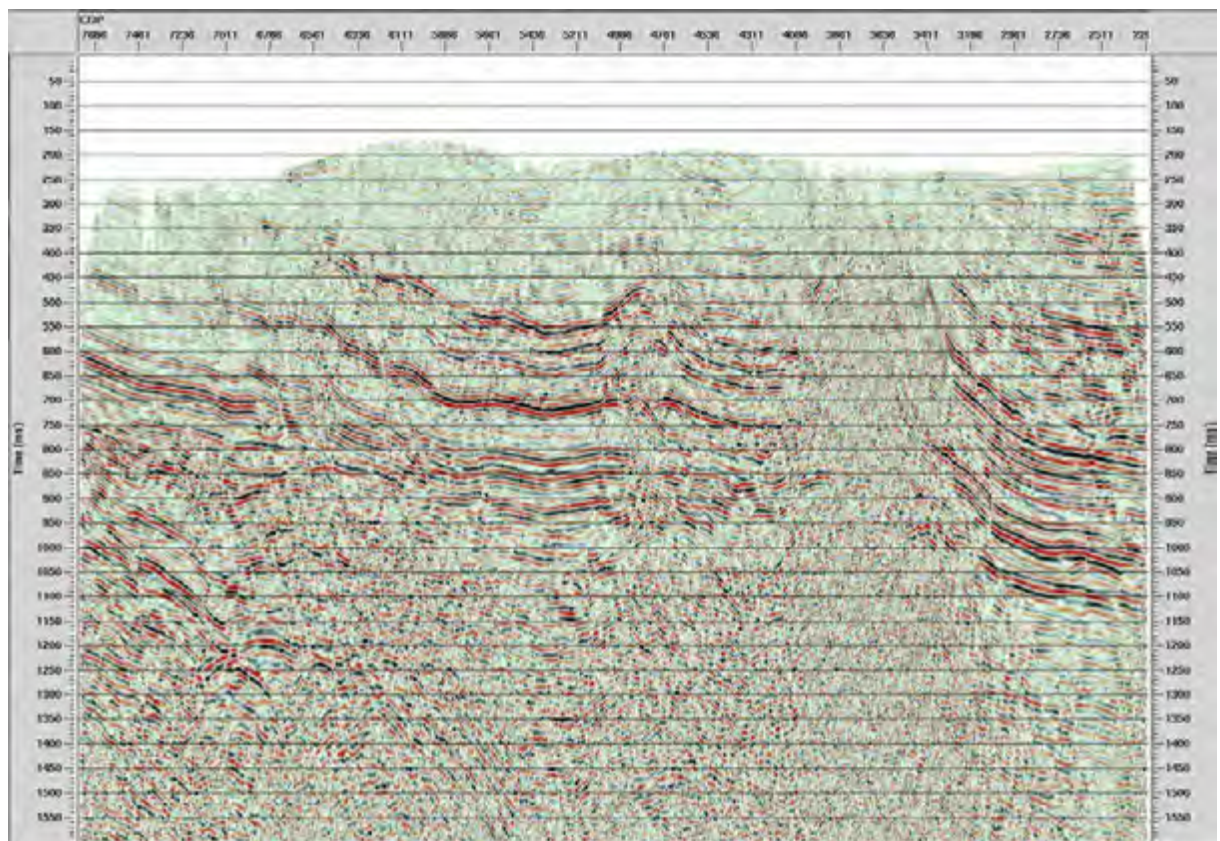
b) 11-NS-18 nach Refraktionsstatik



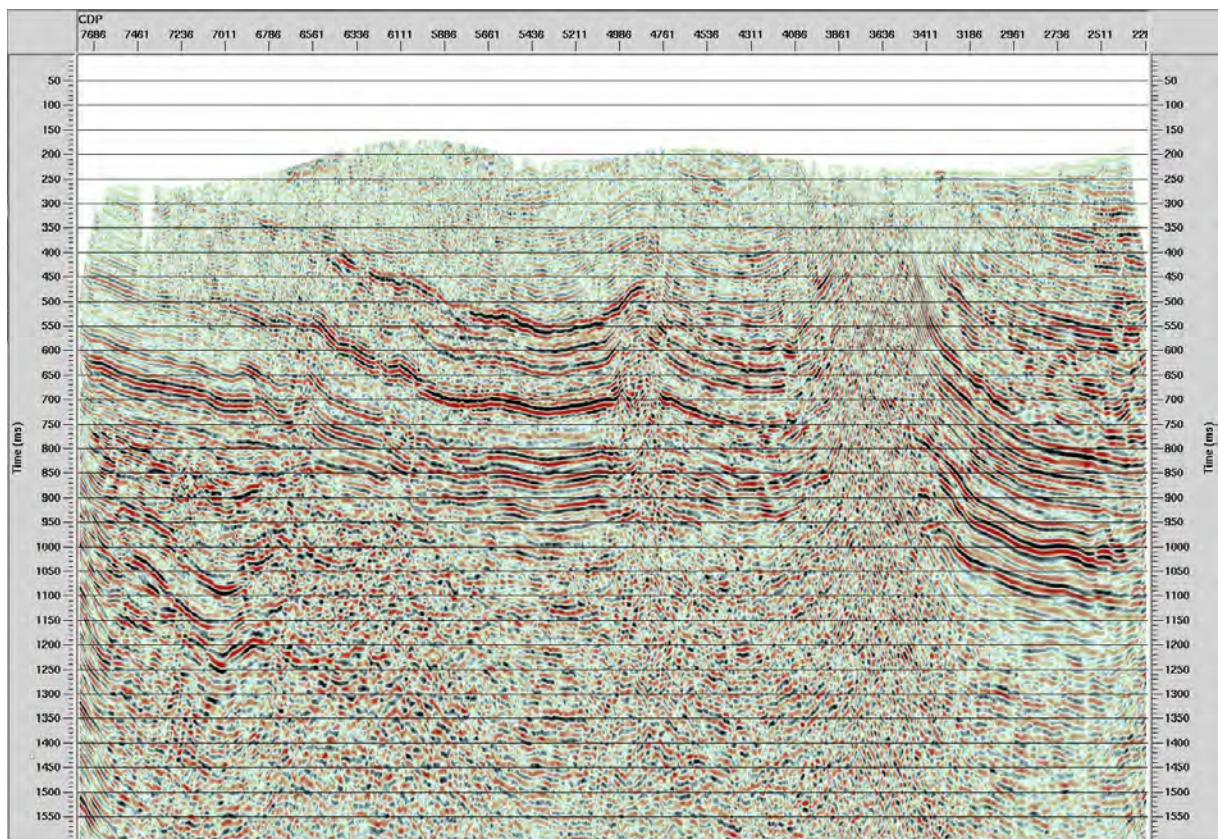
c) 11-NS-18 Finale Stapelung (mit Refraktions- und Reststatik)



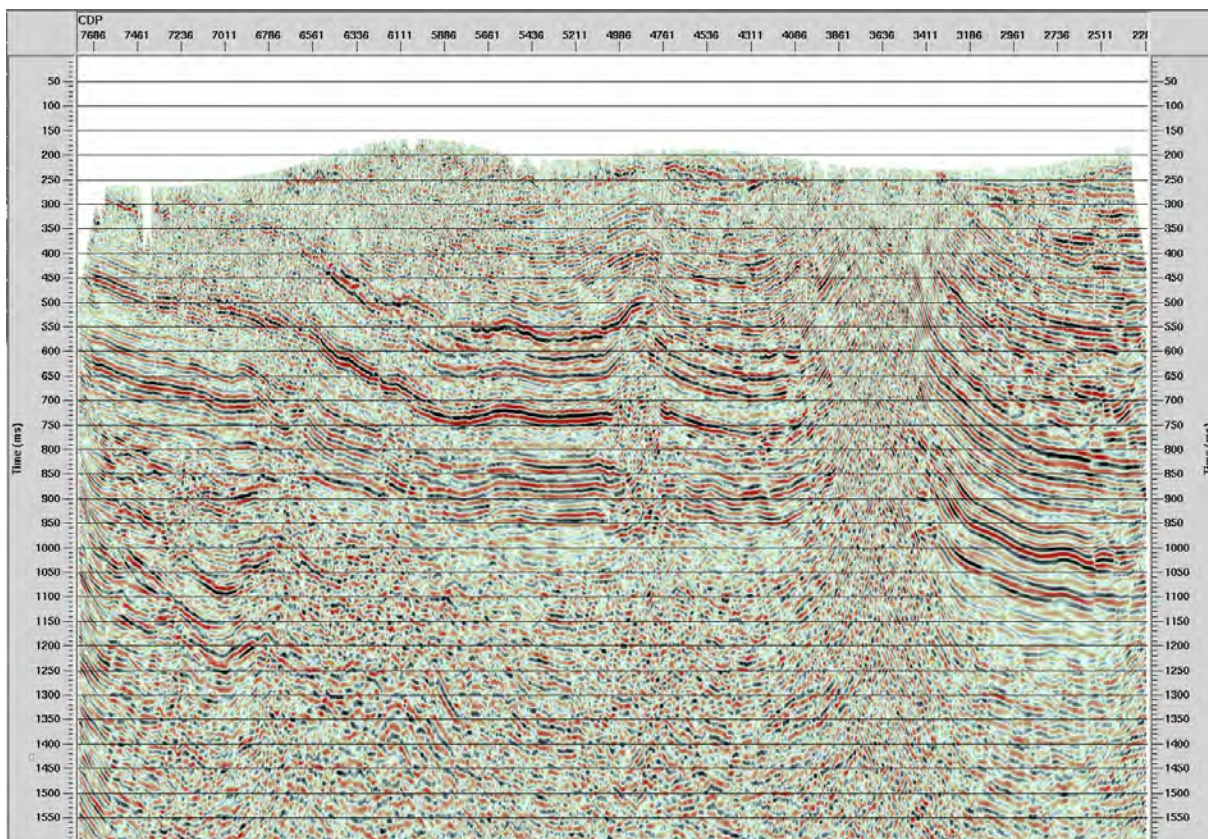
d) 11-NS-18 Finale Stapelung mit Poststack Time Migration



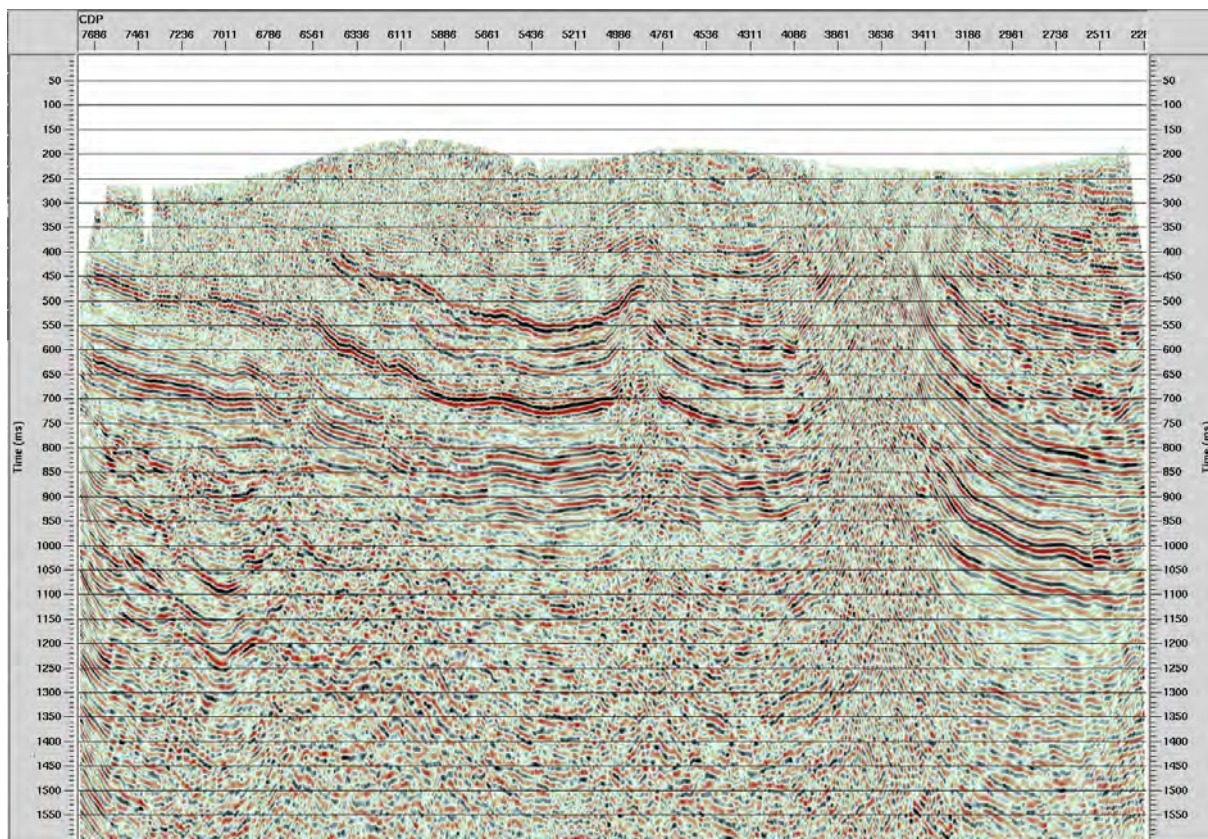
e) 11-NS-18 Finale Stapelung nach CRS Bearbeitung



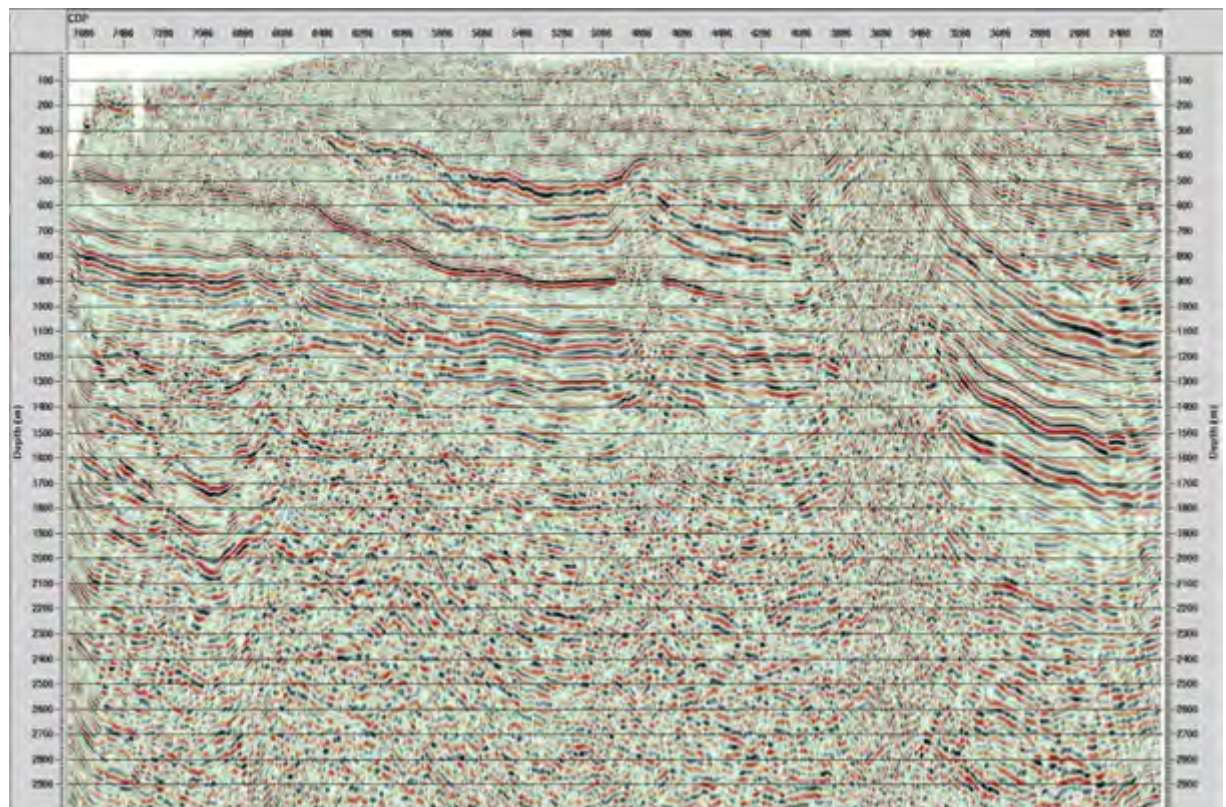
f) 11-NS-18 Finale Stapelung mit CRS Bearbeitung und Poststack-Time Migration



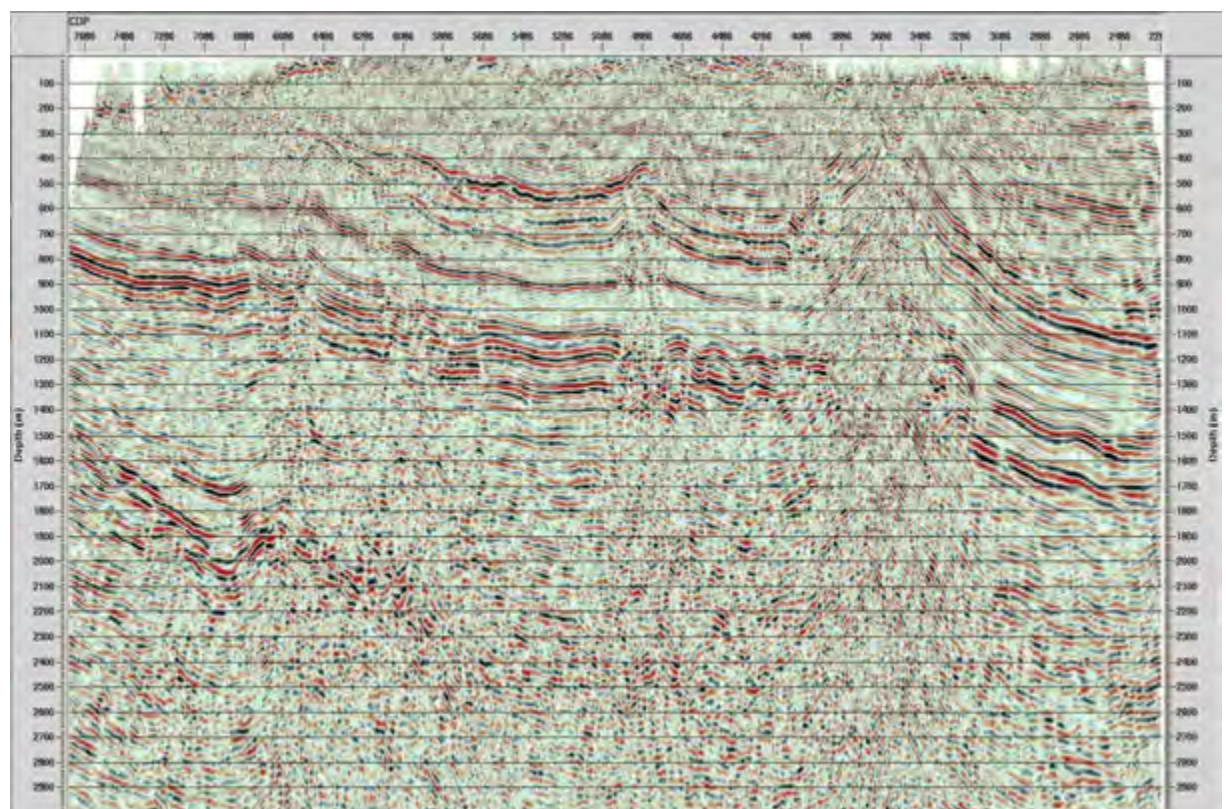
g) 11-NS-18 provisorische Prestack-Time Migration (vor Mistie-Korrektur)



h) 11-NS-18 Finale Prestack-Time Migration (nach Mistie-Korrektur)



i) 11-NS-18 Poststack Tiefenkonversion der Prestack Time Migration



j) 11-NS-18 Prestack Depth Migration

Referenzen:

- Becker, J., Madritsch, H., Schnellmann M., Ruff, M. & Albert, W. (2015): Erläuterungen der für die Abgrenzung von Lagerperimetern verwendeten GIS-Datensätze und ihrer Grundlagen (Revision 1). Unpubl. Nagra Interner Ber.
- Meier, B., Kuhn, P., Roth, Ph., Muff, S. & Madritsch, H. (2014): Tiefenkonvertierung der regionalen Strukturinterpretation der Nagra 2D-Seismik 2011/12. Nagra Arbeitsber. NAB 14-34.
- Nagra (2014): SGT Etappe 2: Vorschlag weiter zu untersuchender geologischer Standortgebiete mit zugehörigen Standortarealen für die Oberflächenanlage. Geologische Grundlagen, Dossier II, Sedimentologische und tektonische Verhältnisse. Nagra Tech. Ber. NTB 14-02.
- Naef, H. & Madritsch, H. (2014): Aktualisierung der tektonischen Karte des Nordschweizer Permokarbons. Nagra Arbeitsber. NAB 14-17.
- Rybarczyk, G. (2012): Abschlussbericht des Reprozessings der regionalen seismischen Profildaten in der Nordschweiz. Unpubl. Nagra Interner Ber.
- Rybarczyk, G. (2013): Seismische Datenverarbeitung der Nagra 2D-Seismik 2011/12 in Zeit. Nagra Arbeitsber. NAB 13-09.
- Rybarczyk, G. (2014): Seismische Datenbearbeitung der Nagra 2D-Seismik 2011/12 in Tiefe. Nagra Arbeitsber. NAB 13-80.

Frage 33: Geologische Entwicklung ZNO

Versandt am 29.05.2015, Antwort erhalten am 21.06.2015.

How do you explain the geological evolution of the Benken horst?

On the line (B 6-14, NAB 14-17, Line 91-NO-75, TWT) we see a large scale anticline. This structure is also visible on the depth version (A 2-2-30, NAB 14-34, PSDM, 91-NO-75, CMP 2500-2680).

All the layers from BMes to Tertiary are gently folded and parallel.

Do we have velocity problem in this area?

If the structural high is real combined with the presence of faults reaching into the Tertiary series (i.e. Neuhausen faults), this suggest neotectonic and possible recent tectonic activity.

Are also other bounding faults of this horst potentially host to recent tectonics?

The Benken Horst is interpreted to reflect a Late Paleozoic structure in the first place, whose bounding faults were repeatedly reactivated later on (e.g. during Mesozoic and Cenozoic times). A neotectonic and possibly recent activity of these faults is not obvious, but cannot be entirely excluded (see conclusion in NTB 14-02 Dossier III chapter 3.8). This is one of the reasons why the "Rafz-Marthalen Flexur" (southern border fault of the Benken horst mildly reactivated in Post-Paleozoic times), which can be traced over several 2D-seismic profiles, was defined as "zu meidende tektonische Zone" and avoided as part of delineating the Lagerperimeters for the "Sicherheitstechnische Vergleich", as was the "Neuhausen Störung" (presumed eastern border fault of the horst with clear signs for Late Tertiary activity) regarded as "Regionale Störungszone" (see NTB 14-02 Dossier II, Kap. 4.5.2).

The other presumed border faults of the Benken Horst are the "Strukturzone von Niderholz" to the West and the "Wildensbacher Flexur" to the North. Both structures have a comparably local character and could only be mapped in detail with the help of 3D-seismic data. Nagra is aware, that similar structures may not yet be detected in other siting regions, where no 3D-seismic data are available in SGT-E2. In order to treat all siting regions equally in the course of the "Sicherheitstechnische Vergleich" of SGT-E2, these "3D-seismic scale structures" were not treated as regional tectonic elements and avoided straight away, but taken into account as "anordnungsbestimmende Störungszonen" (see NTB 14-02, Dossier II, Kap. 4.5.2).

The structure addressed by the ENSI question and visible on profile 91-NO-75 is not considered to stem from a velocity problem. It is known as the "Antiklinale von Trüllikon" and was analysed in detail with the help of 3D-seismic data (see NTB 00-03 by Birkhäuser et al. 2001, sections 4.6.2 page 90). While not directly linkable with a border fault of the Benken Horst, it does show signs for post-Paleozoic (Mesozoic and Cenozoic) activity. Most importantly, the "Antiklinale von Trüllikon" is not traceable over several 2D-seismic profiles (like the above mentioned "Rafz-Marthalen Flexur") and as such, similar to the "Wildensbacher Flexur" and the "Strukturzone von Niderholz" a "3D-seismic scale structure". For this reason it was not regarded as regional tectonic element, but as an "anordnungsbestimmende Störungszone".

Frage 34: Anordnungsbedingte Störung Benken

Versandt am 29.05.2015, Antwort erhalten am 21.06.2015.

How do you explain the fault beneath Benken village as interpreted on the figure A 1-8, NTB 14-02, Dossier II, 91-NO-77, Depth.

A fault cutting layers from Tertiary unit to basement could be a major fault with tectonic implications.

This fault is not present on the seismic interpretation (A-31, NAB 13-10, 91-NO-77, TWT). We can see a bending of some layers, but not an offset. (On this figure, A-31, NAB 13-10, the well is Benken and not Weiach as written).

What would be the geological explanation of this fault? When is this fault active?

The mentioned fault underneath the Benken village, which is visible on profile A1-8 of NTB 14-02, Dossier II, is associated with the "Wildensbucher Flexur". As notified by ENSI this fault is actually not visible on the 2D-seismic profile 91-NO-77. In the geological profile along this seismic section the structural interpretation was complemented according to the interpretation of the 3D-seismic data by Birkhäuser et al. (2001; NTB 00-03), which covers this area (see outline on profile construction by Jordan et al. 2014, NAB 14-105 page 54, 3rd paragraph).

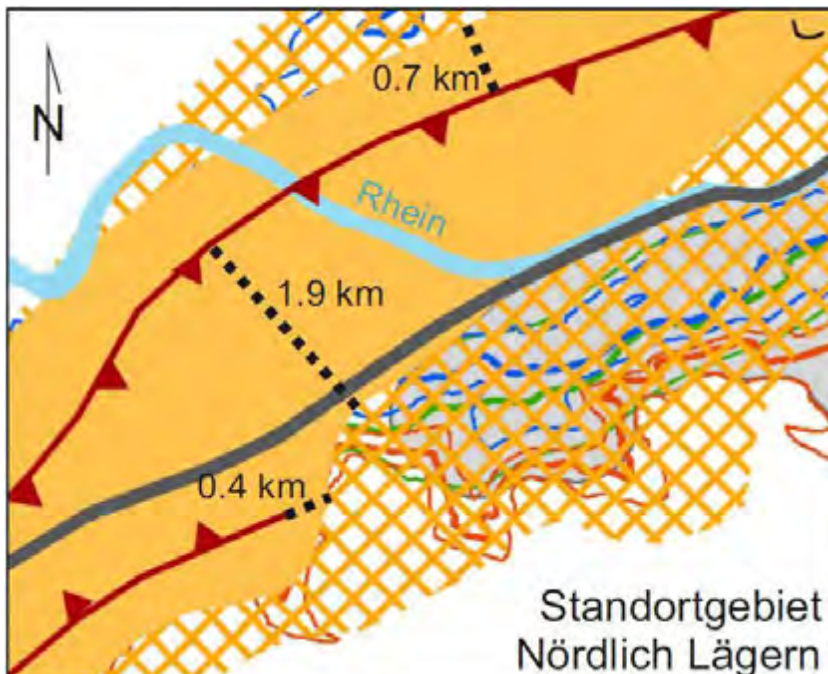
As already outlined in the answer for ENSI Frage 33, the fact that the "Wildensbucher Flexur" could only be fully identified with the help of 3D-seismic data speaks against its classification as "Regionales tektonisches Element" in order to keep up with the SGT-requirement to treat all siting regions equally in the course of the "Sicherheitstechnische Vergleich". The structure is treated as "anordnungsbestimmende Störungszone".

The "Wildensbucher Flexur" was analysed in detail by Birkhäuser et al. (2001, NTB 00-03). It is inferred to be inherited from a Late Paleozoic basement fault (possibly constituting to the northern border of Benken Horst west of profile 91-NO-77). Within the Mesozoic and Cenozoic sedimentary stack it is constituted by an en echelon array of several minor normal faults. The 3D-seismic data suggests a kinematic link with the "Neuhausen Fault". As such the fault was definitely active during Cenozoic times. A neotectonic or even recent activity of the latter regional fault zone is not obvious, but cannot be entirely excluded (see conclusions in NTB 14-02 Dossier III chapter 3.8).

Frage 35: Abgrenzung der Sicherheitsabstände um die regionalen Störungszonen in Etappe 2

Versandt am 04.06.10.2015, Antwort erhalten am 21.06.2015

In NTB 14-01, Fig. 4.1-2, werden alle für die Standortgebiete aus Etappe 1 relevanten regionalen tektonischen Elemente der Nordschweiz dargestellt. In NTB 14-02, Dossier II, S. 72, steht dazu: "Analog zu SGT Etappe 1 wurde für die finale Abgrenzung der regionalen Störungszonen um diesen Einflussbereich ein Sicherheitsabstand von 200 m gezogen." Das Vorgehen dazu wird wie folgt beschrieben (NTB 14-02, Dossier II, S. 72): „Die Abgrenzung der so festgelegten regionalen Störungszonen wurde als Erstes entlang der einzelnen seismischen Profile vorgenommen. Dabei wurden die Verschnittpunkte der regionalen Störungszonen mit den seismischen Markerhorizonten Basis Tertiär und Top Muschelkalk ermittelt. Durch vertikale Projektion dieser Schnittpunkte auf das Niveau der Wirtgesteine wurde im Anschluss der so definierbare Einflussbereich der Störungszone in der Kartenebene abgegrenzt.“ Es fällt auf, dass die orangenen Sicherheitsabstände um die regionalen Störungszonen sehr unterschiedlich dick sind und meist weit über 200 m Dicke aufweisen. Wir bitten die Nagra, das Vorgehen an den folgenden drei Stellen aus Figur 4.2-14 (NTB 14-01) beispielhaft zu erläutern. In der untenstehenden Figur sind drei Strecken von je 1.9, 0.7 und 0.4 km Länge normal zur regionalen Störungszone ausgewiesen bzw. eine in direkter Fortsetzung davon. Wie sieht die Abgrenzung bzgl. Nagra-Vorgehen für diese Stellen im Detail aus? Dabei soll bei der dritten Länge auch auf die Frage des Vorgehens am Ende einer regionalen Störungszone eingegangen werden: Ab wann wird eine Störungszone als solche definiert, welche Tiefe zählt?



Antwort der Nagra vom 21.06.2015

Hier liegt ein Missverständnis vor. Die in den genannten Figuren gezeigten dunkelroten Linien zur Veranschaulichung der Regionalen Störungszonen stellen generalisierte Verläufe der in der Seismik auf unterschiedlichen seismischen Markerhorizonten kartierten Störungsspuren dar. Die generalisierten Verläufe der Störungszonen orientieren sich ca. an der Störungsspur auf Niveau des Markerhorizonts Top Lias, weichen aber aus Ästhetik-Gründen (etwa mittlerer Verlauf der generalisierten Störungsspuren innerhalb der ausgewiesenen regionalen Störungszonen-Polygons) auch des Öfteren mal von dieser ab, so z.B. auch im vom ENSI gezeigten Beispiel. Die genannten Linien haben daher im Sinne einer Berichtsfigur einen rein illustrativen Charakter.

Dies wurde auch im geologischen Grundlagenbericht zu SGT-E1 so gehabt und dort noch etwas ausführlicher illustriert (vgl. Nagra 2008, NTB 08-04 Fig. 5.2-13; Abb.1 unten zeigt eine Kopie dieser Figur). Auf eben diese Figur wurde im Text zur von ENSI angesprochenen Figur im NTB 14-02, Dossier II, ebenfalls explizit verwiesen (S. 71).

Für eine Überprüfung der Abgrenzung der in SGT-E2 verwendeten regionalen Störungszonen und der angewendeten Sicherheitsabstände sollte auf die grundlegende Seismikinterpretation und nicht auf die vom ENSI angesprochenen illustrativen Störungsverläufe zurückgegriffen werden. Die dazu notwendigen Daten (shapefiles zur Seismikinterpretation mit Störungsspuren für die Horizonte Basis Tertiär bis Top Muschelkalk) sind Teil der Datenlieferung, welche dem ENSI mit NIB 15-02 zugestellt wurde (vgl. Kap. 4.2.1). Abb. 2 unten zeigt eine Figur aus diesem Bericht, welche diese Daten illustriert.

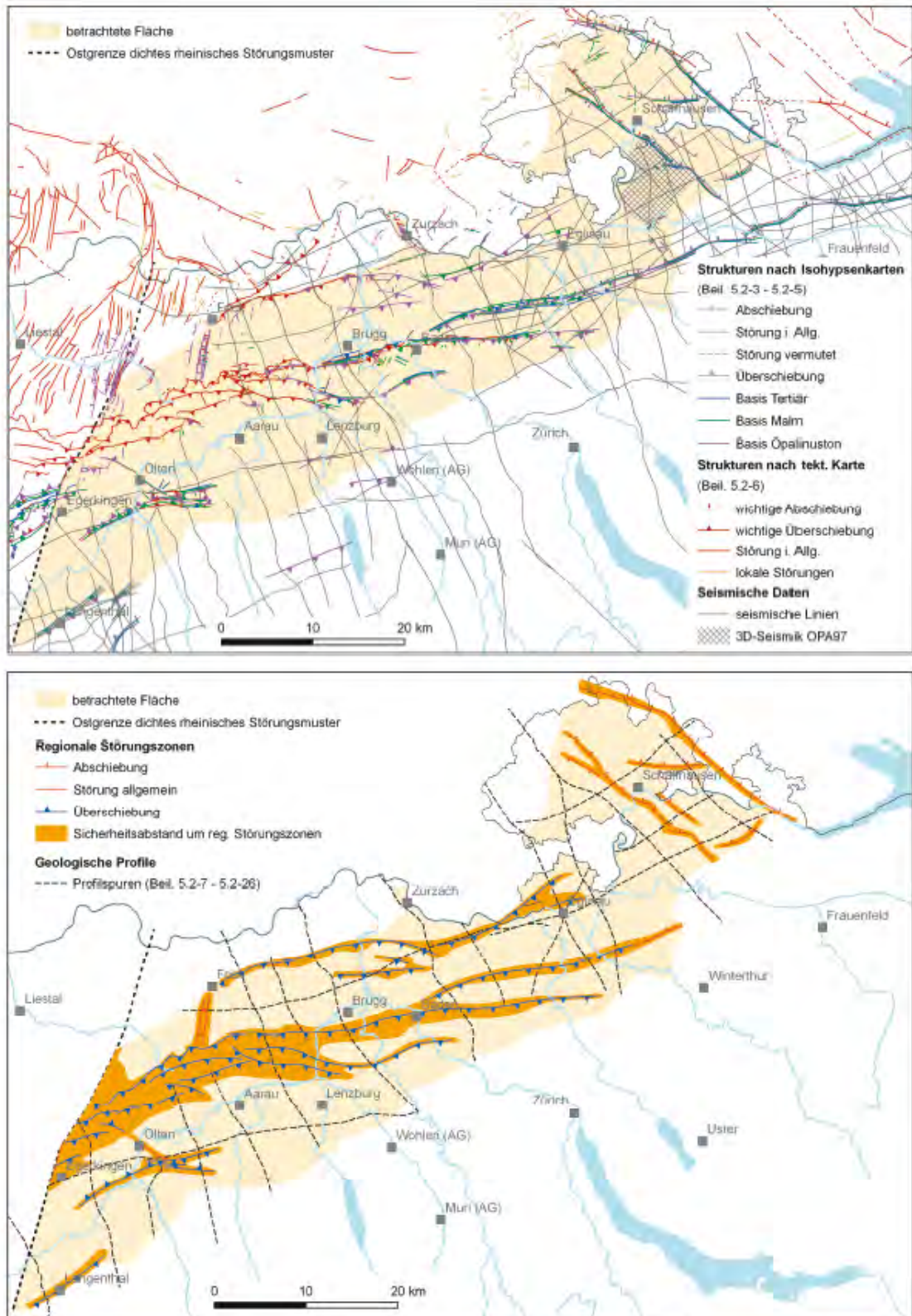
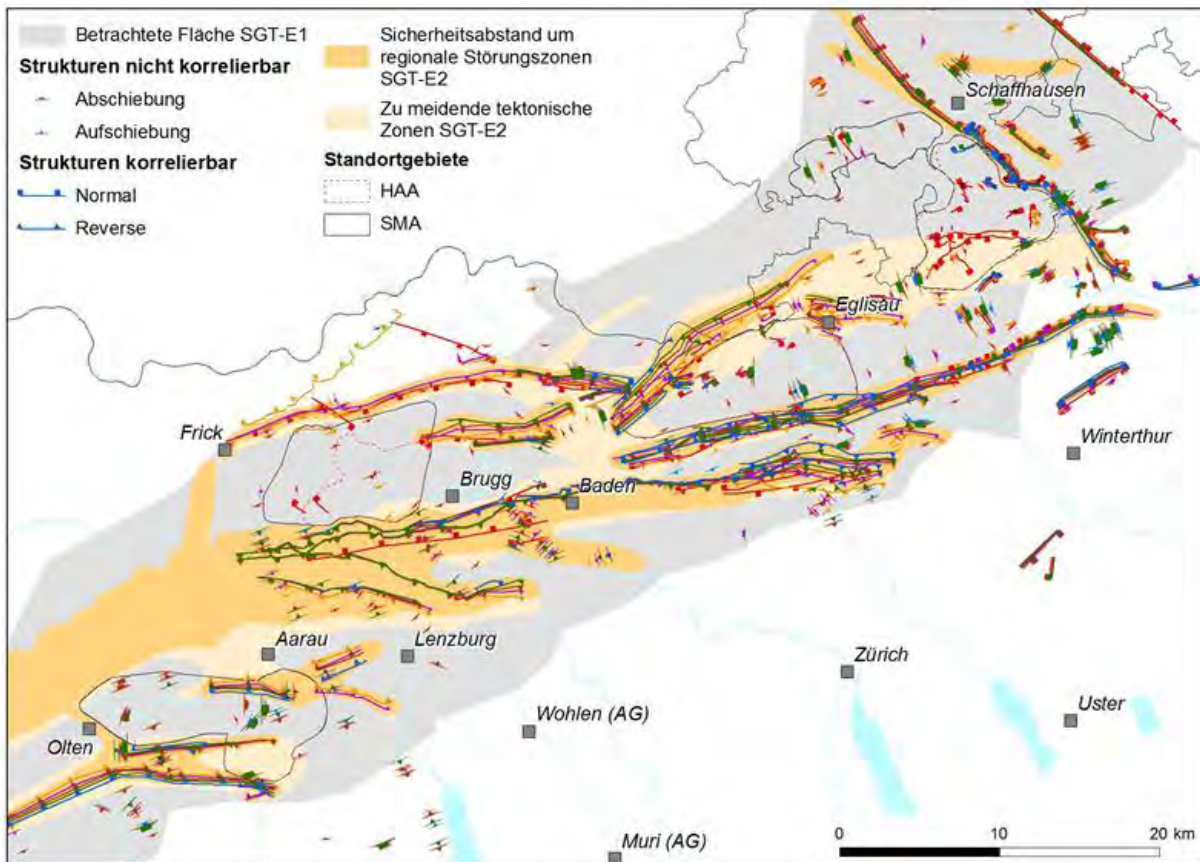


Fig. 5.2-13: Ausscheidung von regionalen Störungszonen mit Sicherheitsabstand.

Oben: Datengrundlage. Unten: Resultate. Detaillierte Erläuterungen im Text.

Frage 35 Abb. 1: Kopie der im NTB 14-02, Dossier II zitierten Figur aus NTB 08-04 (Fig. 5.2-13), welche die graphische Abstraktion von regionalen Störungszonen auf Basis von seismisch kartierten Störungszonen zeigt, wie sie auch in SGT-E2 durchgeführt wurde.



Frage 35 Abb. 2: Figur 4-1 aus NIB 15-02 mit Darstellung der dem ENSI gelieferten seismischen Störungsinterpretation auf Niveaus der verschiedenen seismischen Markerhorizonte zur Nachvollziehbarkeit der Abgrenzung von regionalen Störungszonen.

Rückfrage des ENSI (14.07.2015)

Das ENSI ist mit dem Inhalt der Antwort der Nagra einverstanden, jedoch ist die Antwort nicht ausreichend. Das ENSI möchte das Vorgehen genauer verstehen und nicht nur einen Hinweis auf bereits existierende Figuren. Die mitgeschickte Figur zeigt, dass es auch bei Einzeichnen der Lage der Störungen in den verschiedenen seismischen Horizonten immer noch Bereiche gibt, in denen die gelben Zonen dicker oder dünner sind (z.B. am Südrand von Standortgebiet JO oder entlang der Born-Engelberg-Antiklinale bei JS). Ausserdem wird nichts zum Vorgehen der Nagra an den Enden der Störungen gesagt. Dort würde man erwarten, dass der Sicherheitsabstand rund um das Ende der Störung geht, tut er aber oft nicht, sondern das Ende der Störung ist asymmetrisch zum gerundeten Ende der Störung. Es wird auch nichts gesagt, inwiefern die Dicke des Sicherheitsabstandes ggf. von der Neigung der Störung abhängig ist. Zu Illustrationszwecken wäre es u.U. hilfreich, die in der Frage genannten Beispiele anhand von Profilschnitten darzustellen und zu erläutern.

Es folgen weitere Ausführungen zur Abgrenzung der regionalen Störungszonen:

Abgrenzung im seismischen Profilschnitt:

Aufgrund der oben und auch in NTB 14-02 kurz beschriebenen Vorgehens bei der Abgrenzung von regionalen Störungen anhand der Seismikinterpretation ergeben sich

unterschiedliche Breiten der regionalen Störungszonen. Wesentlich ist hierbei ist das Einfallen der jeweiligen Störungen. Flach einfallende Störungen resultieren in breiteren Störungszonen als steil einfallende (vgl. Abb. 3). Im Falle von flach einfallenden Störungen ergeben sich in der Regel sehr breite Abgrenzungen (Abb. 3a). Die Grenzziehung entlang von vertikalen gedachten Linien wird hier im Sinne der Sicherheitsanalyse gegenüber dem alternativen Vorgehen mit einer Abgrenzung entlang von störungsparallelen Linien als konservativ angesehen (das gewählte Vorgehen führt auf Niveau der Wirtgesteine in der Regel zu einer weiträumigeren Abgrenzung). Im Falle nahezu vertikaler Strukturen wird eine Mindestbreite von 400 m durch den in allen Fällen beidseitig angewandten Sicherheitsabstand von stets 200 m gewährleistet (Abb. 3b).

Abgrenzung im Kartenbild:

Auch die weitere Abgrenzung der regionalen Störungszonen von Profil zu Profil fußt wie schon erwähnt im Wesentlichen auf der seismischen Störungsinterpretation von Madritsch et al. (2013) bzw. Meier et al. (2014), welche auch die Grundlage für die in SGT-E2 aktualisierten Schichtmodelle in den Standortgebieten darstellt (vgl. Nagra 2014 und Becker et al. 2015). Wo vorhanden wurden zusätzlich auch die Oberflächenausbisse regionaler Störungszonen berücksichtigt (z.B. Westende der Mandachüberschiebung oder Nordsegment der Neuhauserstörung im Bereich des Randen; vgl. Abb. 3b). Im Kartenbild kann die Berücksichtigung von diesen zusätzlichen Informationen die Abgrenzungsbreite von regionalen Störungszonen beeinflussen.

Die laterale Abgrenzung der Störungszonen-Enden ist grundsätzlich schwierig, da diese durch das vorliegende 2D-Seismikliniennetz in der Regel nicht präzise lokalisiert werden können. Schon allein deshalb unterliegt dieser Aspekt der Abgrenzung von regionalen Störungszonen einer größeren Interpretationsfreiheit und dementsprechend Ungewissheit. Die Relevanz dieser Ungewissheit wird im Folgenden für jedes Standortgebiet mit den darin abzugrenzenden Lagerperimetern diskutiert:

Standortgebiet Südranden: Die Abgrenzung von lateralen Störungsenden ist für dieses Standortgebiet nicht relevant.

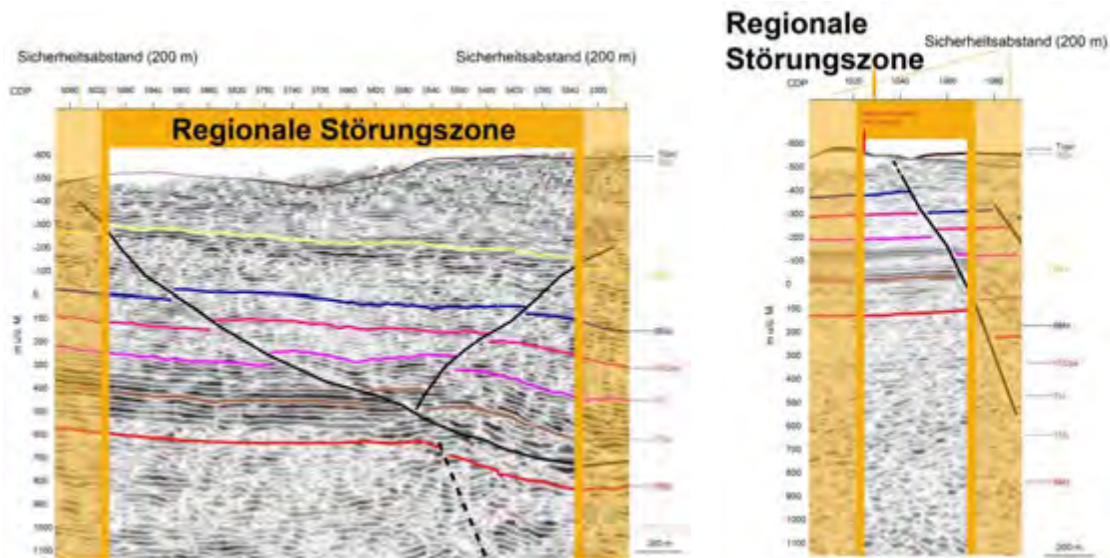
Standortgebiet Zürich Nordost: Der Übergang der regionalen Neuhausen Störungszone in die Wildensbuch Flexur, welche in SGT-E2 analog zu SGT-E1 aufgrund ihrer vergleichsweise kleinsten lateralen Ausdehnung nicht als regionale Störungszone sondern lediglich als anordnungsbestimmende Störung bewertet wurde, kann sehr gut mit Hilfe von in diesem Gebiet zusätzlich vorhandenen 3D-Seismikdaten definiert werden. Die gegenüber SGT-E1 sehr geringfügig weiträumiger Abgrenzung der Neuhausen Störung in SGT-E2 in das Standortgebiet hinein ergibt sich aus der zusätzlichen Mitberücksichtigung einer kleineren Störung aus der 3D-Seismik-Interpretation im unmittelbaren Nahfeld des Störungshauptasts.

Standortgebiet Nördlich Lägern: Die Abgrenzung von lateralen Störungsenden ist für dieses Standortgebiet nicht relevant. Fragliche Enden der Eglisau-Störung und eines Seitenastes der Siglistorf Antiklinale liegen im Bereich einer zu meidenden tektonischen Zone, welche bei der Abgrenzung des Lagerperimeters in diesem Gebiet ohnehin gemieden wurde.

Standortgebiet Jura Ost: Der Aspekt ist für die Westgrenze der Siggenthal Antiklinale relevant, deren Lokation grundsätzlich mit Ungewissheiten behaftet ist (vgl. Antwort zu ENSI Frage 29).

Die aktuelle Abgrenzung wurde jenseits von Seismikprofil 83-NF-31 gezogen, wo die Struktur von Osten kommend das letzte Mal seismisch kartiert klar kartiert werden kann. Der aktuelle Abstand ergibt sich aus einer Grenzziehung ungefähr 100 m westlich jenes Punktes auf dem Streichprofil 11-NS-37, wo der Ausläufer der Struktur von (Meier et al. 2014) schematisch eingezeichnet wurde sowie aus dem Sicherheitsabstand von 200 m, der gemäss dem generell festgelegten Vorgehen noch zusätzlich auf diese Abgrenzung draufgeschlagen wurde. So gesehen wird die aktuelle Abgrenzung im Sinne des generellen Vorgehens und vorbehaltlich der verbleibenden Ungewissheiten über mögliche alternative Verläufe der Störungszone (vgl. Antwort zu ENSI Frage 29) als konservativ eingestuft.

Standortgebiet Jura Südfuss: Die Abgrenzung von lateralen Störungsenden ist für dieses Standortgebiet nicht relevant. Das Westende der Schönenwerd-Eppenberg-Antiklinale sowie das Ostende der Born-Engelberg-Antiklinale liegen im Bereich von zu meidenden tektonischen Zonen, welche bei der Abgrenzung des Lagerperimeters in diesem Gebiet ohnehin gemieden wurde. Das Ostende der Schönenwerd-Eppenberg-Antiklinale, welches eher grosszügig gezogen wurde, liegt nicht im Einflussbereich des Standortgebiets.



a)

b)

Frage 35 Abb. 3: Beispielhafte Illustration der Abgrenzung von regionalen Störungszone bei flachem und steilen Einfallen: a) Abgrenzung der Siglistorf Antiklinale auf Seismik Profil 11-NS-16 (Westteil des Standortgebiets Nördlich Lägern). b) Abgrenzung der Neuhausen Störung auf Profil 91-NO-79 (nördlich des Standortgebiets Südranden). Die in der Abbildung linksseitige Abgrenzung der Neuhausen Störung ergibt sich aus der zusätzlichen Berücksichtigung des an der Oberfläche geologisch kartierten Ausbiss der Störung (markiert durch die vertikale rote Linie; vgl. Geologischer Atlas der Schweiz 1:25'000, Blatt Neunkirch von Hofmann (1981) mit GIS-Datensatz aus Becker et al. (2015)).

Referenzen:

- Becker, J., Madritsch, H., Schnellmann M., Ruff, M. & Albert, W. (2015): Erläuterungen der für die Abgrenzung von Lagerperimetern verwendeten GIS-Datensätze und ihrer Grundlagen (Revision 1). Unpubl. Nagra Interner Ber.
- Hofmann, F. (1981): Geologischer Atlas der Schweiz 1:25'000, Blatt 1031 Neunkirch, mit Erläuterungen. Bundesamt für Landestopografie swisstopo, Wabern (Bern).
- Madritsch, H., Meier, B., Kuhn, P., Roth, P., Zingg, O., Heuberger, S., Naef, H. & Birkhäuser, P. (2013): Regionale strukturgeologische Zeitinterpretation der Nagra 2D-Seismik 2011/12. Nagra Arbeitsber. NAB 13-10.
- Meier, B., Kuhn, P., Roth, Ph., Muff, S. & Madritsch, H. (2014): Tiefenkonvertierung der regionalen Strukturinterpretation der Nagra 2D-Seismik 2011/12. Nagra Arbeitsber. NAB 14-34.
- Nagra (2014): SGT Etappe 2: Vorschlag weiter zu untersuchender geologischer Standortgebiete mit zugehörigen Standortarealen für die Oberflächenanlage. Geologische Grundlagen Dossier II Sedimentologische und tektonische Verhältnisse. Nagra Tech. Ber. NTB 14-02.

Frage 63: Flexur

Versandt am 5.10.2015, Antwort erhalten am 19.10.2015)

How did Nagra define the term “Flexur” used in the reports?

The German term “Flexur” (English: monocline) was not specifically defined in any of the recently submitted Nagra reports. However, a definition was already given in previously published Nagra reports (e.g. glossary of NTB 00-03 by Birkhäuser et al. 2001; see page 152). Besides, at least in German, the term “Flexur” can be considered a standard structural geological term whose definition is given in various geological text books (e.g. Murawski & Meyer 1998, see page 66 and answer below). It is also widely used in the regional geological literature in the respective context (e.g. the annotations to various geological map sheets such as Jordan et al. 2011).

What is the geometry of the flexures?

A “Flexur” is characterized by an s-shape deformation of sediment layers / reflection packages without visible brittle faulting that is caused by vertical (and/or horizontal) movements of underlying tectonic blocks (see Murawski & Meier 1998).

What part of the flexures, precisely, did Nagra map (e.g. Fig. 4.4-4 and Fig. 4.4-5, NTB 14-02, Dossier II)?

The “Flexur” symbols shown in the mentioned figures/maps do not represent the precise traces of flexures (e.g. the “Flexur-Achse” in the sense of Murawski & Meier (1998) which is the line that follows the hinge of the bended layers) but have an illustrative character to roughly show the flexure’s along-strike orientation (similar to the shown red traces of regional fault zones; compare answer to ENSI question 35). The polygons marking flexure – related “Tektonisch zu meidende Zonen” (see Fig. 4.4.1 and polygon outlines in Figs. 4.4.4, 4.4.5 & 4.4.6) cover the entire bended/flexured sediment package.

Flexures are discussed in text report and the flexure trace is shown on the maps (e.g. Fig. 4.4-4 and Fig. 4.4-5, NTB 14-02, Dossier II). But it is not shown/mentioned on the seismic lines. Why?

Only “regional fault zones” are indicated the seismic profiles accompanying NTB 14-02 Dossier II (e.g. Beilagen 4-2 to 4-9 as well as the profiles included in the site specific enclosures). These regional tectonic elements were already introduced in previous seismic interpretation reports (Madritsch et al. 2013, Meier et al. 2014). Flexures are not regarded as “regional fault zones” but as tectonic zones (“zu meidende tektonische Zonen”: compare Nagra 2014, Dossier II, chapter 4.4.).

How did Nagra correlate a flexure from one seismic line to the next (parallel) one?

As outlined in Nagra 2014 Dossier II (see page 75) mapping was done using 2D-seismic data (and 3D-seismic data in the case of the siting region ZNO), whereby the modelled contours of the various interpreted seismic marker horizons were used to track the flexures from one 2D-seismic profile to the next.

The Base Mesozoic horizon contours are hidden by the regional fault zone in the Fig. 4.4-4, 5, 6, 7 NTB 14-02, Dossier II. Do you have a Figure showing relation between Base Mesozoic contours (not hidden) and faults and flexure traces?

We admit that the mentioned NTB figures do not allow to be explored in this regard. This was considered to be acceptable in the context of the NTB, this was acceptable since the overlapping regional fault zone covering the contours was considered as a “no-go” area anyway. The illustrations desired by the reviewer are shown below (Figures. 1, 2 and 3). Please

note though that the flexure traces shown in these, as well as the mentioned NTB figures have an illustrative character (see comment above). Like in the related NTB-figures we therefore also show the outline of the polygons marking the “zu meidende tektonische Zone” (compare Fig. 4.4-1a in NTB 14-02 Dossier II) which covers the entire interpreted flexures.

In this regard, we would also like to draw the reviewer’s attention to the extensive answer to ENSI question 28 related to the delimitation of “zu meidende tektonische Zonen” featuring dip maps of the Top Lias seismic marker horizon.

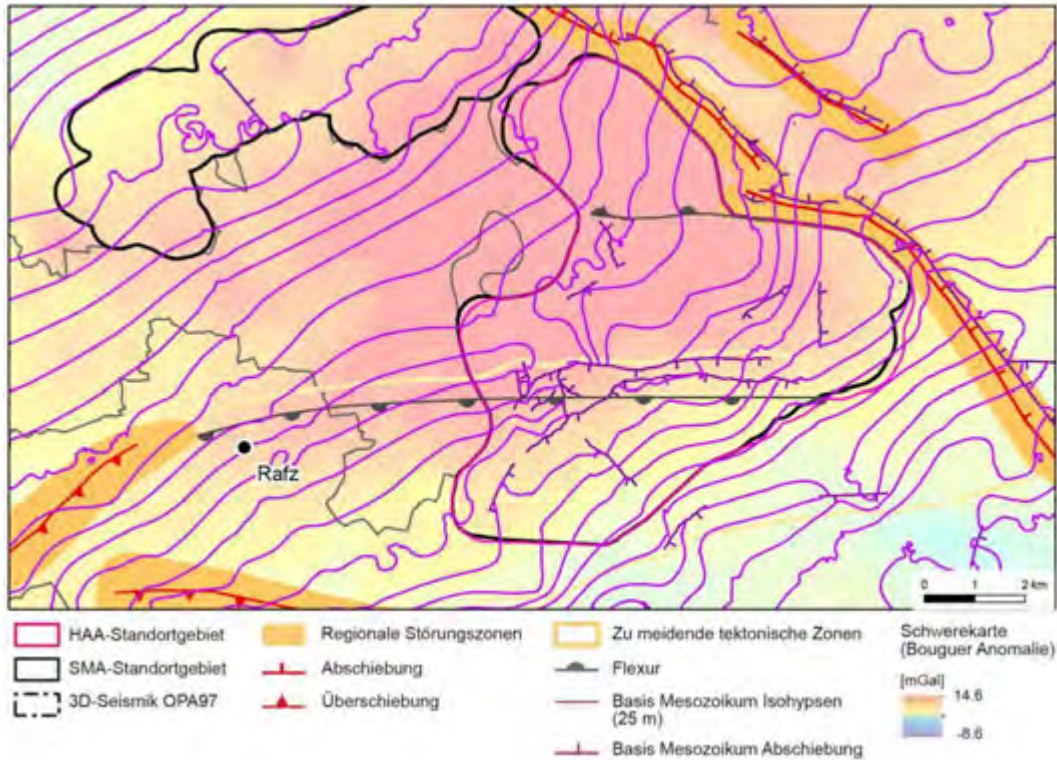


Figure 1: Alternative version of NTB 14-02 Dossier II Fig. 4.4-4 with contours of the Base Mesozoic horizon shown on top of the regional fault zone polygons.

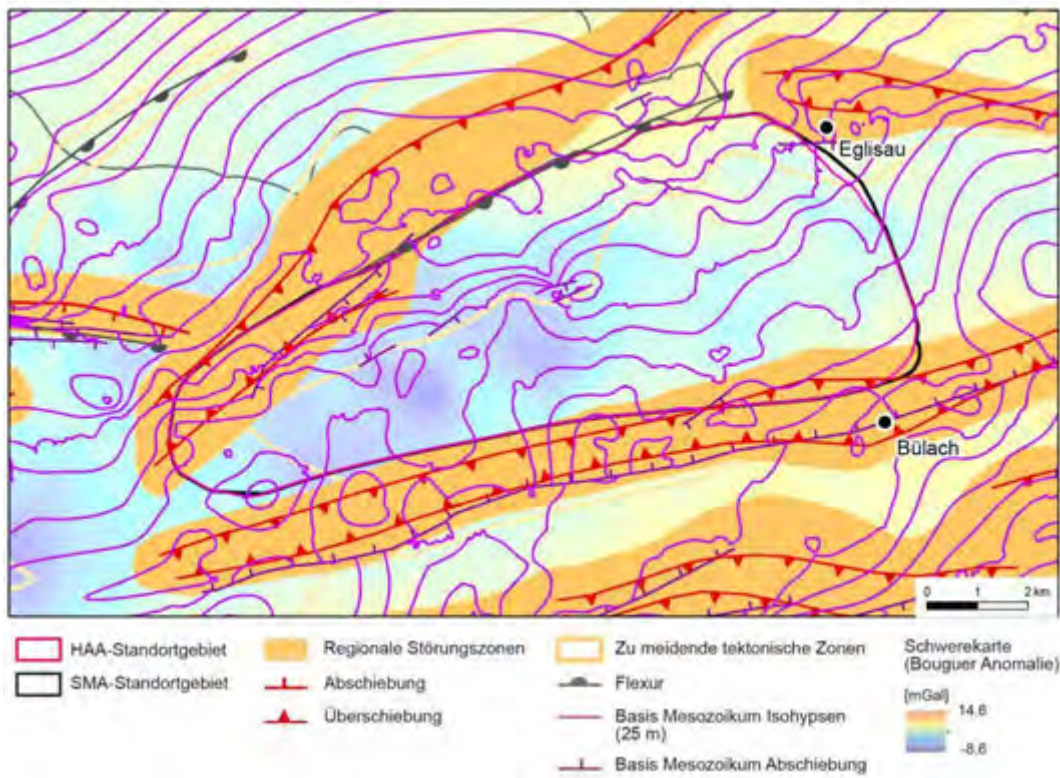


Figure 2: Alternative version of NTB 14-02 Dossier II Fig. 4.4-5 with contours of the Base Mesozoic horizon shown on top of the regional fault zone polygons.

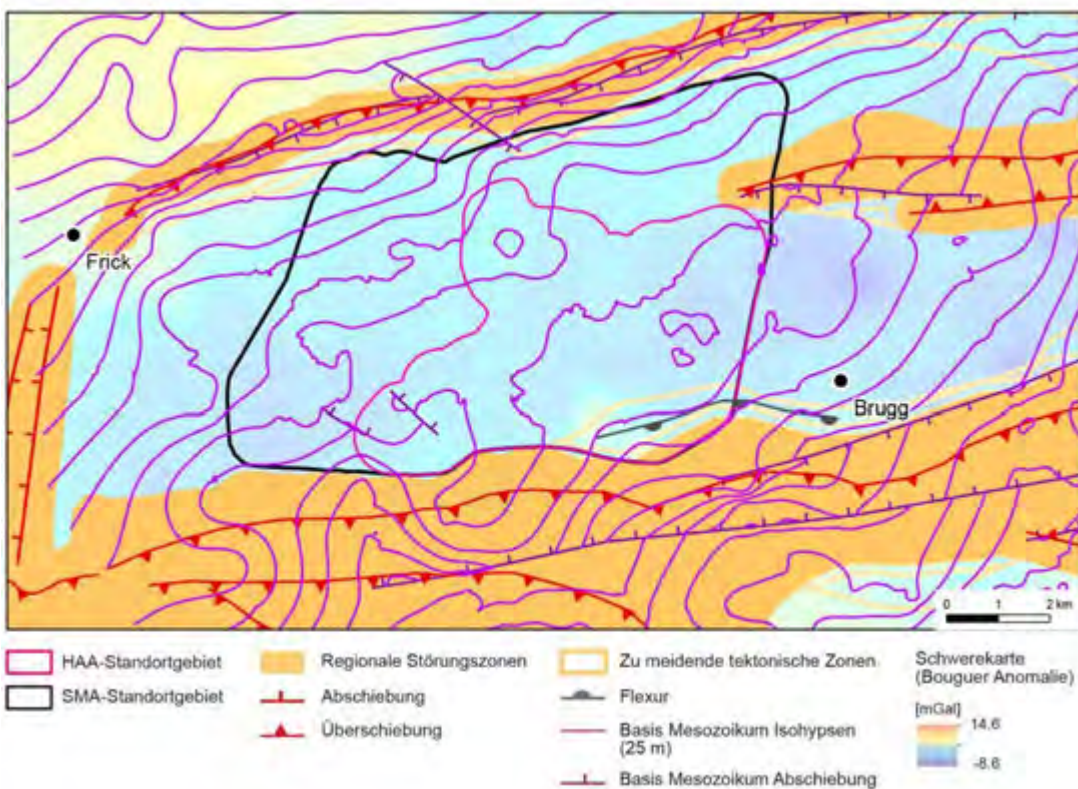


Figure 3: Alternative version of NTB 14-02 Dossier II Fig. 4.4-6 with contours of the Base Mesozoic horizon shown on top of the regional fault zone polygons.

Do all the flexures have a local name?

No. Previously established local names (e.g. Rafz-Marthalen Flexur see Birkhäuser et al. 2001) were used but no new local names were introduced at this stage.

References

- Birkhäuser, Ph., Roth, Ph., Meier, B.P. & Naef, H. (2001): 3D-Seismik: Räumliche Erkundung der mesozoischen Sedimentschichten im Zürcher Weinland. Nagra Tech. Ber. NTB 00-03.
- Jordan, P., Graf, H.R., Eberhard, M., Jost, J., Kälin, D. & Bitterli-Dreher, P. (2011): Geologischer Atlas der Schweiz 1:25'000, Blatt 1089 Aarau (Atlasblatt 135), Erläuterungen. Bundesamt für Landestopografie swisstopo, Wabern (Bern).
- Madritsch, H., Meier, B., Kuhn, P., Roth, P., Zingg, O., Heuberger, S., Naef, H. & Birkhäuser, P. (2013): Regionale strukturgeologische Zeitinterpretation der Nagra 2D-Seismik 2011/12. Nagra Arbeitsber. NAB 13-10.
- Meier, B., Kuhn, P., Roth, Ph., Muff, S. & Madritsch, H. (2014): Tiefenkonvertierung der regionalen Strukturinterpretation der Nagra 2D-Seismik 2011/12. Nagra Arbeitsber. NAB 14-34.
- Murawski, H. & Meyer Wilhelm (1998): Geologisches Wörterbuch. 10. Auflage, Enke Verlag, Stuttgart, 278 p.
- Nagra (2014): SGT Etappe 2: Vorschlag weiter zu untersuchender geologischer Standortgebiete mit zugehörigen Standortarealen für die Oberflächenanlage. Geologische Grundlagen Dossier II Sedimentologische und tektonische Verhältnisse. Nagra Tech. Ber. NTB 14-02.

Rückfrage des ENSI, versendet am 21.10.2015

According to Nagra, the location of the flexures is one of the criteria to determine and delimitate the tectonic zones to be avoided (Antwort Frage 28 ZMTZ). If the mapping of the flexures is rough (Antwort Frage 63), could we think that the mapping of the limit of the tectonic zones to be avoided is also not very precise?

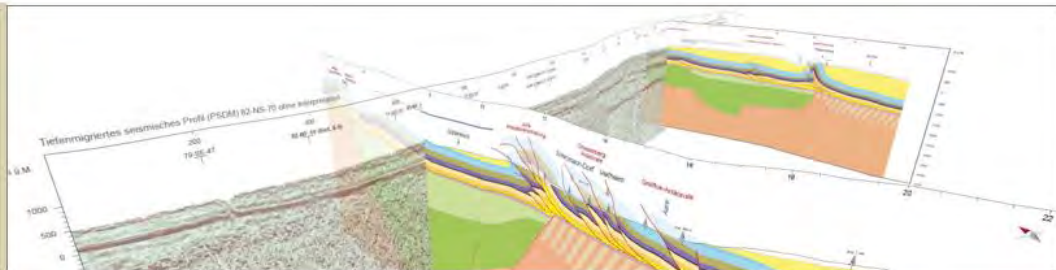
Antwort Nagra (25.10.2015)

It is correctly noted by the reviewer that the location of flexures is a key criterion to delimit the tectonic zones to be avoided. In our earlier reply to the reviewer's initial sub-question number 3 (see above) we did not state that the mapping of these flexures is only rough. What was stated is that the symbol used in the addressed NTB figures only roughly sketches the flexures along the strike orientation. As was explained, it is the shown polygon outlines that delimit the tectonic zones to be avoided, e.g. the flexure zones.

The question raised by the reviewer is still rectified to some extent as the precision of this delimitation is of course affected by uncertainties, in this case stemming from the seismic data density but also the structural geological mapping approach/concept (e.g. expert view). The sensitivity /significance of this uncertainty for the size of the potential disposal perimeters in the various siting regions but in particular Nördlich Lägern was tested in the course of Nagra's evaluation. If desired, we offer to provide further insights into this assessment in the frame of a review meeting / presentation.



4D GEO
Consulting & Training
Structural Geology



APPENDIX 2: 2D Kinematic Modelling Jura Fold-and-Thrust Belt, Switzerland

Author:

Dr. Armelle Kloppenburg (4D Geo/Structural Geology)



Content:

1	Executive summary	5
2	Introduction	7
2.1	Background and Acknowledgements	7
2.2	Rationale of the Study, Aims and Approach	7
2.2.1	Rationale	7
2.2.2	Aim and Approach	8
2.3	Selected Data	9
2.4	Methodology and Workflow	10
2.5	Boundary Conditions, Assumptions and Uncertainty	11
3	Tectono- and mechanical stratigraphy	12
4	Analysis and main results	13
4.1	First Pass Observations combining the Tectonic Map and Sections	13
4.2	Modelling Variables and Preferred Scenario	15
4.2.1	Order of Thrusts	16
4.2.2	Role for Basement Architecture	17
4.2.3	Mechanical Stratigraphy and Main Detachment Levels	19
4.2.4	Folding Mechanism	19
4.2.5	Role of Cross Faults	19
4.3	Forward Modelling of the Jura Ost section (Beilage 6-8 in NAB 14-105)	19
4.3.1	Comparison of Modelled to Present-Day Geometry	28
4.4	Forward Modelling of the Nördlich Lägern section (Beilage 6-6 in NAB 14-105)	31
4.4.1	Comparison of Modelled to Present-Day Geometry	39
5	Summary of the main results	42
6	Conclusion	44
7	Recommendations	45
8	References	46

List of Figures

Figure 2—1: Map showing areas of interest and available sections of the Nagra report NAB-14-105.	8
Figure 2—2: Map with two section insets, illustrating location and orientation of the two selected sections with respect to the location of the two sites of interest.	9
Figure 2—3: Diagram illustrating the five main steps in the applied methodology.	11
Figure 3—1: Tectono-stratigraphic system, following fig. 2-1 (left) and 2-2 (right) of the NAB 14-105 report. The contractional structures that are the focus of this study, thin-skinned folds and thrusts and potential thick skinned thrusts (inverted extensional faults) developed during the most recent part of the tectonic and structural history. The stratigraphic column on the right illustrates the stratigraphic units and contacts that have acted and continue to act as the main detachment levels.	12
Figure 4—1: Tektonische Übersichtskarte (modified Beilage 1-1 of NAB 14-105) highlighting the two sites of interest, and the most significant structures (in bold black stippled lines) as well as the location of the two sections of this study.	14
Figure 4—2: Oblique view looking E at the tectonic map and the two sections of interest (Section 6-6 (Nördlich Lägern) and 6-8 (Jura Ost) taken from report NAB14-105). Top: with tectonic map. Bottom: with clipped tectonic map. Dotted black lines from left to right represent the Mandach Überschiebung, the BIH Lineament and the Jura Main Thrust. The Jura Main Thrust appears to have ‘overridden’ the BIH lineament in the area between the two sections. Alternatively the BIH may stop at a transfer fault system at depth.	15
Figure 4—3: Overview of the most significant modelling variables and optimum scenario for kinematic modelling marked in green.	16
Figure 4—4: In-sequence thrusting order and displacement amount as measured at the base of the Opalinus Clay for the Jura Ost section (section 83-NF-15, Beilage 6-8 in NAB 14-105).	16
Figure 4—5: In-sequence thrusting and consideration for alternative scenario for section 91-NO-58 (from Beilage 6-6 in NAB 14-105). There are no direct constraints from cross-cutting relationships or kinematic considerations for the relative timing of the BIH and Lägern anticline.	17
Figure 4—6: Balanced section 6-8 from the NAB 14-105 report georeferenced in Move and 4x vertically exaggerated to illustrate lateral thickness changes for the Keuper and Dogger formations, and the postulated relationship with basement architecture, with thicker parts of the units overlying grabens, and thinner parts overlying the horst.	18
Figure 4—7: List of the present-day Nördlich Lägern section plus 33 sub-sections in Move™ constituting the sequential kinematic forward model.	20
Figure 4—8: The Jura Ost section (modified from section 83-NF-15, Beilage 6-8 in NAB 14-105) with its present-day geometry with temporal order of faulting and distance of fault offset.	20
Figure 4—9: The Jura Ost section (modified from section 83-NF-15, Beilage 6-8 of NAB 14-105) and the georeferenced illustration of the restored and balanced model with the regional pin placed in the assumed stable block for restoration. Note the detachment level that is near planar.	21
Figure 4—10: Jura Ost section in balanced state (modified from section 83-NF-15, Beilage 6-8 of NAB 14-105) with digitised fault lines and horizons.	21
Figure 4—11: Basement faults adjusted to balanced geometry, with locally modified fault interpretation.	22

Figure 4—12: Potential extensional faults effecting the Triassic and Jurassic units along the Jura Ost section (modified from section 83-NF-15, Beilage 6-8 of NAB 14-105).	22
Figure 4—13: Series of seven forward modelled thrust faults along the Jura Ost section, all in-sequence and with displacements ranging from 50 to 600 m. Note how the hanging wall structures progressively steepen with ongoing thrusting. FPF = Fault Parallel Flow algorithm used.....	25
Figure 4—14: Four faults involved in the development of the Jura Main Thrust system of the Jura Ost section, forward modelled using a combination of the fault propagation (Trishear) and the Fault-Bend-Folding (FBF) algorithm. Also note the use of several detachment levels. See text for further explanation.	26
Figure 4—15: Two stages of the forward modelled Jura Ost section showing thrusts 13 and 14 developing in-sequence, modelled using the Fault-Bend-Folding (FBF) algorithm.	27
Figure 4—16: Final stage: present-day geometry of the forward modelled Jura Ost section. The flat detachment (thick dashed red line above basement top) was adjusted to obtain the shape of the present-day detachment using the Vertical Shear Folding algorithm. This allows comparing and contrasting of the forward modelled and the interpreted geometries.	28
Figure 4—17: Comparing the geometry of the present-day interpretation of the Jura Ost section (from Beilage 6-8 in NAB 14-105) (top) to the geometry as kinematically forward modelled in this study (middle). The Opalinus Clay (violet) has been highlighted to enhance comparison between sections. The bottom figure shows the forward modelled result after vertical adjustment of the planar main detachment level to fit to the present-day geometry. See text for further discussion.....	30
Figure 4—18: List of 21 sections in Move™ constituting the sequential kinematic forward model for the Nördlich Lägern section.	31
Figure 4—19: The Nördlich Lägern section (modified from Section 91-NO-58, Beilage 6-6 in NAB 14-105) with present-day geometry and the order of faulting including the displacement along the fault.	31
Figure 4—20: The balanced Nördlich Lägern section (modified from Section 91-NO-58, Beilage 6-6 in NAB 14-105) with the digitised balanced model using a regional pin placed to the north in the assumed stable block for restoration.....	32
Figure 4—21: The Nördlich Lägern section (modified from Section 91-NO-58, Beilage 6-6 in NAB 14-105) with the original (present-day) basement faults in orange (as in Figure 4—19) and the faults moved down (in red) to the 'balanced geometry' with a planar detachment level.	33
Figure 4—22: The Nördlich Lägern section (modified from Section 91-NO-58, Beilage 6-6 in NAB 14-105) set up for forward modelling. Note the symmetric versus the asymmetric shortening style with NNW-vergent thrusts in the SSE of the section and with a group of both NNW and SSE-vergent wedges and thrusts in the middle of the section, apparently corresponding to the thinner and thicker salt, respectively.	33
Figure 4—23: The Nördlich Lägern section (modified from Section 91-NO-58, Beilage 6-6 in NAB 14-105) with extensional faults in the basement and overlying sequence (shown in blue). These extensional faults appear to have influenced the location and the deformation style in the central zone where shortening is accommodated by multiple wedges.	34
Figure 4—24: The Nördlich Lägern section (based on Section 91-NO-58, Beilage 6-6 in NAB 14-105) focussing on the small displacement of the easternmost thrust.....	34
Figure 4—25: The Nördlich Lägern section (based on Section 91-NO-58, Beilage 6-6 in NAB 14-105) highlighting the next active thrust fault, which was modified to better reflect the present-day fault block shape.	35
Figure 4—26. The Nördlich Lägern section (based on Section 91-NO-58, Beilage 6-6 in NAB	

14-105) with a 575 m displacement along thrust 2 using the Fault-Bend-Folding algorithm. In detail the fold shape is not as tight as the interpreted present-day fold (cf. Figure 4—19). Some pre-thrusting folding is suspected (because of the existing footwall fold, and thickened salt layer).....	36
Figure 4—27: The Nördlich Lägern section (based on Section 91-NO-58, Beilage 6-6 in NAB 14-105) with a 200 m displacement along thrust 3 using the Fault-Bend-Folding algorithm. The step causes further steepening in the hanging wall and formation of an additional thrust, but does not cause a fold/drag in the footwall. In detail the fold shape is not as tight as the present-day fold (cf. Figure 4—19). Some pre-thrusting folding is suspected (because of the existing footwall fold, and thickened salt layer).....	36
Figure 4—28: The Nördlich Lägern section (based on Section 91-NO-58, Beilage 6-6 in NAB 14-105) highlighting the next active thrust fault, which forms a wedge detaching within the Opalinus Clay, and which in turn detaches in the Effinger Schichten unit. Because algorithms in Move™ cannot handle movements over more than two faults, here the back thrust is extended and the artefact offsets are manually transferred into the forward wedge above (see next slides of inset).....	37
Figure 4—29: Detail of the Nördlich Lägern section (based on Section 91-NO-58, Beilage 6-6 in NAB 14-105) showing the stepwise development of the modelled triangle zone. See text for explanation.....	37
Figure 4—30: The Nördlich Lägern section (based on Section 91-NO-58, Beilage 6-6 in NAB 14-105) with a 175 m displacement on the frontal thrust (thrust 6) using the Fault-Bend-Folding algorithm.....	38
Figure 4—31. The Nördlich Lägern section (based on Section 91-NO-58, Beilage 6-6 in NAB 14-105), adjusted by projecting the forward modelled detachment onto the present-day detachment.....	38
Figure 4—32: Comparing the geometry of the present-day interpretation of the Nördlich Lägern section (Section 91-NO-58, Beilage 6-6 in NAB 14-105) (top) to the geometry as kinematically forward modelled in this study (middle). The Opalinus Clay (violet) has been highlighted to enhance comparison between sections. The bottom figure shows the kinematically forward modelled result after vertical adjustment of the planar main detachment level to fit to the present-day geometry. See text for further discussion.....	40

1 Executive summary

ENSI is currently reviewing Nagra's proposal for stage 2 of the Swiss site selection process for radioactive waste repositories, with swisstopo providing scientific support for this review. Selected siting regions of focus include: Jura Ost and Nördlich Lägern, in northern Switzerland.

To support the characterisation of the selected sites, the work reported here focussed on testing the validity of the geological interpretation, and improve the understanding of the tectonic history and structural style. This was achieved by sequentially restoring and forward modelling deformation due to contraction and fold and thrust development on two representative sections, one for each siting region.

Current Nagra section interpretations are viable

It was found that the interpretation of the two sections across the Jura Ost and Nördlich Lägern regions as presented by Nagra (NAB 14-105) is in essence viable. The details of the solution are non-unique, and have room for fine-tuning.

Understanding the structural geological history

The analysis and forward modelling of both sections have led to a valid and internally consistent understanding of the structural development of each cross-section that involved initial detachment folding and fault propagation folding but was dominated by a fault-bent-folding style development of the fold-and-thrust belt. Lateral variation in structural style was observed both across and along the belt. Hence a full understanding will require integration of these sections with others, and with the geological map in 3D. The basement architecture (and the knowledge on the potential reactivation of the basement fault pattern) is expected to have played a significant role in the structural development of both regions.

Structural style and 3D domains

One family of structures was identified, and second was inferred. The first family comprises fold and thrust related structures, parallel to the belt, well imaged on most seismic dip lines (NAB 14-105). A second family of structures, with faults trending at a high angle to the belt, is mapped at the surface only locally. Their lateral extent is inferred by general map patterns. These structures at high angle to the belt are expected to have accommodated the lateral change in intensity and style observed along the belt. They are poorly revealed on the seismic dip lines, but are noticeable on the strike line (Beilage 6-17) which corresponds to those faults on the geological map. These cross-cutting structures are not characterised and may have a range of forms and sizes, including faults, folds and fracture zones.

The two families of structures are expected to be kinematically linked. Both of them need to be considered in assessing availability of deformed/undeformed domains in the areas of interest. Mapping out this relationship requires a 3D approach, based on the availability of 3D seismic data.

Recommendations

Future work would benefit from further integration of the available surface data (geological maps) with the available 2D sections (NAB 14-105), and aim to construct a 3D geological framework model that builds on and further develops the understanding of the kinematic development of both regions.

2 Introduction

2.1 Background and Acknowledgements

4DGeo was commissioned by ENSI and swisstopo to undertake this work in August 2015. The work was performed over a three week period, following a start-up meeting with Meinert Rahn (ENSI) and Christophe Nussbaum (swisstopo) in Wabern on August 3rd, 2015.

Marco Verdon (swisstopo) kindly provided the digitised line work required for the Move™ analysis. This report is accompanied by the PowerPoint set of slides 'Technical Notes 'P1247 - 2D Kinematic Modelling, Jura Fold-and-Thrust Belt, Switzerland.ppt'.

2.2 Rationale of the Study, Aims and Approach

2.2.1 Rationale

ENSI is currently reviewing Nagra's proposal for stage 2 of the Swiss site selection process for radioactive waste repositories, and swisstopo is providing scientific support for this review. Selected siting regions of focus include: Jura Ost and Nördlich Lägern, in northern Switzerland.

The current geological understanding is based on an existing series of 18 profiles across northern Switzerland (Nagra, NAB 14-105), which comprise three sections across the main structural trend of the Jura Ost siting region, and four across the Nördlich Lägern siting region, with one section along-strike of the belt connecting both areas.

Sequential restoration and forward models of one section for each site is required to support the characterisation of the selected sites: to test the validity of the geological interpretation, to optimise the understanding of the structural history, the structural style and the structural domains.

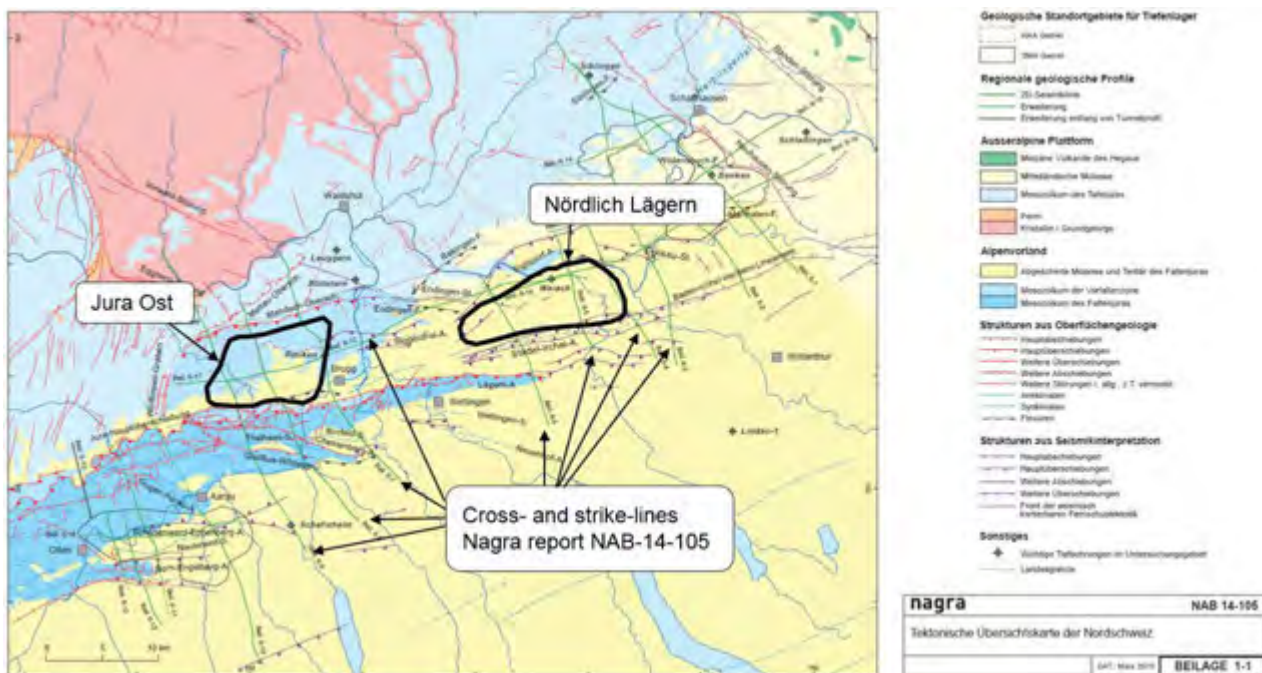


Figure 2—1: Map showing areas of interest and available sections of the Nagra report NAB-14-105.

2.2.2 Aim and Approach

The main aim of this study was to test the validity of the existing section interpretation of two selected representative sections: the Jura Ost section (Section_83-NF-15 in Beilage 6-8 in NAB 14-105) in the Jura Ost siting region, and the Nördlich Lägern section (Section_91-NO-58 in Beilage 6-6, NAB 14-105) in the Nördlich Lägern siting region. Figure 2—2 shows the location and orientation of these two sections with respect to the two siting regions of interest. We refer to these sections as the Jura Ost and the Nördlich Lägern section, respectively.

The validity of the existing section interpretation was tested by sequentially restoring and forward modelling deformation due to contraction and fold and thrust development.

The results support the development of a consistent and valid model for the structural history, a better understanding of the sequence and timing of the key structures, the structural style(s) and structural domains.

The tools and workflows available in Move2015.1 were applied.

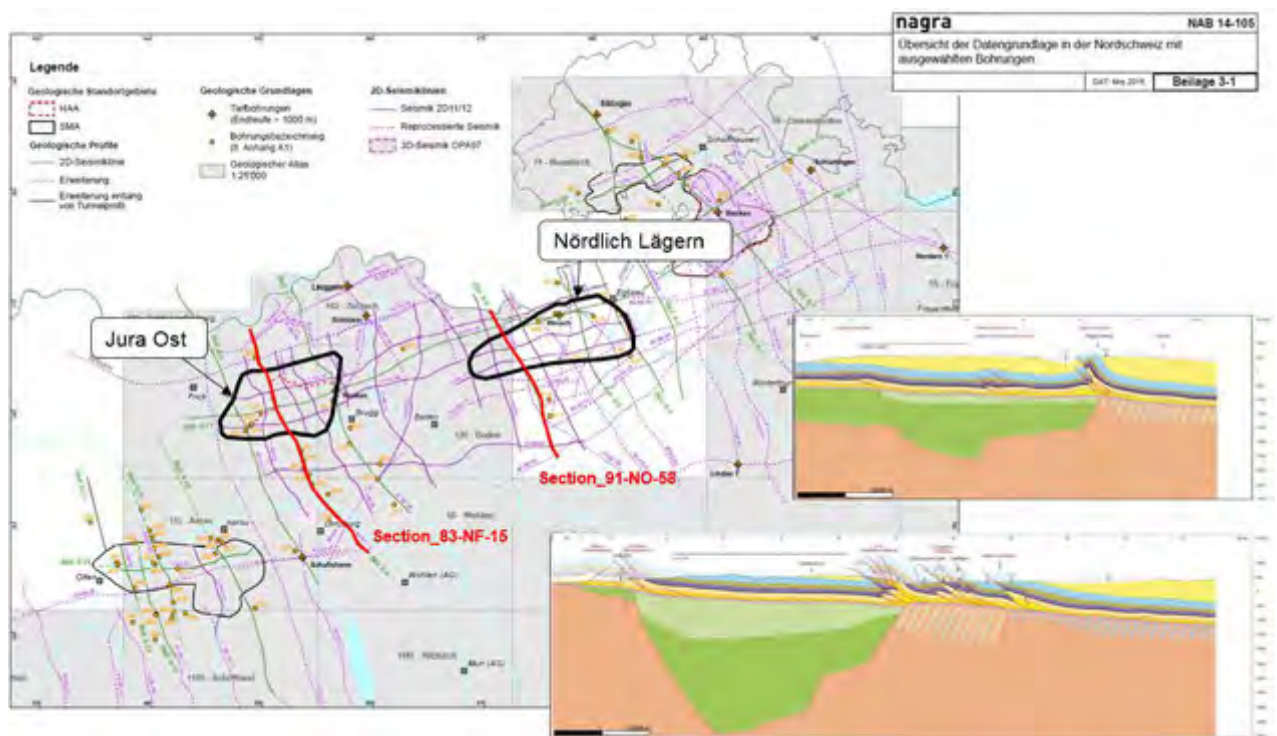


Figure 2—2: Map with two section insets, illustrating location and orientation of the two selected sections with respect to the location of the two sites of interest.

2.3 Selected Data

The two sections selected for this study are displayed in the Nagra report NAB 14-105.

Available imagery for each section included:

- Interpretation of the present-day fault and horizon geometry;
- Seismic imagery (in the depth domain);
- Balanced interpretation.

A hard copy of the report was made available for the duration of the project, with all imagery provided in .pdf format as well. The above images for the two sections were made available in georeferenced files in Move™, with digitised fault and horizon interpretation of both the present-day and balanced sections. These files also included a Digital Elevation Model (DEM) and georeferenced geological maps.

In addition, two selected peer reviewed papers were provided for background reading and served as a reference for the regional geological context:

Malz, A., H. Madritsch, J. Kley. (2015): Improving 2D seismic interpretation in challenging settings by integration of restoration techniques: A case study from the Jura fold-and-thrust belt (Switzerland). *Interpretation* 3 (4), p. SAA37-SAA58.

Malz, A., H. Madritsch, B. Meier, J. Kley. Triangle zone formation and associated thrust front development in thin-skinned foreland fold belts: A case study from the Eastern Jura

Mountains. Tectonophysics, under review.

2.4 Methodology and Workflow

To test the validity of the two sections, a five step methodology was applied (see Figure 2—3).

Both the present-day interpretation as well as the balanced sections were studied using the kinematic modelling software Move™. The sections were digitised and georeferenced in 3D space and were studied in context with the topography and draped geological maps, as well as the other 16 sections that were available from the NAB 14-105 study (step 1).

Move™ allows kinematic restoration and forward modelling of deformation, including folding and faulting. It has a series of algorithms that mimic different styles of deformation, such as fault-bend-folding, detachment folding and fault propagation folding. Whereas balancing tests the consistency of line-length between pre- and post-deformation geometries, the benefit of kinematic restoration and forward modelling is that it tests and quantifies the nature and order of deformation through time, and the geometry of horizons and faults at sequential steps in time.

Taking the balanced sections as a starting point, first-pass observations led to the identification of the most significant modelling variables (step 2) in context with the regional setting, and information from adjacent profiles and the geological map.

Forward modelling was expected to be an iterative process, where forward modelled geometries are compared and contrasted, and modelling variables are adjusted accordingly. For both sections, the key modelling variables were identified, the sensitivity of the results to the various settings were tested, and an optimum scenario was selected (step 3, reported in paragraph 4.2).

Deformation was then applied to cause fault displacements for each individual fault in a number of steps forward in time. This created geometries for the faults and fault blocks that are similar to the interpreted present-day section. Based on the outcome, adjustments were made to the algorithm details, the 'starting geometry' (the balanced sections), the local fault shapes and salt thicknesses, to converge towards better forward modelling results (step 4).

Step 5 involved the forward modelling of fault displacement. This comprised – for each profile - a series of individual subordinate steps that represent particular points in time. Each subordinate step shows the displacement of one fault plus the resulting geometry of the stratigraphic units above and below. The starting position (i.e. the unfolded and balanced sections) assume a planar detachment level, therefore the last forward step has to project the fully evolved fold-and-thrust structures onto the present-day detachment with an irregular shape (using the Vertical Shear Folding algorithm, part of the Move set of algorithms). This allows for direct comparison of the original interpretation and the forward modelled sections. Results are reported in paragraphs 4.3 and 0 of this report. The subordinate steps when viewed in sequence form an animation that is best viewed in the appended PowerPoint presentation.

Final forward models were then compared and contrasted with the existing interpretation and mis-matches highlighted and discussed. Also, suggestions for basement fault interpretation were made based on observed systematics with overlying structures.

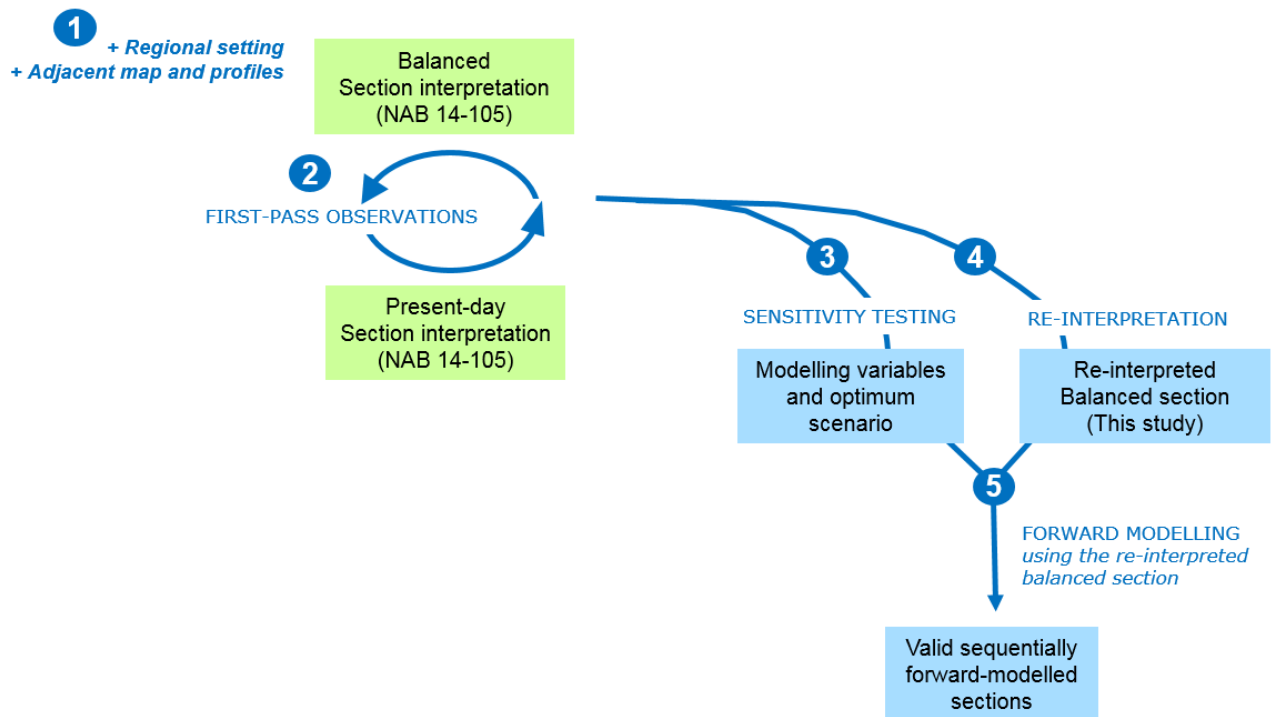


Figure 2—3. Diagram illustrating the five main steps in the applied methodology.

2.5 Boundary Conditions, Assumptions and Uncertainty

This study was undertaken during a limited three-week period. Hence, a full study of the regional geology, as well as a detailed study of individual profiles was beyond the scope of this work due to time constraints.

Regional stratigraphic and tectonic context followed the Nagra report NAB 14-105 and two selected papers:

1. Improving 2d-seismic interpretation in challenging settings by integration of restoration techniques: A case study from the Jura fold-and-thrust belt (Switzerland). A. Malz, H. Madritsch, J. Kley. *Interpretation* 3 (4), p. SAA37-SAA58.
2. Triangle zone formation and associated thrust front development in thin-skinned foreland fold belts: A case study from the Eastern Jura Mountains. A. Malz, H. Madritsch, B. Meier, J. Kley. *Tectonophysics*, in review.

The 18 geological sections of the Nagra NAB 14-105 report, other than the two selected for detailed study, were not validated in this study, and taken at face value.

Tools and workflows available in Move2015.1 were used.

3 Tectono- and mechanical stratigraphy

This study will follow the tectonostratigraphic context as outlined in the NAB 14-105 report. Figure 3—1 illustrates the stratigraphic units, their age and relationship with the main tectonic phases (left) as well as the main detachment levels (right).

The left diagram shows that the development of the fold and thrust belt (Miocene-Pliocene) was strongly influenced by the existing Palaeozoic horsts and graben structures (filled with Permo-Carboniferous sediments) in a crystalline basement (“Kristallines Grundgebirge”). Basement and grabens were covered by a sequence of Triassic and Jurassic sediments. This sequence includes Triassic Muschelkalk (salt) near its base. The Triassic salt forms the primary regional detachment level.

The mechanical stratigraphy, i.e. the vertical occurrence of relatively strong and weak stratigraphic units and contacts, shows that apart from the primary detachment in the Triassic Salt of Mittlerer Muschelkalk age, second order detachments are formed at the base of the Keuper, the base of the Opalinus Clay, and the Effinger Schichten.

During deposition of the Triassic and Jurassic unit, differential subsidence may have reactivated the basement faults along the graben structures and may have affected the depositional thicknesses.

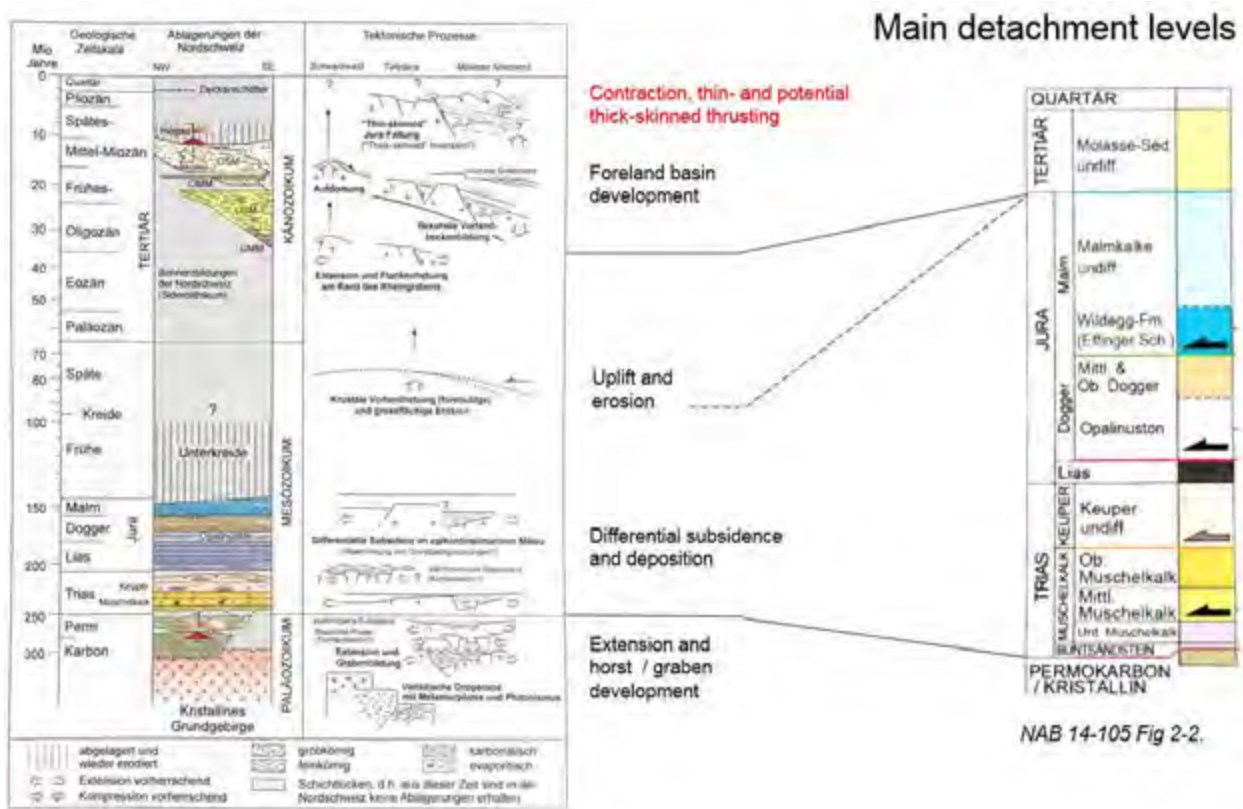


Figure 3—2: Tectono-stratigraphic system, following fig. 2-1 (left) and 2-2 (right) of the NAB 14-105 report. The contractional structures that are the focus of this study, thin-skinned folds and thrusts and potential thick skinned thrusts (inverted extensional faults) developed during the most recent part of the tectonic and structural history. The stratigraphic column on the right illustrates the stratigraphic units and contacts that have acted and continue to act as the main detachment levels.

4 Analysis and main results

4.1 First Pass Observations combining the Tectonic Map and Sections

Both the Jura Ost and the Nördlich Lägern sections (Figure 2—2) are compared and contrasted to find similar and different structures, to assess cylindricity and lateral continuity of the folds and faults, with the aim to identify structures that can tie the development of one section to the development of the other.

The two sections and the Tektonische Übersichtskarte (Beilage 1-1 in NAB 14-105) were integrated in the digital model '*4DGeo Jura Kinematic Modelling.move*' in 3D modelling space. Figure 4—2 highlights the most significant structures for the two sites of interest.

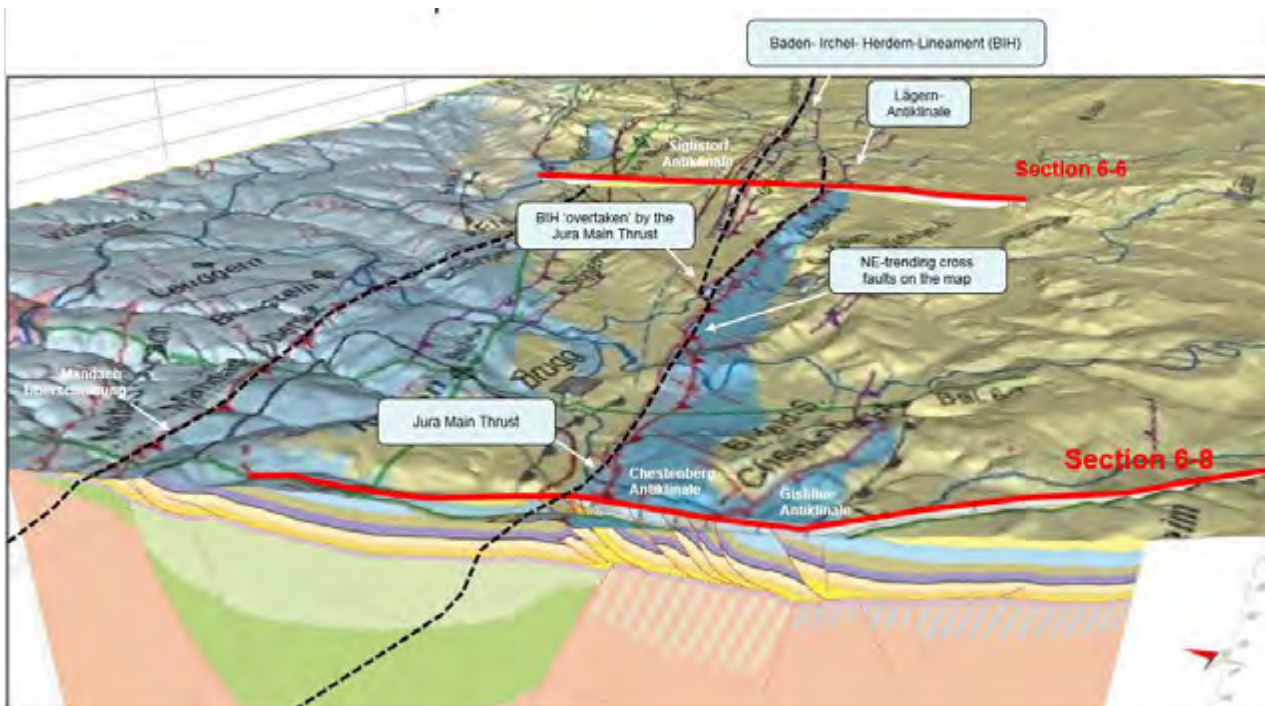
It can be seen that both Nördlich Lägern and Jura Ost are bound by two main thrust zones. The Jura Ost site is situated in between the Mandach-Überschiebung and the Jura Hauptüberschiebung (Jura Main Thrust, Figure 4—1). In-between the two siting areas Jura Ost and Nördlich Lägern is the Siggenthal anticline which laterally does not reach the Jura Ost section. The Nördlich Lägern siting area is situated in-between the Siglistorf and the Lägern anticlines and related thrusts. In addition, the Baden–Irchel-Herdern-Lineament (BIH) is located in-between, but merges with the Jura Main Thrust north of Wettingen, where several NE-SW-trending faults are mapped to cut across the general trend of the overall belt. We refer to them as 'cross faults'. If the Jura Main Thrust is offset by cross faults, these faults must be younger than the Main Thrust, or at least have developed last as part of a family of structures related to the thrust zone.

It appears that these NE-trending cross-faults seen on the map have accommodated differences in amount of thrust displacement with intensity increasing towards the E. This can be explained by the angle between the ENE basement fault trend and the more E-W fold and thrust belt.

The BIH zone may continue to the WSW under the Jura Main Thrust, or it may end at a transfer fault system. The seismic section of Beilage 6-17 (NAB 14-105), which runs across the siting regions Jura Ost and Nördlich Lägern and approximately parallel to the orogenic direction of the Jura thrust belt, shows a major step in vertical level of the stratigraphy and a number of interpreted faults along strike of the NE-trending faults indicated on the map, which may point to a transfer system at basement level. This observation indicates that there may be a significant role for additional (not yet known) cross faults.



Figure 4—2: Tektonische Übersichtskarte (modified Beilage 1-1 of NAB 14-105) highlighting the two sites of interest, and the most significant structures (in bold black stippled lines) as well as the location of the two sections of this study.



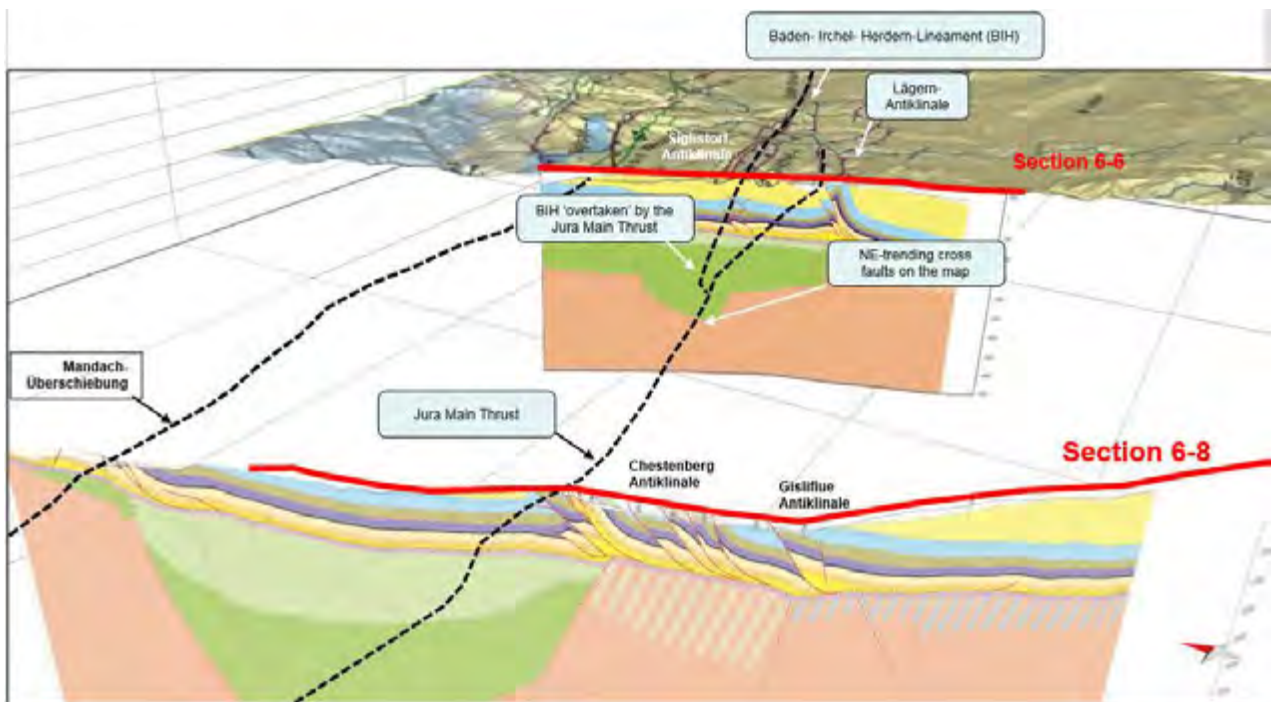


Figure 4—3: Oblique view looking E at the tectonic map and the two sections of interest (Section 6-6 (Nördlich Lägern) and 6-8 (Jura Ost) taken from report NAB14-105). Top: with tectonic map. Bottom: with clipped tectonic map. Dotted black lines from left to right represent the Mandach Überschiebung, the BIH Lineament and the Jura Main Thrust. The Jura Main Thrust appears to have ‘overridden’ the BIH lineament in the area between the two sections. Alternatively the BIH may stop at a transfer fault system at depth.

4.2 Modelling Variables and Preferred Scenario

The preferred scenario for the kinematic modelling is presented in Figure 4—4 and comprises the following aspects:

- (i) The thrusts have developed in-sequence;
- (ii) The basement plays a passive role in which the basement topography nucleated the thrusts;
- (iii) The Triassic Salt is the main detachment but with the Effinger Beds and the Opalinus Clay forming significant second order detachments;
- (iv) Fault-bend-folding is the main mechanism by which the sequence contracted, with local fault-propagation-folding, and in which
- (v) The cross faults have not influenced the style and kinematics as seen on the sections.

The reasoning behind selecting this scenario, and significance for the modelling of alternatives, is briefly discussed below. For both sections the ‘regional pin’ was taken W of the Mandach-Überschiebung, taken to be the frontal thrust representing the end of the system of significant shortening.

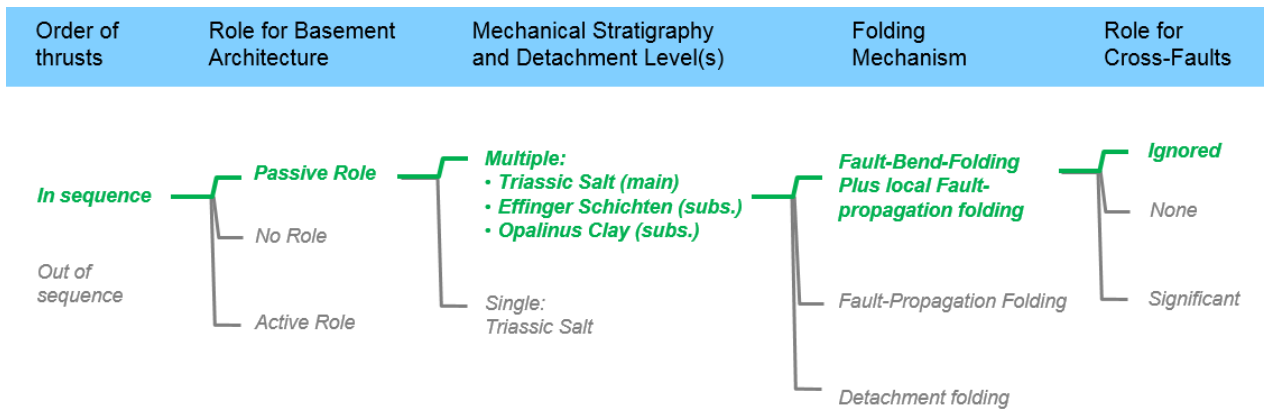


Figure 4—4: Overview of the most significant modelling variables and optimum scenario for kinematic modelling marked in green.

4.2.1 Order of Thrusts

For the Jura Ost section (Beilage 6-8 in NAB 14-105) a largely in-sequence order of thrusting is assumed, with thrusts formed from the SSE to the NNW. Figure 4—5 shows the faults numbered 1 to 12 corresponding to their order of ‘appearance’. This order is common in thrust systems and is consistent with the observation that faults in the hangingwall are steepened by displacement on the thrust below: Fault 3 in the SSE formed first, then faults 4, 5 and 6 towards the NNW. For each fault the displacements as measured at the base of the Opalinus Clay (Purple) is recorded.

Faults of the Jura Main Thrust (faults 9, 10, 11 and 12) are considered to have formed largely coevally, as part of progressive development of this structure. However, the displacement of the footwall fold by fault 12 indicates that the footwall folds/thrusts formed first.

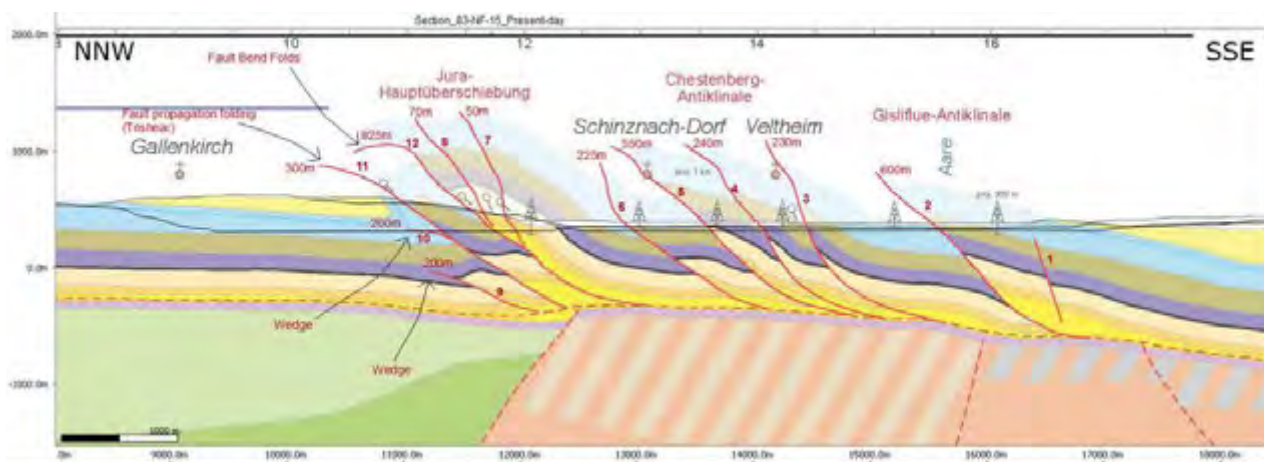


Figure 4—5: In-sequence thrusting order and displacement amount as measured at the base of the Opalinus Clay for the Jura Ost section (section 83-NF-15, Beilage 6-8 in NAB 14-105).

Also for the Nördlich Lägern section (Section 91-NO-58, Beilage 6-6 in NAB 14-105) a normal in-sequence order of thrusting is assumed, progressing from SSE to NNW (see Figure 4—6). This order is allowable, i.e. geologically and kinematically reasonable, but is not constrained by the geometry of thrusts as observed on the present-day section.

In an alternative solution, Malz et al. (2015) interpreted the BIH to have formed first, situated above a reactivated extensional basement fault that can be seismically tracked for circa 40 km to the NE. The deformation front then back-stepped to the SE to form the Lägern anticline and associated thrusts. The Siglistorf anticline and associated thrust to the NW of the BIH formed last.

The Nördlich Lägern section provides no direct cross-cutting or kinematic constraints to prefer one interpretation over the other. Accordingly, both solutions are equally viable based on the constraints included in this study.

A third scenario is postulated in this report. It is noted that the Jura Ost section does not show a separate BIH lineament structure, as was expected from observations on the map (Figure 4—2). The third scenario would consider the BIH to have formed first (located above a reactivated basement fault), and the Jura Main Thrust Front to not yet have reached the BIH in the Nördlich Lägern section, whilst it has overtaken the BIH in the Jura Ost section. This scenario is also kinematically viable. It emphasizes the angular relationship between the basement extensional faults and the thin-skinned thrust front. This scenario makes some assumptions on the continuity of structures between both sections, testing this scenario would, however, require a model construction in 3D.

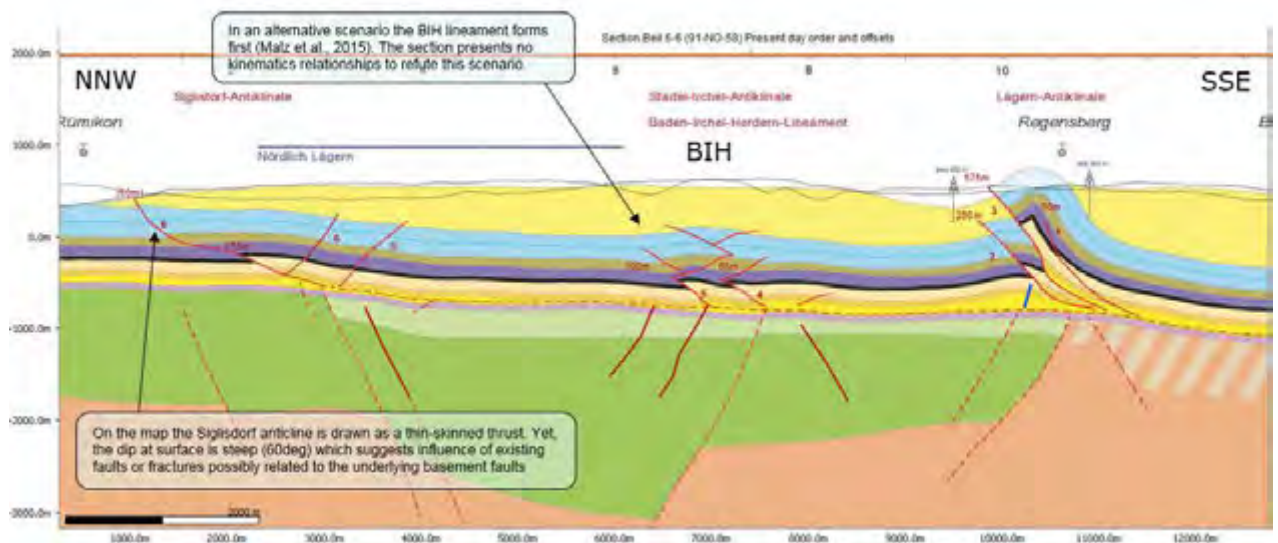


Figure 4—6: In-sequence thrusting and consideration for alternative scenario for section 91-NO-58 (from Beilage 6-6 in NAB 14-105). There are no direct constraints from cross-cutting relationships or kinematic considerations for the relative timing of the BIH and Lägern anticline.

4.2.2 Role for Basement Architecture

At least two aspects are significant for the modelling and understanding of the two sections: the basement fault block topography nucleating the thrusts, and the presence of deep grabens across which reactivation and/or differential compaction may trigger accommodating extensional faults.

4.2.2.1 Basement Fault Block Crests Initiating Thrusts

A spatial relationship is observed between interpreted thrusts and the fault tips of basement horst, particularly at the Jura Main Thrust. This is a mechanically common relationship (refs). Therefore, interpretation should aim for consistency with location of basement fault tips and thrusts in the overlying rocks. Note: this relationship may be displaced with time by displacement along the detachment.

We assume (at least) a passive role for the basement faults during contraction and have aimed for a spatial relationship between 'fault topography' in the basement and thrusts in the overlying sequence. The sections do not require significant thick-skinned inversion displacement after deposition of the Triassic and Jurassic sequence.

4.2.2.2 Basement extensional growth faults post-salt sequence

Basement fault block topography appears to correspond to subtle thickness variation of the Triassic salt, with thicker salt layers in (half)-grabens. Also the Keuper and Dogger units appear to be thicker towards the basement extensional faults (see Figure 4—7).

This can be caused by active basement extension, or more likely by differential compaction across the km-thick graben fill. Differential compaction may trigger extensional faults in the rocks overlying the sides of the graben (with or without actual reactivation of the basement faults themselves).

RISK: Basement faults that run at a high angle to the belt (transfer or cross faults and associated faults/fractures) will be under-represented on seismic dip lines because they are parallel. When (even modestly) reactivated, these basement faults may cause cross-cutting faults/fracture zones in the overlying cover sequence. Models are generally at risk of under-representing these fault zones.

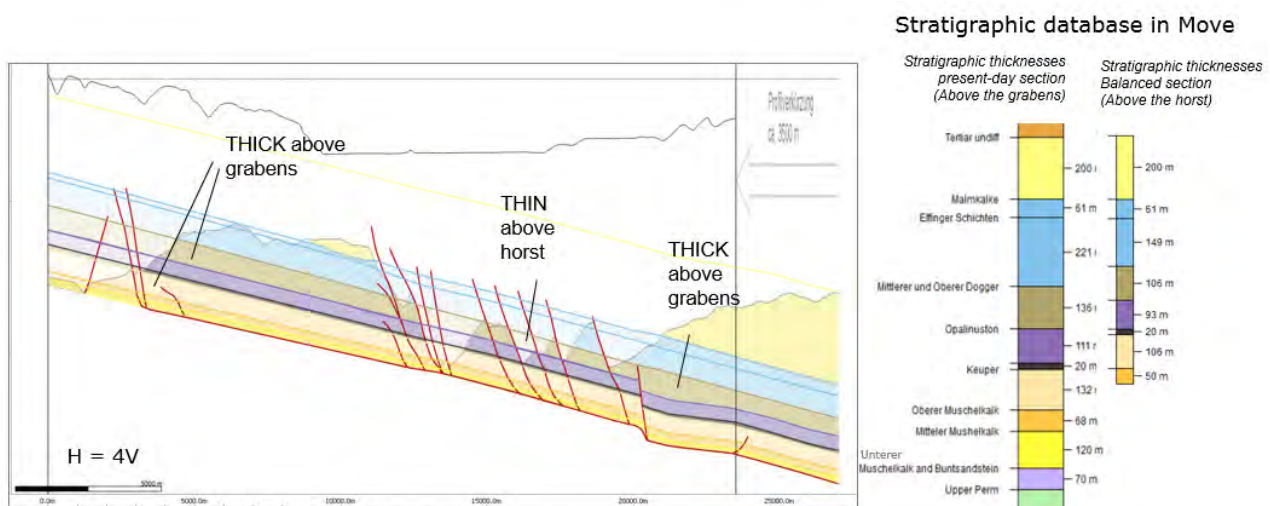


Figure 4—7: Balanced section 6-8 from the NAB 14-105 report georeferenced in Move and 4x vertically exaggerated to illustrate lateral thickness changes for the Keuper and Dogger formations, and the postulated relationship with basement architecture, with thicker parts of the units overlying grabens, and thinner parts overlying the horst.

4.2.3 Mechanical Stratigraphy and Main Detachment Levels

The mechanically weaker units and the four main detachment levels as proposed in the NAB 14-105 report (Figure 3—2) have clearly played a role in the development of the available sections in the NAB 14-105 report. They will be used as a guide and constraint for the kinematic modelling of the Jura Ost and the Nördlich Lägern section.

4.2.4 Folding Mechanism

Observations of present-day geometries, and initial iterative restoration and forward modelling on selected faults show that the most important cause for folding is movement over thrusts with ramps and flats. The appropriate algorithm to mimic such development is the Fault-Bend-Fold algorithm. This algorithm is available as part of the Move kinematic modelling software package.

Locally, apparently in areas where the salt layer was thicker, thrust faults have developed in which detachment folding played an initial role: it can be seen that both the footwall and the hangingwall are folded. After initial detachment folding fault-propagation folding played a role, cutting through the fold and causing differential displacement from deeper to more shallow parts of the fault. For these faults we use the Trishear algorithm, which is part of the Move2015.1 modelling software.

Some of the faults did not reach the surface but propagated into shallower detachments to form a triangle zone, or wedge. Triangle zones can be modelled using Move by modelling displacement on two coevally active faults. However, complex triangle zones with multiple wedges cannot be modelled kinematically using the available algorithms in Move, and require some manual translations. Required manual translations were systematically documented and illustrated.

4.2.5 Role of Cross Faults

Even though faults at a high angle to the thrust belt are seen on the tectonic map (Figure 4—8) the direct effect on both the Jura Ost and the Nördlich Lägern sections is minimal. It is not expected that these cross faults effect the kinematic analysis of the two sections in a fundamental way as the faults do not intersect the sections.

It must be noted, however, that a system of cross faults at the surface (possibly related to sidewall ramps, and possibly related to reactivation of underlying transfer system in the basement) has been observed on the geological map (see Figure 4—2) and may explain the lateral variation in structural style and amount of shortening in this part of the Jura Fold-and-Thrust Belt. This is further discussed below.

For the section kinematic modelling, an influence of cross faults is neglected.

4.3 Forward Modelling of the Jura Ost section (Beilage 6-8 in NAB 14-105)

The kinematic forward modelling sequence for the Jura Ost section comprised 34 individual annotated files (sections in Move) to communicate each step in the analysis. The file name reflects the focus of the kinematics of each individual time step.

This written (printed) report shows the most significant deformation steps in a series of figures with notes on the main observations and outcomes of the analysis. The appended PowerPoint presentation is better suited to show all 34 files in sequence to produce an animation style presentation.

- 4 Section Beil 6-8 (83-NF-15) Present-day (33)
 - Section_83-NF-15_balanced
 - Section_83-NF-15_Digitised with thickness variation
 - Section_83-NF-15_Basement interp
 - Section_83-NF-15_Setup
 - Section_83-NF-15_Post Salt pre-thrust extension
 - Section_83-NF-15_Thrust 2
 - Section_83-NF-15_Thrust 2_600m
 - Section_83-NF-15_Thrust 3
 - Section_83-NF-15_Thrust 3_230m
 - Section_83-NF-15_Thrust 4
 - Section_83-NF-15_Thrust 4_240m
 - Section_83-NF-15_Thrust 5
 - Section_83-NF-15_Thrust 5_550m
 - Section_83-NF-15_Thrust 6
 - Section_83-NF-15_Thrust 6_225m
 - Section_83-NF-15_Thrust 7
 - Section_83-NF-15_Thrust 7_50m
 - Section_83-NF-15_Thrust 8
 - Section_83-NF-15_Thrust 8_70m
 - Section_83-NF-15_Thrust 9
 - Section_83-NF-15_Thrust 9_200m Trishear wedge
 - Section_83-NF-15_Thrust 10
 - Section_83-NF-15_Thrust 10_200m
 - Section_83-NF-15_Thrust 11
 - Section_83-NF-15_Thrust 11_300m
 - Section_83-NF-15_Thrust 12
 - Section_83-NF-15_Thrust 12_900m
 - Section_83-NF-15_Thrust 13
 - Section_83-NF-15_Thrust 13_200m FBF
 - Section_83-NF-15_Thrust 14
 - Section_83-NF-15_Thrust 14_50m
 - Section_83-NF-15_Fold to target detachment
 - Section_83-NF-15_Additional seismic considerations

Figure 4—9: List of the present-day Nördlich Lägern section plus 33 sub-sections in Move™ constituting the sequential kinematic forward model.

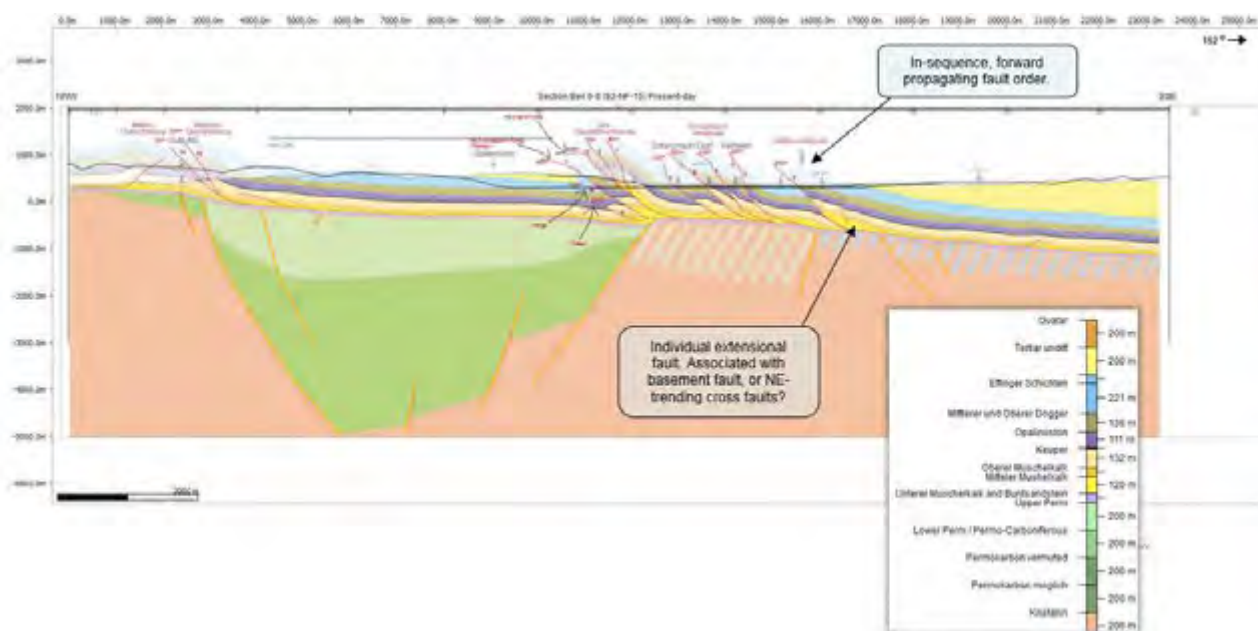


Figure 4—10: The Jura Ost section (modified from section 83-NF-15, Beilage 6-8 in NAB 14-105) with its present-day geometry with temporal order of faulting and distance of fault offset.

Figure 4—10 shows the present-day geometry with the temporal order of faulting and the metric distances of the individual fault offsets. The fault offsets were measured at the Opalinus Clay level. Some faults display a vertical displacement gradient because of fault-propagation during thrusting (causing larger displacements at depth compared to higher up on the fault).



Figure 4—11: The Jura Ost section (modified from section 83-NF-15, Beilage 6-8 of NAB 14-105) and the georeferenced illustration of the restored and balanced model with the regional pin placed in the assumed stable block for restoration. Note the detachment level that is near planar.

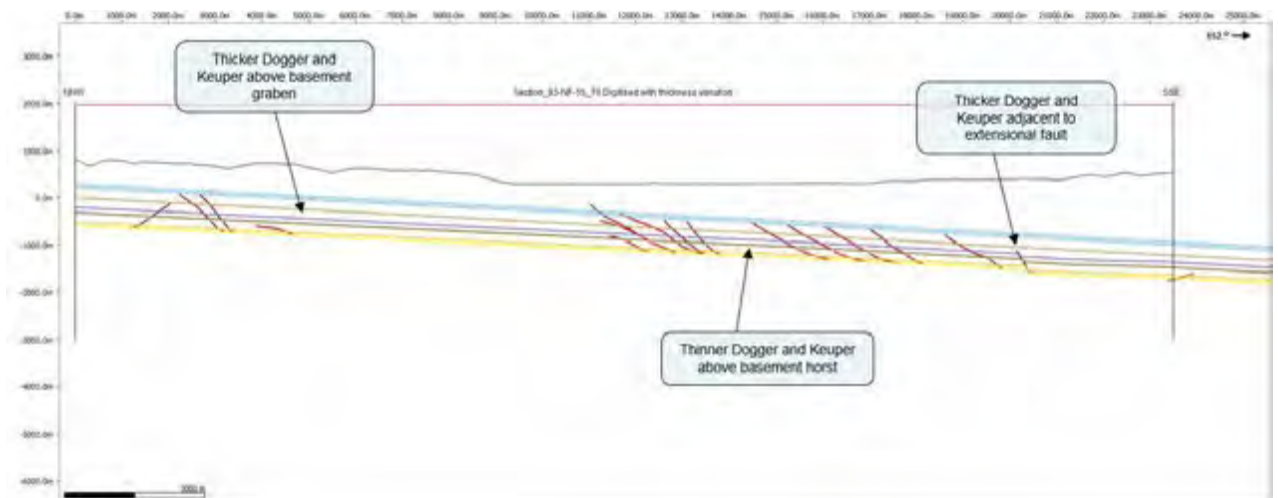


Figure 4—12: Jura Ost section in balanced state (modified from section 83-NF-15, Beilage 6-8 of NAB 14-105) with digitised fault lines and horizons.

Figure 4—12 shows the balanced section with the digitised stratigraphic horizons and fault lines. Thicker sections of Dogger and Keuper are locally recorded above basement grabens, and in the SSE thicker units also correspond to a small extensional fault in the lower units.

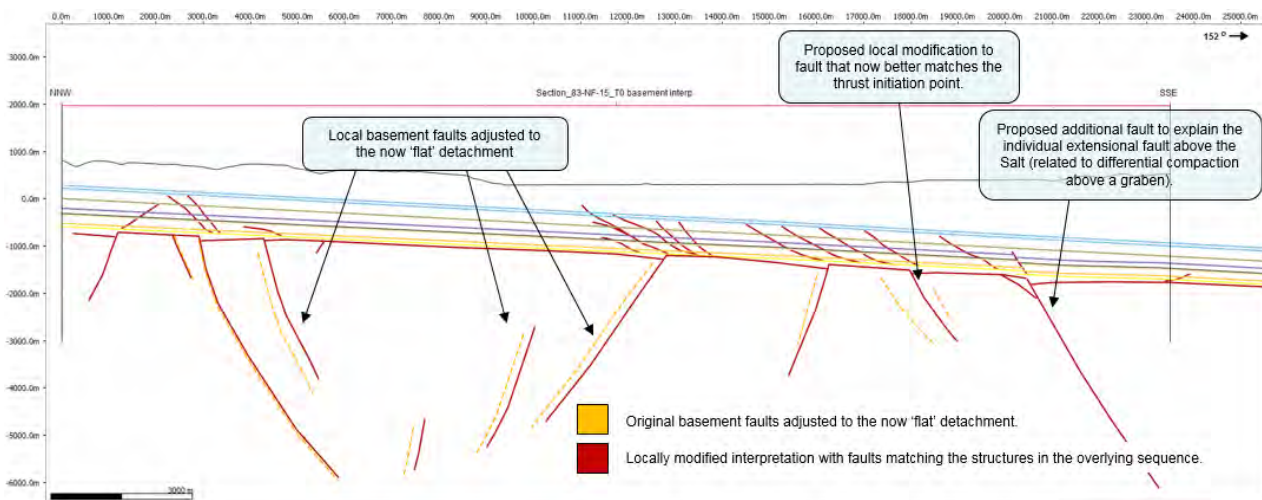


Figure 4—13: Basement faults adjusted to balanced geometry, with locally modified fault interpretation.

Figure 4—13 shows the present-day basement faults adjusted to the ‘balanced geometry’ of a flat detachment plane. Local modifications to the basement faults were made to be more consistent with the thrust initiation points and/or with the seismic imagery (Report NAB 14-105). Modifications of specific faults are pointed out in Figure 4—13. These modifications do not affect the kinematic analysis of the overlying units directly. Merely, they aim to improve the understanding of the basement architecture to provide context for the deformation of the overlying stratigraphic units of interest.

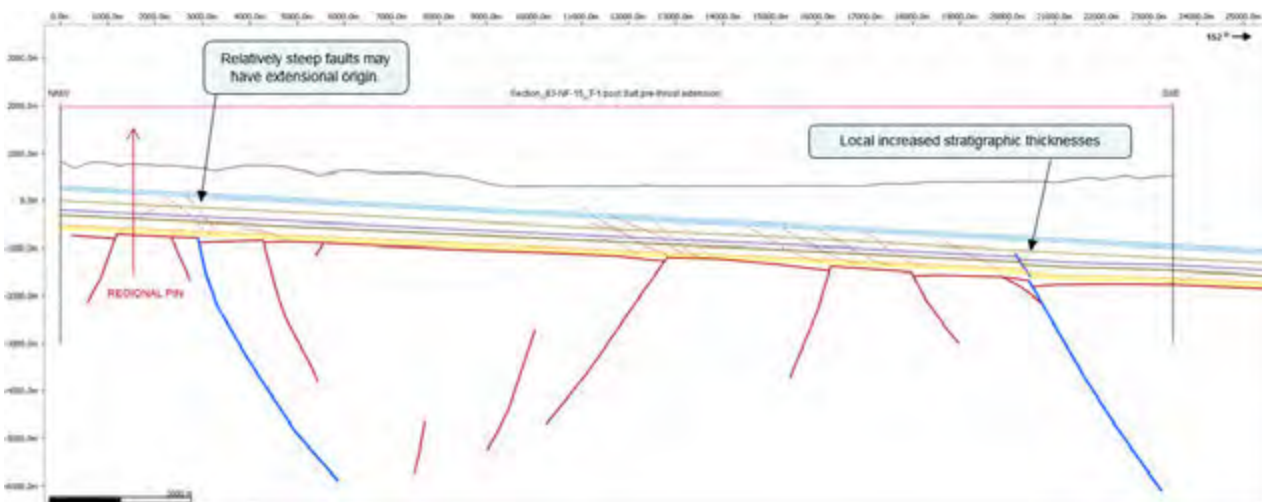
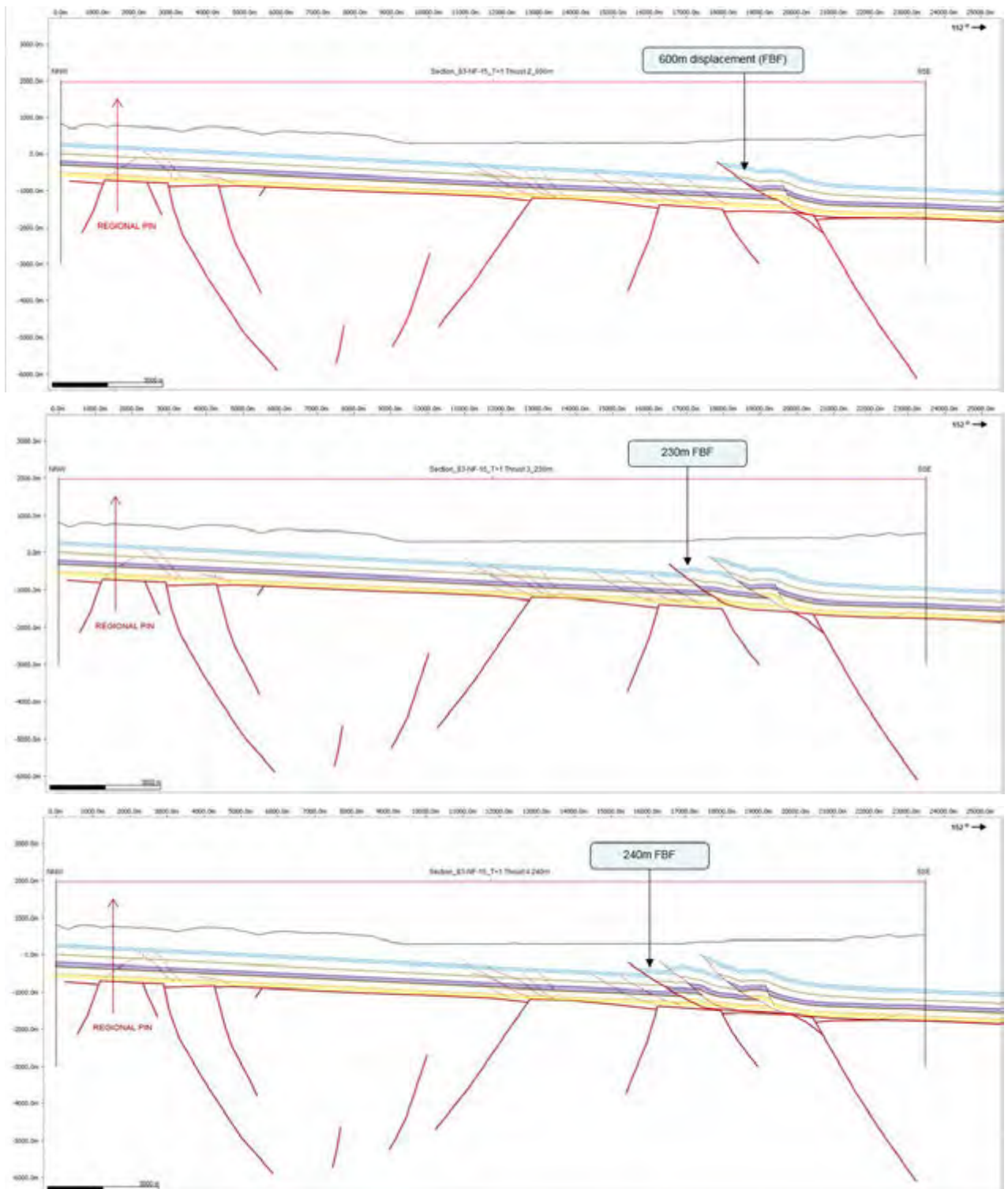
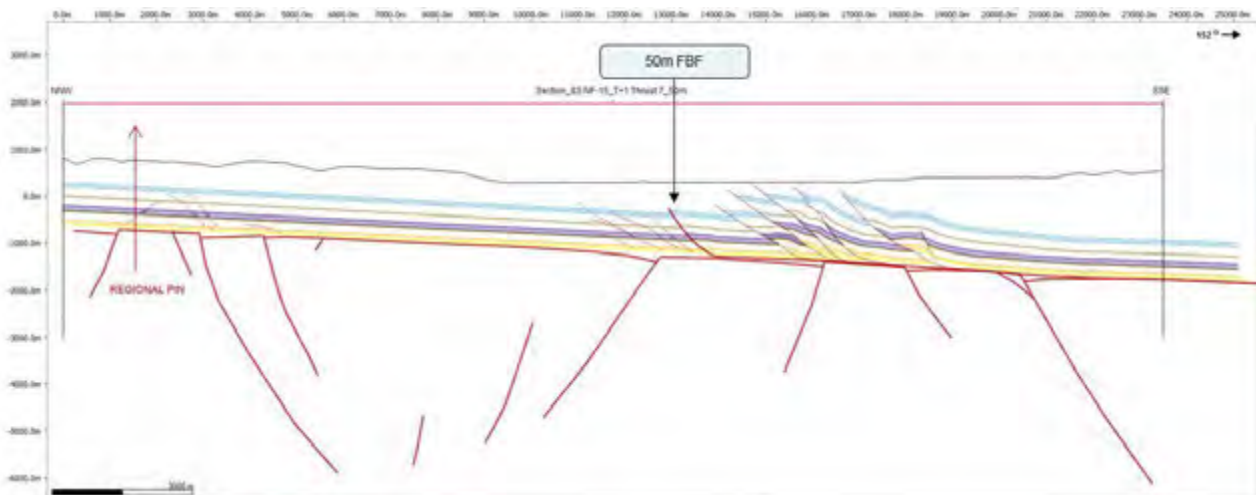
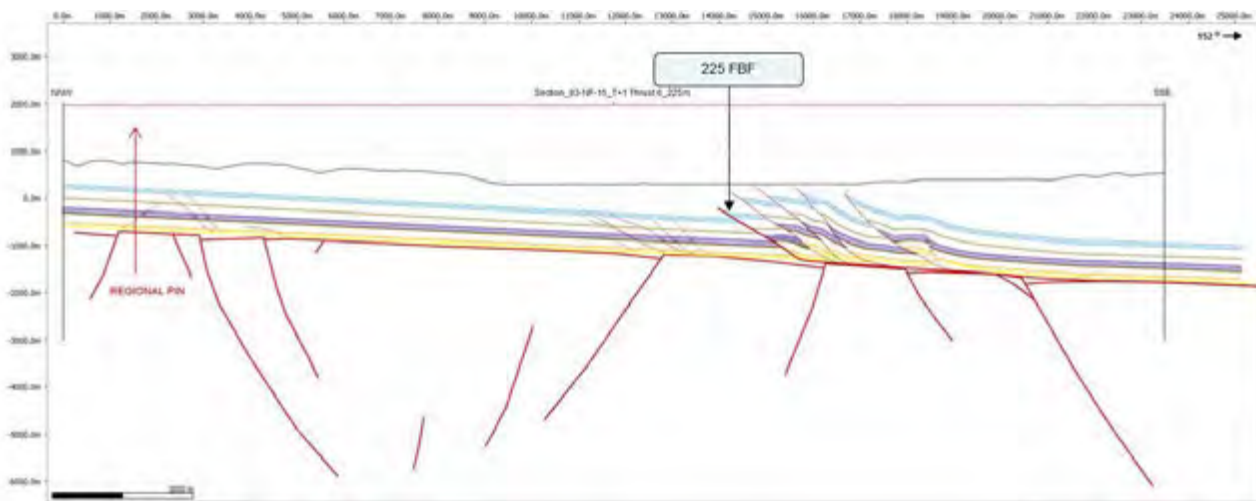
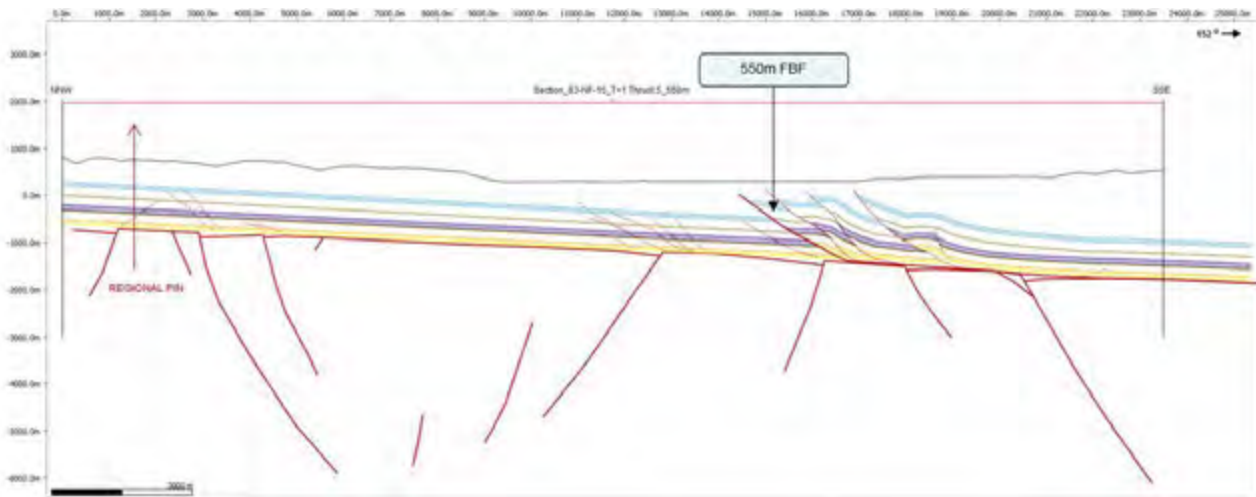


Figure 4—14: Potential extensional faults effecting the Triassic and Jurassic units along the Jura Ost section (modified from section 83-NF-15, Beilage 6-8 of NAB 14-105).

Figure 4—14 shows two faults (in blue) that may have caused extensional structures in the overlying sequence, either due to reactivation of the underlying basement fault or to differential compaction and subsidence-accommodating extensional adjustment faults in the overlying sequence.





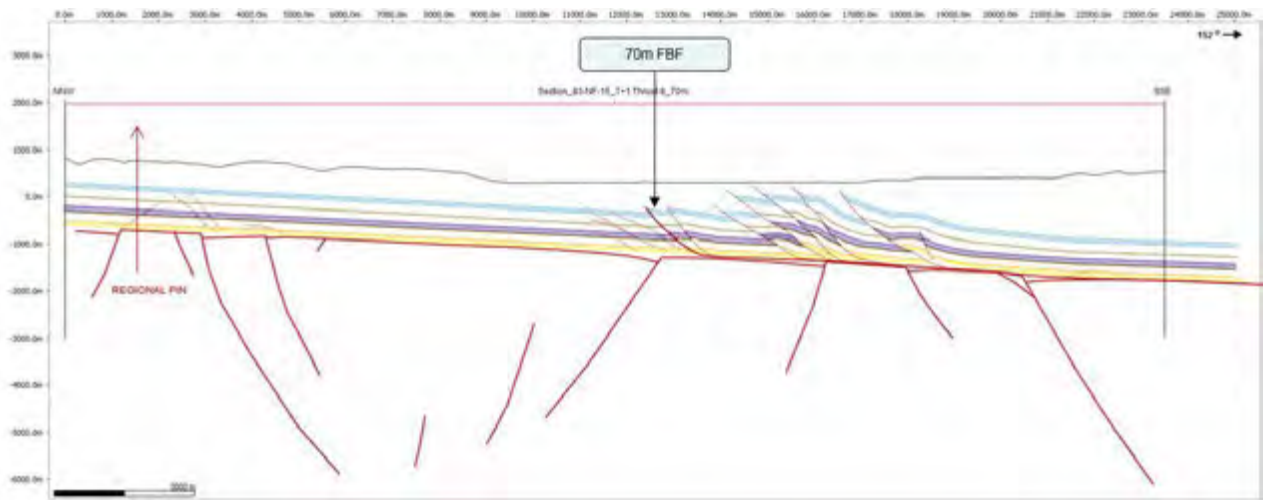
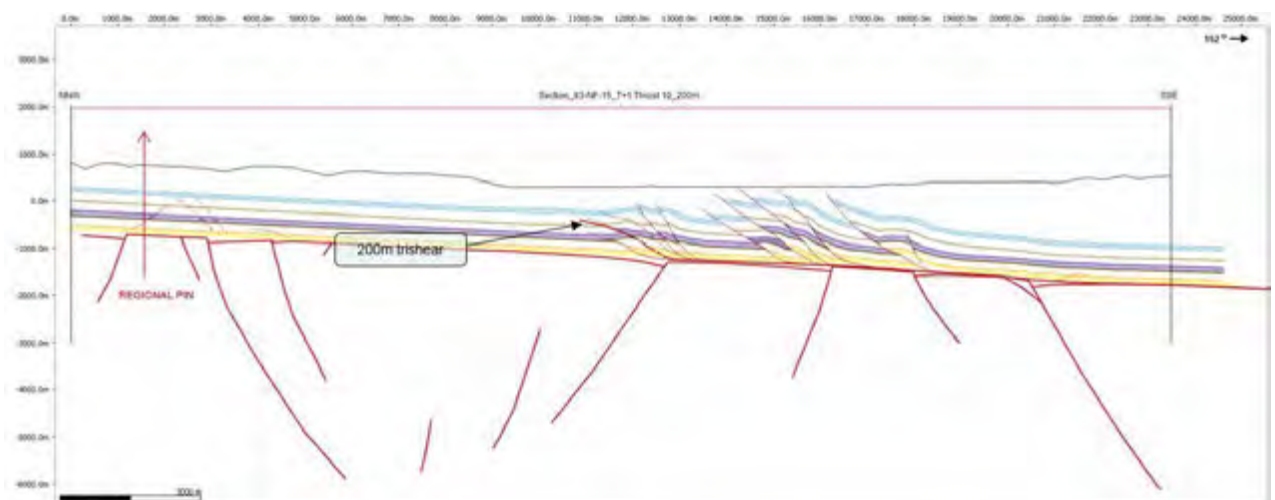
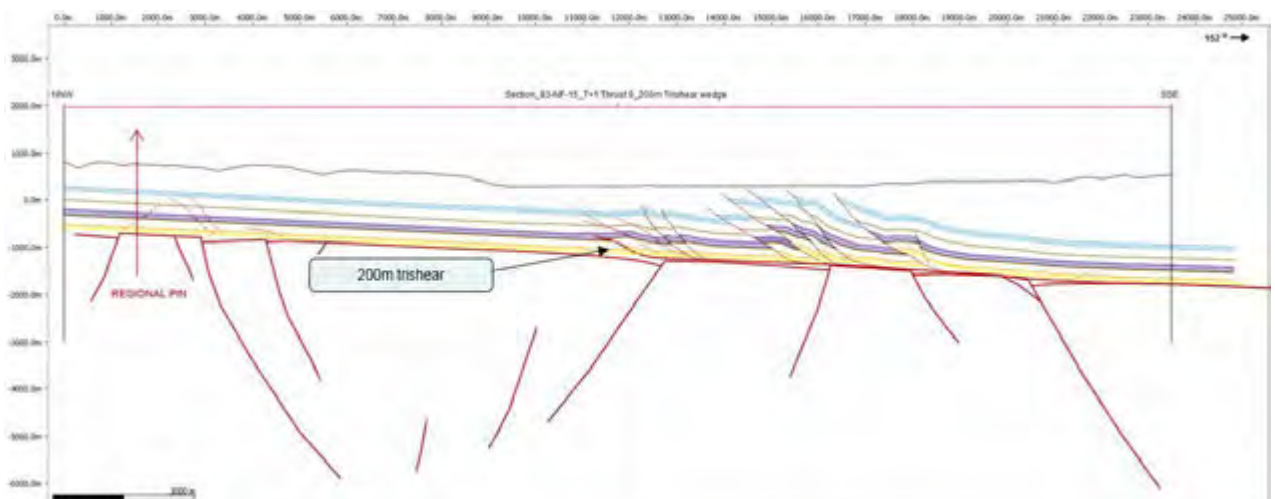


Figure 4—15: Series of seven forward modelled thrust faults along the Jura Ost section, all in-sequence and with displacements ranging from 50 to 600 m. Note how the hanging wall structures progressively steepen with ongoing thrusting. FPF = Fault Parallel Flow algorithm used.



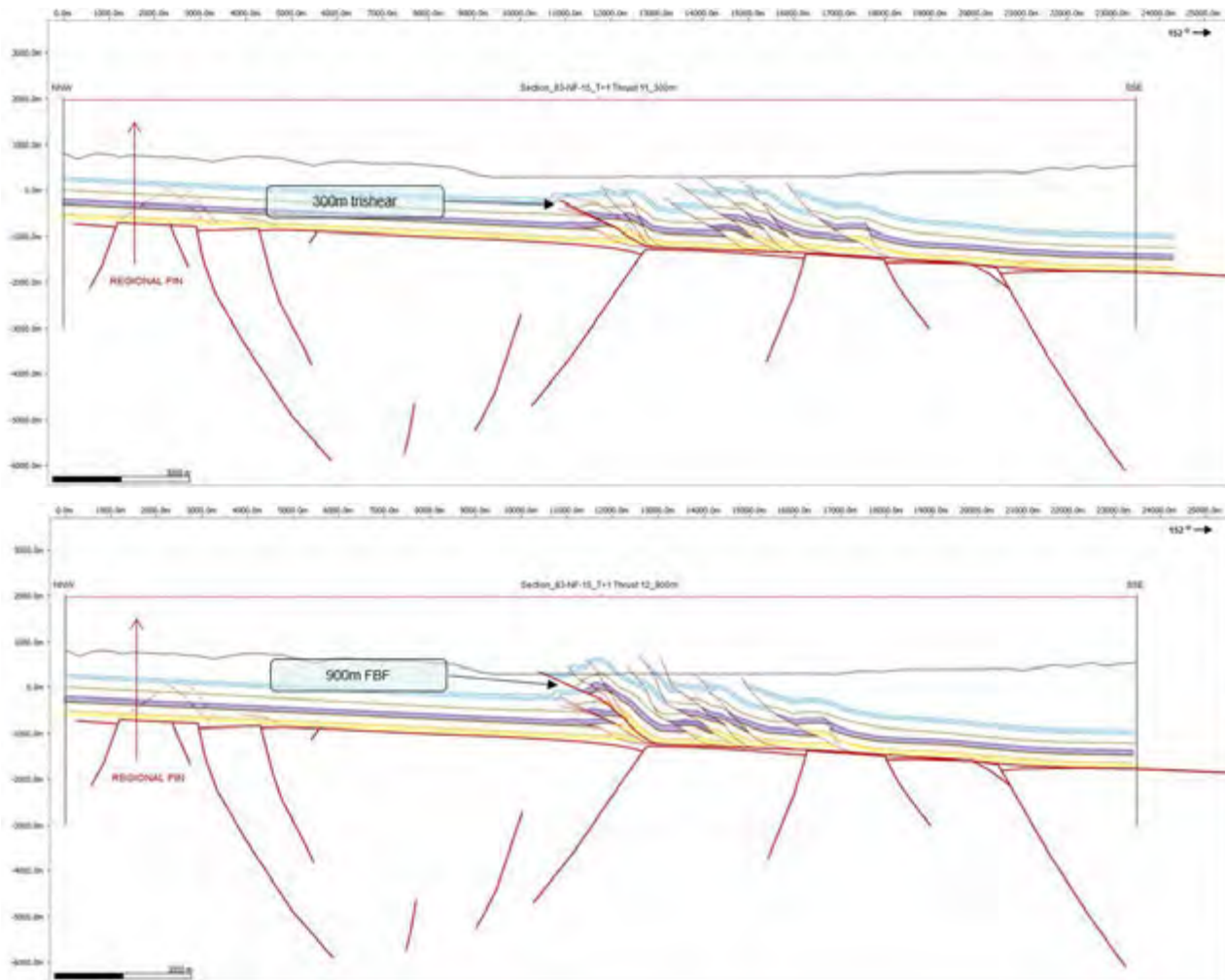


Figure 4—16: Four faults involved in the development of the Jura Main Thrust system of the Jura Ost sectio, forward modelled using a combination of the fault propagation (Trishear) and the Fault-Bend-Folding (FBF) algorithm. Also note the use of several detachment levels. See text for further explanation.

Figure 4—16 shows the four faults involved in the progressive development of the Jura Main Thrust zone. Deformation has been forward modelled using the fault propagation (Trishear) algorithm for the lower most three faults. The first fault in the footwall detaches into the Opalinus Clay (top), the second and third detach in the next detachment level up, displacements of 200m, 200m and 300m respectively. The youngest fault is the Jura Main Thrust, the offset of which is modelled at 900m using Fault-Bend-Folding algorithm (below).

Trishear settings for the three lower faults include:

Trishear Apex: Left 26.00

Trishear Angle: 10.00

Angle Offset: 0.50

Propagation/Slip Ratio: 4.50

Trishear Zones: 1

Movement Type: Forward

Angular Shear: 0.00 deg

Fault Tip Position: 0.00

Last in sequence is the development of the Mandach Überschiebung, modelled here using the Fault-Bend-Fold algorithm with a collective 250 m displacement on the two faults forming the thrust zone (Figure 4—17).

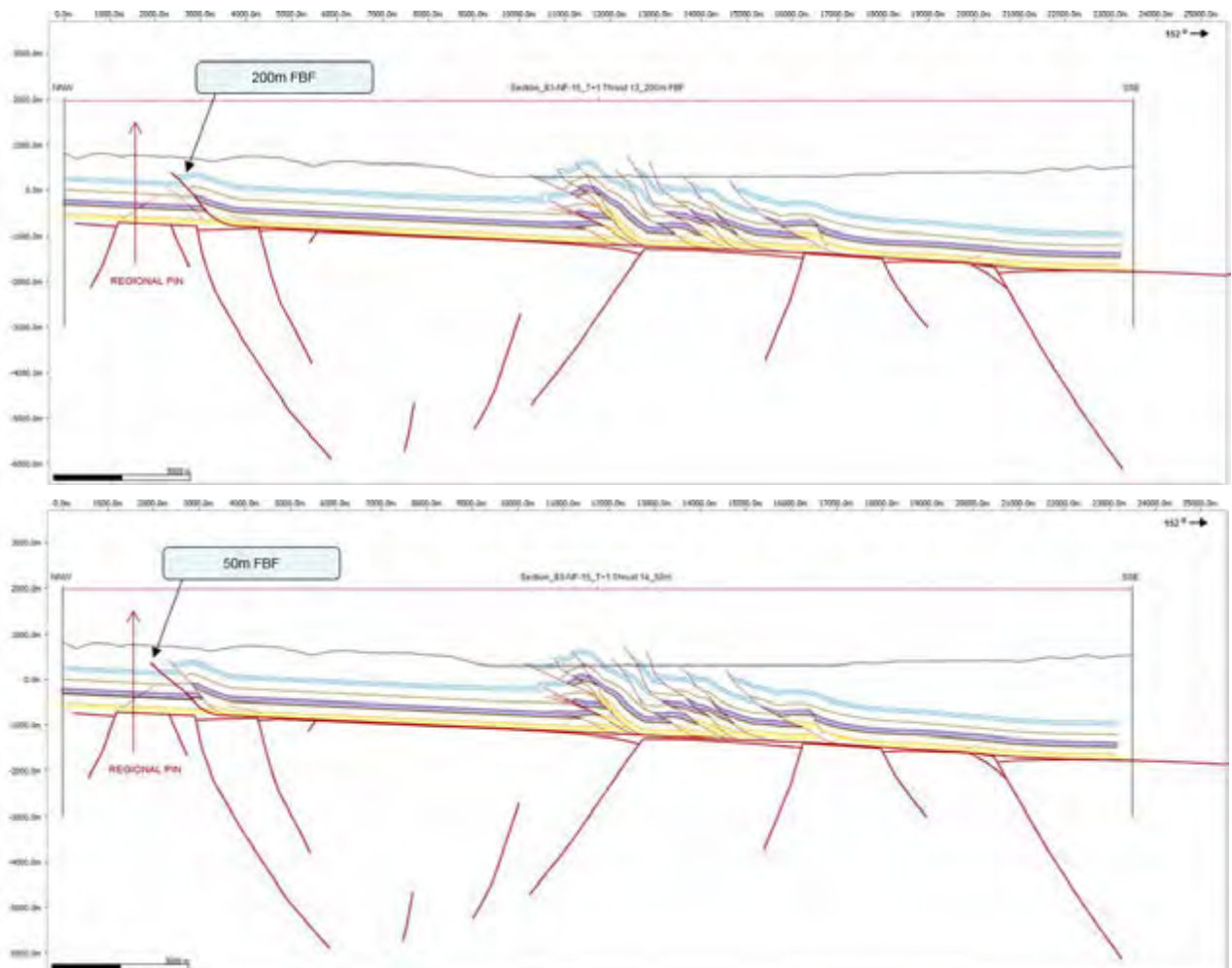


Figure 4—17: Two stages of the forward modelled Jura Ost section showing thrusts 13 and 14 developing in-sequence, modelled using the Fault-Bend-Folding (FBF) algorithm.

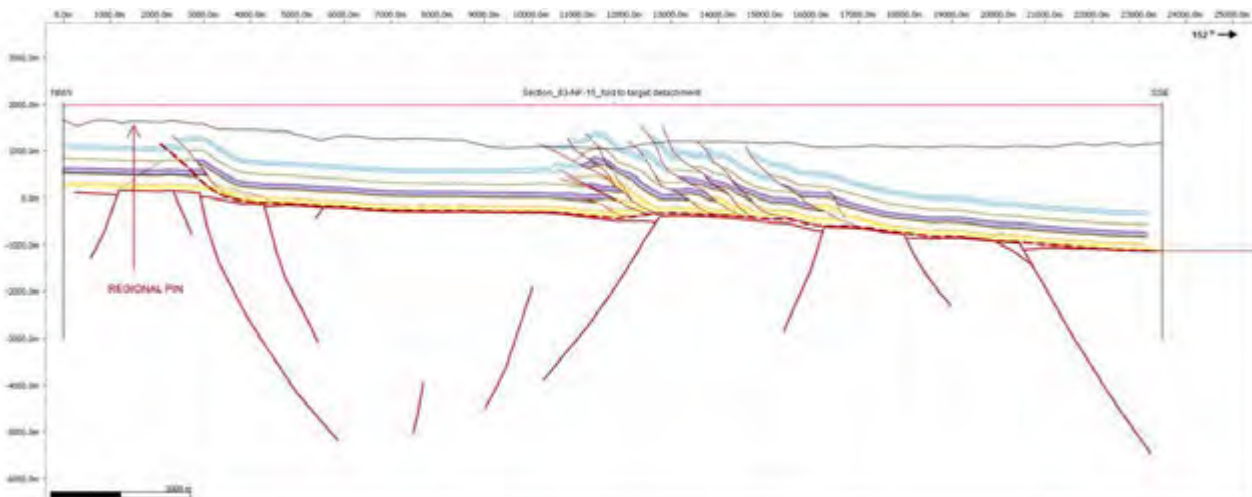


Figure 4—18: Final stage: present-day geometry of the forward modelled Jura Ost section. The flat detachment (thick dashed red line above basement top) was adjusted to obtain the shape of the present-day detachment using the Vertical Shear Folding algorithm. This allows comparing and contrasting of the forward modelled and the interpreted geometries.

The final step of the forward modelling involved a vertical adjustment of the section, and a local projection of the main detachment (interpreted to have originated as a planar structure) to the interpreted present-day detachment (with local highs and lows), compare Figure 4—10 and Figure 4—11. This adjustment is not kinematic and does not take into account any specific geological cause. It merely involves projection of the forward modelled planar detachment plus overlying beds and faults onto the present-day geometry, to allow comparison of the fold and fault shapes in georeferenced space. The adjustment was done using the Vertical Shear algorithm in Move. The resulting section is presented in Figure 4—18. The geological significance of this adjustment is further discussed below.

4.3.1 Comparison of Modelled to Present-Day Geometry

Figure 4—19 gives a comparison of the present-day geometry (proposed by Nagra, top) with the forward modelled geometry (resulting out of this report, middle). It can be seen that the overall geometry shows a good fit of the structural style, the thrust slices and their tilts, and the units correspond generally well to the mapped surface geology. It can be concluded that the current interpretation and structural concept in essence is valid, structurally and kinematically feasible.

Local mismatches do occur. Differences in local hangingwall dips, detail of fold shapes, and salt thickness are indicated in Figure 4—19. The reason for these differences is most likely an oversimplification of the forward modelling scenario and not of the initial interpretation as the dips and fold shapes are well constrained by surface measurements.

The most significant mismatches in hangingwall fold shapes appears to correlate to a difference in interpreted and assumed salt thickness, also indicated in Figure 4—19. The salt interpretation is constrained by the seismic interpretation and has uncertainty.

In the current modelling scenario the salt unit was assumed to initially be of constant thickness above the detachment, and the detachment was assumed planar. The salt did not change

thickness during folding and thrusting. Alternative scenarios may be considered:

1. A scenario in which a component of salt-cored detachment folding prior to failure and thrusting is included (with a planar detachment);
2. A scenario in which differential compaction of the graben sequence may have caused locally deeper basins at the time of salt deposition, leading to locally thicker salt unit prior to folding and thrusting (either with a planar detachment or with some local low on the detachment due to differential compaction);
3. A scenario that includes a component of basement inversion that pushes part of the salt above regional and above the detachment, leading to the salt to be 'decapitated' and incorporated into the thrust slices, which in turn affects the hangingwall shape.

Future modelling iterations may test different forward modelling scenarios aiming for a better fit in detail.

The significance of the potential of these scenarios is that if basement faults have played a role in the development of the fold and thrust belt, these faults are possibly active structures in the future and carry risk of future displacement affecting the overlying units, and/or may form conduits for focused fluid flow.

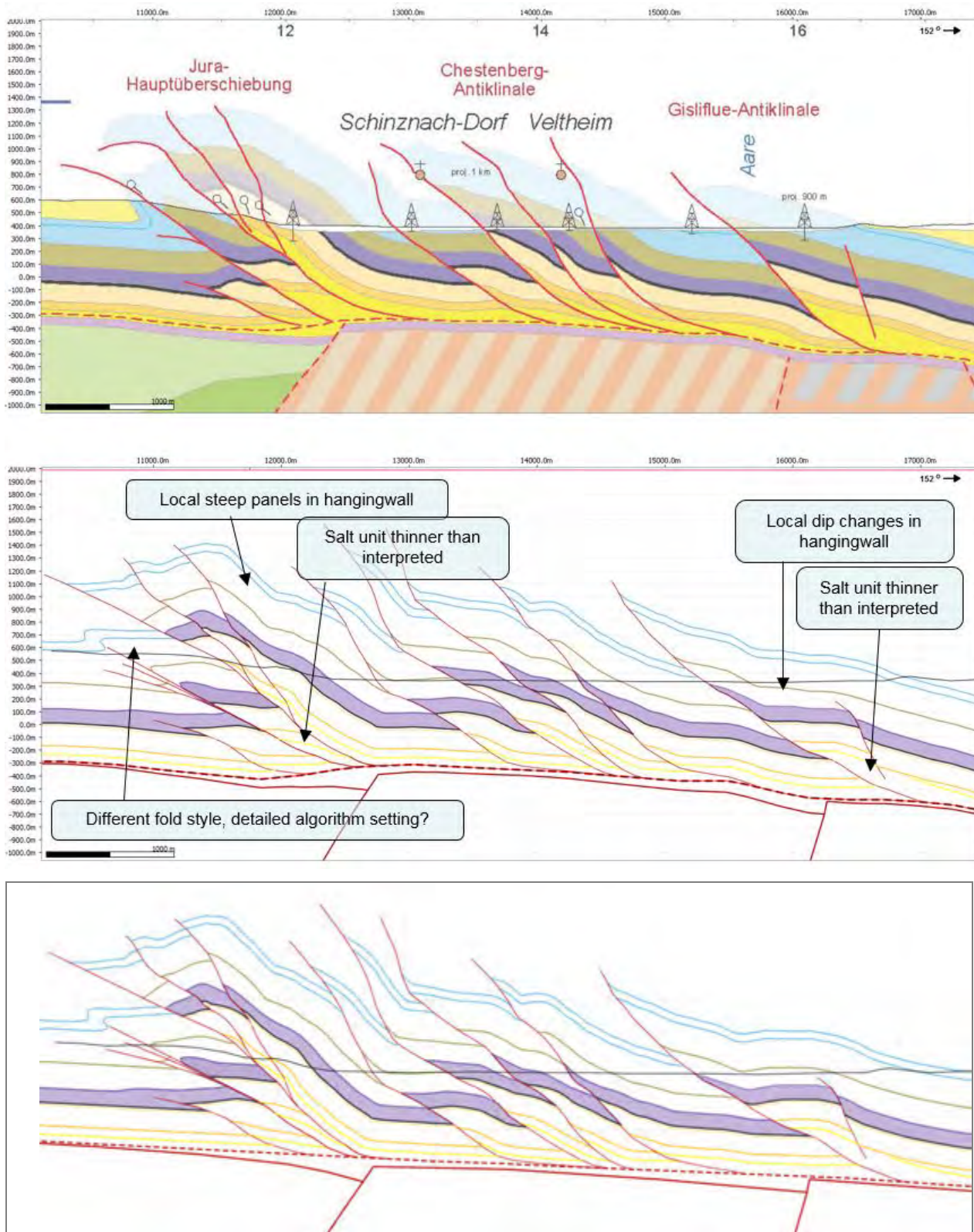


Figure 4—19: Comparing the geometry of the present-day interpretation of the Jura Ost section (from Beilage 6-8 in NAB 14-105) (top) to the geometry as kinematically forward modelled in this study (middle). The Opalinus Clay (violet) has been highlighted to enhance comparison between sections. The bottom figure shows the forward modelled result after vertical adjustment of the planar main detachment level to fit to the present-day geometry. See text for further discussion.

4.4 Forward Modelling of the Nördlich Lägern section (Beilage 6-6 in NAB 14-105)

The kinematical forward modelling sequence for the Nördlich Lägern section comprised 21 individual time steps (called “sections” below). Each section-name reflects the focus of the applied kinematics of that particular section.

The sections can be view as series of single time steps in Move™ and in the appended PowerPoint presentation. Here, the most important sections are shown with notes on the main observation and outcomes of the analysis.

- Section Beil 6-6 (91-NO-58) Present day order and offsets (20)
 - Section Beil 6-6 (91-NO-58) Balanced
 - Section Beil 6-6 (91-NO-58) Digitised
 - Section Beil 6-6 (91-NO-58) Basement interp
 - Section Beil 6-6 (91-NO-58) Set up
 - Section Beil 6-6 (91-NO-58) Extensional faults Pre-thrust
 - Section Beil 6-6 (91-NO-58) Thrust 1
 - Section Beil 6-6 (91-NO-58) Thrust 1_50m FBF
 - Section Beil 6-6 (91-NO-58) Thrust 2
 - Section Beil 6-6 (91-NO-58) Thrust 2 FBF
 - Section Beil 6-6 (91-NO-58) Thrust 3
 - Section Beil 6-6 (91-NO-58) Thrust 3_200m FBF
 - Section Beil 6-6 (91-NO-58) Thrust 4
 - Section Beil 6-6 (91-NO-58) Thrust 4_65m FBF wedge
 - Section Beil 6-6 (91-NO-58) Thrust 4_65m FBF wedge edited
 - Section Beil 6-6 (91-NO-58) Thrust 5
 - Section Beil 6-6 (91-NO-58) Thrust 5_100m on FBF wedge
 - Section Beil 6-6 (91-NO-58) Thrust 5_100m on FBF wedge_edited
 - Section Beil 6-6 (91-NO-58) Thrust 6
 - Section Beil 6-6 (91-NO-58) Thrust 6_175m FBF
 - Section Beil 6-6 (91-NO-58) folded to detachment

Figure 4—20: List of 21 sections in Move™ constituting the sequential kinematic forward model for the Nördlich Lägern section.

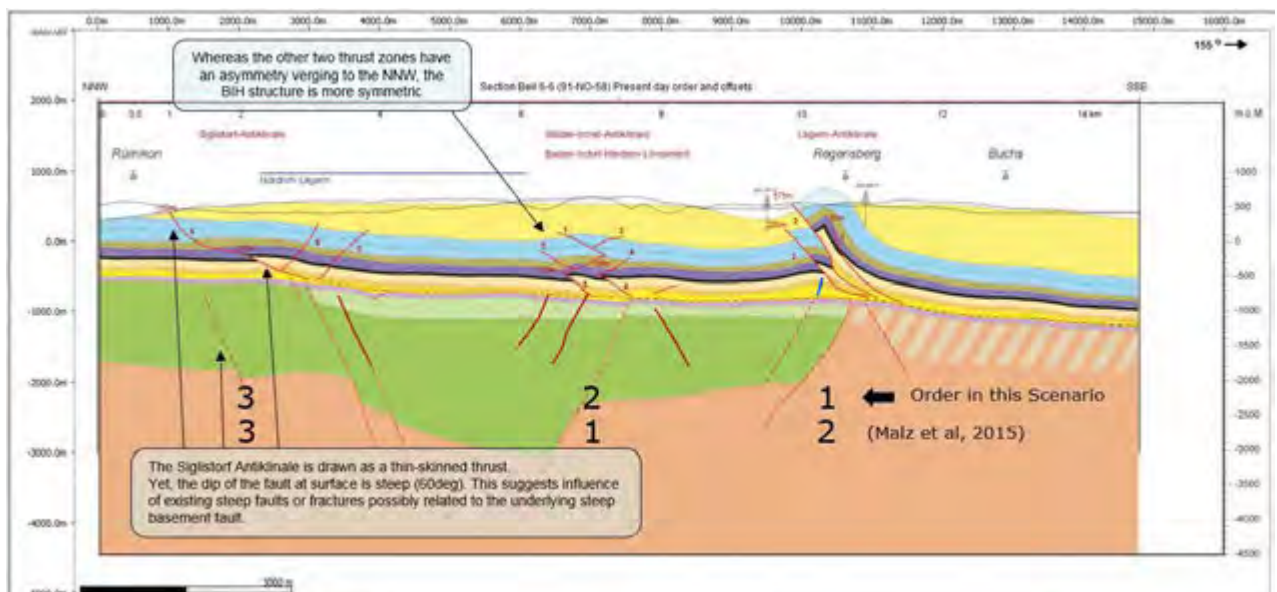


Figure 4—21: The Nördlich Lägern section (modified from Section 91-NO-58, Beilage 6-6 in NAB 14-105) with present-day geometry and the order of faulting including the displacement along the fault.

Figure 4—21 shows the present-day interpretation of the geometry with the temporal order of faulting (small red numbers from 1 to 6) assuming an in-sequence thrust development. The assumed order of faulting will not affect the timing nor the style of the fold and thrust belt. It may influence the understanding of the role of the basement.

One argument in favour of an alternative to in-sequence order of thrusting, is the position of thrusts 1-3. Assuming the basement horst played a role in initiating the thrusts, its position with respect to thrusts 1-3 suggests thrusts 1-3 were initiated after the sequence was displaced to the NNW due to displacement on thrusts 4-6. This is further illustrated in the forward modelling steps. The indicated offsets along the fault lines were measured at the Opalinus Clay level.

In the present-day interpretation (Figure 4—21) the Siglistorf anticline is drawn as a thin-skinned thrust. Note, however, that the dip of the fault at surface is too steep (60°) for a typical 30° thrust angle and suggests an influence of previously existing faults or fractures possibly related to the underlying steep basement fault. The balanced section (Figure 4—21) shows a shallower angle.

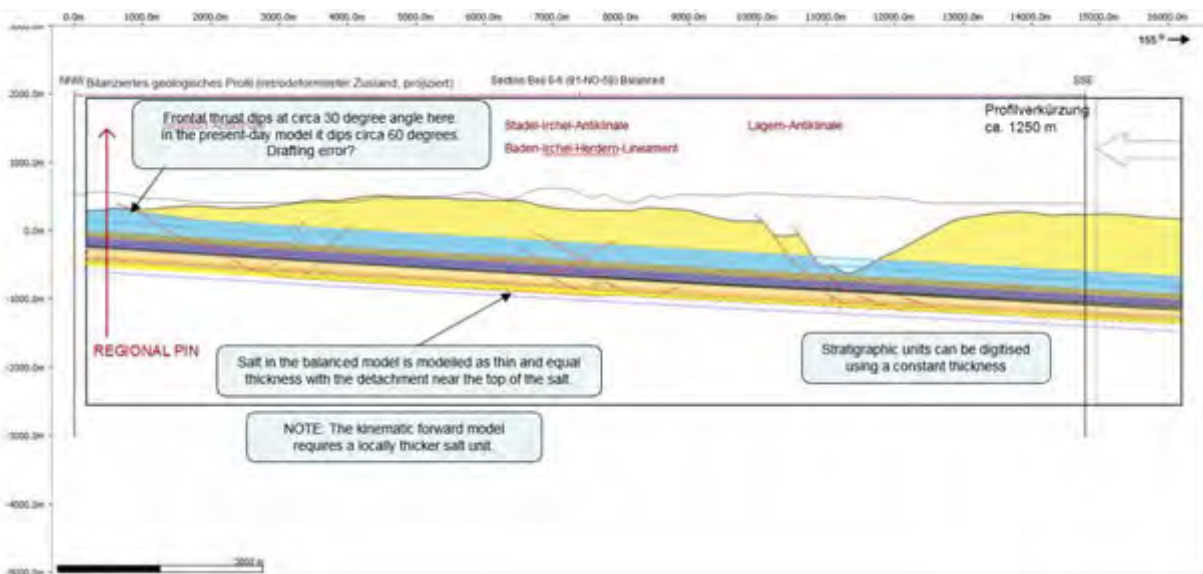


Figure 4—22: The balanced Nördlich Lägern section (modified from Section 91-NO-58, Beilage 6-6 in NAB 14-105) with the digitised balanced model using a regional pin placed to the north in the assumed stable block for restoration.

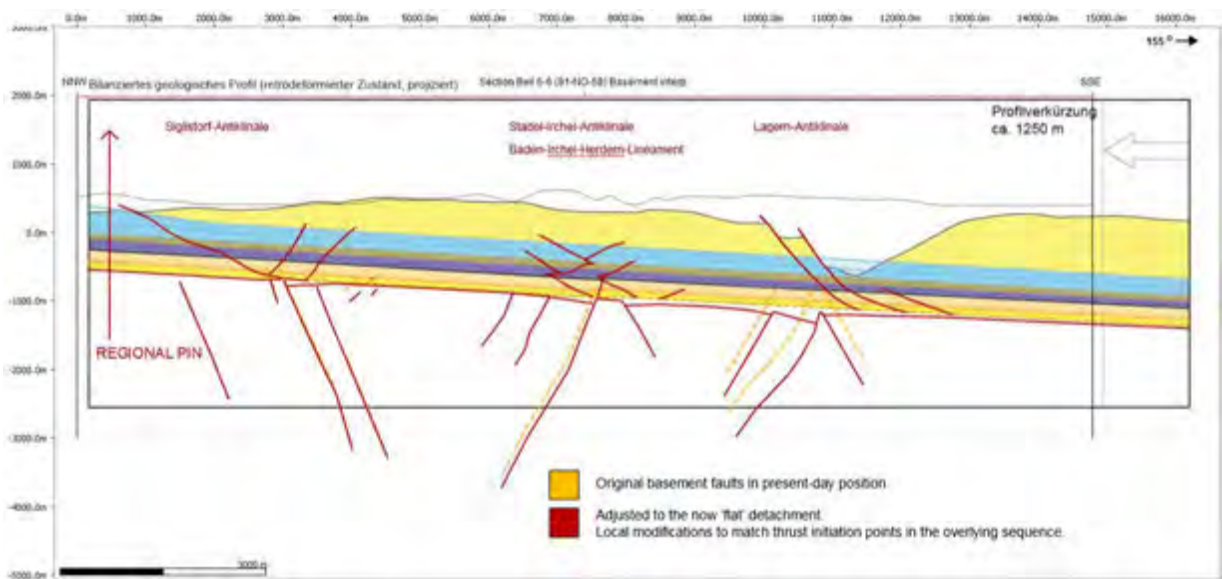


Figure 4—23: The Nördlich Lägern section (modified from Section 91-NO-58, Beilage 6-6 in NAB 14-105) with the original (present-day) basement faults in orange (as in Figure 4—21) and the faults moved down (in red) to the 'balanced geometry' with a planar detachment level.

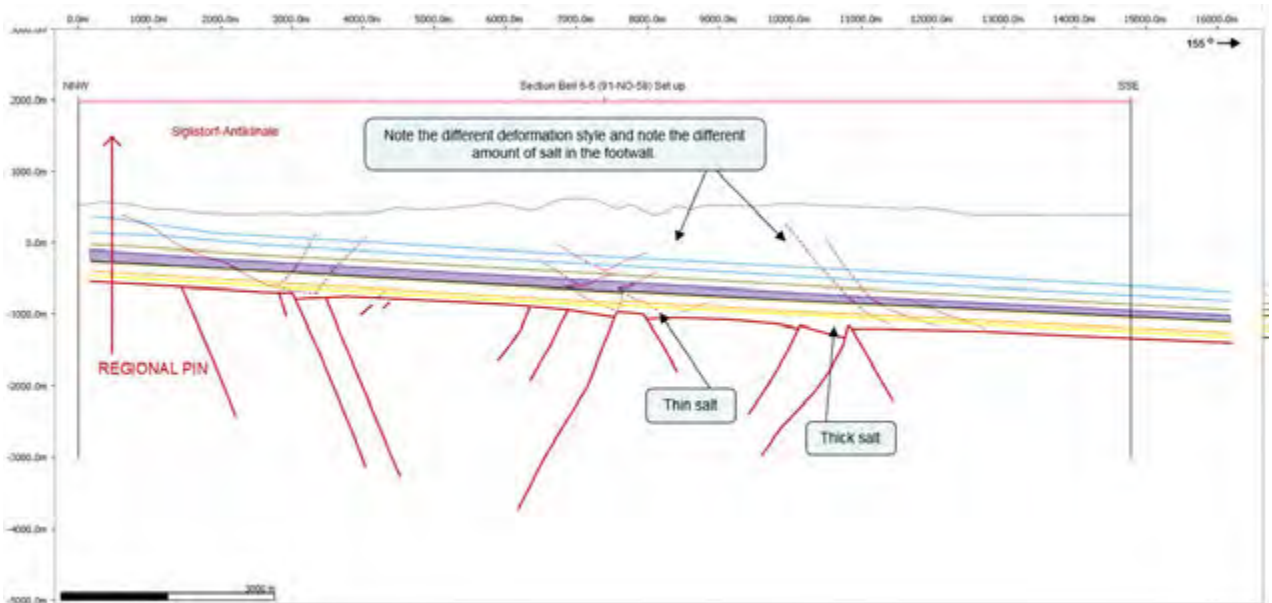


Figure 4—24: The Nördlich Lägern section (modified from Section 91-NO-58, Beilage 6-6 in NAB 14-105) set up for forward modelling. Note the symmetric versus the asymmetric shortening style with NNW-vergent thrusts in the SSE of the section and with a group of both NNW and SSE-vergent wedges and thrusts in the middle of the section, apparently corresponding to the thinner and thicker salt, respectively.

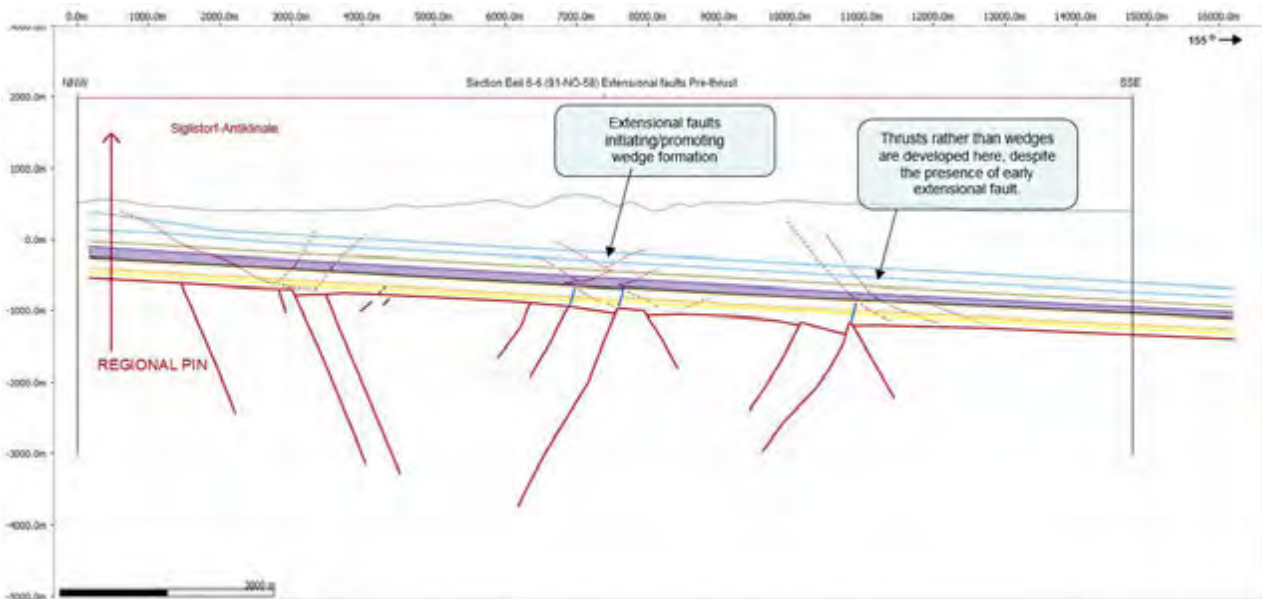


Figure 4—25: The Nördlich Lägern section (modified from Section 91-NO-58, Beilage 6-6 in NAB 14-105) with extensional faults in the basement and overlying sequence (shown in blue). These extensional faults appear to have influenced the location and the deformation style in the central zone where shortening is accommodated by multiple wedges.

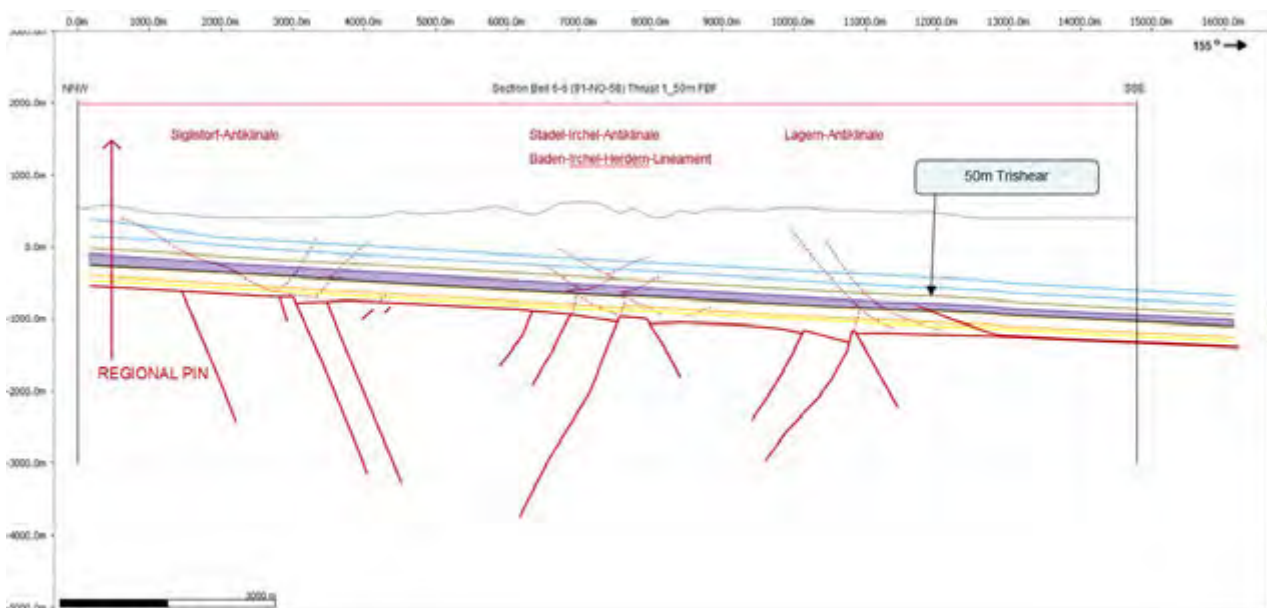


Figure 4—26: The Nördlich Lägern section (based on Section 91-NO-58, Beilage 6-6 in NAB 14-105) focussing on the small displacement of the easternmost thrust.

Initial thrusting focusses on the small displacement of the easternmost thrust (Figure 4—26). This thrust connects the basal detachment with the Opalinus Clay secondary detachment. A 50 m displacement is measured at the base of the Opalinus Clay. The units above the Opalinus Clay are not affected and displacement is modelled with a fault-propagation folding algorithm (Trishear).

Trishear settings include:

Trishear Apex: Left 26.00

Trishear Angle: 10.00

Angle Offset: 0.50

Propagation/Slip Ratio: 4.50

Trishear Zones: 1

Movement Type: Forward

Angular Shear: 0.00 degrees

Fault Tip Position: 0.00

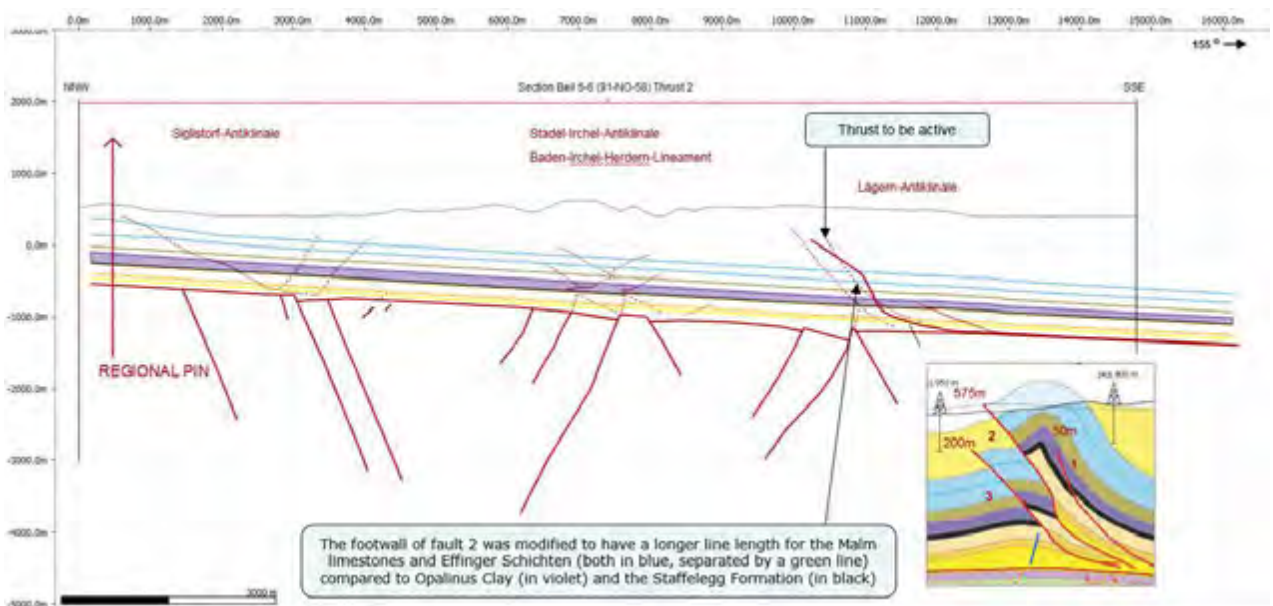


Figure 4—27: The Nördlich Lägern section (based on Section 91-NO-58, Beilage 6-6 in NAB 14-105) highlighting the next active thrust fault, which was modified to better reflect the present-day fault block shape.

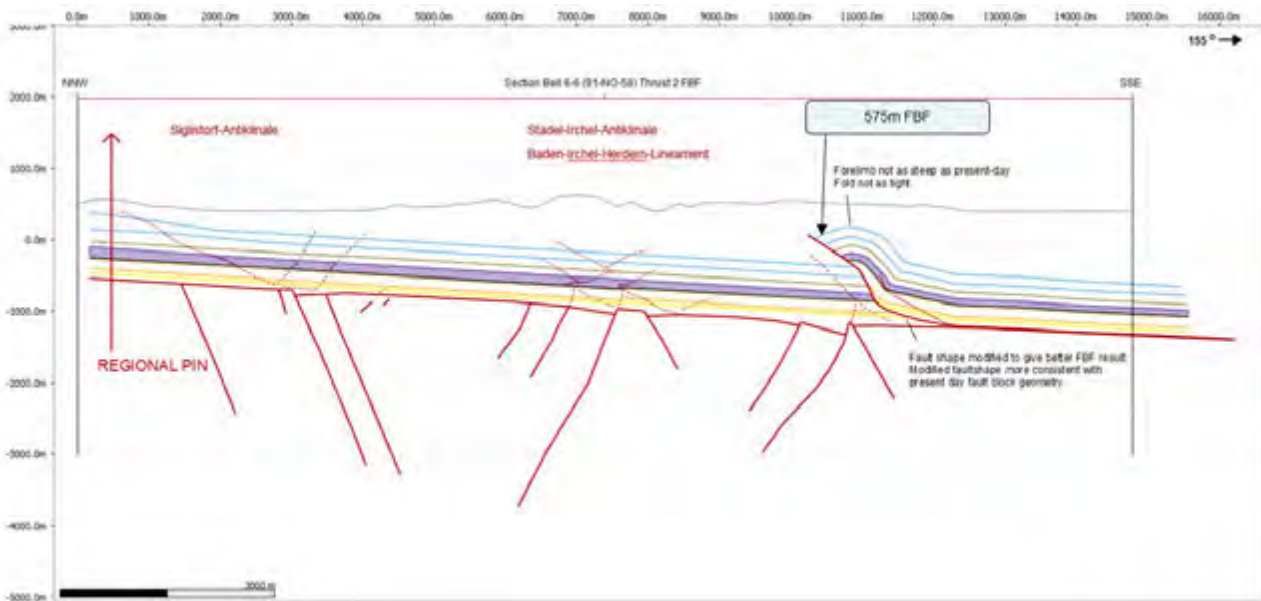


Figure 4—28. The Nördlich Lägern section (based on Section 91-NO-58, Beilage 6-6 in NAB 14-105) with a 575 m displacement along thrust 2 using the Fault-Bend-Folding algorithm. In detail the fold shape is not as tight as the interpreted present-day fold (cf. Figure 4—21). Some pre-thrusting folding is suspected (because of the existing footwall fold, and thickened salt layer).



Figure 4—29: The Nördlich Lägern section (based on Section 91-NO-58, Beilage 6-6 in NAB 14-105) with a 200 m displacement along thrust 3 using the Fault-Bend-Folding algorithm. The step causes further steepening in the hanging wall and formation of an additional thrust, but does not cause a fold/drag in the footwall. In detail the fold shape is not as tight as the present-day fold (cf. Figure 4—21). Some pre-thrusting folding is suspected (because of the existing footwall fold, and thickened salt layer).

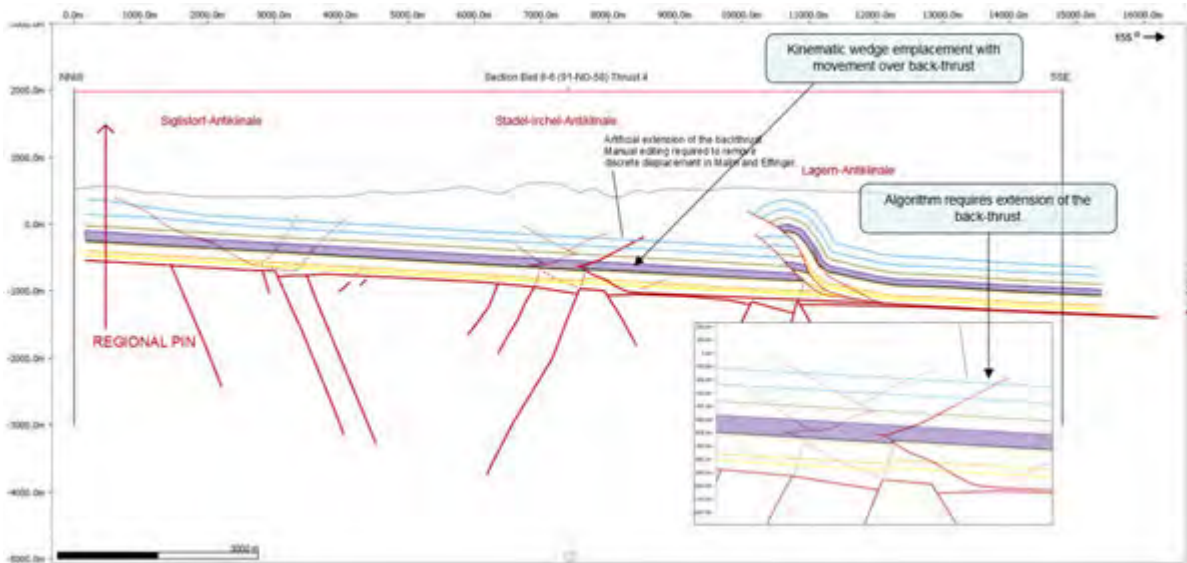


Figure 4—30: The Nördlich Lägern section (based on Section 91-NO-58, Beilage 6-6 in NAB 14-105) highlighting the next active thrust fault, which forms a wedge detaching within the Opalinus Clay, and which in turn detaches in the Effinger Schichten unit. Because algorithms in Move™ cannot handle movements over more than two faults, here the back thrust is extended and the artefact offsets are manually transferred into the forward wedge above (see next slides of inset).

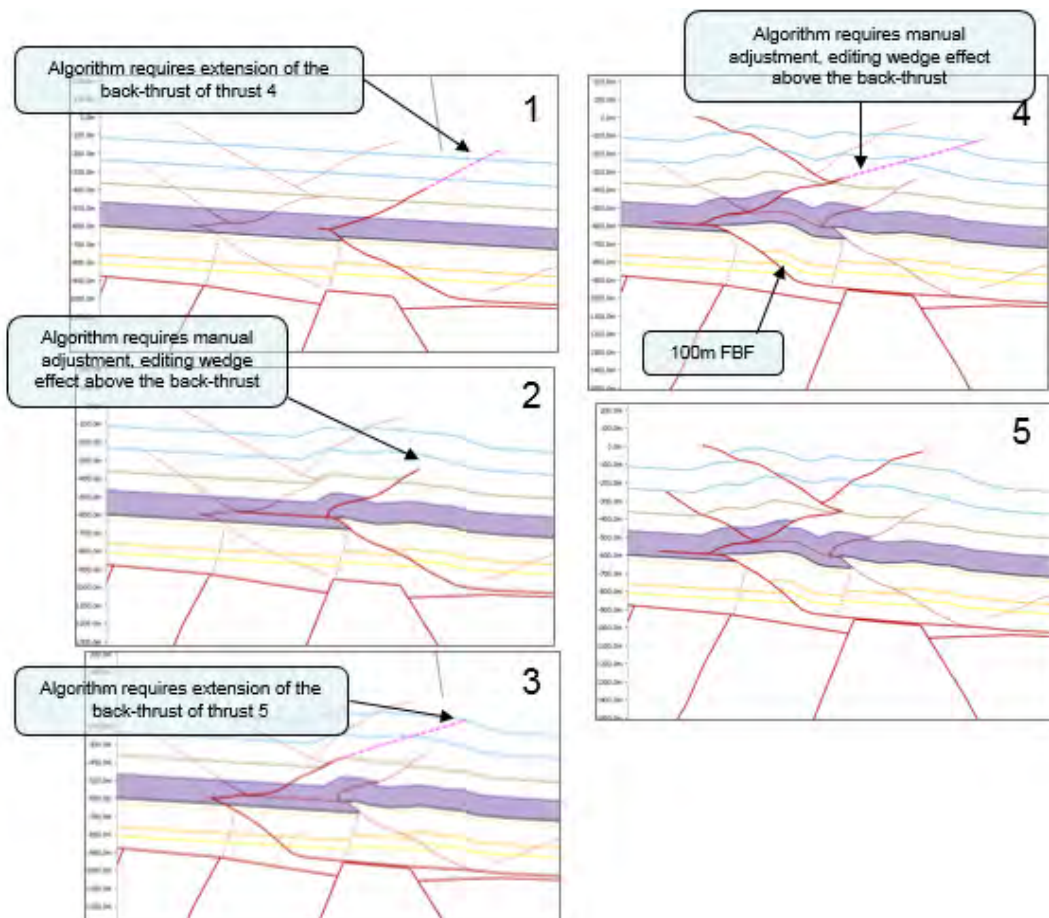


Figure 4—31: Detail of the Nördlich Lägern section (based on Section 91-NO-58, Beilage 6-6 in NAB 14-105) showing the stepwise development of the modelled triangle zone. See text for explanation.

Development of the wedged zone in the centre of the modelled section involves a series of displacements (Figure 4—31) that will have to be modelled sequentially using the current kinematic tools in Move™ (version 2015.1). Fault 4 was extended (Figure 4—31.1) and offset was modelled using the Fault-Bend-Folding algorithm with a coeval connected back-thrust to form a wedge (Figure 4—31.2). Because algorithms in Move™ cannot handle movements over more than two faults at the same time, the back thrust is extended and the unwanted part of the offset manually transferred to the forward wedge above. Subsequently, a 100 m displacement along thrust 5 was modelled with the Fault-Bend-Folding algorithm and a wedge fault. Fault 5 and the above wedge was edited manually to transfer the offsets on the artificially extended fault to the forward wedge above (see top left fault in Figure 4—31.5).

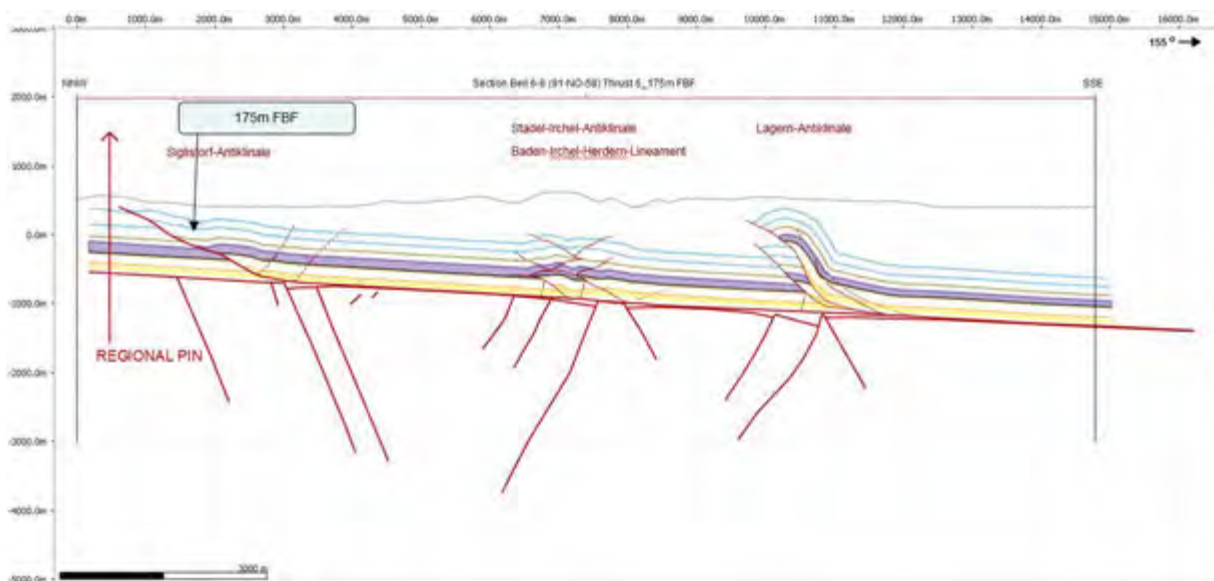


Figure 4—32: The Nördlich Lägern section (based on Section 91-NO-58, Beilage 6-6 in NAB 14-105) with a 175 m displacement on the frontal thrust (thrust 6) using the Fault-Bend-Folding algorithm.

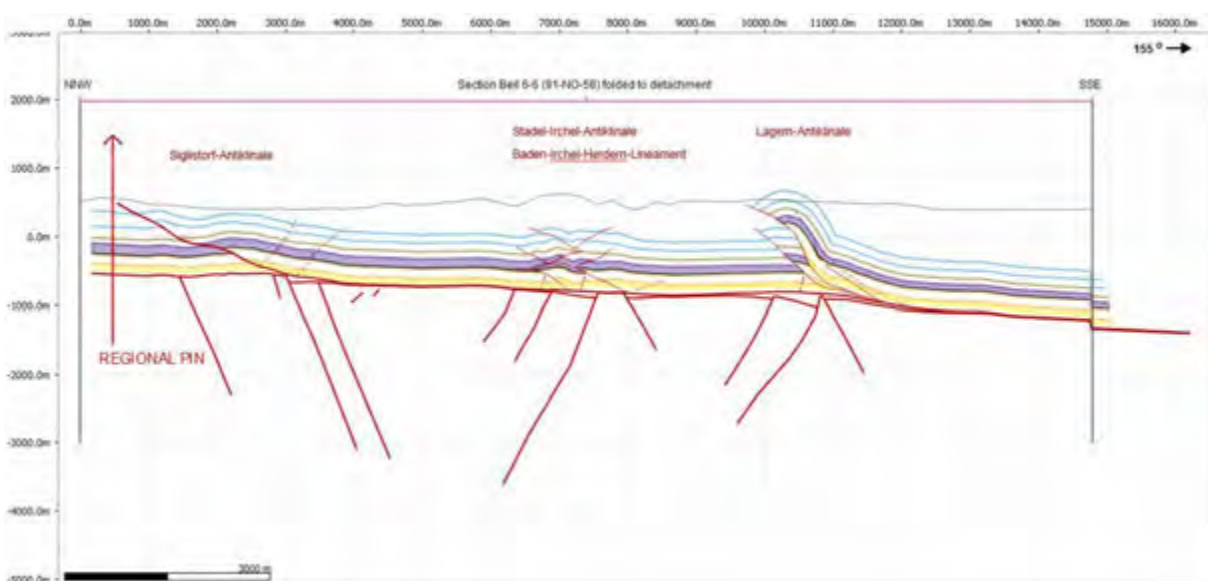


Figure 4—33. The Nördlich Lägern section (based on Section 91-NO-58, Beilage 6-6 in NAB 14-105), adjusted by projecting the forward modelled detachment onto the present-day detachment.

As with the Jura Ost section, the final step of the forward modelling involved a vertical adjustment of the section, and a local projection of the main detachment to the interpreted present-day detachment, compare Figure 4—11. This allowed comparison of the fold and fault shapes in georeferenced space. The adjustment was done using the Vertical Shear algorithm in Move.

4.4.1 Comparison of Modelled to Present-Day Geometry

Figure 4—34 gives a comparison between the present-day geometry (as proposed by Nagra, top) with the forward modelled geometry (as resulting from this report, middle). Note that the overall geometry is a good fit and corresponds generally well to the vertical position with respect to the surface geology.

One discrepancy is observed for the frontal thrust, which has a forward-modelled geometry that is not as steep as in Nagra's present-day interpretation (Figure 4—21). This was expected, because in our starting section (Nagra's *balanced* section, Figure 4—22) the dip of the frontal thrust on was significantly shallower than in Nagra's present-day interpretation (Figure 4—21).

A second mismatch concerns the Lägern anticline, which in the forward model is less tightly folded compared to the present-day interpretation of Nagra (Section 83-NF-15, Beilage 6-6 in NAB 14-105). It is possible that the Fault-Bend-Folding algorithm alone is not adequate to geometrically model this structure, and a pre-thrusting detachment folding stage must be considered.

Additional discrepancies occur in the footwall of the Jura Main Thrust. A difference in salt layer thickness is observed, and the footwall is slightly folded, suggesting some salt-cored detachment folding, accommodated by salt-layer-internal deformation and accumulation prior to thrusting. Alternatively, the underlying extensional basement fault inverted some hundred meter, increasing the salt layer thickness to values above 'regional' average ('salt buckling'), and folding the footwall of the structure.

These geometrical discrepancies between the modelling result of Nagra and 4DGeo have no significant influence on the fundamental kinematic scenario and may be addressed in future iterations, based e.g. on a more detailed seismic data set.

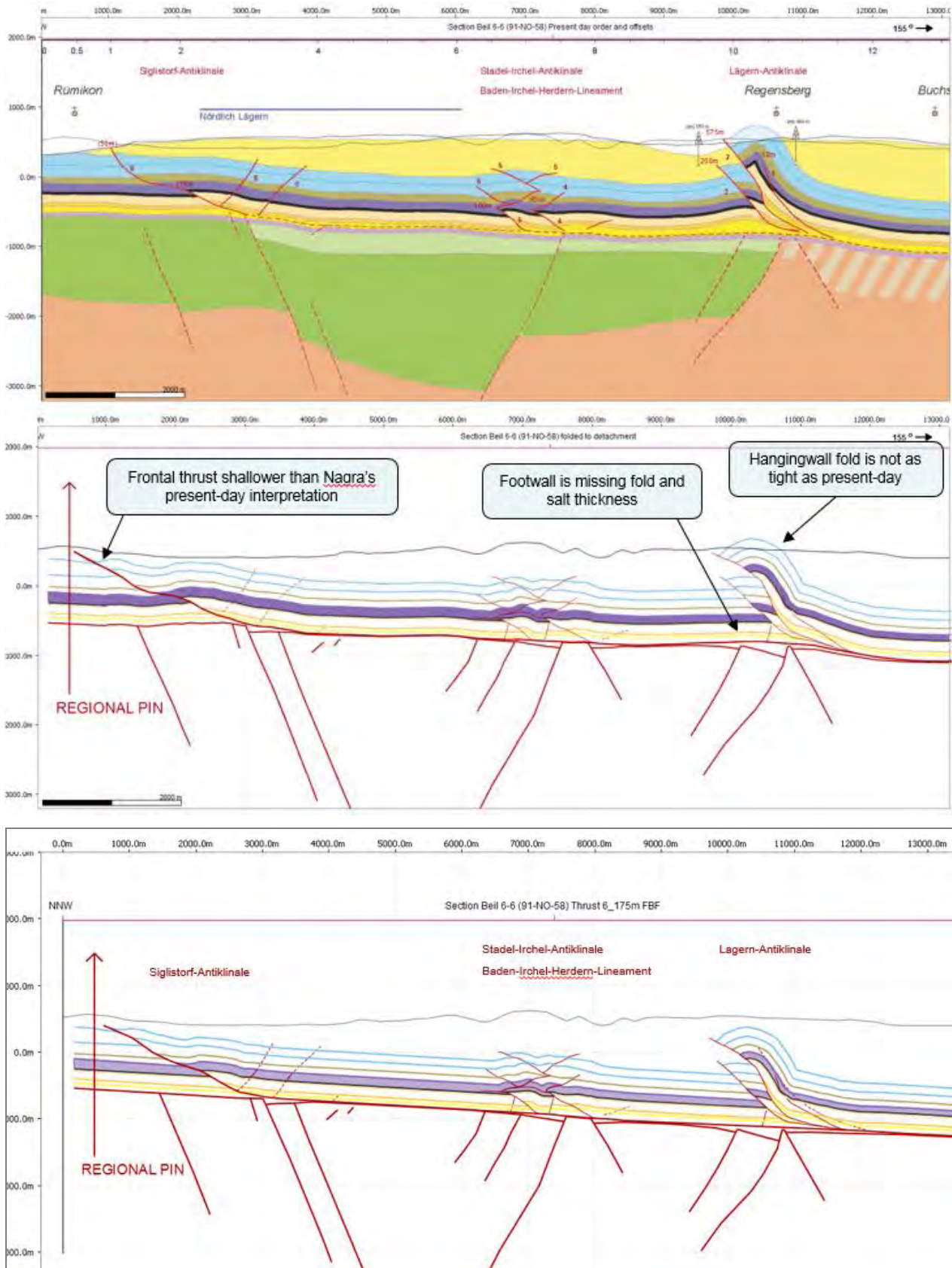


Figure 4—34: Comparing the geometry of the present-day interpretation of the Nördlich Lägern section (Section 91-NO-58, Beilage 6-6 in NAB 14-105) (top) to the geometry as kinematically

forward modelled in this study (middle). The Opalinus Clay (violet) has been highlighted to enhance comparison between sections. The bottom figure shows the kinematically forward modelled result after vertical adjustment of the planar main detachment level to fit to the present-day geometry. See text for further discussion.

5 Summary of the main results

1. The forward modelled scenarios for two sections across the siting regions Jura Ost and Nördlich Lägern indicate that the current interpretation of Nagra (NAB 14-105) is in essence viable.
2. The current study has identified that the main modelling variables included deformation algorithm, (local) thickness of salt, and faulting order. A preferred forward modelling scenario was formulated.
3. Forward modelling iterations have pointed to a geological structural history with the following components:
 - An in-sequence fault order, with new faults forming in the same direction as the transport direction is required due to the steepness of structures in the Jura Ost section and a viable solution for the Nördlich Lägern section.
 - A spatial and causal relationship is found between basement topography and initiation of thrusts at horst/graben contacts (and likely local pre-thrust extensional faults).
 - The structural style is controlled by the mechanical stratigraphy that contains one main detachment (Triassic Salt) and two subsidiary detachment levels (Effinger Schichten, Opalinus Clay) facilitating the main thrust stacks in both sections and the development of wedges in the Nördlich Lägern section, respectively.
 - A significant role for fault-bent-folding is observed, with fault propagation folding being significant locally, particularly for the Jura Main Thrust. Local intra-sequence triangle (wedge or fish-tail) structures nucleated above older extensional faults, perhaps due to reduced salt thickness at this site.
 - The contractional structural style appears to be dictated by the combined basement topography and thickness of salt, with thicker salt promoting detachment folding, and a fault-propagation folding component.
 - Faults observed on the geological map that trend at a high angle to the fold-and-thrust belt, typically (N)NE in the area between the Jura Ost and Nördlich Lägern sections (Figure 4—2), correspond to a zone of reflector offset on the seismic line that runs parallel to the belt (Beilage 6-17). The nature and extent of these faults is as yet unknown, and the current 2D seismic design is not suited to image them. Hence, this family of faults and their influence on both siting regions may be re-evaluated in full detail when a 3D seismic data set will be available.
4. Both forward modelled sections show in essence a similar structural style compared to the interpreted present-day geometry in the sections presented by Nagra (NAB 14-105), with only minor differences, including:
 - Local vertical position;
 - Local hangingwall fold shape;
 - Local fault shape;
 - Local salt thickness.

These differences may in part reflect the over-simplification inherent when applying deformation algorithms, rather than an inconsistent interpretation, but may also indicate a need for adjustment and/or further fine-tuning of the modelling variables and assumptions.

5. Whereas the influence of cross-faults on the structural style of the two studied sections is currently considered to be minimum, cross faults do occur in between the Jura Ost and the Nördlich Lägern siting regions and their effect on these areas needs to be assessed.

6 Conclusion

The current Nagra section interpretations are viable

It was found that the interpretation of the two sections across the Jura Ost and Nördlich Lägern regions as presented by Nagra (NAB 14-105) is in essence viable. The details of the solution are non-unique, and have room for fine-tuning.

Understanding the structural geological history

The analysis and forward modelling of both sections have led to a valid and internally consistent understanding of the structural development of each cross-section that involved initial detachment folding and fault propagation folding but was dominated by a fault-bent-folding style development of the fold-and-thrust belt. Lateral variation in structural style was observed both across and along the belt. Hence a full understanding will require integration of these sections with others, and with the geological map in 3D. The basement architecture (and the knowledge on the potential reactivation of the basement fault pattern) is expected to have played a significant role in the structural development of both regions.

Structural style and 3D domains

One family of structures was identified, and second was inferred. The first family comprises fold and thrust related structures, parallel to the belt, well imaged on most seismic dip lines (NAB 14-105). A second family of structures, with faults trending at a high angle to the belt, is mapped at the surface only locally. Their lateral extent is inferred by general map patterns. These structures at high angle to the belt are expected to have accommodated the lateral change in intensity and style observed along the belt. They are poorly revealed on the seismic dip lines, but are noticeable on the strike line (Beilage 6-17) which corresponds to those faults on the geological map. These cross-cutting structures are not characterised and may have a range of forms and sizes, including faults, folds and fracture zones.

The two families of structures are expected to be kinematically linked. Both of them need to be considered in assessing availability of deformed/undeformed domains in the areas of interest. Mapping out this relationship requires a 3D approach, based on the availability of 3D seismic data.

7 Recommendations

To address the uncertainty and improve the understanding of the geological framework of the two siting regions Jura Ost and Nördlich Lägern, future work should focus on further integration of the available surface data (geological maps) with the available 2D sections (NAB 14-105), and the insights into the kinematic development that were gained in this report, to aim for the construction of a 3D geological framework model.

A 3D geological framework model of the current siting regions can be built on the combination of direct observations, the validly interpreted sections, and on extrapolations for areas without direct (seismic) observations. Extrapolations can be made with confidence based on the valid understanding of the kinematic development of the region.

Efforts should focus on:

1. Performing additional iterations on the section forward modelling to address and minimise the differences between the interpreted present-day and the forward modelled geometries. Improvements may lead to smaller discrepancies in local vertical position of hanging wall beds, local hangingwall fold shape, local fault shape, and salt thickness.
2. Characterizing the nature and significance of the faults that run at high angle to the belt, the 'cross-faults'. What is their extent and have they formed in relation to the basement architecture?
3. Constructing a 3D geological framework model for the areas of interest:
 - For the units above the salt; to address the lateral changes in shortening amount and deformation style, and the role/existence of cross-faults.
 - For the basement; to address basement architecture, with faults blocks and steps in the extensional faults, a possible transfer system in relation to the faults at high angle to the belt.

8 References

Arbeitsbericht NAB 14-105. Jordan, P., A. Malz, S. Heuberger, J. Pietsch, J. Kley and H. Madritsch. Regionale geologische Profilschnitte durch die Nordschweiz und 2D-Bilanzierung der Fernschubdeformation im östlichen Faltenjura: Arbeitsbericht zu SGT-Etappe 2, Nagra, March 2015.

Malz, A., H. Madritsch, J. Kley. (2015): Improving 2D seismic interpretation in challenging settings by integration of restoration techniques: A case study from the Jura fold-and-thrust belt (Switzerland). Interpretation 3 (4), p. SAA37-SAA58.

Malz, A., H. Madritsch, B. Meier, J. Kley. Triangle zone formation and associated thrust front development in thin-skinned foreland fold belts: A case study from the Eastern Jura Mountains. Tectonophysics, under review.



Schweizerische Eidgenossenschaft
Confédération suisse
Confederazione Svizzera
Confederaziun svizra

Eidgenössisches Departement für Verteidigung,
Bevölkerungsschutz und Sport VBS

armasuisse

Bundesamt für Landestopografie swisstopo, Landesgeologie

APPENDIX 3:

Mechanical analysis of the eastern end of the Jura (NE Switzerland): role of basement ramps and inherited faults

Authors:

Typhaine Caër, Prof. Dr. Bertrand Maillot, Dr. Pascale Leturmy, Dr. Pauline Souloumiac
(University of Cergy-Pontoise, France)

© 2016 **swisstopo**
Bundesamt für Landestopographie
Office fédéral de topographie
Ufficio federale di topografia
Uffizi federal da topografia
Federal Office of Topography
www.swisstopo.ch

Landesgeologie
Seftigenstrasse 264
CH-3084 Wabern
Tel: +41 58 469 05 87



E-mail: christophe.nussbaum@swisstopo.ch

Content:

1	Introduction	5
2	The seven selected cross sections	6
3	Method of analysis of a cross section	10
3.1	Principles and implementations of Limit Analysis	10
3.2	Attribution of mechanical properties to materials of the cross sections	11
3.2.1	Properties of the décollement level	11
3.2.2	Properties of the other layers	12
3.3	Response to compression in the current state (Optum G2 software)	14
3.3.1	Presentation of the prototype	14
3.3.2	Results	14
3.4	Evolution in the near future (SLAMTec software)	16
3.4.1	Presentation of the prototype	16
3.4.2	Results	17
4	Results for all seven cross sections	19
4.1	Description	19
4.1.1	Cross section 3 (across Südranden siting region)	19
4.1.2	Cross section 4 (across Nördlich Lägern siting region)	19
4.1.3	Cross section 6 (across Nördlich Lägern siting region)	20
4.1.4	Cross section 7 (across Jura Ost siting region)	20
4.1.5	Cross section 8 (across Jura Ost siting region)	20
4.1.6	Cross section 10 (across Jura Südfuss siting region)	20
4.1.7	Cross section 13 (across Jura Südfuss siting region)	20
4.1.8	Maps of results	21
4.2	Comments on the results	21
5	Reliability of the results	32
5.1	Verification and validation	32
5.2	Rheological data	32
5.3	Initial conditions	33
5.4	Boundary conditions: Thin- or thick-skin?	33
6	Conclusion	38
7	Perspectives	40
8	References	41

List of Figures

Figure 2—1: Correspondence table between the name of the cross sections in this report and the corresponding seismic line number in Jordan et al. (2015). 6

Figure 2—2: Map of the seismic lines and of the cross sections of NAGRA (modified after Jordan et al., 2015). We here studied the seven cross sections labelled 3, 4, 6, 7, 8, 10 and 13. 7

Figure 2—3: The seven cross sections of NAGRA studied in this report (continued in Figure 2—4)..... 8

Figure 2—4: The seven cross sections of NAGRA studied in this report (continuation of Figure 2—3) 9

Figure 3—1: Principles of Limit Analysis. We use here extensively the kinematic approach to determine the failure geometries, i.e., zones of deformation and active faulting. For illustration, the internal approach is used to compute stress fields in cross section 8. 11

Figure 3—2: Stratigraphic log, redrawn after Figure 2—2.1 of Jordan et al., 2015, and mechanical properties with ranges of values used for computations with Optum G2, and with SLAMTec. Note that faults are weaker than pristine materials in Optum G2 computations, while SLAMTec considers only uniform properties, except for the decollement which has its own, uniform, properties. 13

Figure 3—3: Prototype for Optum G2 for the cross section nbr. 8, a). Different typical results classified by common zones of deformation, colours are proportional to the horizontal component of the optimal virtual velocity field V_x , b). Distribution of zones of deformation in a space spanning the friction and cohesion values of the material of the decollement, c.). The Jura Ost siting region, crossed by the cross section is represented by a blue segment. 15

Figure 3—4: Prototype for Optum G2 for the cross section nbr. 8. The static approach of Limit Analysis determines a lower bound to the unknown tectonic force by optimising a statically admissible stress field. This optimal field is shown here. Units are MPa σ_1 and σ_3 are respectively the maximum and minimum principal stress..... 16

Figure 3—5: Prototype for SLAMTec for the cross section nbr. 8, at zero shortening (current situation) a), then at successive steps of shortening up to 1000 m in b). G-gram presenting the position of the roots of the thrust and the width of the deformed area during shortening, c). We can remark that the second ramp develops southward of the first one. A first activation of this second ramp occurs at 360m of shortening, then the first ramp becomes active again and after several hundred meters of shortening accommodated on it, the second ramp becomes active again. 18

Figure 4—1: Prototype for Optum G2 for the cross section nbr. 3 and legend, a). Different typical results classified by common zones of deformation, and extrapolations of deformation using SLAMTec for selected results, b). Distribution of zones of deformation in a space spanning the friction and cohesion values of the material of the decollement, c). The Südranden siting region crossed by the cross section is represented by a blue segment. 22

Figure 4—2: Prototype for Optum G2 for the cross section nbr. 4 and legend, a). Different typical results classified by common zones of deformation, and extrapolations of deformation using SLAMTec for selected results, b). Distribution of zones of deformation in a space spanning the friction and cohesion values of the material of the decollement, c). The Nördlich Lägern siting region crossed by the cross section is represented by a blue segment. 23

Figure 4—3: Prototype for Optum G2 for the cross section nbr. 6 and legend, a). Different typical results classified by common zones of deformation, and extrapolations of deformation using SLAMTec for selected results, b). Distribution of zones of deformation in a space

- spanning the friction and cohesion values of the material of the decollement, c). The Nördlich Lägern siting region crossed by the cross section is represented by a blue segment.....24
- Figure 4—4: Prototype for Optum G2 for the cross section nbr. 7 and legend, a). Different typical results classified by common zones of deformation, and extrapolations of deformation using SLAMTec for selected results, b). Distribution of zones of deformation in a space spanning the friction and cohesion values of the material of the decollement, c). The Jura Ost siting region crossed by the cross section is represented by a blue segment.....25
- Figure 4—5: Prototype for Optum G2 for the cross section nbr. 8 and legend, a). Different typical results classified by common zones of deformation, and extrapolations of deformation using SLAMTec for selected results, b). Distribution of zones of deformation in a space spanning the friction and cohesion values of the material of the decollement, c). The Jura Ost siting region crossed by the cross section is represented by a blue segment.....26
- Figure 4—6: Prototype for Optum G2 for the cross section nbr. 10 and legend, a). Different typical results classified by common zones of deformation, b). Distribution of zones of deformation in a space spanning the friction and cohesion values of the material of the decollement, c). The Jura Südfuss siting region crossed by the cross section is represented by a blue segment.....27
- Figure 4—7: Prototype for Optum G2 for the cross section nbr. 13 and legend, a). Different typical results classified by common zones of deformation, b). Distribution of zones of deformation in a space spanning the friction and cohesion values of the material of the decollement, c). The Jura Südfuss siting region crossed by the cross section is represented by a blue segment.....28
- Figure 4—8: Map view showing the interpolation of the deformation front between cross sections. Note that the different deformation fronts correspond to the various hypotheses on the friction angle of the decollement. This map was made using a cohesion on the decollement of 0 MPa.....29
- Figure 4—9: Map view showing the interpolation of the deformation front between cross sections. Note that the different deformation fronts correspond to the various hypotheses on the friction angle of the decollement. This map was made using a cohesion on the decollement of 0,1 MPa.....30
- Figure 4—10: Map view showing the interpolation of the deformation front between cross sections. Note that the different deformation fronts correspond to the various hypotheses on the friction angle of the decollement. This map was made using a cohesion on the decollement of 1 MPa.....31
- Figure 5—1: Illustration of the hypotheses on the thin-skin tectonic (a) or the activation of the basement, i.e. thick-skin tectonics (b). Cross section C (Figure 21 and Figure 22) and Optum G2 prototype considered for the thin-/thick-skin tectonics analysis c). D1 and D2 indicate respectively the Muschelkalk and the mid-crustal detachments. The red arrows at the southern edge show the applied tectonic compression. The other boundaries are kept rigid (green hash signs along the base), or allow movement parallel to them (green vertical equal sign at the northern edge and at the base of the southern edge). Top surface is free of any traction.355
- Figure 5—2: Surface positions of the thick-skin deformation fronts in map view, interpolated from three cross sections (A, B, C) for different values of ϕ_{D2} , a), and examples of results for three different values of ϕ_{D2} , b). Note that as the friction on the mid-crustal decollement ϕ_{D2} decreases, the thick-skin deformation front moves to the north. In cross section C which is of particular interest here, the deformation front is either in the area, or north of it. The region of interest of this report is represented by the black rectangle. Note that in all cases above, the Muschelkalk.....36
- Figure 5—3: Results of the Optum G2 analysis of the thick-skin hypothesis: The two prototypes, cross section 13 at local scale a)i) and in the frame at regional scale b)i). Graph of results for

local scale study, identical to figure 16, a)ii); for regional scale study with $cD2 = 0$ MPa and $\varphi D2 = 3^\circ$, b)ii); $\varphi D2 = 7^\circ$, b)iii); $\varphi D2 = 10^\circ$, b)iv). Examples of the different types of results obtained and represented by colours in the graphs c)..... 37

1 Introduction

The Swiss Federal Office of Topography (swisstopo) has asked the laboratory Geosciences et Environnement Cergy (GEC), of the University of Cergy-Pontoise (France), to provide mechanical analyses of the structural interpretations by NAGRA for the Eastern termination of the Jura fold belt and its transition to the tabular Jura in the North of Switzerland. Swisstopo was itself mandated by ENSI to provide expertise of the NAGRA interpretation of the seismic lines. This region contains four potential nuclear waste underground siting regions named Jura Südfuss, Jura Ost, Nördlich Lägern, and Südranden-Zürich Nordost. Nagra's geological interpretation of this region is largely based on 20 new seismic lines acquired in 2011 and 2012 and on reprocessed older lines.

In this report we analyse seven of the thirteen cross sections of NAGRA that were published in the NAGRA report NAB 14-105 (Jordan et al., 2015). The mechanical analyses aim at predicting the 2D deformation in a given cross section by applying a horizontal compressive force on a vertical rigid wall placed at its southern limit. In section 2 we briefly describe the seven cross sections selected for analysis. Section 3 starts with a short description of the mechanical methods and softwares used to predict deformation: Limit Analysis ("Optum G2" software), and sequential Limit Analysis ("SLAMTec" software). We then develop our choice of rheological parameters and their ranges of values for the various rock types and faults found in the cross sections. A detailed analysis of a single cross section is performed first using Optum G2 to determine the first response to compression, i.e. at the first increment of shortening. These calculations provide the displacement and stress fields that are optimal with respect to the compressive force. Next, we use SLAMTec, to follow the evolution of deformation up to 1 km of shortening and thus estimate whether the onset of deformation detected by Optum G2 is long-lived or only transient. The choice of 1 km corresponds to 1 mm/a over 1 Ma, i.e. the average shortening velocity in the Jura during the peak phase of its formation. A parametric analysis of the decollement layer reveals the main types of distribution of deformation that can be expected. In section 4 we perform the same analysis for the six remaining cross sections and we draw a map of the deformation limits by interpolation of results obtained with cross sections. Section 5 opens the analyses to the hypothesis of thick-skin tectonics. The cross section 13 is extended southward to the central Alps and the pushing wall reaches the lower-upper crust limit. This allows us to discuss the relevance of the thin-skin assumption and to propose richer kinematic scenarios involving the reactivation of pre-existing basement normal faults.

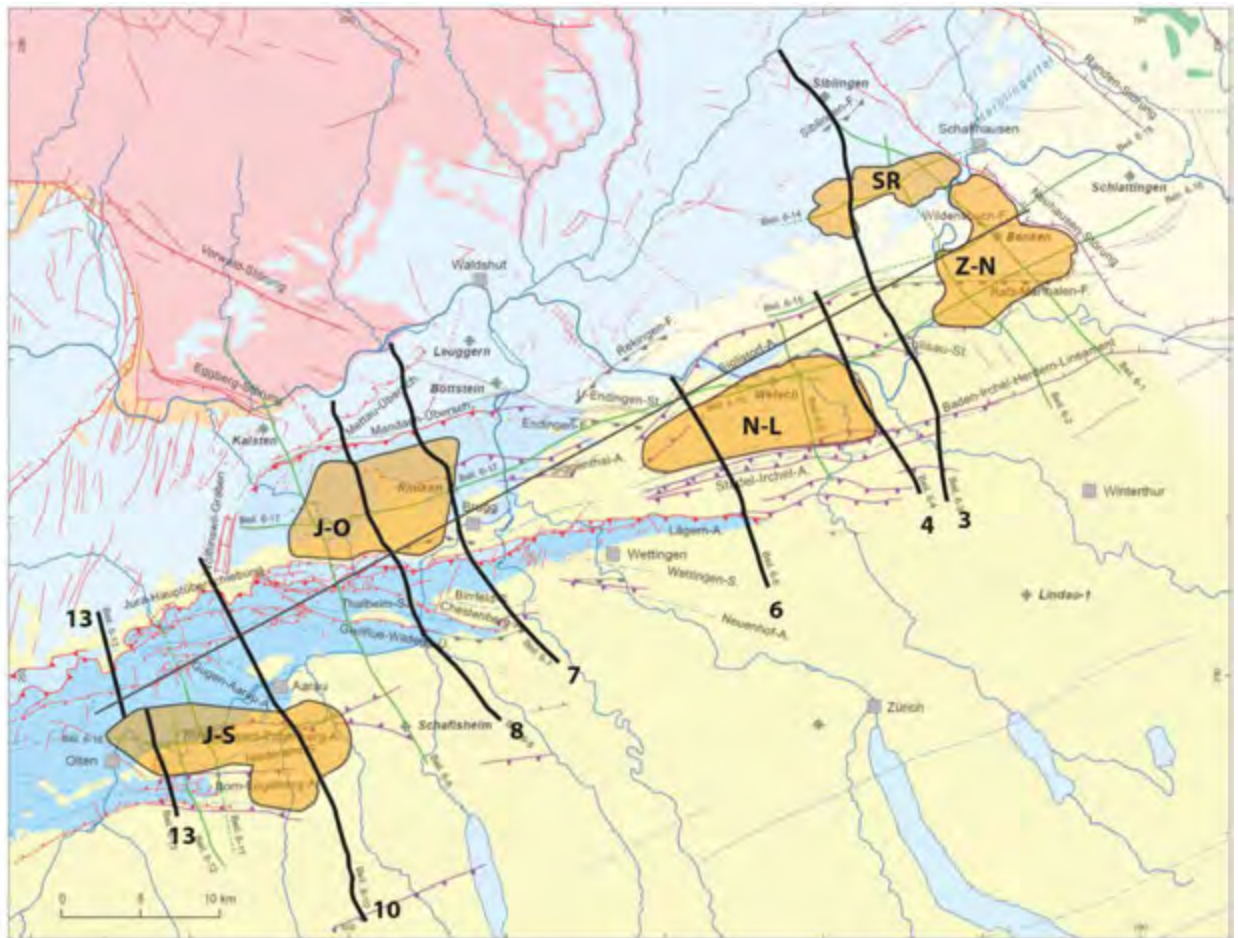
2 The seven selected cross sections

The seven selected cross sections studied in this report have been chosen in order to cut through the different regions of potential radioactive waste siting. We selected two cross sections per region for the three westernmost potential siting regions (cross sections 4, 6, 7, 8, 10 and 13 (the correspondences with the real names of the seismic lines are given in Figure 2—1) and one cross section through the easternmost (cross section 3) which is located in an area weakly deformed by the compressive Alpine deformation responsible for the Jura folds (Figure 2—2). The oriental end of the folded Jura is located above a ENE-WSW trending Permo-Carboniferous graben easy to see on the interpreted seismic profiles (Figure 2—3). The normal faults bordering this graben constitute disruptions in the continuity of the Triassic decollement layer and explain why, in the seven cross sections most of the shortening is accumulated just above the southern normal fault of the Permo-Carboniferous graben (Figure 2—3 and Figure 2—4). The offsets of the decollement by the normal faults indeed represent hampering staircases in the propagation of the deformation. These catching points localized a ramp until the topographic load created is sufficient to block the ongoing deformation on this ramp allowing its propagation farther along the offset portion of the decollement level (T. Caer PhD, work in progress). On cross sections 3 and 4, small folds and thrusts are confined below the Swiss Tertiary Molasse, they belong to the “tabular Jura” zone (Figure 2—2 and Figure 2—3). In cross section 6 a fold clearly outcrops at the southern edge of the Permo-Carboniferous graben. Two other compressive structures develop above the centre and the northern edge of the graben but they accommodate small shortening (Figure 2—3). To the west, on cross section 7 and then 8 (Figure 2—4), several major structures are stacked above the southern border of the Permo-Carboniferous graben while the frontal structure is located above the northern border and shows small shortening (between 250 and 500 m according to Jordan et al., 2015, Tables 8-1 and 8-2). To the north we note the presence of a back thrust whose structure has undergone very significant erosion. This structure results from a gravitational instability, sliding southward because of the uplift of the basement in the black forest (Jordan et al., 2015). On cross section 10 and 13 the deformation front is localized above the southern border of the graben and is characterized by two or three major thrusts.

All these cross sections therefore present pre-existing structures more or less developed that can likely be reactivated in the future, threatening the safety of the siting regions.

Name of cross sections in this report	Corresponding seismic line
3	84-NF-65
4	91-NO-62
6	91-NO-58
7	83-NF-31/82-NF-30
8	83-NF-15
10	83-SE-12
13	12-NS-42

Figure 2—1: Correspondence table between the name of the cross sections in this report and the corresponding seismic line number in Jordan et al. (2015).



Geologische Standortgebiete für Tiefenlager

- HAA Gebiet
- SMA Gebiet

Regionale geologische Profile

- 2D-Seismiklinie
- Erweiterung
- Erweiterung entlang von Tunnelprofil

Auseralpine Plattform

- Miozäne Vulkanite des Hegaus
- Mittelländische Molasse
- Mesozoikum des Tafeljuras
- Perm
- Kristallin / Grundgebirge

Alpenvorland

- Abgescherte Molasse und Tertiär des Faltenjuras
- Mesozoikum der Vorfaltenzone
- Mesozoikum des Faltenjuras

Strukturen aus Oberflächengeologie

- Hauptabschiebungen
- Hauptüberschiebungen
- Weitere Überschiebungen
- Weitere Abschiebungen
- Weitere Störungen i. allg., z.T. vermutet
- Antiklinalen
- Synklinalen
- Flexuren

Strukturen aus Seismikinterpretation

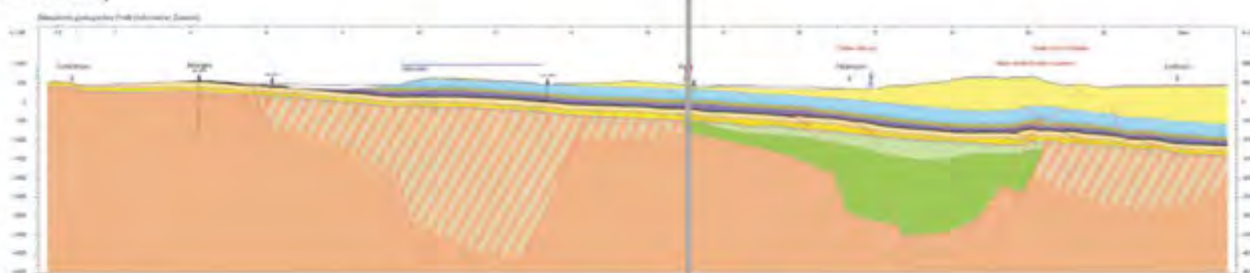
- Hauptabschiebungen
- Hauptüberschiebungen
- Weitere Abschiebungen
- Weitere Überschiebungen
- Front der seismisch kartierbaren Fernschubtektonik

Important features for this report

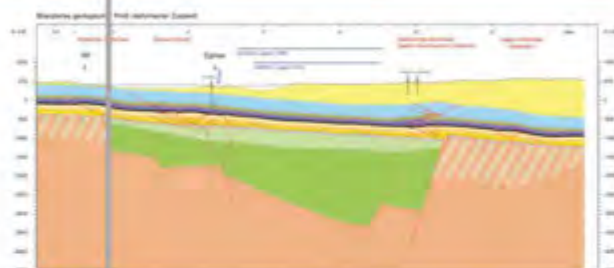
- Areas studied for radioactive waste disposal
J-S : Jura Südfuss; J-O : Jura Ost;
N-L : Nördlich Lägern; Z-N : Zürich Nordost
SR: Südranden
- 10** Cross sections studied in this report
- Reference line (Fig. 2)

Figure 2—2: Map of the seismic lines and of the cross sections of NAGRA (modified after Jordan et al., 2015). We here studied the seven cross sections labelled 3, 4, 6, 7, 8, 10 and 13.

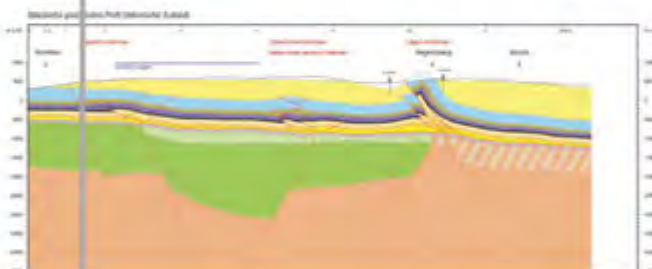
3. (84-NF-65)



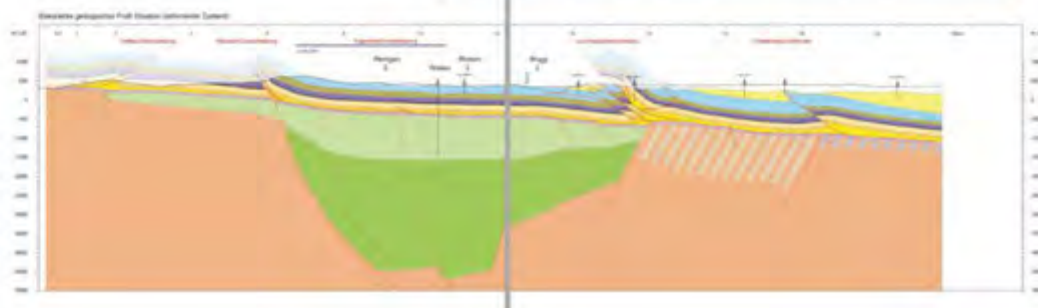
4. (91-NO-62)



6. (91-NO-58)



7. (83-NF-31/82-NF-30)



0 1 5 km

Figure 2—3: The seven cross sections of NAGRA studied in this report (continued in Figure 2—4)

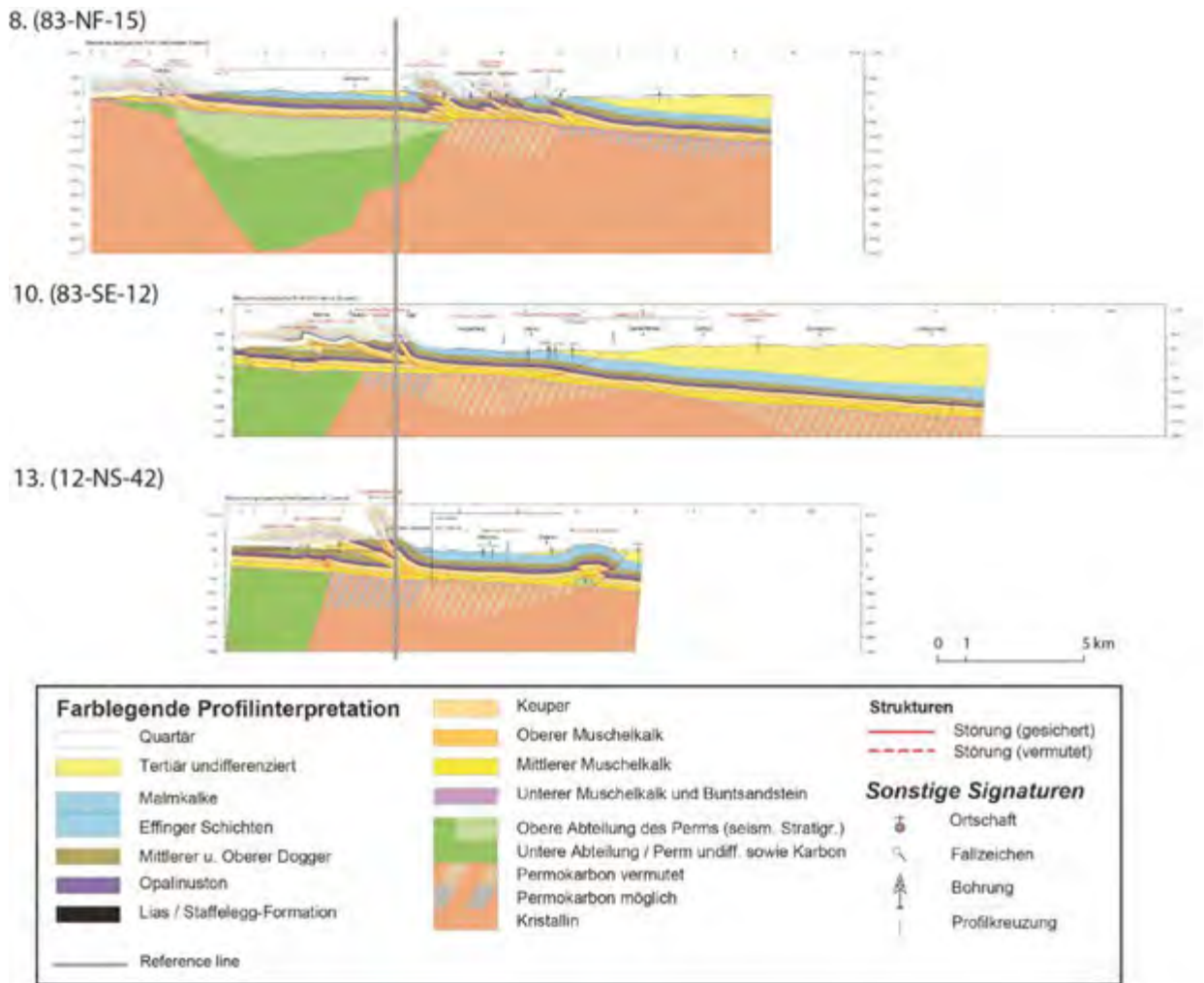


Figure 2—4: The seven cross sections of NAGRA studied in this report (continuation of Figure 2—5)

3 Method of analysis of a cross section

We have chosen the cross section nbr. 8 (Figure 2—4) to illustrate in detail the procedure of analysis because it contains the most complicated structures and will produce varied results in the parametric analysis that can be recognized in the other sections. Analyses of the seven other cross sections follow the same methodology and will be presented in section 4.

3.1 Principles and implementations of Limit Analysis

The following brief description of Limit Analysis is adapted from Caër et al. (2015). We follow a simplified mechanical approach originally developed in Civil Engineering and named Limit Analysis (Salençon, 2002). The kinematic approach of Limit Analysis consists in calculating an upper bound of the tectonic force Q associated to a given distribution of deformation, by accounting for mechanical equilibrium and for the maximum resistance of rocks, described by the Coulomb criterion (Figure 3—1). By upper bound, we mean that, although the tectonic force is unknown, its exact value cannot be above the upper bound. An optimization procedure then allows us to determine the distribution of deformation associated to the least upper bound. We use two numerical implementations of this general method. The first one is a commercial software called Optum G2 (Krabbenhøft and Lyamin, 2014) based on the theoretical and numerical developments of Krabbenhøft and Damkilde (2003), Krabbenhøft et al (2005), Lyamin et al (2005), Souloumiac et al (2009), Souloumiac et al (2010). Diffuse deformation and faulting is described by a spatial discretization with automatic mesh refinement as part of the optimization procedure. This is an implementation of classical Limit Analysis: only the onset of failure is detected and the subsequent evolution is not addressed. The second one is a semi analytical formulation whereby the deformation is restricted to a set of three planar faults in a uniform material: a planar decollement continued by a planar thrust ramp reaching the surface, and a shear plane that acts as a migrating hinge between material above the decollement and material in the thrust hanging wall). The optimization consists in finding the location and dips of the two latter faults, rooting at a common point on the decollement. Once determined, an increment of slip is applied on the optimal faults, and a new optimization is performed before applying the next slip increment. This procedure is known as Sequential Limit Analysis (Yang, 1993; Maillot and Leroy, 2006; Cubas et al, 2008) and used here with the software called SLAMTec (Mary, 2012; Mary et al, 2013a; Mary et al, 2013b). SLAMTec has the advantage to simulate the evolution of folding, but does not yet take into account former faults, non-planar decollements, or heterogeneous properties.

We mostly use Optum G2 which has the advantage of putting no constraints on the deformation field (apart from mesh discretization), including faults as true velocity discontinuities. Also, pre-existing faults and heterogeneity of the mechanical parameters are accounted for, allowing us to analyse our structural interpretations in detail. Optum G2 also performs the static approach of Limit Analysis which complements the kinematic approach by computing a lower bound of the tectonic force associated to a given distribution of stress (Figure 3—1). An optimization procedure yields the max lower bound (Lyamin et al, 2005). In order to estimate the lifetime of the failure geometries predicted by Optum G2, we use SLAMTec to simulate the potential evolution of deformation in some of the cross sections over 1000 m of applied shortening, corresponding to 10 Ma at 0.1 mm/a, or to 1 Ma at 1 mm/a. This investigation is done only in cases where both SLAMTec and Optum G2 predict the same geometry. Indeed, the simplifications assumed in SLAMTec are sometimes too strong and the results differ.

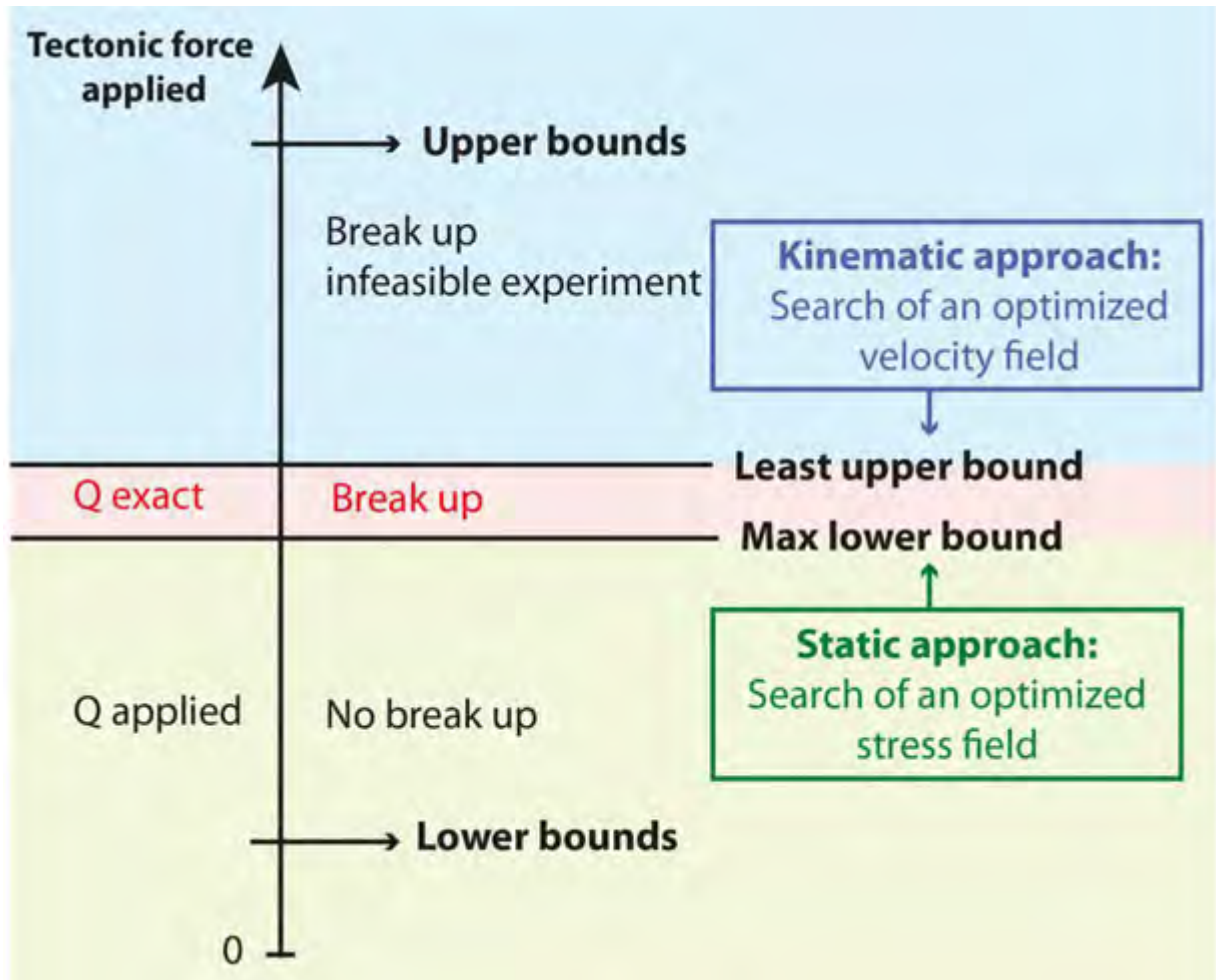


Figure 3—1: Principles of Limit Analysis. We use here extensively the kinematic approach to determine the failure geometries, i.e., zones of deformation and active faulting. For illustration, the internal approach is used to compute stress fields in cross section 8.

3.2 Attribution of mechanical properties to materials of the cross sections

In both softwares the necessary mechanical parameters includes the material density ρ and the Coulomb parameters (friction angle Φ_B and cohesion c_B) of each material. In SLAMTec, an additional friction angle Φ_{Rf} specifies the softened friction on any optimal thrust ramp after its first slip increment (Cubas et al, 2008), and the decollement has its own Coulomb parameters Φ_D, c_D . The ranges of values for these parameters (Figure 3—2), have been chosen in order to fit the rheology of the different layers according to the log presented in the Figure 2—2.1 of the report NAB 14-105. Besides, recall that SLAMTec can only consider a uniform material above the decollement.

3.2.1 Properties of the decollement level

In the Jura Mountains, the Triassic decollement is the middle Muschelkalk (Figure 3—2). It is composed of evaporites which have a rheology better approximated as a Newtonian fluid than as a frictional (Coulombian) solid. Because the layer is rather thin, sliding of material above it

must result in a Couette type flow where the top and bottom limits of the decollement layer remain parallel to each other, the top sliding past the bottom one. In that situation, it is possible to mimic the fluid resistance to sliding by specifying a particular cohesion in the decollement layer (c_D) and setting its friction angle (Φ_D) to zero (no dependence to pressure). In view of the cross sections, we estimate a mean thickness of the evaporite layer $e = 120$ m, and choose a viscosity $\nu = 10^{18}$ Pa.s, and a velocity of sliding $V = 0.5$ mm/a. Thus the shear stress at the base of the sliding body

$$\tau = \nu V / e = 0.13 \text{ MPa.} \quad (1)$$

For consistency with the Coulomb friction used in Limit Analysis, we must have

$$\tau = \tan \Phi_D \sigma_n + c_D = 0.13 \text{ MPa.} \quad (2)$$

Choosing $\Phi_D = 0$ and $c_D = \nu V / e = 0.13$ MPa ensures that we will properly describe the shear stress at the base of the sliding material. In the following analyses, we consider c_D in the range $[0 ; 2]$ MPa, i.e., a substantial range around the reference value in (1) to account for uncertainties on e , V and ν . This range of values encompasses for example variations of the thickness from, say, 10 m, up to 1000 m (keeping V and ν constant). Alternatively, choosing $V = 0.1$ mm/a, gives $c_D = 0.025$ MPa, a value within the range considered in the analyses. Φ_D in the range $[0 ; 12]$ keeps low values, but allows to scan a large range of parametric combinations.

Cross section 3 has a feature that we did not include here: the Muschelkalk changes of facies from the south, where it is made of evaporites, to the north where no evaporites are found.

3.2.2 Properties of the other layers

For the other layers, the friction angle and the cohesion stay fixed for all the experiments. In Optum G2 each layer has its own properties, the friction angle is considered to be 30° in limestones (Malm, Dogger), 25° in sandstones (Tertiary Molasse), 20° in marly-calcareous (Lias, Permo-Carboniferous) and 15° in diverse incompetent rocks (clays, or clays and evaporites mixture, i.e Aalenian, Keuper, Upper Muschelkalk and Bundsandstein). The friction on the faults is always 15° , excepted along faults segments that are in contact with one of the incompetent rocks listed above; in that case, the friction along the fault segment is lowered to 10° . To the faults segments in contact with the evaporites of the decollement layer in Optum G2, we confer the friction value of the evaporites, and zero cohesion. For each layer, the chosen cohesion is the smallest cohesion for which no cross section undergoes gravitational collapse according to Optum G2. We thus make sure that all prototypes are topographically stable. In SLAMTec we consider $\Phi_B = 30^\circ$ and we choose $c_B = 0.4$ MPa, the average the cohesion we put in the different layers in Optum G2.










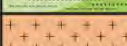

Rheology	Unit	Parameters in OptumG2				Parameters in SLAMTec				Common parameters
		Layer		Faults		Layer		Faults		
		$\Phi_B(^{\circ})$	$c_B(\text{MPa})$	$\Phi_f(^{\circ})$	$c_f(\text{MPa})$	$\Phi_B(^{\circ})$	$c_B(\text{MPa})$	$\Phi_f(^{\circ})$	$c_f(\text{MPa})$	
	Tertiary (Molasse)	25	0.5	15	0					
	Malm (undifferentiated)	30	0.6	15	0					
	Dogger	30	0.6	15	0	30	0.4	25	0	2300
	Aalenian (Opalinus clays formation)	15	0.1	10	0					
	Lias	20	0.1	15	0					
	Keuper (undiff.)	15	0.2	10	0					
	Upper Muschelkalk	15	0.5	10	0					
	Middle Muschelkalk	[0-12]	[0-2]	[0-12]	0	-	-	[0-12]	[0-2]	
	Lower Musch. and Buntsandstein	15	0.2	10	0					
	Permo-Carbon.	20	0	15	0	-	-	-	-	
	Kristaline basement	30	0	15	0					2700

Figure 3—2: Stratigraphic log, redrawn after Figure 2—2.1 of Jordan et al., 2015, and mechanical properties with ranges of values used for computations with Optum G2, and with SLAMTec. Note that faults are weaker than pristine materials in Optum G2 computations, while SLAMTec considers only uniform properties, except for the decollement which has its own, uniform, properties.

3.3 Response to compression in the current state (Optum G2 software)

3.3.1 Presentation of the prototype

We built our prototype by re-drawing the cross section nbr. 8 (Figure 2—4) in the Optum G2 interface and applying the selected rheological properties to each layer and to each fault as presented in Figure 3—2. Regarding the boundary conditions, the southern edge of the prototype is composed by a moving rigid wall from the surface to the middle of the decollement layer (i.e. the Middle Muschelkalk), on which we apply a horizontal compressive force (in cross sections 10 and 13 the force is applied perpendicular to the decollement which has a slight slope). The force distribution is such that the wall remains vertical. The other part of the southern wall and the northern wall are fixed, but vertical movements are allowed on the other parts of the vertical walls (both north and south). The base wall passing through the geological basement is fixed.

The experiments consist in looking on the effect of a variation of Φ_D and c_D on the geometry and the localization of the deformation. We thus realize a parametric study with the kinematic approach of the Limit Analysis in the Optum G2 software.

3.3.2 Results

The kinematic approach allows us to obtain results in terms of velocity fields. In this report the Optum G2 results will be only presented in terms of horizontal component of this velocity field (V_x) because it shows well the geometry and the localization of the deformation (Figure 3—3, b). The red areas undergo no movement (zero velocity) and the dark blue areas undergo the maximum velocity. The colour gradient in between thus corresponds to a velocity gradient. Recall that Optum G2 gives only the onset of the deformation.

In the case of cross section 8, we classified the results in five different types, by common zones of deformation front (Figure 3—3, b). A colour has been attributed to each type. The grey case is a particular case, in which Optum G2, before applying any compressive force on the back-wall, detects a gravitational movement in the Muschelkalk layer in the North of the cross section. In this area, the middle Muschelkalk reaches the surface, and the friction and cohesion are so low that the topography is not stable. The blue case is the other end-member where the deformation is restricted to the neighbourhood of the moving rigid wall. The three other colours each correspond to different locations of the deformation front: in red, the northernmost duplex is active, in orange, the central one is active, and in green, the southernmost ramp is active. The distribution of these types of results in the (Φ_D, c_D) space is presented in Figure 3—3, c. Only the boxes with a black spot have been calculated. The other boxes are filled by extrapolation of the calculated results towards higher c_D values.

The gravitational collapse corresponds to the very low values of Φ_D and c_D (grey areas), and for the high values of Φ_D it is impossible to activate the central structures, at least with the current topography. The three cases in between correspond respectively to an increasing mechanical resistance of the decollement, although the green case dominates largely the Φ_D, c_D space. Note that the use of only five colours is a simplification of the exact deformation fields. However, the transition between colours is indeed sharp, representing sharp changes of types of

deformation, especially for the green and blue end-member cases. The results of this cross section show that if no gravitational collapses are detected by Optum G2, the deformation localizes south of the Jura Ost siting region (orange, red, green and blue cases), which stays undeformed.

Optum G2 also allows to use the static approach of the Limit Analysis, and thus, to obtain the stress field. Figure 3—4 illustrates an optimum stress field. We have not dealt this type of results here, but that could be an interesting perspective to this work.

Cross section 8

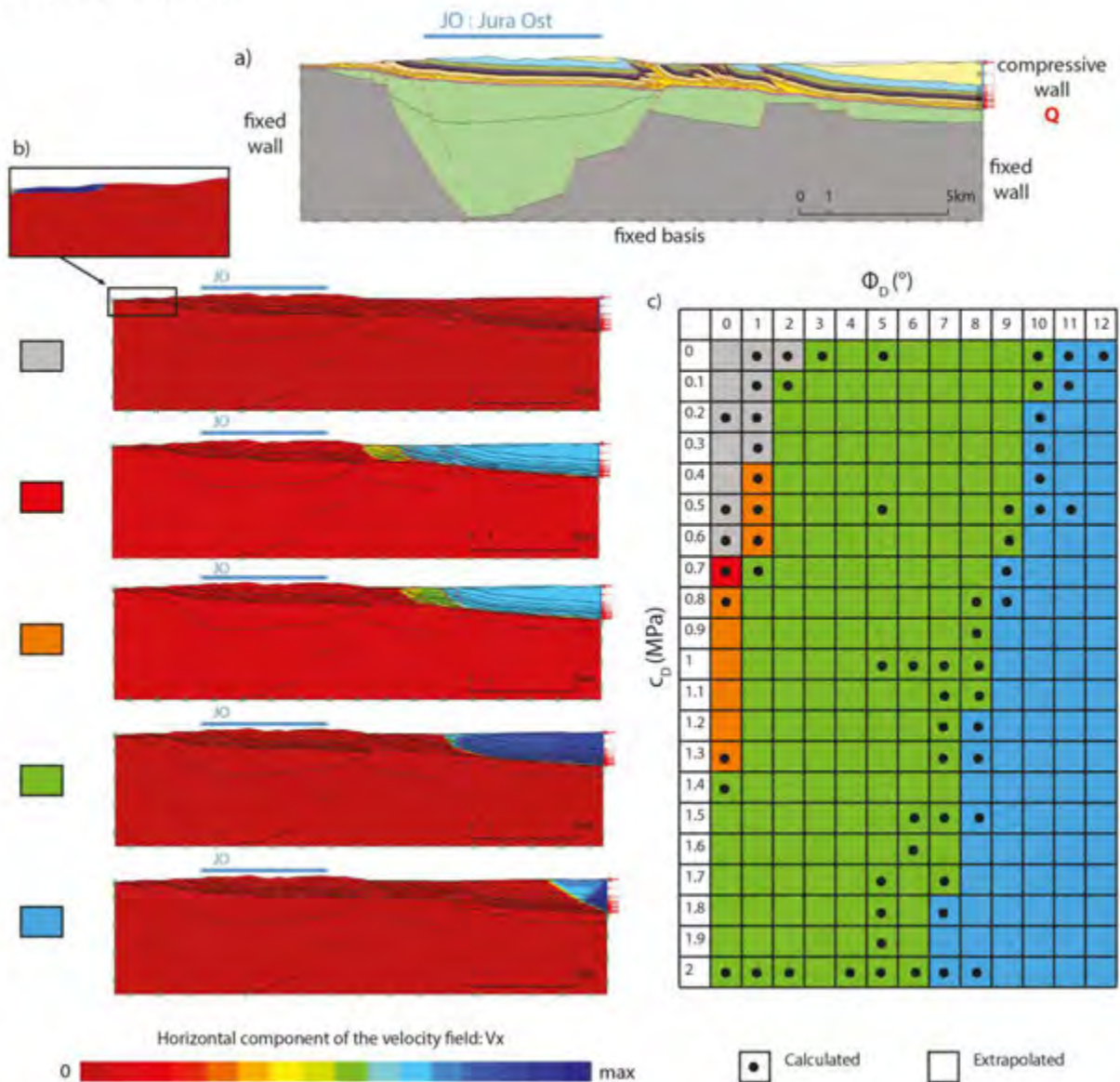


Figure 3—3: Prototype for Optum G2 for the cross section nbr. 8, a). Different typical results classified by common zones of deformation, colours are proportional to the horizontal component of the optimal virtual velocity field V_x , b). Distribution of zones of deformation in a space spanning the friction and cohesion values of the material of the decollement, c.). The Jura Ost siting region, crossed by the cross section is represented by a blue segment.

Cross section 8

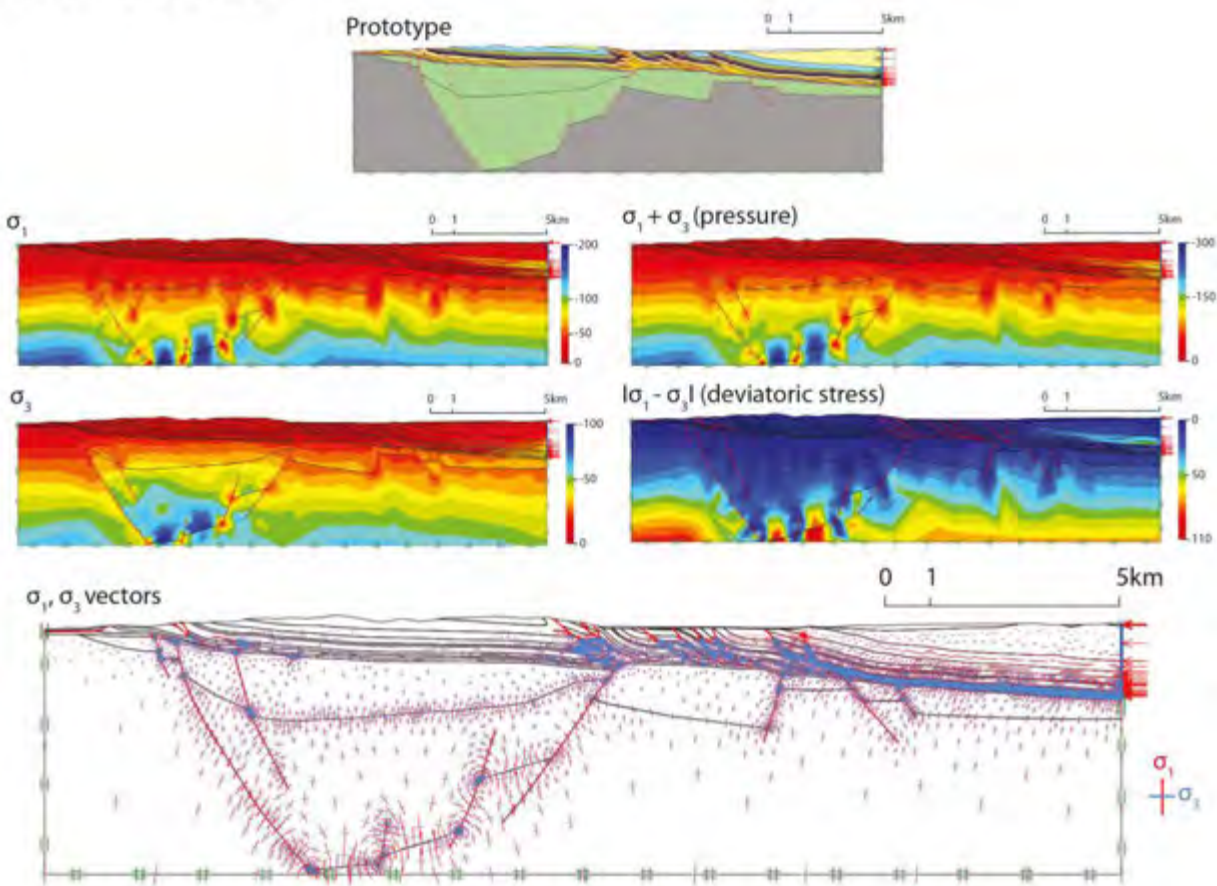


Figure 3—4: Prototype for Optum G2 for the cross section nbr. 8. The static approach of Limit Analysis determines a lower bound to the unknown tectonic force by optimising a statically admissible stress field. This optimal field is shown here. Units are MPa σ_1 and σ_3 are respectively the maximum and minimum principal stress.

3.4 Evolution in the near future (SLAMTec software)

3.4.1 Presentation of the prototype

Recall that in SLAMTec the geometry of the prototype cannot consider as much complexities that the one in OptumG2, it is composed of one planar decollement tilted at an angle β underlying a homogeneous sedimentary body, no pre-existing faults, no interruption in the decollement (Figure 3—5, a). The decollement is drawn by estimating a linear average of the disrupted and non-planar real decollement. The topography is the real topography of the cross section. For each cross section we add a super-critical prism in the back (south) to assure that the deformation will not reach the rigid back wall.

The experiment consists in looking at the effect of Φ_D and c_D on the localization and the evolution of a geological structure, through a parametric study with the sequential Limit Analysis software, SLAMTec. The prototype in SLAMTec is more simplified than in Optum G2, and this may lead to different results; so the aim is to select the cases in which the first deformation is at

the same location as in Optum G2 and to note how long this structure is actively deforming before the deformation jumps to another location. By the term “same location” we mean that SLAMTec produces a result that would have the same colour as the Optum G2 result, i.e., belongs to the same type of deformation. The actual active fault may not be exactly at the same place, because in Optum G2, the location depends on the topography and the local weak zones (layers or faults), but in SLAMTec, the location depends only on the topography since the sedimentary body is homogeneous.

3.4.2 Results

After the run, SLAMTec produces two output types: a movie that shows the evolution of the deformation, from which we extracted a few steps, (Figure 3—5) and a graph, called “G-gram” of the position of the root of the ramp on the decollement (point G) and of the surface outcrop of the ramp and its associated shear plane (Figure 3—5, c, black dots and blue curves respectively), throughout the shortening.

Based on Figure 3—5b and c, we note that, at first glance, the deformation location changes suddenly toward 880 m of shortening, but if we take a closer look to the G-gram, we realize that toward 380 m of shortening, a second ramp develops, accommodates very low shortening (10m) and is then abandoned for several hundred meters of shortening, before being reactivated. Such short transient events occur often in SLAMTec and are interpreted as diffuse deformation rather than nucleation of a new fault. Therefore, in SLAMTec, the first ramp nucleates at the same position that the one of the green type of OptumG2 results, and is followed by a southward retreat of deformation, i.e an evolution from green to blue deformation types (Figure 3—3, c).

Cross section 8
 $\Phi_D = 8^\circ, c_D = 0.5\text{MPa}$

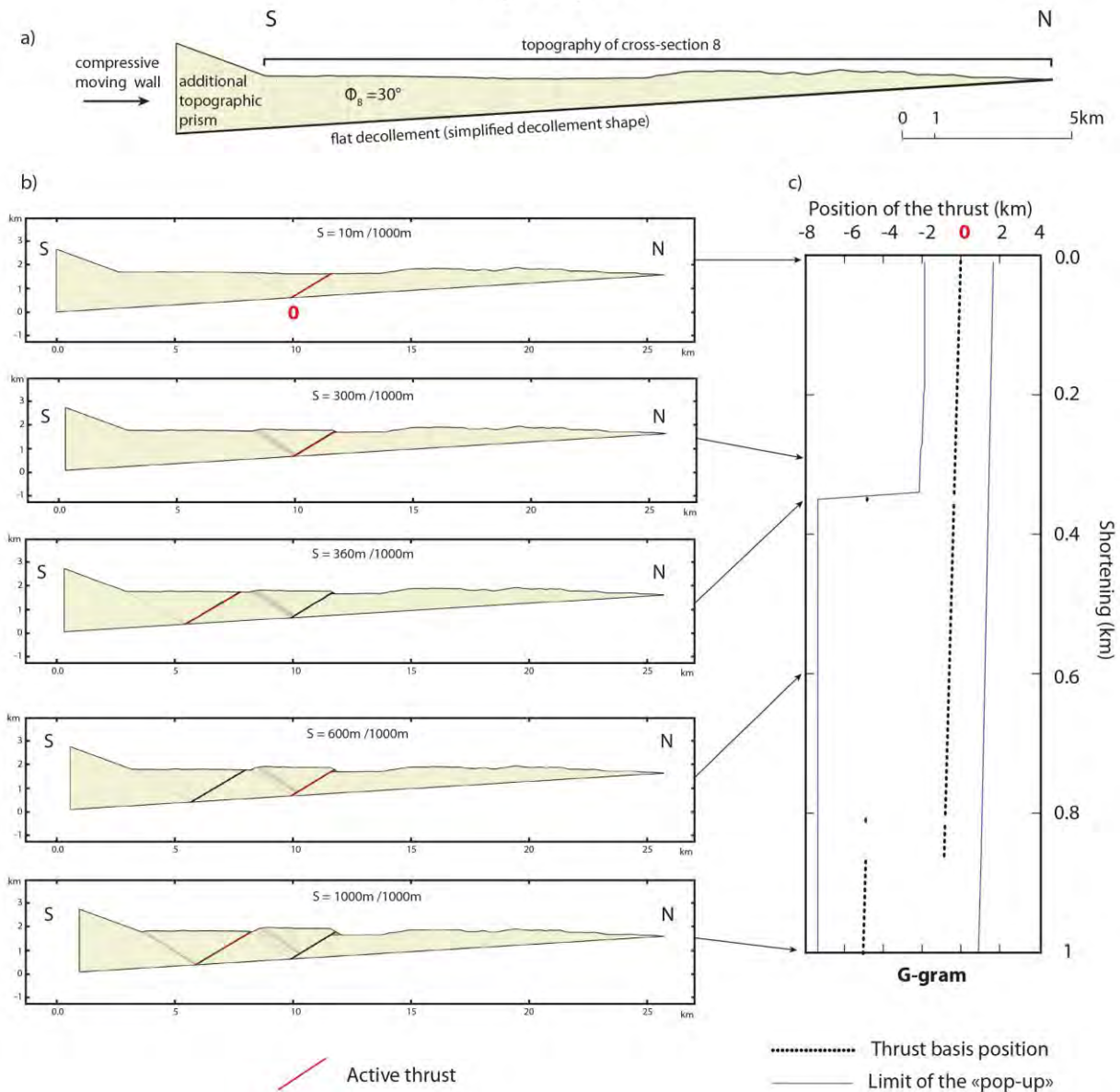


Figure 3—5: Prototype for SLAMTEC for the cross section nbr. 8, at zero shortening (current situation) a), then at successive steps of shortening up to 1000 m in b). G-gram presenting the position of the roots of the thrust and the width of the deformed area during shortening, c). We can remark that the second ramp develops southward of the first one. A first activation of this second ramp occurs at 360m of shortening, then the first ramp becomes active again and after several hundred meters of shortening accommodated on it, the second ramp becomes active again.

4 Results for all seven cross sections

4.1 Description

We used the same methodology described previously to study all seven cross sections. A synthesis of the results of each cross section is presented into Figure 4—. For each cross section we present the prototype used in Optum G2, the different types of results obtained, classified by common zone of deformation front, and the graph showing the distribution of these results according to Φ_D and c_D . For each type of results for which we found a similar solution with SLAMTec, we select a specific case (Φ_D, c_D) and we present the evolution of the structure for the next 1km of shortening. The stability of the first structure that develops in the cross section can be assessed by looking at the S_{min} value. The S value is defined as the displacement accommodated on the first active thrust ramp before another ramp or diffuse deformation takes over. The S_{min} value is the minimum value of S among all the tested parameters. For all cross sections, in light grey and dark grey cases Optum G2 detects movements inside the Muschelkalk layer, before applying any compressive force on the backwall (to Figure 4—). The friction Φ_D and the cohesion c_D of this layer, are too low to maintain the sedimentary prism stable. For light grey cases it results in a gravitational collapse inside a Muschelkalk outcrop (Figure 4—1, Figure 4—4, , Figure 4— and Figure 4—, Figure 4—7), and for dark grey cases, the cross section does not contain Muschelkalk outcrops and thus it results in a global instability of the prototype (Figure 4—2 and Figure 4—). Note finally that the blue cases (Figure 4—1 to Figure 4—), where the deformation is close to the pushing wall, represent either a physically acceptable solution (if the deformation does not touch the pushing wall), or a bias due to the presence of the rigid wall. In the latter case, the true solution would exhibit a deformation at or south of the pushing wall.

4.1.1 Cross section 3 (across Südranden siting region)

On cross section 3 the Permo-Carboniferous graben is divided in two parts. For the orange and yellow cases, a ramp nucleates at different locations North of the northern part of this graben (Figure 4—1, a). In the green case it emplaces between the two parts of the graben and for the blue case, the deformation stays south of the southern part of the graben (Figure 4—1 b, c). With SLAMTec we succeed in reproducing the yellow, green and blue cases. For the yellow case, the minimal shortening accommodated by the first emplaced structure is $S_{min} = 850$ m, for the green case, $S_{min} = 260$ m, and for the blue case, $S_{min} = 220$ m (Figure 4—1 b). Recall that the northern extent of the deformation front in section 3 is overestimated due to the fact that the Muschelkalk is considered to consist of evaporites all along the section. In fact the evaporites die out somewhere in the central part of the cross section. Therefore the orange and yellow cases are probably not realistic, due to the absence of evaporites in the north.

4.1.2 Cross section 4 (across Nördlich Lägern siting region)

In the red case of cross section 4, the deformation propagates until the north of the cross section, in the green case it reactivates a ramp located just above the northern edge of the Permo-Carboniferous graben, and in the blue case the structure located just above the southern edge of the deepest area of the graben is reactivated (Figure 4—2 b, c). With SLAMTec we succeed in reproducing the red, green and blue cases. For the red case, $S_{min} = 440$ m, for the

green case, $S_{min} = 400$ m, and for the blue case, $S_{min} = 440$ m (Figure 4—2 b).

4.1.3 Cross section 6 (across Nördlich Lägern siting region)

In the red case of cross section 6, the deformation propagates beyond the northern boundary of the cross section, as shown by the apparent back thrust (only due to boundary effects) (b). This result is obtained only for ($\Phi_D = 0$, $c_D = 0.1$ MPa) (c). In all the other situations tested, the structure located above the southern edge of the deepest part of the graben is reactivated (green case). For this cross section, the result is quite clear, if the friction and the cohesion are enough to maintain the current topography stable, then the first deformation is almost sure to occur as in the green case. With SLAMTec we succeed in reproducing the green case, and we found that $S_{min} = 330$ m (b).

4.1.4 Cross section 7 (across Jura Ost siting region)

In the green case of cross section 7, the pre-existing structures stacked above the southern edge of the deepest part of the graben are reactivated, and in the blue case, the ramp located above the extreme southern edge of the graben is reactivated (Figure 4— b, c). The deformation never propagates across the Permo-Carboniferous graben. With SLAMTec we succeed in reproducing the green and the blue cases. For the green case, $S_{min} = 780$ m and for the blue case, $S_{min} = 190$ m (Figure 4— b).

4.1.5 Cross section 8 (across Jura Ost siting region)

Results were presented in chapters 3.3 and 3.4. We list it here again for completeness. On cross section 8 several major structures are stacked above the southern border of the Permo-Carboniferous graben (Figure 2—4, a); the red, orange and green cases correspond to the reactivation of these structures (b, c). In the blue case the deformation localizes completely south of the cross section. With SLAMTec we succeed in reproducing the green and the blue cases. For the green case, $S_{min} = 330$ m, and for the blue case, $S_{min} = 410$ m (b).

4.1.6 Cross section 10 (across Jura Südfuss siting region)

In cross section 10, the deformation propagates up to the pre-existing backthrust located in the centre of the cross section (green case), but never further north to reactivate the different thrust stacked above the southern edge of the main Permo-Carboniferous graben of the region (Figure 4—6). If the Φ_D and c_D are high, the deformation remains localized completely in the south of the cross section (blue case). With SLAMTec we don't succeed in reproducing any case. This is probably due to the strong curvature of the decollement, which when simplified to a plane does not provide a solution compatible with observation.

4.1.7 Cross section 13 (across Jura Südfuss siting region)

In cross section 13, the thrusts stacked above the southern edge of the main Permo-Carboniferous graben of the region can be reactivated but only for $\Phi_D = 0^\circ$ and $c_D > 0.9$ MPa (red cases) (Figure 4—7). For $\Phi_D < 2^\circ$, the deformation localizes in the large syncline between the two main pre-existing zones of deformation. And if $\Phi_D \geq 2^\circ$, the deformation affects the anticline pre-existing in the south of the cross section. With SLAMTec we don't succeed in reproducing any case, probably for the same reason as for cross section 10, or due to pre-

existing weaknesses (stacked ramps) that are not accounted for in SLAMTec.

4.1.8 Maps of results

On Figure 4—8, Figure 4—9 and Figure 4—10, we insert the different deformation zones obtained with Optum G2 on the map of the area, and we interpolate the results between the cross sections in order to assess the position and the shape of the deformation front for all the friction values ($\Phi_D = [0-12]^\circ$). Results are shown for the three cohesion values $c_D = [0.01; 0.1; 1]$ MPa. Recall that these three values of cohesion correspond to $\nu = 10^{16}$; respectively, 10^{18} Pa.s, with $e = 120$ m and $V = 0.5$ mm/a (section Attribution of mechanical properties to materials of the cross sections). Note that the results are indicated only when a deformation front is defined, i.e., when the overall cross section is gravitationally stable. For very weak decollement ($c_D = 0$ MPa, $\Phi_D = 0^\circ$), all cross sections are unstable and collapse. For such a case, no map was constructed.

4.2 Comments on the results

The first interesting result is that the lowest S_{min} is 190 m, obtained for ($\Phi_D = 4^\circ$, $c_D = 1$ MPa) on the cross section 7 (Jura Ost). This shows that the first structures predicted by Optum G2 and SLAMTec are relatively stable in time (1.9 Ma if we consider a shortening rate of 0.1 mm/a, or 190 ka for 1 mm/a). The different maps show that the Jura-Ost siting region will never be reached by the deformation front in a future compressive regime. The Zürich Nordost and Südranden siting region appear also be rather isolated from the different deformation fronts. The Jura Ost siting region is located just above the Permo-Carboniferous graben, and the deformation is always blocked at the southern edge of this graben. However we can see on cross sections 7 and 8 that in the past the deformation reached the northern edge of the graben. That means that this structure is not the youngest one to have been active and has been emplaced when the topography of the Jura folds was not too high compared to the topography of the Molasse basin, to represent a “catching point” of the propagation of the deformation.

This siting region could even so be attained by deformation if we are in the cases for which Optum G2 detects gravitational collapses (light and dark grey cases of all the cross sections). In these cases, Φ_D and c_D are too low to maintain the current topography of the sedimentary prism of the cross sections. Even before applying a compressive force, Optum G2 detects that the prototype is not stable, and thus, stops, giving no information on the tectonic deformation that will emplace with the compressive action. The friction and the cohesion being very low in these cases, it is likely that the deformation would propagate up to the siting region. GPS measurements could answer this problem. If no topographic collapses are detected, the deformation front will remain south of the siting region for any shortening below S_{min} . If topographic collapses are detected, we cannot determine whether or not the deformation front will affect the siting region. The results obtained from Optum G2 have been classified by common zones of deformation fronts. It is important to keep in mind that in the back of this deformation front, the sedimentary prism cannot be considered to be in rigid translation. Indeed, in some cases, a structure is reactivated southward of the frontal current thrust and accommodates substantial shortening (for example the green case presented on cross section 7, Figure 4—3). In other cases, although only the frontal current thrust is active, some diffuse deformation could occur south of it.

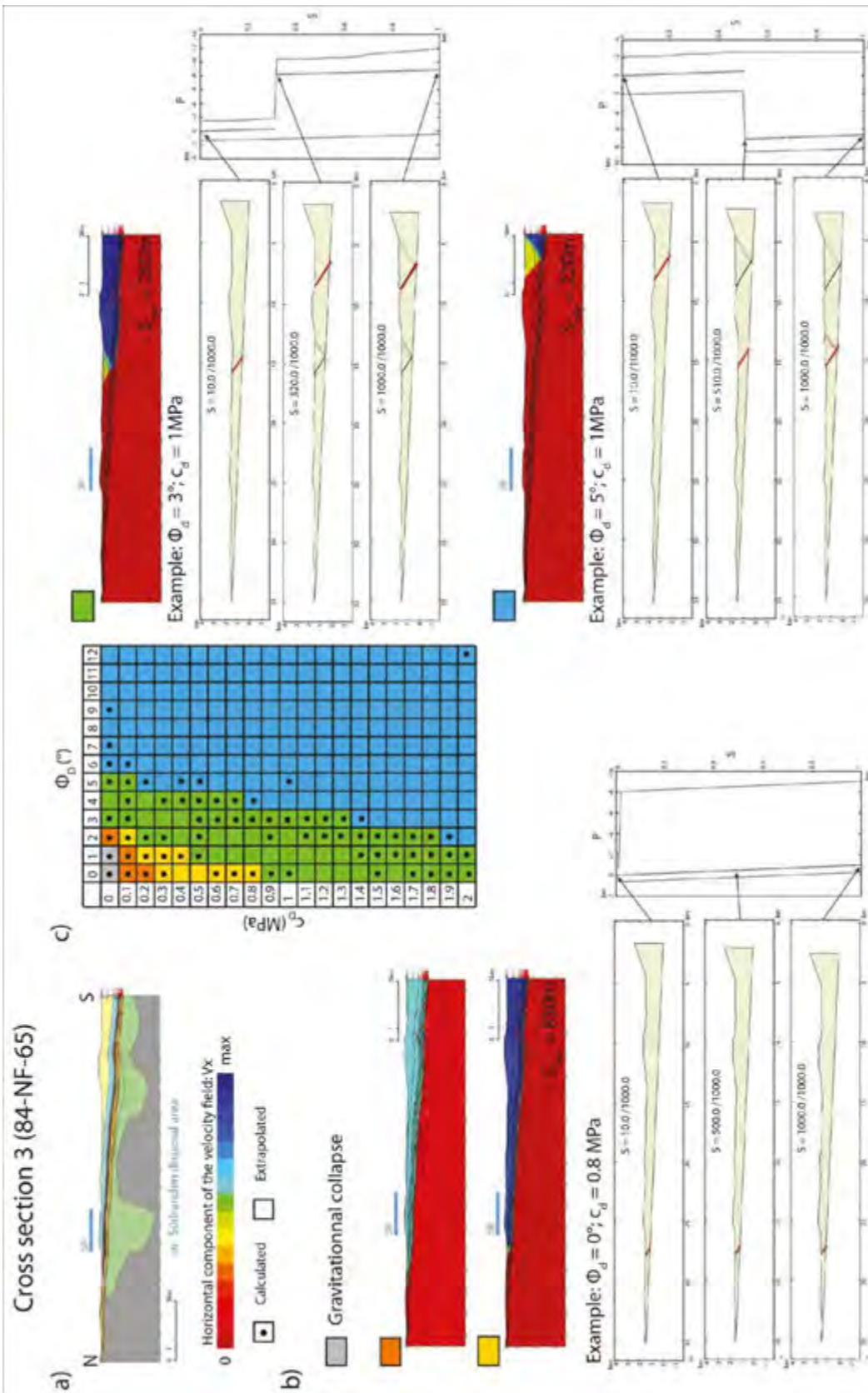


Figure 4—1: Prototype for Optum G2 for the cross section nbr. 3 and legend, a). Different typical results classified by common zones of deformation, and extrapolations of deformation using SLAMTec for selected results, b). Distribution of zones of deformation in a space spanning the friction and cohesion values of the material of the decollement, c). The Südanden siting region crossed by the cross section is represented by a blue segment.

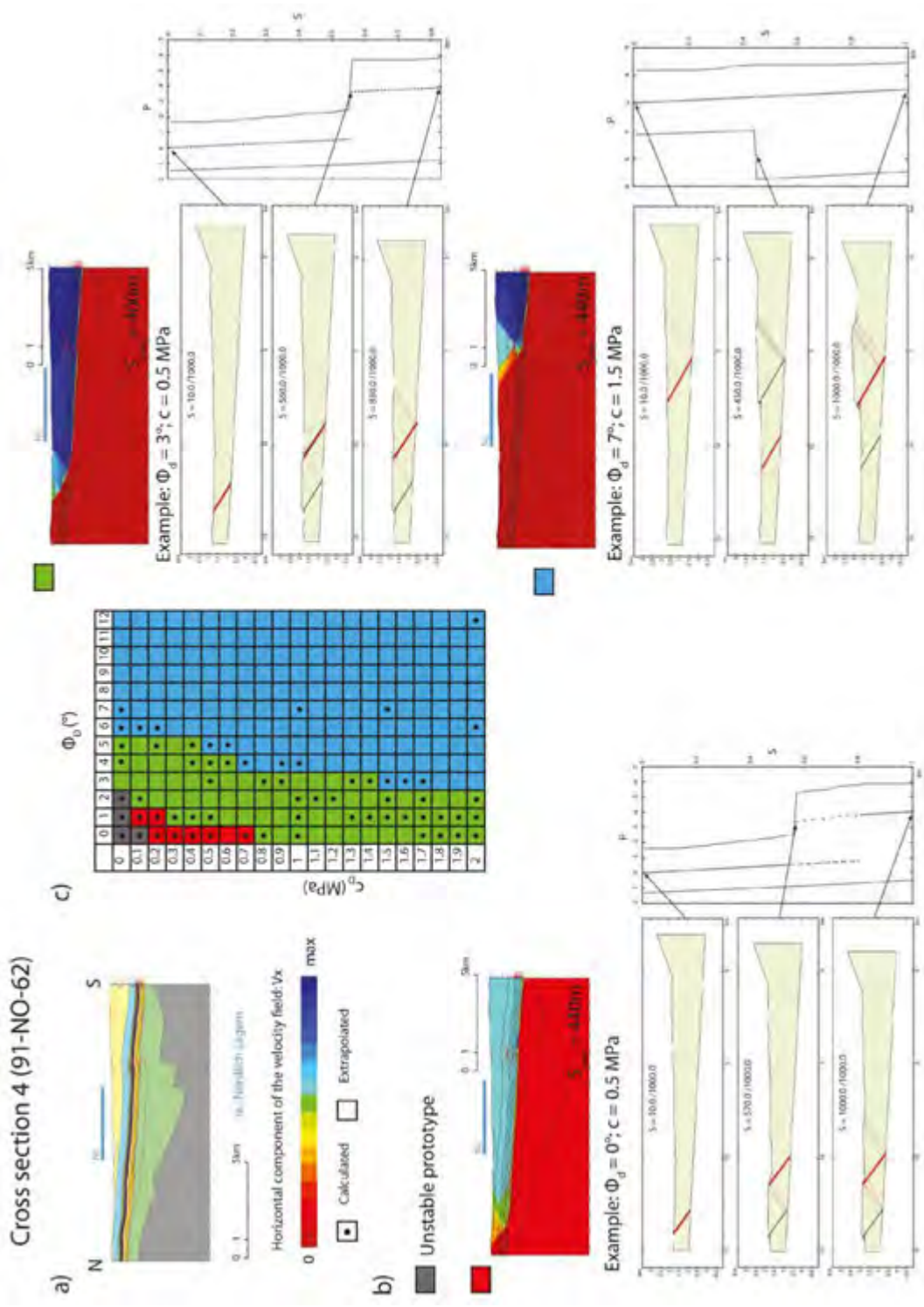


Figure 4—2: Prototype for Optum G2 for the cross section nbr. 4 and legend, a). Different typical results classified by common zones of deformation, and extrapolations of deformation using SLAMTec for selected results, b). Distribution of zones of deformation in a space spanning the friction and cohesion values of the material of the decollement, c). The Nördlich Lägern sitting region crossed by the cross section is represented by a blue segment.

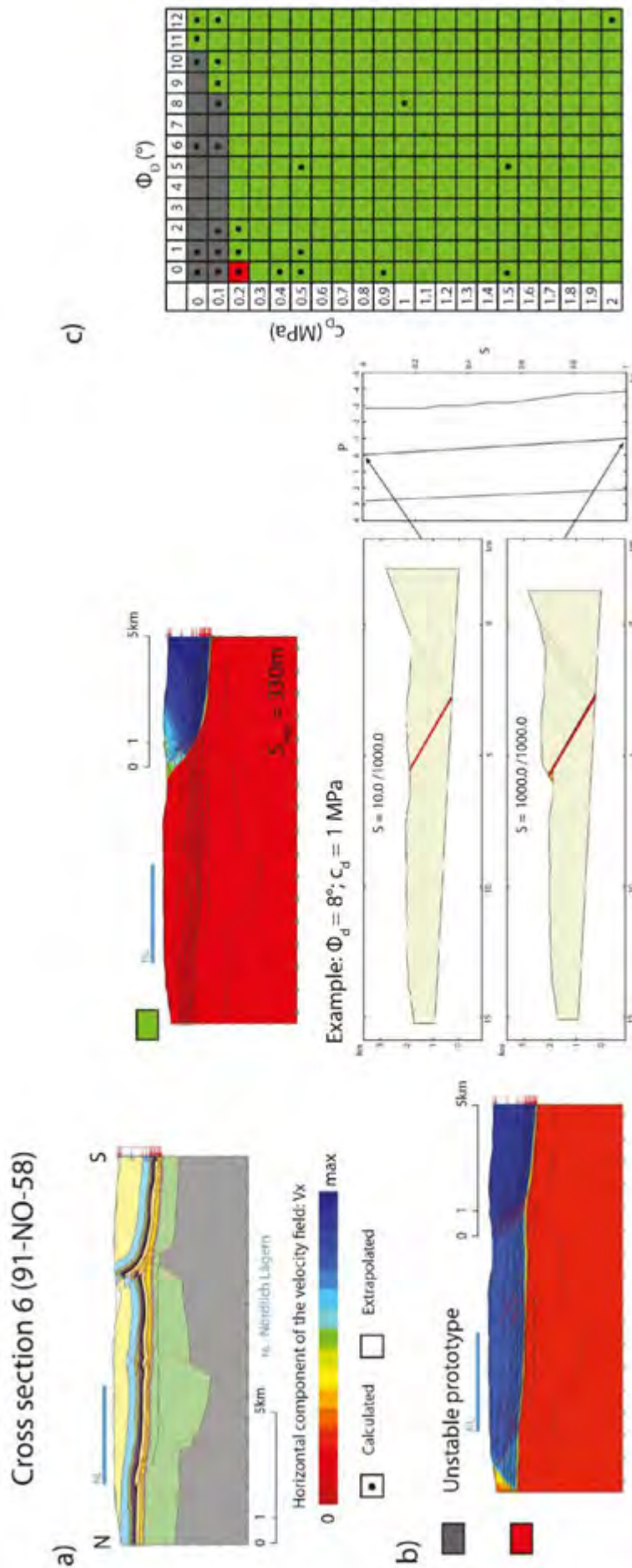


Figure 4—3: Prototype for Optimum G2 for the cross section nbr. 6 and legend, a). Different typical results classified by common zones of deformation, and extrapolations of deformation using SLAMTec for selected results, b). Distribution of zones of deformation in a space spanning the friction and cohesion values of the material of the decollement, c). The Nördlich Lägern siting region crossed by the cross section is represented by a blue segment.

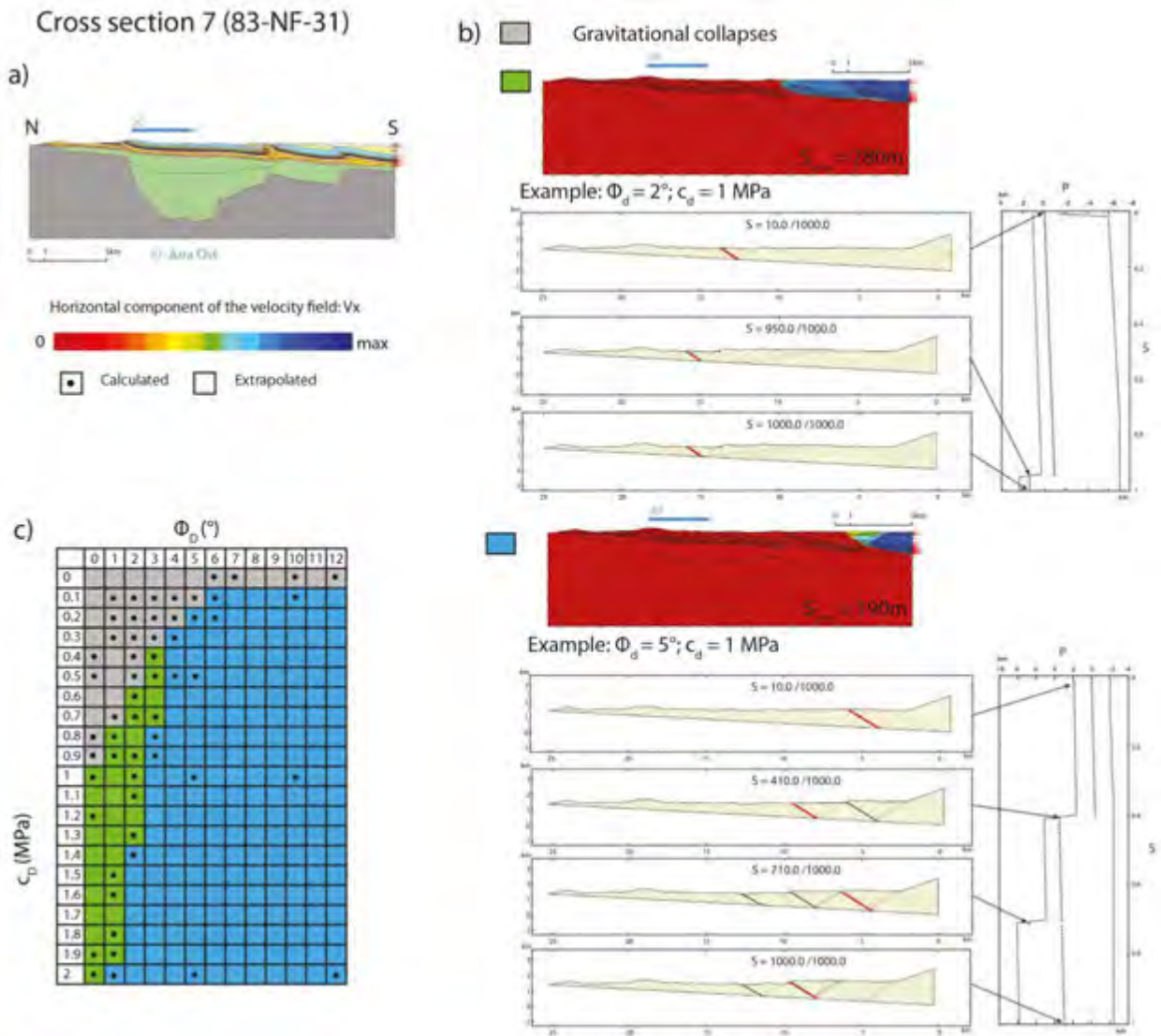


Figure 4—4: Prototype for Optum G2 for the cross section nbr. 7 and legend, a). Different typical results classified by common zones of deformation, and extrapolations of deformation using SLAMTec for selected results, b). Distribution of zones of deformation in a space spanning the friction and cohesion values of the material of the decollement, c). The Jura Ost siting region crossed by the cross section is represented by a blue segment.

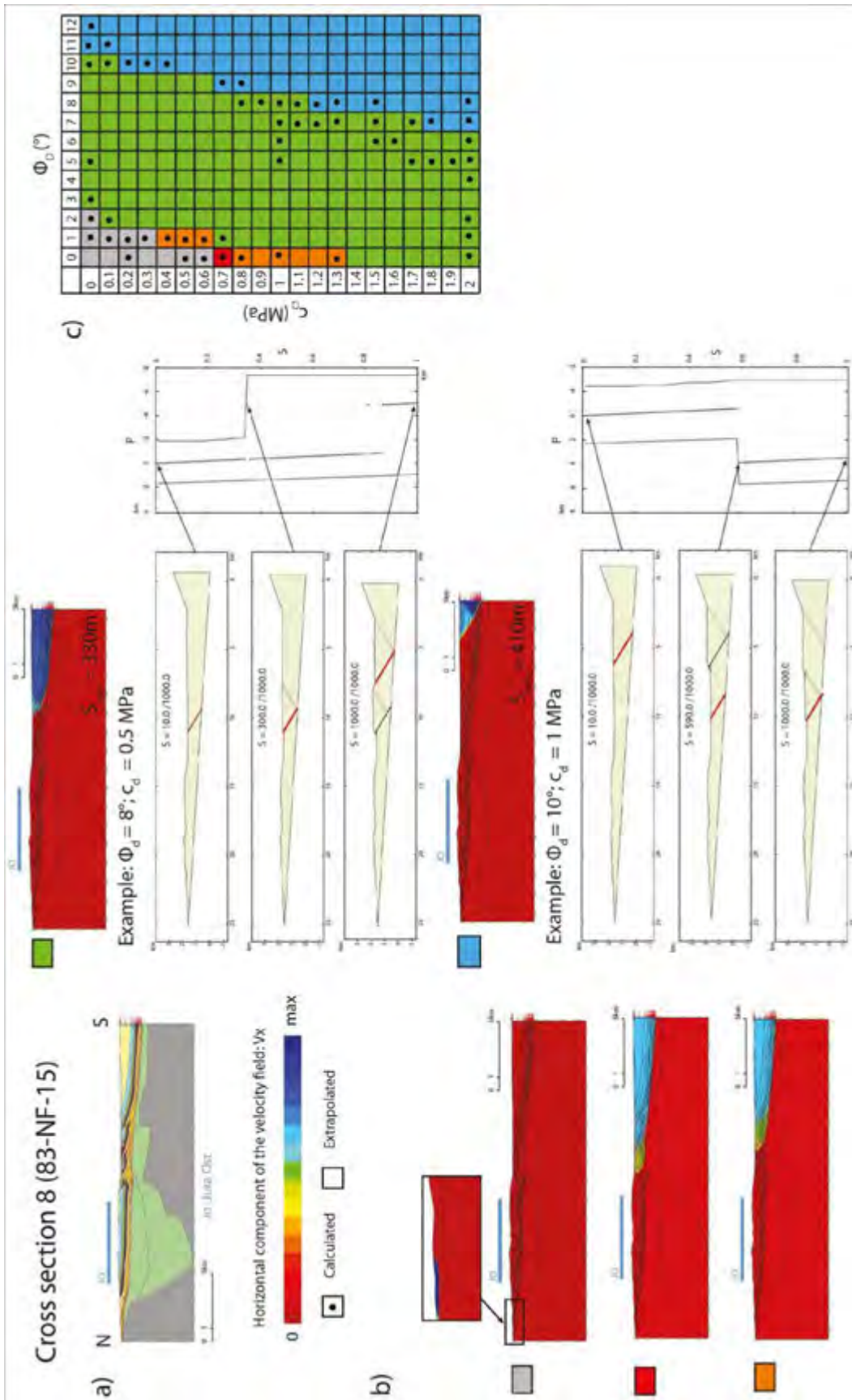


Figure 4—5: Prototype for Optum G2 for the cross section nbr. 8 and legend, a). Different typical results classified by common zones of deformation, and extrapolations of deformation using SLAMTec for selected results, b). Distribution of zones of deformation in a space spanning the friction and cohesion values of the material of the decollement, c). The Jura Ost siting region crossed by the cross section is represented by a blue segment.

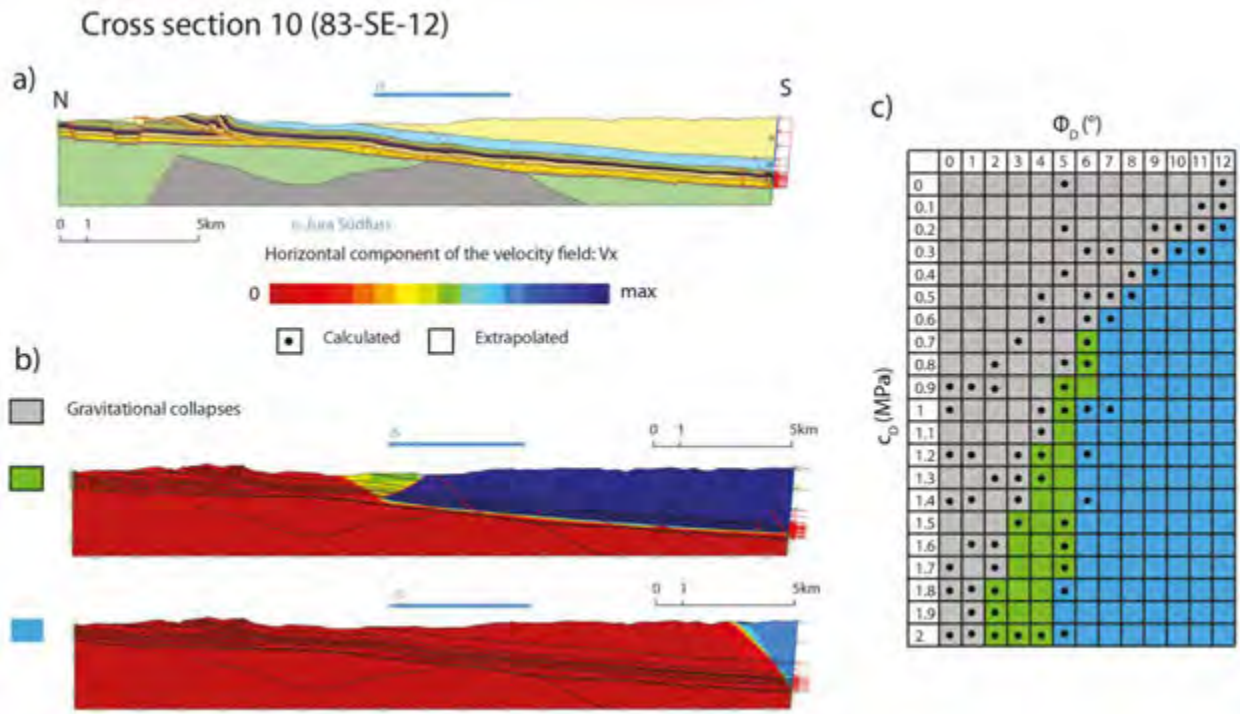


Figure 4—6: Prototype for Optum G2 for the cross section nbr. 10 and legend, a). Different typical results classified by common zones of deformation, b). Distribution of zones of deformation in a space spanning the friction and cohesion values of the material of the decollement, c). The Jura Südfuss siting region crossed by the cross section is represented by a blue segment.

Cross section 13 (12-NS-42)

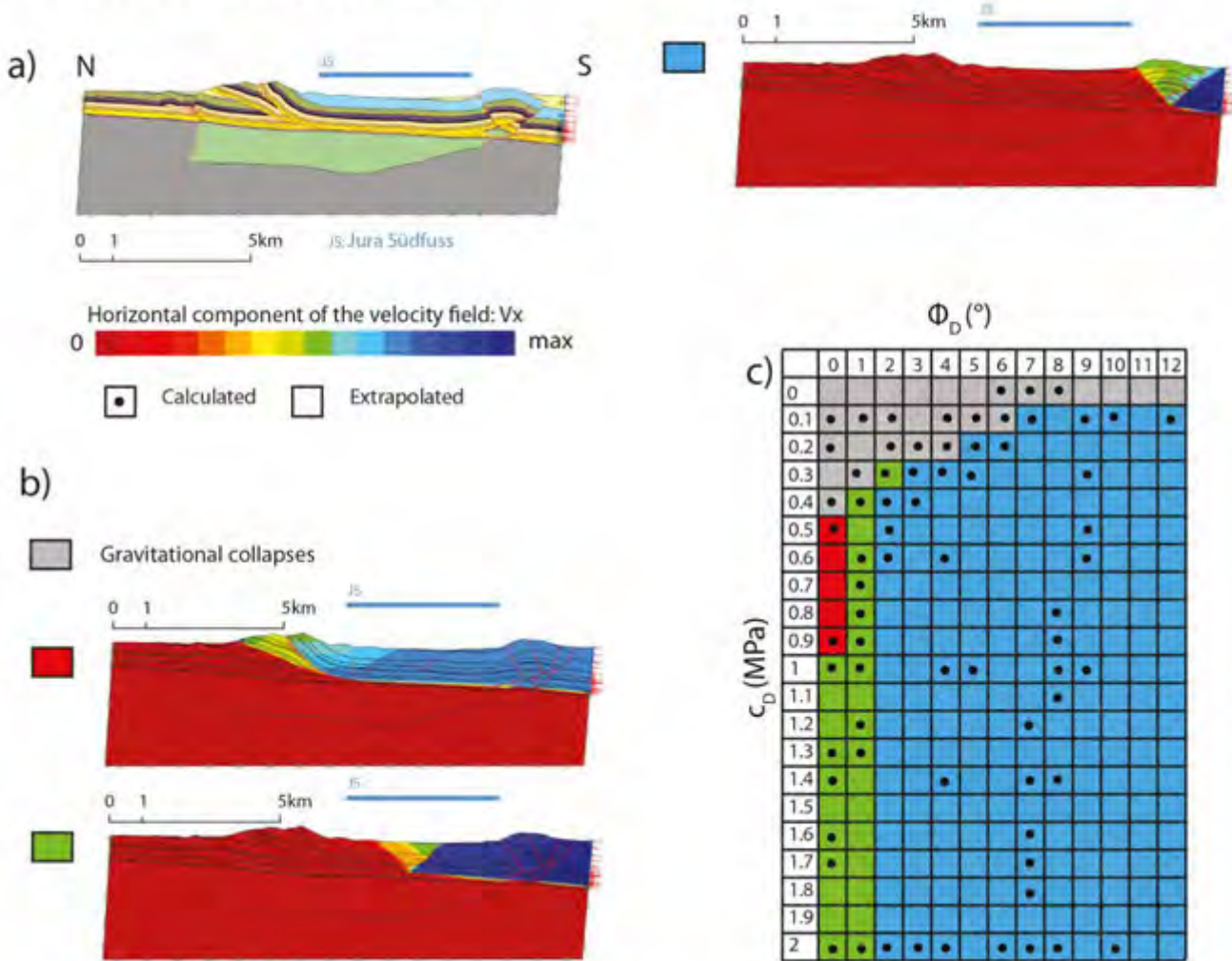


Figure 4—7: Prototype for Optum G2 for the cross section nbr. 13 and legend, a). Different typical results classified by common zones of deformation, b). Distribution of zones of deformation in a space spanning the friction and cohesion values of the material of the decollement, c). The Jura Südfuss siting region crossed by the cross section is represented by a blue segment.

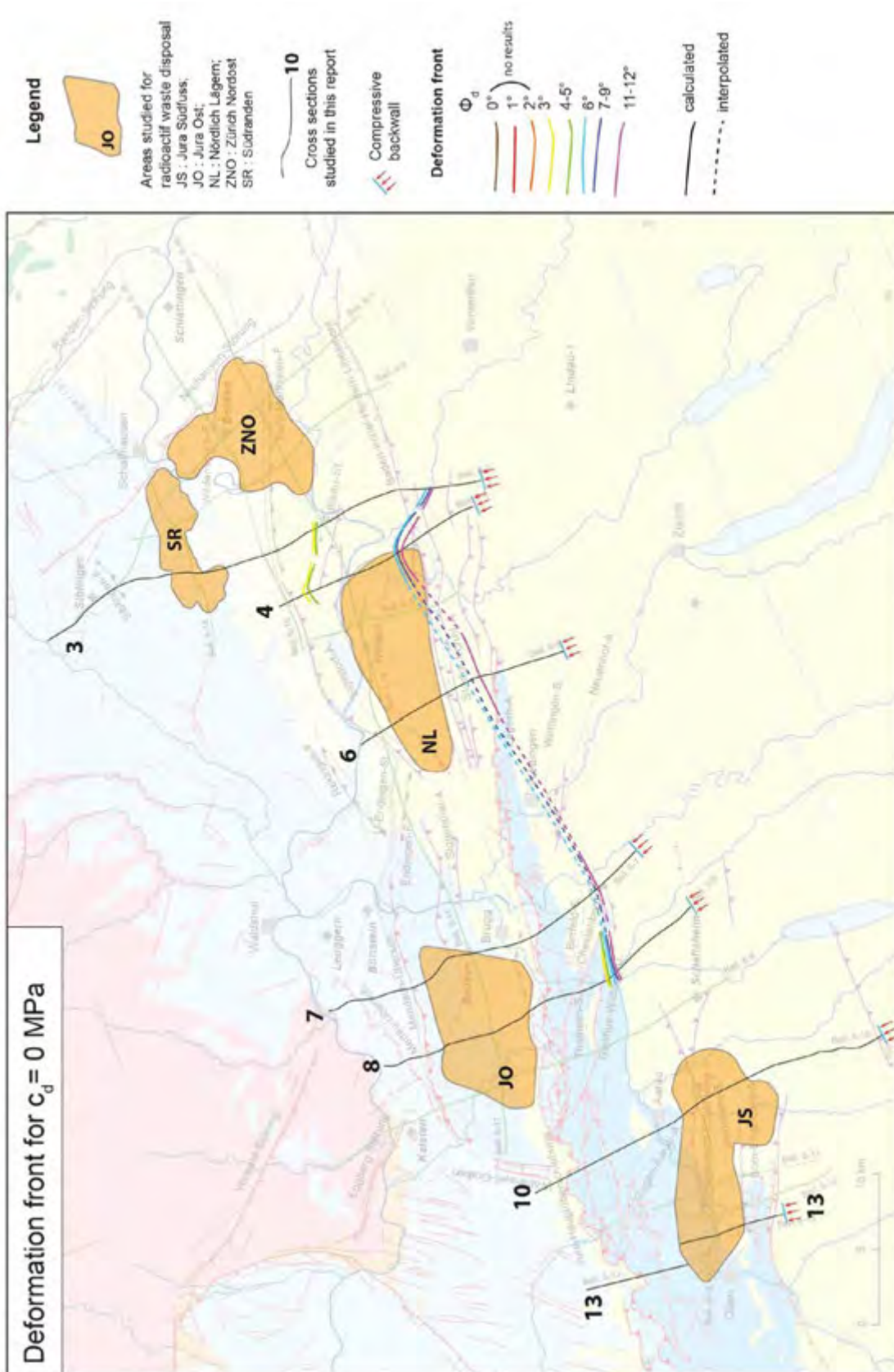


Figure 4—8: Map view showing the interpolation of the deformation front between cross sections. Note that the different deformation fronts correspond to the various hypotheses on the friction angle of the decollement. This map was made using a cohesion on the decollement of 0 MPa.

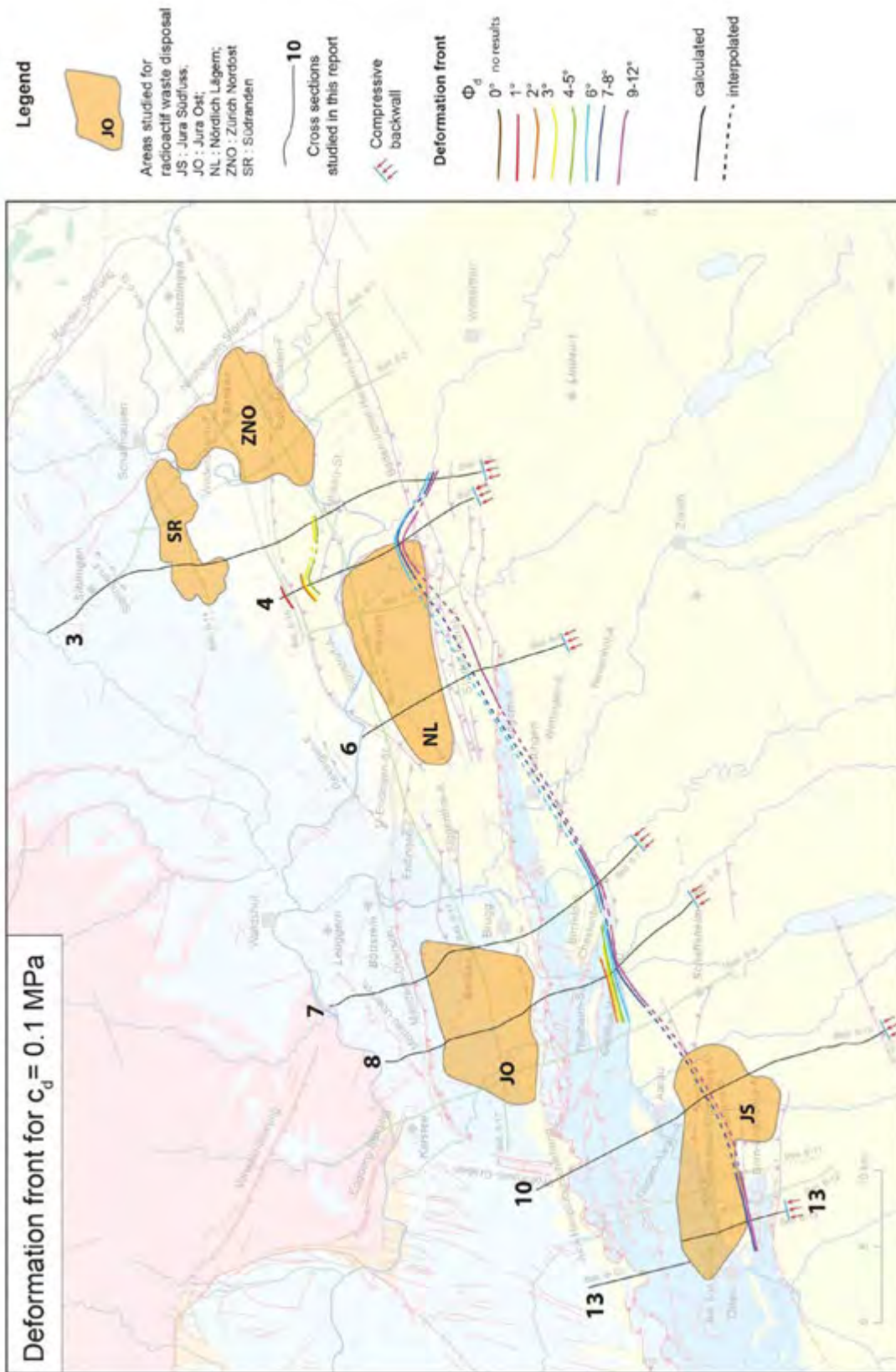


Figure 4—9: Map view showing the interpolation of the deformation front between cross sections. Note that the different deformation fronts correspond to the various hypotheses on the friction angle of the decollement. This map was made using a cohesion on the decollement of 0.1 MPa.

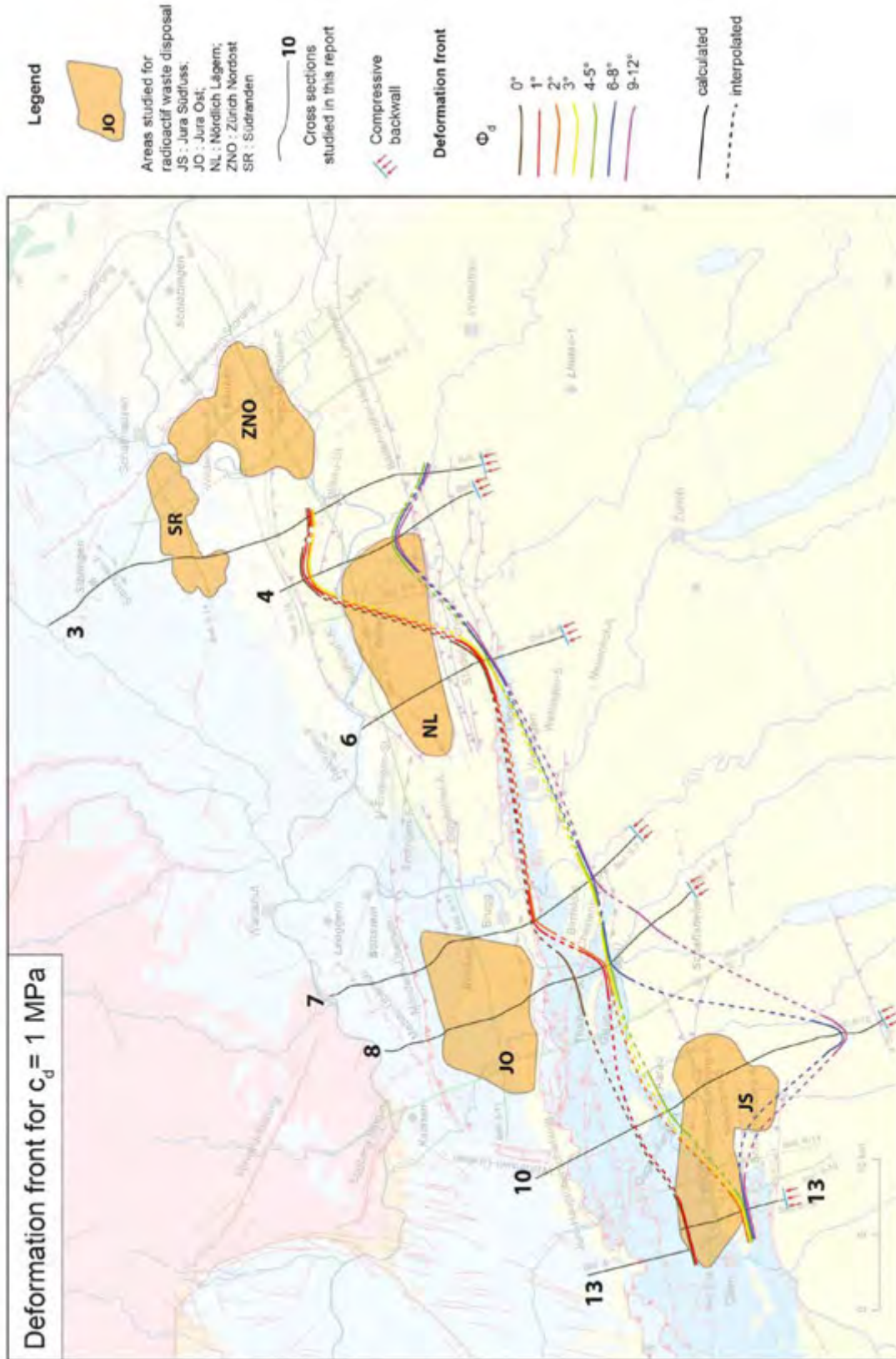


Figure 4—10: Map view showing the interpolation of the deformation front between cross sections. Note that the different deformation fronts correspond to the various hypotheses on the friction angle of the decollement. This map was made using a cohesion on the decollement of 1 MPa.

5 Reliability of the results

There is no protocol today that would allow us to calculate error bars associated to the numerical simulation of tectonic activity, in particular in small regions and over one million years as is the goal here. First, because the numerical solution cannot be compared to an experiment. Second, because we lack of precise rheological data, especially over such time scales. Third, because both initial and boundary conditions are subject to unknown uncertainties. Let us now precise these general statements one by one.

5.1 Verification and validation

Confidence in a numerical simulation depends first on its verification, and its validation. Both numerical methods and softwares used here have been verified in a number of different cases using analytical solutions, and their convergence properties (refinement of the solution when using finer spatial and temporal discretisation) have been measured so that all solutions presented here are most probably free of numerical errors and do represent precise solutions. References to these works are given in the Method section of the present report. Therefore, our solutions are actually solutions of the mechanical problem as it was stated: they are verified.

The second step is called "validation" in numerical analysis and consists in comparing the solution to an experiment to conclude whether the equations describing the mechanical problem are pertinent descriptions of the physical phenomena at stake. We have done validation of SLAMTec using analogue experiments with dry sand (Cubas et al., 2013). For OptumG2, again, validations can be found in the references found in the Method section. Therefore, both softwares are valid when dealing with frictional Coulomb materials (recall that SLAMTec makes further simplifying assumptions like planarity of the decollement level, and uniformity of material properties above the decollement). But, in real settings, other deformation mechanisms than just Coulomb friction occur, for example the pressure solution in carbonates or the ductile flow of evaporites. Changes in the local shortening rates due to far field geodynamics may also trigger switches between ductility and friction in the same material. The presence and flow of pore fluids may modify the effective stress, and influence the friction parameters through chemical processes. Part of the deformation may also be stored as elastic energy and released as earthquakes. Also, surface processes redistribute the mass in a way that cannot be precisely accounted for in the 2D vertical cross sections we analysed here.

5.2 Rheological data

Thanks to the simplicity of the deformation process adopted in our limit analysis approach, i.e., the assumption that all deformation is expressed as Coulomb friction, there are only three parameters needed to describe the properties of materials (cohesion, friction angle, density), and two for the properties of interfaces, or faults (cohesion and friction angle). The density is a relatively uniform parameter and is treated as such, the other material properties were set to fixed values (Figure 3—2). We concentrated our analysis on the most important material property: that of the Muschelkalk evaporites which form the major decollement level. To answer the problem of uncertainty on the friction parameter values of the Muschelkalk rocks, we made a parametric study, i.e., we considered all physically realistic values.

5.3 Initial conditions

The present day structures in each cross sections are issued from state of the art acquisition and interpretation of seismic and other data (wells, gravimetry, ...). Obviously, they influence strongly the predictions of failure in the near future so that errors in location of faults or layer boundaries, and the absence of structures below the seismic resolution, could have important effects on our results, and these are very difficult to estimate.

5.4 Boundary conditions: Thin- or thick-skin?

In this study, the results have been obtained by considering thin-skin tectonics (Figure 5—1a): the compressive force was applied only above the Muschelkalk decollement (here called $D1$). However, whether the Jura Mountains today undergo thin- or thick-skin deformation is a debated question (Laubscher, 1986; Becker, 1989; Becker, 2000; Ustaszewski & Schmidt, 2007; Madritsch, 2008; Madritsch et al, 2008; Madritsch et al, 2010a, Madritsch et al, 2010b) (Figure 5—1a, b). To address this question, we modify our prototypes by Figure 5—1 extending the pushing wall down to the Upper- lower-crust limit where we set another decollement, called $D2$, or “mid-crustal decollement” (Figure 5—1c). This is also an on-going study carried out by T. Caër as part of her PhD project: she studies this question throughout the Jura with the same methods as applied here and with prototypes considering the whole crust and part of the mantle. She considers four cross sections from the Alps to the foreland scanning the whole Jura (Figure 5—2). The southernmost one is the ECORS profile interpretation redrawn after Schmidt and Kissling (2000) and Philippe (1995). The three cross sections have been realized using different data sources allowing to constrain the depth of the basement, the thickness of the Triassic bed, the position of the Permo Carboniferous graben, and the depth of the upper-lower crust limit ($D2$) (Pfiffner et al., 1990; Sommaruga, 1999; Rotstein et al., 2006; Ustaszewski and Schmidt, 2007; Sommaruga et al., 2012). One of these cross sections, the easternmost one, is presented in Figure 5—1. This study suggests so far that it is possible to have thick-skin deformation associated with slip on the Muschelkalk detachment in the Eastern Part of Jura (Figure 5—2). Here we focus on cross section C (Figure 5—2), whose axis is located only a few kilometres west of the cross section 13 of this report (Figure 2—2, Figure 2—34, Figure 4—). We then process exactly in the same manner that we did for the beginning of this report by setting fixed friction angle and cohesion values to each material (Figure 3—2) except for the Muschelkalk decollement where they vary exactly like in the local scale study (section 3 of this report). As the behaviour of the lower crust is very difficult to estimate; we vary its friction from $\Phi_{D2} = 0^\circ$ to $\Phi_{D2} = 30^\circ$ to scan a large range of results. Note that the friction on $D2$ is considered to be the same than the one of the lower crust. Pictures of results are presented as examples in Figure 5—2b, and illustrate the behaviour of the thick-skin tectonics: We can see that the deformation uses the decollement $D2$ and northward, a crustal ramp develops and either reaches the surface or connects to the Triassic decollement. The map in Figure 5—2a shows the location of the arrival in the sedimentary cover of this crustal ramp, for different values of Φ_{D2} . Thick-skin conditions dominate for a wide range of friction values on the $D2$ decollement (Figure 5—2). We can then distinguish two situations: for the highest range ($\Phi_{D2} = 10$ to 30°) the crustal ramp emerges in the region of interest, i.e. the map presented in Figure 2—2, potentially causing damage in this area. For lower values, the ramp emerges further north and the region is expected to be passively transported as part of the crustal ramp hanging wall. Deformation would then be only due to the reactivation of the $D1$ decollement. We then study what happen precisely in the region of interest, i.e. the map presented in Figure 2—2, and for

that, we select three different values of $\Phi D2$ that corresponds to three different position of the crustal ramp according to the region of interest: $\Phi D2=3^\circ$ the crustal ramp emerges far beyond the north of the region of interest, $\Phi D2=7^\circ$ the crustal ramp emerges precisely in the north of the region of interest and $\Phi D2=10^\circ$ the crustal ramp emerges in the region of interest. For each value of $\Phi D2$, we realize a parametric study varying the friction $\Phi D1$ and the cohesion $cD1$ in the Muschelkalk layer (Figure 5—3).

In order to verify the applicability of the conclusions drawn in the thin-skin hypothesis (section 3 and 4) we now place cross section nbr. 13 into the large scale prototype (Figure 5—3) and we perform the same parametric study as before on the friction parameters of $D1$ (Figure 5—3c, d). We consider three different cases corresponding to the two different situations detailed in the previous paragraph (Figure 5—2, Figure 5—3). In the first one, we consider $\Phi D2=3^\circ$ corresponding to a crustal ramp emerging beyond the north of the studied area (Figure 5—2, Figure 5—3). In the second one, we consider $\Phi D2=10^\circ$ corresponding to a crustal ramp emerging in the region of interest (Figure 5—2, Figure 5—3). And the third case is an intermediate case in which $\Phi D2=7^\circ$.

The results of these three different situations are presented in graphs b)ii), b)iii) and b)iv) of Figure 5—3. Graph a)ii) presents the results for the local study presented in the previous section (Figure 4—7). Graph b)ii) presents the results for a regional scale study with $\Phi D2=3^\circ$ (Figure 5—2, Figure 5—3b)ii)). In this situation, the crustal ramp emerges beyond the north of the cross section, and the different types of results that we obtain are the same than for the local study, but their repartition in the graph is different. The propagation of the deformation needs lower cohesion than at local scale. The dark grey cases are cases in which the friction on $D1$ is too high to allow any sliding on it. At the local scale this corresponds to the blue case (see section 4 for further explanations). Graph b)iii) presents the results for a regional scale study with $\Phi D2=7^\circ$ (Figure 5—2, Figure 5—3b)iii)), and we observe that the results are very close to the ones of graph b)ii). Graph b)iv) presents the results for a regional scale study with $\Phi D2=10^\circ$ (Figure 5—2, Figure 5—3b)iv)). In this graph, the yellow and dark blue cases are similar respectively to green and blue cases of the other graphs, but with an additional reactivation of the two thrusts present south of the Permo-Carboniferous graben. According to the colour gradients on the figure, this reactivation occurs at very low velocity compared to the main structure that is developing (in the middle of the flat underformed area for the yellow case and in the anticline for the dark blue case).

It is surprising to obtain the same types of results and the same distribution in the ($\Phi D1$, $cD1$) domain for graphs b)ii), b)iii) and b)iv), i.e. for different frictions on $D2$ and so different positions of the crustal ramp. That means that whatever the expression of the thick-skin tectonics, if the properties on the Muschelkalk decollement ($D1$) are low enough to allow its activation, the deformation of near surface is expressed in the same manner as thin-skin. The basement faults bordering the Permo-Carboniferous grabens do not play a major role here.

The results obtained with the local study (Figure 5—2) and section 3 and 4 of this report), are important because they highlight the different zones that will undergo present-day and future deformation. If we knew better the real $\Phi D1$ and $cD1$, then regional studies would be interesting for all cross sections, but these values are difficult to estimate precisely, and then, local scale studies, simpler to realize, already provide much information, and allow to trace the worst deformation front that can develop in the next million years (or rather the next 1 km of

shortening).

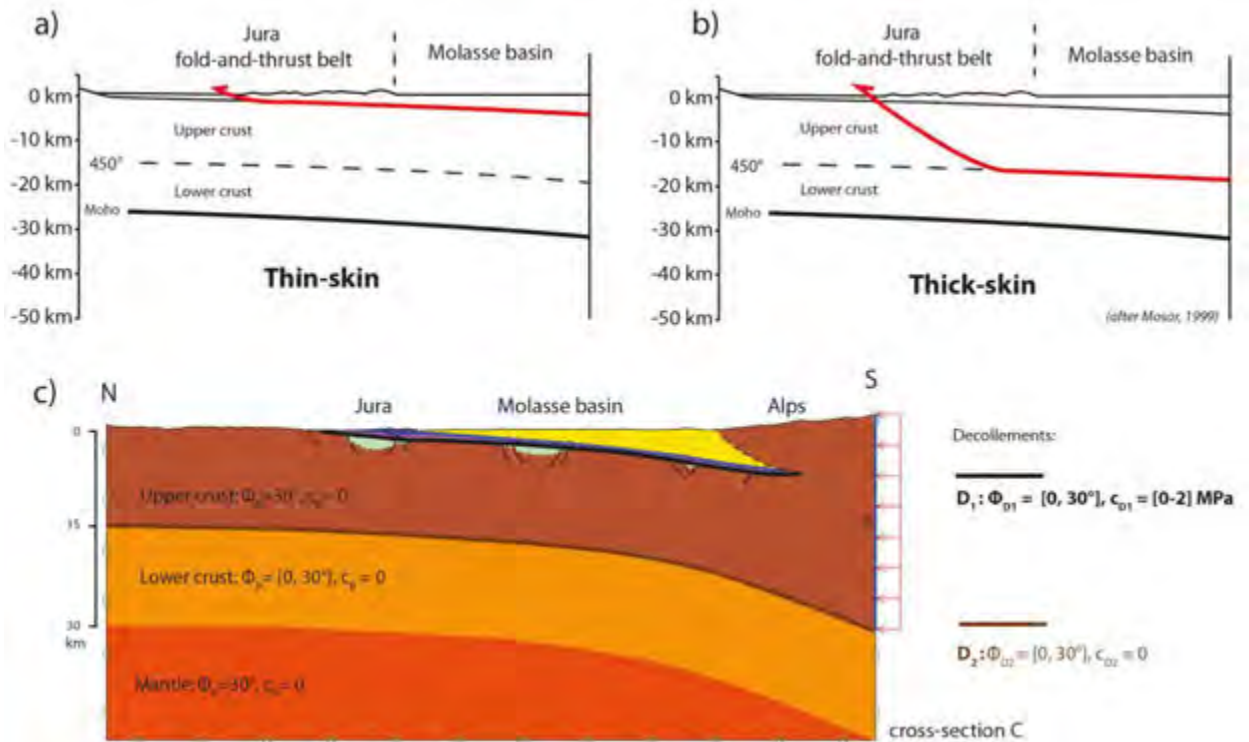


Figure 5—1: Illustration of the hypotheses on the thin-skin tectonic (a) or the activation of the basement, i.e. thick-skin tectonics (b). Cross section C (Figure 21 and Figure 22) and Optum G2 prototype considered for the thin-/thick-skin tectonics analysis c). D1 and D2 indicate respectively the Muschelkalk and the mid-crustal detachments. The red arrows at the southern edge show the applied tectonic compression. The other boundaries are kept rigid (green hash signs along the base), or allow movement parallel to them (green vertical equal sign at the northern edge and at the base of the southern edge). Top surface is free of any traction.

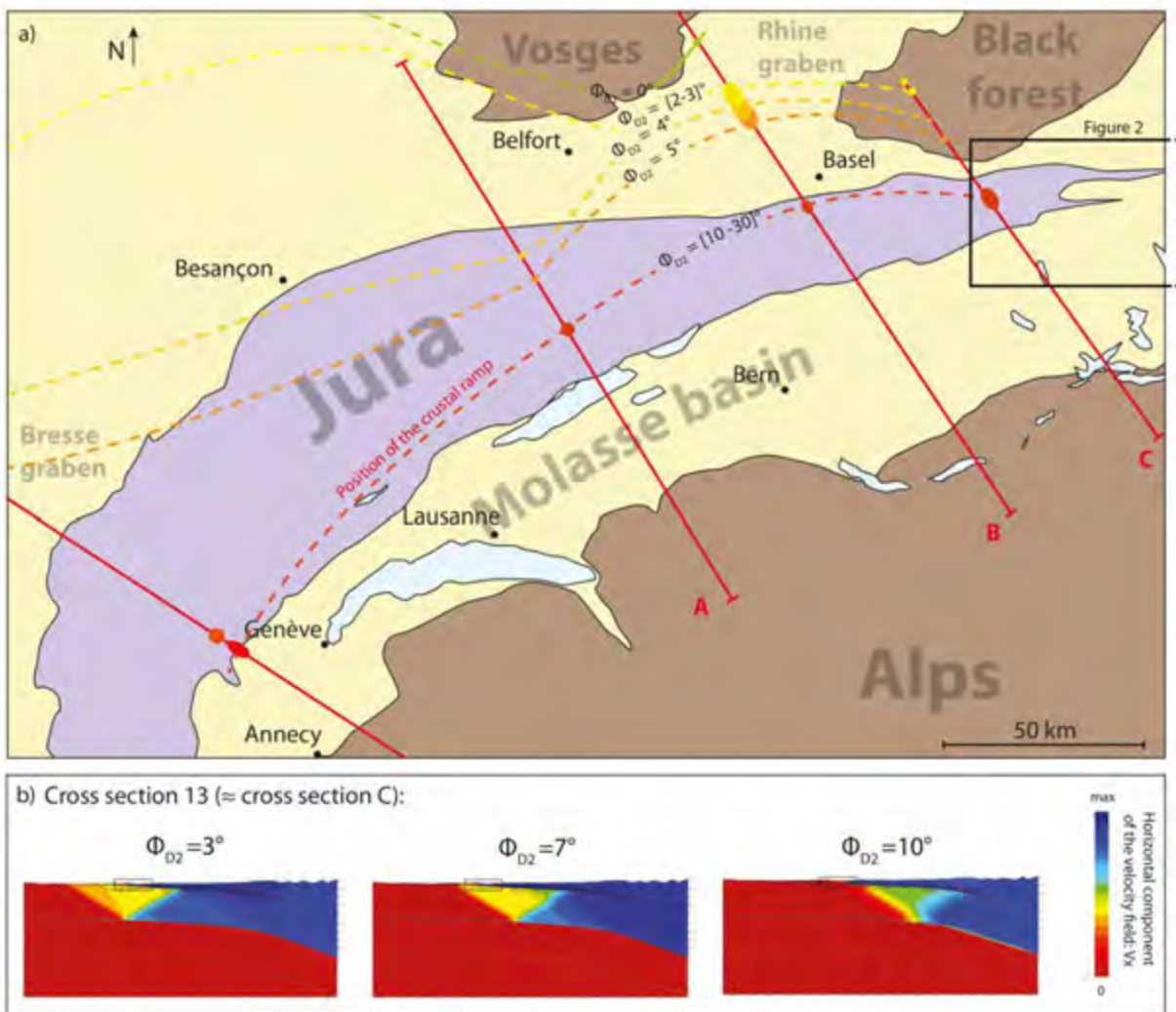


Figure 5—2: Surface positions of the thick-skin deformation fronts in map view, interpolated from three cross sections (A, B, C) for different values of Φ_{D2} ,a), and examples of results for three different values of Φ_{D2} ,b). Note that as the friction on the mid-crustal decollement Φ_{D2} decreases, the thick-skin deformation front moves to the north. In cross section C which is of particular interest here, the deformation front is either in the area, or north of it. The region of interest of this report is represented by the black rectangle. Note that in all cases above, the Muschelkalk

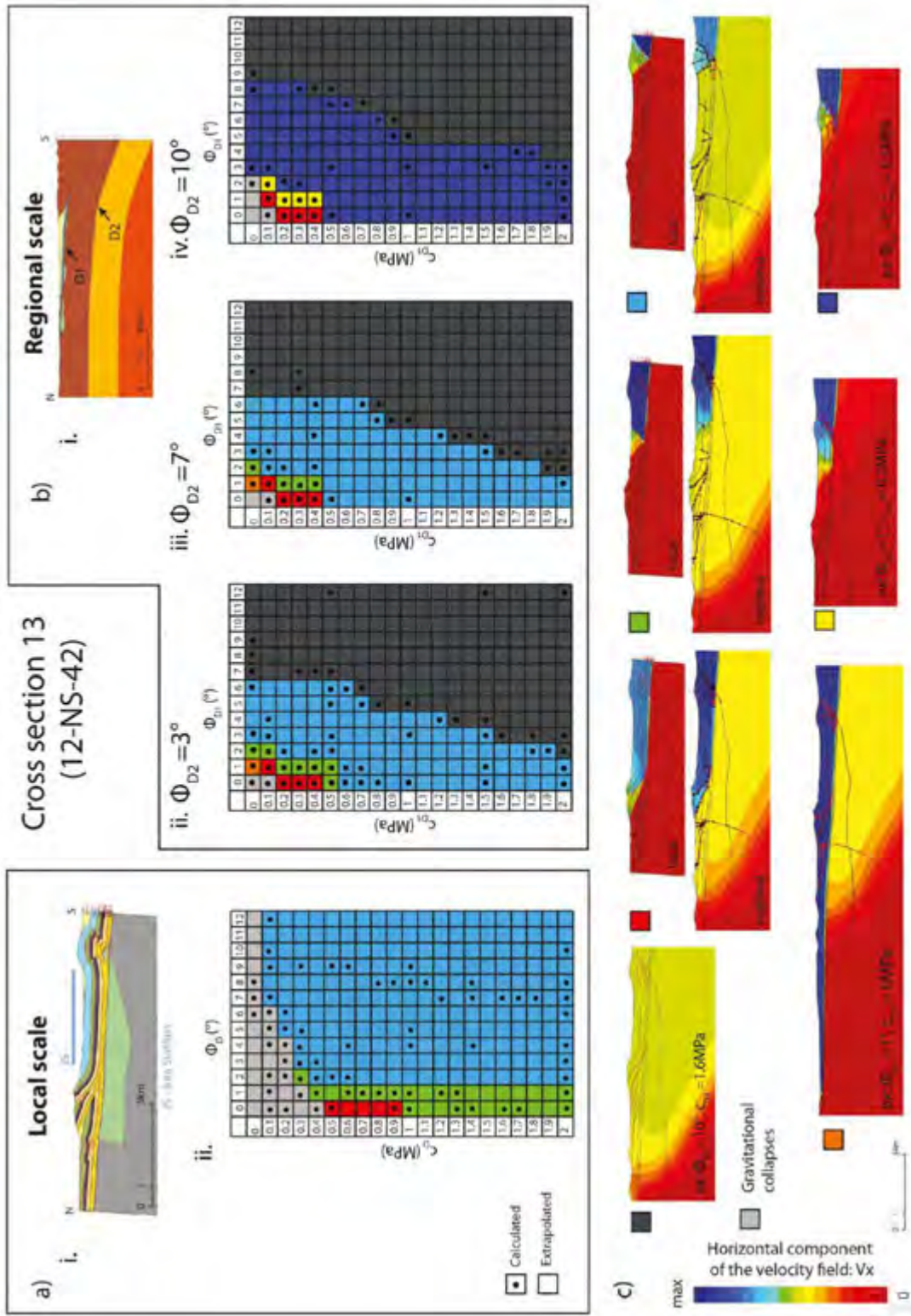


Figure 5—3: Results of the Optum G2 analysis of the thick-skin hypothesis: The two prototypes, cross section 13 at local scale a)) and in the frame at regional scale b)). Graph of results for local scale study, identical to figure 16, a)ii); for regional scale study with $c_{D2} = 0$ MPa and $\phi_{D2} = 3^\circ$, b)ii); $\phi_{D2} = 7^\circ$, b)iii); $\phi_{D2} = 10^\circ$, b)iv). Examples of the different types of results obtained and represented by colours in the graphs c).

Conclusion

Two software packages based on the theory of Limit Analysis were used to predict the deformation and stress fields resulting from horizontal compression in seven cross sections proposed by Jordan et al., 2015 in the Eastern end of the Swiss Jura Mountains. Limit Analysis is based here on the Coulomb criterion defined by friction angles and cohesions. No elastic or viscous parameters are considered. Velocity, deformation and stress fields are obtained by optimization of the tectonic compressive force applied at the southern end of the cross sections. The commercial software Optum G2 provides the onset of deformation, accounting for rheological contrasts between lithology and for the weakness of existing faults. To gain insight on the future evolution of deformation we used a second software, SLAMTEC, which uses Limit Analysis sequentially, applying one deformation step between each optimization step, at the cost however of limiting the predictions to rheologically uniform materials sliding on a planar, uniform, decollement. Based on this simplifications, we conducted systematic parametric investigations of the decollement properties (friction angle ΦD and cohesion cD) for each cross section. The resulting velocity fields can be classified in few groups defined essentially by the position of emergence of the active ramp rooted in the Muschelkalk decollement. For a very weak decollement, whole (dark grey cases in figures 11 and 12) , or parts (light grey cases in figures 10, 13, 14, 15 and 16) of the cross sections are gravitationally unstable and collapse under their own weight by sliding on such a weak base. For a strong decollement, deformation is concentrated at or near the pushing southern wall, precluding the activation of most structures found in the cross sections. Between these two end-members we find velocity fields that mostly activate existing faults and folds drawn in the cross sections at the northern and southern limits of the Permo-Carboniferous graben, and sometimes predict the occurrence of new ramps in pristine parts. Also, as expected, the northern extent of the deformation front (defined as the surface position of emergence of the active ramp) depends on the weakness of the decollement. Next, for a given set of rheological parameters, we interpolated the deformation fronts of each cross section to draw a map of the northern limit of the deformation. Drawing such limits for several sets of rheological parameters spanning all physically realistic values between the above mentioned end-members allowed us to define the zones in map view that will likely not be deformed in the near future. The main result is that there are indeed intersections between the deformation fronts and some regions considered for nuclear waste siting. However, the Jura-Ost zone and the Zurich Nordost remain mostly north of the deformation front in all calculations. The SLAMTEC simulations provided predictions on the future evolution of the active structures detected with Optum G2. The active structures would stay active for at least 190 m of shortening (about 200 Ka at 1 mm/a).

In the first part of the study we assumed thin-skin tectonics: the pushing rigid wall extends from the surface down to the Muschelkalk decollement, and the basement below is considered fixed, i.e. not subjected to the horizontal compression. To address the possibility of thick-skin tectonics, we have extended cross section 13 to the south down into the central Alps, and applied a compressive force to that new southern limit on a rigid wall extending vertically from the surface down to the upper-lower crust limit. The main result is that studies at regional scale differ from studies at local scale only by the repartition of the different types of results in the ϕ/c graph, but these different types of results are the same. Whatever the position of the thick-skin crustal ramp, if the Muschelkalk decollement is active, the deformation is expressed in the same manner at near-surface. However, for a value of 10° of the friction coefficient in the lower crustal decollement ($\Phi D2$), we showed that a crustal ramp would form and emerge in the Jura Südfuss

siting region, potentially generating substantial deformation. As long as we do not know precisely the values of $\Phi D2$ and $cD2$, regional scale studies will probably not bring further information. Be aware that for certain $\Phi D2$ values (around 10°), a crustal ramp would cross the siting region in cross section 13 and could therefore generate deformation within the siting region (Figure 21 and yellow and dark blue cases in Figure 22). The other cross sections are expected to follow the same conclusions on the kinematics, but probably for different values of $\Phi D2$. Therefore, this large scale analysis raises new kinematic solutions that may affect all siting regions.

It should be kept in mind that it is not possible today to predict in details the deformation in a given tectonic region over a time scale of one million years. Our predictions and conclusions are based on a simple mechanical and rheological description of materials and faults. They are also based on cross sections which themselves carry an unknown uncertainty and they also partly depend on the choice of rheological parameter values. It is therefore not possible to quantify the uncertainty of each result. This is why we have conducted parametric studies of the most important parameters (the decollement levels), and we have grouped the results in global types of deformation to forbid the over-interpretation of particular details of single simulations. The global outcome is that there are sharp boundaries between the types of deformation in the parametric space so that a small change in friction of a decollement level can produce a major change in the location of the active fault, for example. We think that both the types of deformations, and their sharp boundaries when varying parameters, are robust features of our results and not merely the imprint of our assumptions.

6 Perspectives

Thick- or thin-skin?

The test of the thick-skin hypothesis in cross section 13 has shown two features: (i) The thin-skin structures that were observed in the first part (where compression is applied only above the Muschelkalk decollement) are retrieved when using a more extended prototype that permits thick-skin deformation; (ii) the bigger prototype has in addition revealed the possibility of the emergence of a crustal ramp in the zone of the siting region, depending on the friction value set on the lower to upper crust limit. Since all other cross sections are further to the East, it is important to check whether similar conclusions would be drawn on the other cross sections.

The stress field

The Limit Analysis approach used here can also be used to determine an optimal stress field. We have shown the stress field issued from one of the simulations of cross section 8. The stress field could be used in two ways. First, it is an additional observable that could be compared to field data on stress measurements. Similarly to fitting the cross sections using the predicted velocity field as done here, we could perform a parametric study to constrain friction parameters with regard to the fit to the stress data. Second, the fitted stress fields would then help in the interpolation of the stress data between wells, or their extrapolation at depth, to estimate the evolution of the pressure and deviatoric stress levels in the siting regions. In that respect, smaller scale analyses around the disposal could be conducted.

Other mechanical methods

The present analyses were made with simplified mechanical and numerical tools: We describe material properties only with friction (Coulomb) parameters and independently determine the velocity and the stress fields. Thanks to this simplicity we were able to explore important portions of the parametric space (essentially regarding the resistance to slip of the two major decollements levels) and to prepare the grounds for the use of more complete methods. In a full mechanical problem, stress and strains are linked through rheological relations requiring more materials parameters (elastic, viscous, and plastic). It could be of interest to compare our results to simulations obtained with other available softwares, for example using the finite-element method, to estimate the detailed effects of the simplifications adopted in each method and thus better determine the uncertainty of the predictions.

Finally, analyses in three dimensions are certainly highly desirable and are the subject of ongoing developments. A 3D version of Optum G2, called Optum G3, is in preparation, and we have also our own 3D implementation of Limit Analysis, but it is currently limited to simple geometries which cannot yet describe the complexity of the cross sections studied here.

7 References

- Becker, A. (1989). Detached neotectonic stress field in the northern Jura Mountains, Switzerland. *Geol. Rundsch.* 78(2), pp. 459-475
- Becker, A. (2000). The Jura Mountains—an active foreland fold-and-thrust belt? *Tectonophysics*, 321(4), 381-406.
- Caër, T., Maillot, B., Souloumiac, P., Leturmy, P., de Lamotte, D. F., & Nussbaum, C. (2015). Mechanical validation of balanced cross-sections: The case of the Mont Terri anticline at the Jura front (NW Switzerland). *Journal of Structural Geology*, 75, 32-48. Doi:10.1016/j.jsg.2015.03.009
- Cubas, N., Leroy, Y. M., & Maillot, B. (2008). Prediction of thrusting sequences in accretionary wedges. *Journal of Geophysical Research: Solid Earth (1978–2012)*, 113(B12), 1-21. Doi:10.1029/2008JB005717.
- Jordan, P., Malz, A., Heuberger, S., Pietsch, J. Kley, J., Madritsch, H. (2015). Regional geologische Profilschnitte durch die Nordschweiz und 2D-Bilanzierung der Fernschubdeformation im stlichen Faltenjura: Arbeitsbericht zu SGT-Etape 2. Arbeitsbericht NAB 14-105. Nagra.
- Krabbenhøft, K., Damkilde, L. (2003). A general non-linear optimization algorithm for lower bound limit analysis. *International Journal for Numerical Methods in Engineering* 56, 165-184.
- Krabbenhøft, K., Lyamin, A.V., 2014. Optum g2 (2014). optum computational engineering, www.optumce.com.
- Krabbenhøft, K., Lyamin, A.V., Hjjaj, M., Sloan, S.W. (2005). A new discontinuous upper bound limit analysis formulation. *International Journal for Numerical Methods in Engineering* 63, 1069-1088.
- Laubscher, H. P. (1986). The eastern Jura: relations between thin-skinned and basement tectonics, local and regional. *Geologische Rundschau*, 75(3), 535-553.
- Lyamin, A.V., Sloan, S.W., Krabbenhøft, K., Hjjaj, M. (2005). Lower bound limit analysis with adaptive remeshing. *International journal for numerical methods in engineering* 63, 1961-1974.
- Madritsch, H. (2008). Structural evolution and neotectonics of the Rhine-Bresse Transfer Zone (Doctoral dissertation, University of Basel).
- Madritsch, H., Schmid, S. M., & Fabbri, O. (2008). Interactions between thin-and thick-skinned tectonics at the northwestern front of the Jura fold-and-thrust belt (eastern France). *Tectonics*, 27(5).
- Madritsch, H., Fabbri, O., Hagedorn, E. M., Preusser, F., Schmid, S. M., & Ziegler, P. A. (2010a). Feedback between erosion and active deformation: geomorphic constraints from the frontal Jura fold-and-thrust belt (eastern France). *International journal of earth sciences*, 99(1), 103-122.
- Madritsch, H., Preusser, F., Fabbri, O., Bichet, V., Schlunegger, F., & Schmid, S. M. (2010b). Late Quaternary folding in the Jura Mountains: evidence from syn-erosional deformation of fluvial meanders. *Terra Nova*, 22(2), 147-154.
- Maillot, B., Leroy, Y.M. (2006). Kink-fold onset and development based on the maximum strength theorem. *Journal of the Mechanics and Physics of Solids* 54, 2030-2059. doi:10.1016/j.jmps.2006.04.004.
- Mary, B., Maillot, B., Leroy, Y.M. (2013a). Deterministic chaos in frictional wedges revealed by convergence analysis. *Int. J. Numer. Anal. Meth. Geomech.* doi:10.1002/nag.2177.
- Mary, B., Maillot, B., Leroy, Y.M. (2013b). Predicting orogenic wedge styles as a function of analogue erosion law and material softening. *Geochemistry, Geophysics, Geosystems* 14. doi:10.1002/ggge.20262.

- Mary, B.C.L. (2012). Au-delà du prisme critique de Coulomb par l'analyse limite séquentielle et contributions expérimentales. Doctoral thesis. Université de Cergy-Pontoise, France.
- Pfiffner, O. A., KLAPER, E. M., Mayerat, A. M., & HEITZMANN, P. (1990). Structure of the basement-cover contact in the Swiss Alps. *Mémoires de la Société géologique de France*, 156, 247-262.
- Philippe, Y. (1995). Rampes latérales et zones de transfert dans les chaînes plissées. Unpublished PhD thesis, Université de Savoie
- Rotstein, Y., Edel, J. B., Gabriel, G., Boulanger, D., Schaming, M., & Munsch, M. (2006). Insight into the structure of the Upper Rhine Graben and its basement from a new compilation of Bouguer Gravity. *Tectonophysics*, 425(1), 55-70.
- Salençon, J. (2002). De l'élasto-plasticité au calcul à la rupture. Ecole Polytechnique, Palaiseau, and Ellipses, Paris.
- Schmid, S. M., & Kissling, E. (2000). The arc of the western Alps in the light of geophysical data on deep crustal structure. *Tectonics*, 19(1), 62-85.
- Sommaruga, A. (1999). Décollement tectoniques in the Jura foreland fold-and-thrust belt. *Marine and Petroleum Geology*, 16(2), 111-134.
- Sommaruga, A., Eichenberger, U., & Marillier, F. (2012). Seismic atlas of the Swiss molasse basin. E. Kissling (Ed.).
- Souloumiac, P., Krabbenhoft, K., Leroy, Y.M., Maillot, B. (2010). Failure in accretionary wedges with the maximum strength theorem: numerical algorithm and 2D validation. *Computational Geosciences* doi:doi: 10.1007/s10596-010-9184-4.
- Souloumiac, P., Leroy, Y.M., Krabbenhoft, K., Maillot, B. (2009). Predicting stress in fault-bend fold by optimization. *J. Geophys. Res.* 114, B09404. doi:doi:10.1029/2008JB005986.
- Ustaszewski, K., & Schmid, S. M. (2007). Latest Pliocene to recent thick-skinned tectonics at the Upper Rhine Graben–Jura Mountains junction. *swiss Journal of Geosciences*, 100(2), 293-312.
- Yang, W.H. (1993). Large deformation of structures by sequential limit analysis. *International Journal of Solids and Structures* 30, 1001-1013. URL: <http://www.sciencedirect.com/science/article/pii/002076839390023Z>, doi:10.1016/0020-7683(93)90023-Z.

ENSI 33/470

ENSI, CH-5200 Brugg, Industriestrasse 19, Telefon +41 56 460 84 00, E-Mail Info@ensi.ch, www.ensi.ch